Development of Group 10 Metal Catalyzed Decarbonylative Catalysis and Undergraduate Organic Chemistry 2 Lab Modules

by

Naish Lalloo

A dissertation submitted in partial fulfillment
of the requirements for the degree of
Doctor of Philosophy
(Chemistry)
at The University of Michigan
2022

Doctoral Committee:

Professor Melanie S. Sanford, Chair
Professor Tim Cernak
Professor Alison H. Narayan
Professor Nathaniel Szymczak

Naish Lalloo

nlalloo@umich.edu

ORCID iD: 0000-0001-9926-0387

DEDICATION

It is with enormous gratitude and regard that I dedicate this work to the people who supported me throughout this challenging academic process in becoming an educator of chemistry. I worked extremely hard in grade school and university to achieve academic success, ultimately leading to my attending graduate school in chemistry at The University of Michigan. To attend graduate school at the University of Michigan, I sacrificed time with my family and loved ones. This dedication is an acknowledgment of that sacrifice.

Despite our distance, I could not have had this success without the support of my mother, Usha Lalloo, and my father, Jayesh Lalloo. Mom, you have guided me with a loving and strong hand throughout this journey and remain my biggest fan to this day. Dad, you have been an example of discipline, diligence, effort, and dedication. Through everything, you remain supportive of me, and I am excited to make you proud as the first Dr. Lalloo in our family.

To my brothers, Shahil and Nikheel, I remember vividly when I didn't "have time" to come to Wilmington and do a brother vacation and when I didn't "have time" to see you two in Raleigh. I want you both to know that I would not be where I am without you two. Shahil, your sensibility and wisdom have helped me see how to be compassionate, how to be strong, and how to become my own person. Nikheel, your compassion and calm continually teach me how to be a kind, grateful person that appreciates all things, small and big. I love you both so much.

This work is also dedicated to Thomas Gilliam, my best friend from age 10. Thomas, you have been instrumental in my life and in my success. I treasure you as a brother and know we have a lifetime full of experiences to enjoy together. Thank you for your unending support, your advice, and your critical thinking. It is an honor to be your best friend.

This work would not have been completed without the support of my partner over four years, Chloe Weise. Chloe, you have been my champion throughout this process. You have supported me day in and day out. You have taught me so much and I am so grateful that we met in 2018.

This work is also dedicated to my Master Sensei, Mark Slocum. Those of you who know me best know that martial arts have been a critical and impactful part of my life. Sensei Mark passed away after being intubated for week due to complications related to COVID-19. Sensei, I thought you would be there for my defense, for my future marriage, and for the birth of my future children. You taught me to be strong, to be fierce, to be kind, to be empathetic, to be wise, and so much more. I will remember you forever and will continue to make you proud. Thank you for gracing my life. I only wish we had more time together.

ACKNOWLEDGEMENTS

I would like to gratefully acknowledge all those who have helped me complete by journey and finish this document. First, I would like to thank my family here in the US and abroad, as well as Sensei Mark Slocum, Sensei Brian Villegas, and Sensei Rick Bondi for their unconditional support. I would like to thank my friends, Thomas Gilliam (and the Gilliam family) and Adam Johnson (and the Johnson family) for their love and acceptance of me. Growing up with you all has been one of the greatest pleasures of my life. I would also like to thank Nick Ragazzone for his awesome friendship and support over these five years.

I would not be attending graduate school in chemistry in the first place if it wasn't for Professor Joshua G. Pierce at North Carolina State University (NCSU). During my time as an undergraduate at NCSU, you were an excellent example for me of what a dedicated college professor could accomplish and the impact that position holds in the lives of students. I remember reaching out to you regularly for over a year to gain an opportunity to conduct research in your lab. I cannot thank you enough for believing in me and giving me that initial opportunity. Since then, you have constantly supported me in my academic career and helped me immensely during my application process for graduate school. Also during my time at NCSU, I was fortunate to interact with and learn from Dr. Ana Ison, who has been just a pleasure to engage with throughout this process. I must also thank my first research mentors, Dr. Yunlong Shi (Scripps – Florida) and Dr. Yasamin Moazami. It was so much fun working with you guys. All of the people in the Pierce Lab at the time – Dr. Grant Edwards, Dr. Chrissi Martinez, Professor Jonathan Mills, Dr. Patrick Parker, Dr. Kaylib Robinson, Dr. Anna Cholowczynski, Alain Valery, Alex Cusumano, Dr. You-Chen Lin – thank you for all of your support and for the great memories. I miss you all.

I must acknowledge my research mentors at the University of Michigan (UM): Professor Courtney Roberts (University of Minnesota) and Professor Christian Malapit (Northwestern University) for their invaluable teachings and guidance. I must also thank Dr. Andrew Higgs for his relentless support and awesome friendship over these five years. Additionally, I would like to

thank Professor Patrick Melvin for his support of me when we taught CH419 together at UM. Without each of you, I would not be the chemist and educator I am today. I would like to specifically mention a few members of the Sanford Lab. First, Conor Brigham. I am so appreciative of you for your comradery and friendship through these five years. To the students I have been privileged to mentor, Frances and Alex, you both are wonderful people, and I look forward to seeing where your lives take you.

My last and greatest acknowledgement is to Professor Melanie Sanford. Melanie, you have been an inspiration to me. I am so grateful that I was fortunate enough to join your lab. Your knowledge, compassion, and passion have continuously amazed and excited me over these five years. Thinking back to 2017, it feels like ages ago. In these five years you have helped me to be more confident, more concise (despite my wordiness), and have been an exemplar to me of an excellent professor and person.

I remember our first in-person interaction was during recruitment in Winter 2017 in a scheduled recruitment meeting in 1706 Chem. At that time, I had no idea that you would become my advisor, that we would develop a fantastic working relationship, and that you would support me relentlessly over these five years. I remember meeting with you in my second year to discuss the status of my platinum project. While that first interaction about it was very challenging for me, I remember vividly when you asked to meet again to have a productive and supportive conversation. This conversion is what led to my working on the awesome chemistry that is now reported in this thesis. Since that meeting, I feel that we have had a fantastic rapport. I appreciate so much how compassionate you are as a leader and person. You have made this challenging experience for me an absolute pleasure. You have constantly supported me in my pursuit of becoming an educator of chemistry. I look forward to our professional relationship continuing and am excited to see how the research in your lab develops moving forward. This experience has been invaluable, and it has been an honor to learn from you and teach for you.

TABLE OF CONTENTS

LIST OF TABLES

LIST OF SCHEMES

LIST OF FIGURES

Abstract

The development of novel methods to install fluoroalkyl groups into organic molecules is highly desirable due to the effects that fluorine atoms impart, such as metabolic stability and lipophilicity. Due to the commercial availability of fluorocarboxylic acid derivatives ($R_FC(O)X$), we aimed to utilize these reagents and their derivatives in decarbonylative fluoroalkylative cross-coupling reactions. This works builds on literature examples of related decarbonylative reactions that form C–C bonds.

Chapter 1 briefly introduces transition-metal catalyzed decarbonylative cross-coupling reactions and delineates the goal of this thesis, which is to use fluorocarboxylic acid derivatives to incorporate fluoroalkyl groups into molecules via decarbonylative coupling. The key considerations for reaction development (metal, ligand, $R_FC(O)X$ electrophile, aryl nucleophile) are discussed.

Chapter 2 describes the development of a decarbonylative Pd-catalyzed aryl–difluoromethylation reaction that couples difluoroacetylfluoride (DFAF) with aryl boronate esters. This reaction was developed by interrogating the elementary steps of the catalytic cycle (oxidative addition, carbonyl de-insertion, transmetalation, and reductive elimination) to identify a pair of compatible coupling partners and a suitable Pd catalyst system, (SPhos)Pd^0. Additionally, computational analysis established the presence of a stabilizing F_2C–H---X electrostatic interaction that contributes to accelerating the key carbonyl de-insertion step of this transformation.

Chapter 3 begins with the development of a decarbonylative C–H difluoromethylation reaction of azoles catalyzed by (XantPhos)Pd^0. Stoichiometric syntheses revealed an unusual geometry of the putative catalytic intermediate, (XantPhos)Pd(CHF_2)($OCOCHF_2$), which likely plays a role in the unique efficacy of Xantphos compared to other phosphine ligands for this reaction. Chapter 3 also details a systematic approach to building in complexity into the carboxylic acid coupling partner towards the ultimate goal of developing decarbonylative cross-coupling

reactions of chiral acid derivatives. In this context, a $(AdBu_2P)Pd^0$-catalyzed difluorobenzylation is developed that is effective for a range of aryl organometallics with varying electronic properties.

Chapter 4 details parallel investigations into the development of a Ni-catalyzed decarbonylative difluoromethylation reaction that couples DFAF with tributyl(aryl)stannanes. Thees studies reveal that tBuPPF is the optimal ligand for $Ni^{0/II}$ catalysis and that the Ni-catalyzed reaction exhibits a complementary substrate scope to the $(SPhos)Pd^0$ one described in Chapter 2. Organometallic synthesis of model complexes was conducted and a catalytically-relevant $Ni(CHF_2)(F)$ complex was characterized by X-ray crystallography. These complexes will be used to elucidate the origins of the selectivity and electronic trends observed in our catalytic decarbonylative fluoroalkylation reactions.

Chapter 5 shifts away from decarbonylative cross-coupling reactions and details the development of an organic chemistry 2 lab module for the CH216 course at the University of Michigan. The protocol was translated from a literature report that utilized deoxyfluorination of a carboxylic acid to access amide products. This project will be continued in a second FFGSI project with focus on developing an argument-based post-lab assignment to help students gain mechanistic insight from the experiment.

.

Chapter 1 – Introduction

Decarbonylative cross-coupling reactions between carboxylic acid-derived electrophiles and a diverse variety of nucleophiles have recently emerged as an attractive strategy for C–C and C–heteroatom bond formation.[1a] In comparison to more traditional and widely studied cross-coupling reactions of aryl halide electrophiles[1b], this approach offers several key advantages. First, carboxylic acids are abundant[1] and can be used to generate a variety of carboxylic acid-derived electrophiles (RCOY), including amides, acid halides, esters, and anhydrides.[1] Second, the tunability of the RCOY electrophiles enables control over the ligands at the transition metal center and thus the barriers of each of the elementary steps of the catalytic cycle. Third, oxidative addition, a step that is often slow in reactions of aryl halides, is often facile for reactive carboxylic acid derivatives like acid halides and anhydrides.[2] Fourth, decarbonylative cross-coupling reactions can be tuned by modulating metal, ligand, acyl electrophile, and organometallic nucleophile to achieve an extremely broad range of bond-forming reactions via a common mechanistic manifold.

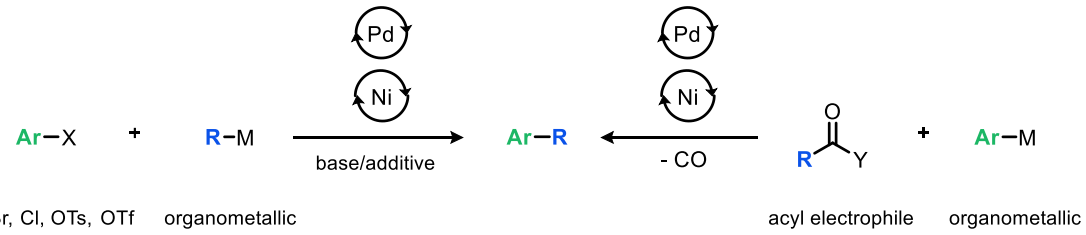

Scheme 1.1. Traditional cross-coupling of aryl (pseudo)halides and decarbonylative cross-coupling of acyl electrophiles.

Transition metals have been known to undergo oxidative addition into C(acyl)–Y bonds since the mid 1900's. The Tsuji decarbonylation reaction is a known system for the conversion of aldehydes to alkanes using Wilkinson's catalyst (Scheme 1.2).[4]

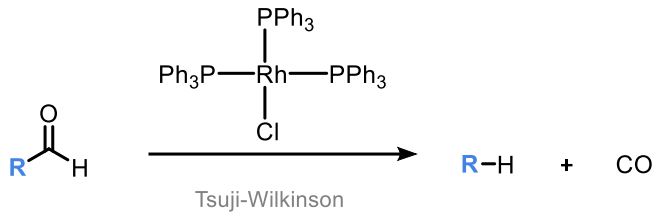

Scheme 1.2. Tsuji-Wilkinson decarbonylation of aldehydes.[4]

Since these early investigations, the development of decarbonylative transformations has seen the extensive use of Ni and Pd catalysts for the activation of novel electrophiles and for challenging bond formations.[1,3] The work in this thesis focuses on optimization of the identity of the metal (Ni or Pd), ligand, and the coupling partners of the reaction to achieve high yield and selectivity for a targeted decarbonylative couplings, with a focus on fluoroalkylation reactions. Further, we demonstrate that identification, isolation, and characterization of catalytically-relevant intermediates and model complexes can be effective for studying the mechanisms and decomposition pathways within the various catalytic process. We expect these studies to engender interest in the novel decarbonylative processes of acyl electrophiles that are available at Ni and Pd catalysts.

1.1 Catalytic Cycle of Decarbonylative Cross-Coupling Reactions

A general catalytic cycle for cross-coupling reactions of RC(O)Y electrophiles via group 10 metals is shown in Scheme 1.3. The first step (*i*) involves oxidative addition of the C-Y bond at the M^0 catalyst to generate a [M^{II}]-acyl intermediate **I**. Carbonyl de-insertion then proceeds to release CO along with [M^{II}]–R (**II**, step *ii*). An intermolecular cross-coupling reaction is then possible via the addition of an appropriate organometallic nucleophiles to promote transmetalation to form **III**. Finally, complex **III** can undergo reductive elimination to yield the cross-coupled product.

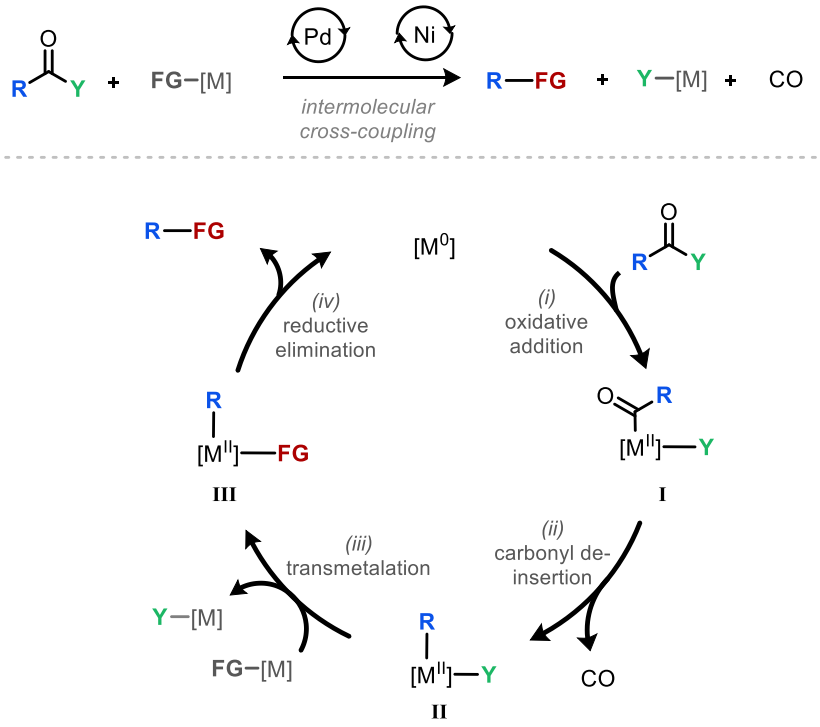

Scheme 1.3. Proposed catalytic cycle for decarbonylative cross-coupling reactions of acid derivatives.

1.2 Reaction Parameters and General Trends

In the development of our decarbonylative coupling reactions, we iteratively optimize the identity of metal, ligand, and electrophile with respect to the hypothesized rate-determining step of the desired transformation. Some key considerations for each of these reaction components are discussed below.

Selection of metal catalyst. Although the majority of aryl halide cross-coupling reactions utilize palladium as the catalyst, reactions involving RC(O)Y electrophiles have seen extensive development with both palladium and nickel-based catalysts (as well as, to a lesser extent, other transition metals).[1a] Nickel is more electropositive (1.91) than palladium (2.20), and this property appears to facilitate oxidative addition reactions of acyl electrophiles. As such, the use of Ni^0-based catalysts in decarbonylative coupling reactions often leads to fast oxidative addition, even

with weakly electrophilic coupling partners like esters and amides. In contrast, Pd^0 catalysts are often inert towards oxidative addition of these weakly electrophilic carboxylic acid derivatives. However, $Pd^{II}(R)(X)$ intermediates (where X = a heteroatom such as nitrogen, oxygen, or halogen) are generally much more reactive towards C–X bond forming reductive elimination than their Ni^{II} analogues. Thus, depending on the energetic demands of the catalytic process and the hypothesized rate-determining step, either Pd or Ni could be the most suitable choice.

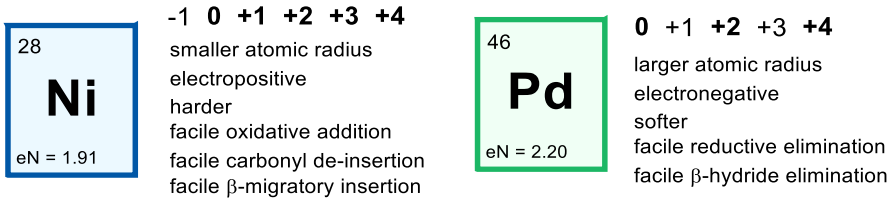

Figure 1.1. Description of central reactivity profiles for Ni and Pd transition metals. Adapted from ref 2.

Furthermore, as an electropositive first-row transition metal, Ni interacts favorably with CO to form stable $Ni(CO)_n$ complexes.[2] Accordingly, a strong thermodynamic driving force exists for carbonyl deinsertion at Ni–(C(O)R) complexes to form (CO)Ni–R complexes (assuming R and the supporting ligand are competent for carbonyl deinsertion). Also, ligand substitution is generally easier at Ni. Since carbonyl de-insertion generally requires an open site for coordination, this likely contributes to the faster rate for carbonyl de-insertion at Ni compared to at Pd.[2] As such, for reactions in which carbonyl de-insertion is posited as the rate-determining step, Ni is often selected as a precatalyst rather than Pd. However, due to their stability, $Ni(CO)_mL_n$ complexes have been observed as catalyst sinks in various catalytic processes involving carbon monoxide and nickel catalysts. For this reason, the use of nickel in decarbonylative processes often requires high reaction temperatures to liberate CO from Ni.

Selection of ligand. Early work in Pd-catalyzed cross-coupling reactions typically used simple phosphine ligands, such as PPh_3. Efforts over the past several decades have led to the development of designer phosphine ligands to meet the demands of challenging bond breaking and forming processes. For instance, it is now well-established that sterically large and electron-rich ligands, such as bulky trialkylphoshines or N-heterocyclic carbenes, promote oxidative addition into

relatively inert chemical bonds via L_1Pd^0 intermediates. Electron-withdrawing and sterically encumbering ligands can enhance the rate of reductive elimination. Thus, an initial choice of ligand (denticity, basicity, acidity, etc…) may be informed by the posited rate-determining step.

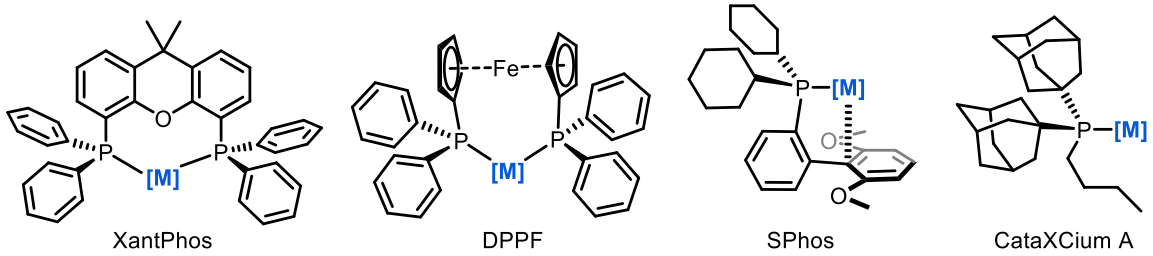

Figure 1.2. Sample of metal-ligand complexes that are reported herein.

Selection of RC(O)Y electrophile. For decarbonylative coupling processes, the choice of R and Y must be selected with respect to metal/ligand. To form cross-coupled products from RC(O)Y electrophiles via a decarbonylative process requires that: (1) the electrophile is sufficiently reactive to undergo oxidative addition with the catalyst to form **I** (Scheme 1.3), (2) that the R group of RC(O)Y can undergo carbonyl deinsertion at either Ni or Pd to form **II** (Scheme 1.3) and (3) that the metal–Y intermediate **II** is active for transmetalation with an organometallic, and (4) that the catalyst is competent (and selective) for the desired bond formation. Regarding the first requirement, highly reactive acyl electrophiles such as acid chlorides or anhydrides are sufficiently electropositive to undergo facile oxidative addition at Pd. For electrophiles that are less reactive, including esters, amides, and acid fluorides, Pd may not be effective for oxidative addition, and nickel may be a more appropriate choice. Furthermore, the identity of R has a strong impact on the rate of carbonyl-deinsertion, with larger and less electronegative R groups undergoing slower de-insertion.[5] With regard to the transmetalation-activity of complex **II**, we optimize the identity of RCOY and the organometallic reagent to achieve high selectivity for the desired decarbonylative process.

Selection of Ar–M organometallic. The selection of an organometallic nucleophile must be selected based on the desired rate of transmetalation, assuming the compatibility of the electrophile

and nucleophile. As described in this Thesis, the optimization of the organometallic reagent is often informed by the reactivity of the electrophile such that background decomposition is minimized. Assuming compatibility, the selected organometallic must also selectively transmetalate with intermediate **II** in Scheme 1.3, rather than intermediate **I**. In this Thesis we utilize the varying reactivity between Zn-, Sn-, and B-based organometallics to promote selectivity in our fluoroalkylation reactions.

At present, few examples for decarbonylative fluoroalkyl have been reported.[6,7,8] A seminal report[6] on this challenging process was reported by Shoenebeck and co-workers in 2018 (Scheme 1.4). They successfully develop a Pd-catalyzed decarbonylative aryl trifluoromethylation reaction using aroyl fluorides and $TESCF_3$ as a nucleophile source of the $–CF_3$ group. This reaction indeed demonstrates that decarbonylative fluoroalkylation is possible at Pd.

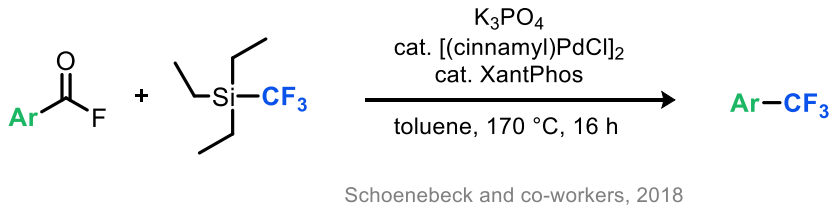

Scheme 1.4. Decarbonylative aryl trifluoromethylation by Schoenebeck and co-workers.[6]

However, in contrast to the reaction reported by Schoenebeck and co-workers (Scheme 1.4), we were motivated to utilize fluorocarboxylic acid derivatives as electrophiles, given their commercial availability, ease of handling, and native electrophilicity.[9] To our best knowledge, the only known reactions of this type are an early report from our lab[7] that demonstrated the feasibility of the stoichiometric decarbonylation and cross-coupling of trifluoroacetic anhydride (TFAAn) to form trifluoromethylarene products. However, all attempts to translate this stoichiometric process into a catalytic reaction led to the competitive decomposition of TFAAn into trifluoromethyl ketone by-products due to a rapid, uncatalyzed background reaction. As such, we determined that the compatibility of the fluorocarboxylic acid derivative and organometallic reagent is a critical feature for the development of catalytic decarbonylative fluoroalkylation reactions.

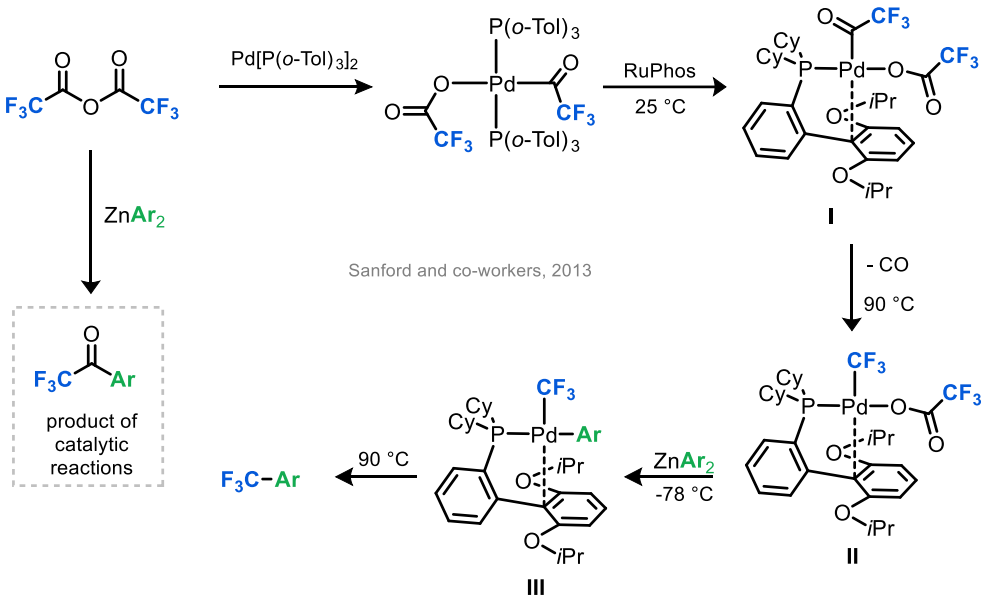

Scheme 1.5. Stoichiometric decarbonylative trifluoromethylation of arenes at a (RuPhos)Pd complex.[7]

Informed by these previous studies[6,7], this Thesis described the development of a Pd-catalyzed catalyzed difluoromethylation reaction of aryl boronate esters using difluoroacetyllfluoride (DFAF) as the electrophile (Chapter 2).[8] In Chapter 3 demonstrates that feasibility of Pd-catalyzed decarbonylative difluoromethylation via C–H activation strategies as well as the development of a Pd-catalyzed decarbonylative difluorobenzylation reaction. We then demonstrate the feasibility of Ni-catalyzed decarbonylative difluoromethylation of aryl tin nucleophile and synthesize model Ni complexes to study trends in transmetalation (Chapter 4). Finally, in Chapter 5 we describe the development of a novel amide-bond forming lab module for a large-enrollment organic chemistry 2 lab course at the University of Michigan.

1.3 References

1. (a) Guo, L.; Reuping, M. Transition-metal-catalyzed decarbonylative coupling reactions: concepts, classifications, and applications. *Chem. Eur. J.* **2018**, *24*, 7794–7809..(b) Gooßen, L. J,; Gooßen, K.; Rodríguez, N.; Blanchot, M.; Linder, C.; Zimmermann, B. New catalytic transformations of carboxylic acids. *Pure Appl. Chem.*, **2008**, *80*, 1725–1733. (c) Liu, C.; Szostak, M. Decarbonylative cross-coupling of amides. *Org. Biomol. Chem*., **2018**, *16*, 7998-8010. (d) Guo, L.; Reuping, M.; Decarbonylative cross-coupling: nickel catalyzed functional group interconversion strategies construction of complex organic molecules. *Acc. Chem. Res*. **2018**, *51*, 1185 –1195.
2. Zhang, Y-F.; Shi, Z-J. Upgrading cross-coupling reactions for biaryl synthesis. *Acc. Chem. Res.* **2019**, *52*, 161–191.
3. Tasker, S. Z.; Standley, E. A.; Jamison, T. F. Recent advances in homogenous nickel catalysis. *Nature* **2014**, *509*, 299–309.
4. (a) Tsuji, K.; Ohno, K. Organic syntheses by means of noble metal compounds: XXXi. Carbonylation of olefins and decarbonylation of acyl halides and aldehydes. *Tet. Lett.* **1965,** *6*, 3969–3971. (b) Ohno, K.; Tsuji, J. Organic synthesis by means of noble metal compounds. XXXV. Novel decarbonylation reactions of aldehydes and acyl haldies using rhodium complexes. *J. Am. Chem. Soc.* **1968**, *90*, 99−107.
5. For relative rates in carbonylation reactions, see: (a) Shusterman, A. J.; Tamir, I.; Pross, A. The mechanism of organometallic migration reactions. A configuration mixing approach. *J. Organomet. Chem.* **1988**, *340*, 203−222. (b) Ortuno, M. A.; Dereli, B.; Cramer, C. J. Mechanism of Pd-catalyzed decarbonylation of biomass-derived hydrocinnamic acid to styrene following activation as an anhydride. *Inorg. Chem*. **2016**, *55*, 4124−4131.
6. Keaveney, S. T.; Schoenebeck, F. Palladium-catalyzed decarbonylative trifluoromethylation of acid fluorides. *Angew. Chem., Int. Ed***. 2018**, *57*, 4073−4077. X
7. Maleckis, A.; Sanford, M. S. Catalytic cycle for palladium-catalyzed decarbonylative trifluoromethylation using trifluoroacetic esters as the CF3 source. *Organometallics* **2014**, *33*, 2653−2660.

8. Lalloo, N.; Malapit, C. A.; Taimoory, S. M.; Brigham, C. E.; Sanford, M. S. Decarbonylative fluoroalkylation at palladium(II): from organometallic studies to catalysis. *J. Am. Chem. Soc.* **2021**, *143*, 18617–18625.
9. For reviews on carboxylic acids and their derivatives as electrophiles in cross-coupling: (a) Baudoin, O. New approaches for decarboxylative biaryl coupling. *Angew. Chem., Int. Ed.* **2007**, *46*, 1373−1375. (b) Gooßen, K.; Rodriguez, N.; Gooßen, L. J. Carboxylic acids as substrates in homogenous catalysis. *Angew. Chem., Int. Ed.* **2008**, *47*, 3100−3120. (c) Yu, D. G.; Li, B. J.; Shi, Z. J. Exploration of new C−O electrophiles in cross-coupling reactions. *Acc. Chem. Res.* **2010**, *43*, 1486−1495. (d) Rodriguez, N.; Gooßen, L. J. Decarboxylative coupling reactions: a modern strategy for C−C bond formation. *Chem. Soc. Rev.* **2011**, *40*, 5030−5048. (e) Cornella, J.; Larrosa, I. Decarboxylative carbon-carbon bond-forming transformations of (hetero)aromatic carboxylic acids. *Synthesis* **2012**, *44*, 653−656. (f) Hoover, J. M. Mechanistic aspects of copper-catalyzed decarboxylative coupling reactions of (hetero)aryl carboxylic acids. *Inorg. Chem.* **2017**, *37*, 169−200. (g) Takise, R.; Muto, K.; Yamaguchi, J. Cross-coupling of aromatic esters and amides. *Chem. Soc. Rev.* **2017**, 46, 5864−5888. (h) Guo, L.; Rueping, M. Decarbonylative cross-couplings: Nickel catalyzed functional group interconversion strategies for the construction of complex organic molecules. *Acc. Chem. Res.* **2018**, *51*, 1185−1195. (i) Meng, G.; Szostak, M. N-Acyl-glutarimides: Privileged scaffolds in amide N−C bond cross-coupling. *Eur. J. Org. Chem* **2018**, 2352−2365. (j) Zhao, Q.; Szostak, M. Redox-neutral decarbonylative cross-couplings coming of age. *Chem. Sus. Chem* **2019**, *12*, 2983−2987. (k) Blanchard, N.; Bizet, V. Acid fluorides in transition-metal catalysis: a good balance between stability and reactivity. *Angew. Chem., Int. Ed.* **2019**, *58*, 6814−6187. (l) Ogiwara, Y.; Sakai, N. Acyl fluorides in late transition-metal catalysis. *Angew. Chem., Int. Ed.* **2020**, *59*, 574−594. (m) Wang, Z.; Wang, X.; Nishihara, Y. Nickel or palladium-catalyzed decarbonylative transformations of carboxylic acid derivatives. *Chem. Asian J.* **2020**, *15*, 1234−1247. (n) Zheng, Y.-L.; Newman, S. G. Cross-coupling reactions with esters, aldehydes, and alcohols. *Chem. Commun.* **2021**, *57*, 2591−2604. (o) Fahandej-Sadi, A.; Lundgren, R. J. Copper-mediated synthesis of monofluoro aryl acetates via decarboxylative cross-

coupling. *Synlett* **2017**, *28*, 2886− 2890. (p) Moon, P. J.; Yin, S.; Lundgren, R. J. Ambient decarboxylative arylation of malonate half-esters via oxidative catalysis. *J. Am. Chem. Soc.* **2016**, *138*, 13826−13829.

Chapter 2 – Development of Decarbonylative Difluoromethylation of Aryl Boronate Esters

2.1 Introduction

Due to the prevalence of fluoroalkyl (R_F) substituents in bioactive molecules, there is a high demand for reagents and synthetic methods for the formation of (heteroaryl)aryl–R_F bonds.[1,2] The prevailing approach involves transition metal-catalyzed cross-coupling of aryl halide electrophiles (ArX) with fluoroalkyl nucleophiles (R_F–M) (Scheme 2.1, A).[3,4] Despite extensive work in this area, the scope and broad utility of these transformations remain limited, largely due to challenges associated with the fluoroalkyl nucleophiles.[4] The most common fluoroalkyl nucleophiles, R_3SiR_F, have limited availability for diverse R_F substituents, undergo sluggish transmetalation in the absence of bases, and exhibit poor stability in the presence of the basic additives required for transmetalation.[4,5] While some designer Ag and Zn-based fluoroalkyl nucleophiles have been developed to address these challenges, these reagents still have limitations with respect to synthetic accessibility and/or broad availability, particularly for diverse R_F groups.[4,6,7]

A. Traditional cross-coupling with fluoroalkyl nucleophiles

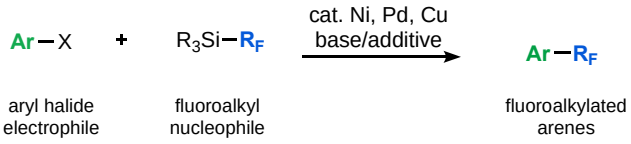

B. This work:
Decarbonylative fluoroalkylation with $R_FC(O)X$ electrophiles

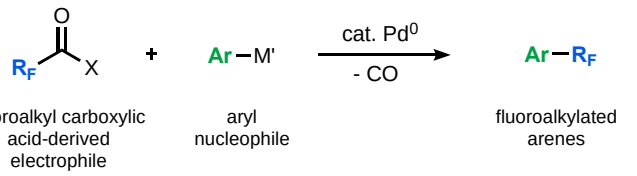

Scheme 2.1. (A) Traditional cross-coupling for fluoroalkylation and (B) decarbonylative fluoroalkylation with R_FCOX electrophiles.

A complementary cross-coupling approach to form (hetero)aryl–R_F bonds would involve the reaction of fluoroalkyl carboxylic acid-derived electrophiles ($R_FC(O)X$) with (hetero)aryl nucleophiles (Ar–M', Scheme 2.1, B).[8-13] This strategy eliminates the challenges associated with transmetalation from a weakly nucleophilic R_F reagent.[4,5] Furthermore, it leverages the abundance, low cost, and high stability of fluoroalkyl carboxylic acid derivatives.[13]

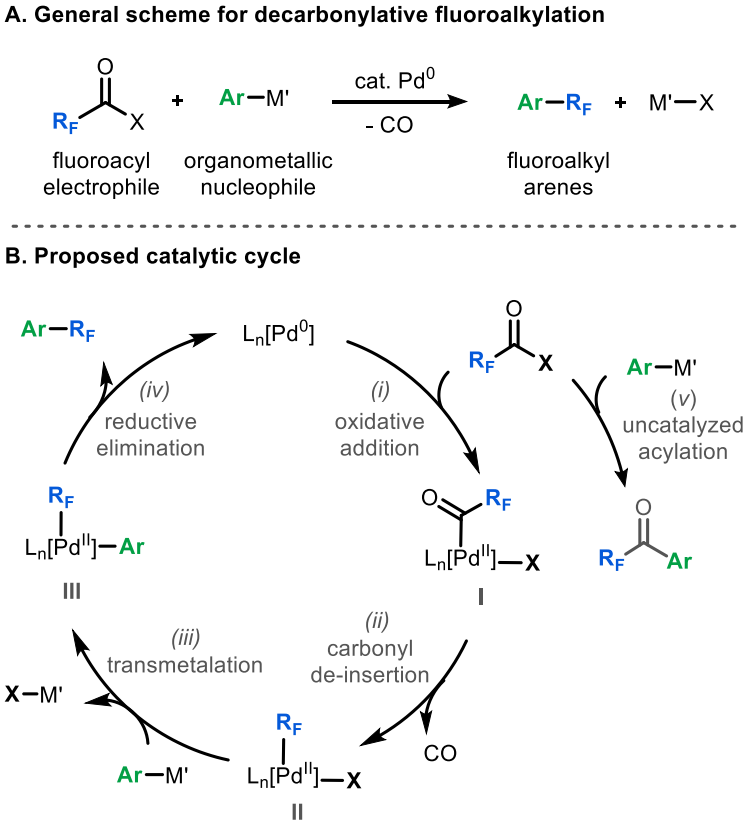

Scheme 2.2. (A) General reaction scheme for decarbonylative fluoroalkylation. (B) Proposed catalytic cycle with undesired acylation shown.

A putative catalytic cycle for this transformation is shown in Scheme 2.2, B and involves (*i*) oxidative addition of $R_FC(O)X$ to form [M]–acyl complex **I**, (*ii*) carbonyl de-insertion to generate [M]–R_F intermediate **II**, (*iii*) transmetalation of the aryl nucleophile (Ar–M') to form complex **III**, and (*iv*) aryl–R_F bond-forming reductive elimination to release the product. A

previous study from our group established the feasibility of each of these individual steps using trifluoroacetic anhydride and diphenyl zinc as the coupling partners, and Pd[P(*o*-Tol)$_3$]$_2$/RuPhos as [M] (Scheme 2.3).[13a] However, catalytic turnover was not viable in this system due to a rapid uncatalyzed background reaction between the reagents to form trifluoromethyl ketones (Scheme 2.2, B, uncatalyzed acylation, *v*).

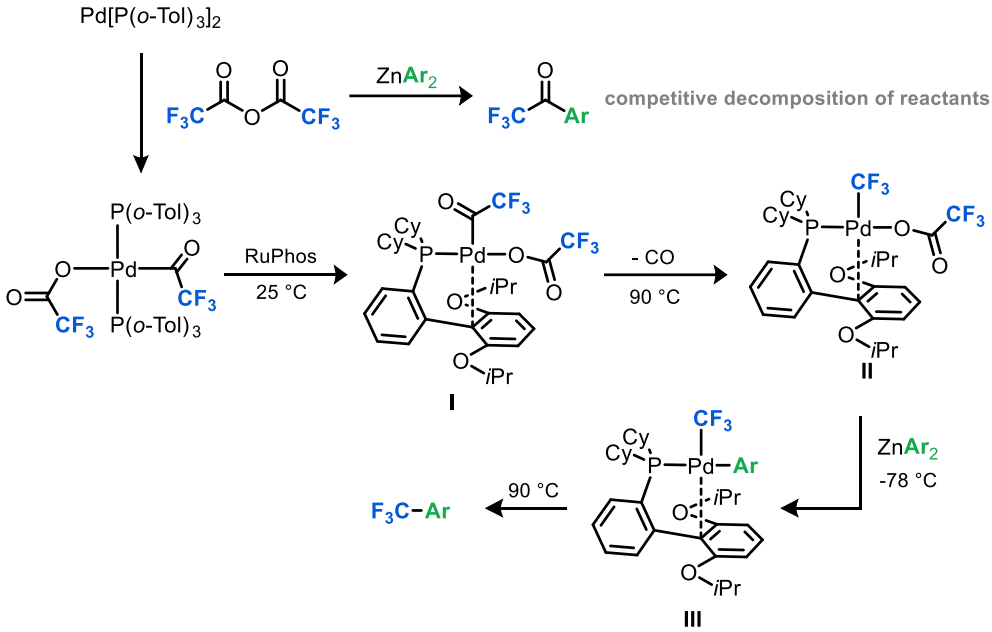

Scheme 2.3. Previous stoichiometric studies [ref 13a].

In addition to the competing background reaction, this previous work identified several other limitations associated with individual steps of the catalytic cycle.[13a] For instance, direct oxidative addition of trifluoroacetic anhydride at (RuPhos)Pd^0 (Scheme 2.2, step *i*) proved challenging. As such, a two-step sequence involving initial oxidative addition at Pd(P(o-Tol)$_3$)$_2$ followed by a separate ligand exchange between P(o-Tol)$_3$ and RuPhos was required. Furthermore, both carbonyl de-insertion (Scheme 2.2, step *ii*) and aryl–CF$_3$ bond-forming reductive elimination (step *iv*) were slow and/or low yielding. Finally, transmetalation (Scheme 2.2, step *iii*) was limited to strongly nucleophilic organometallic reagents like diphenyl zinc.[13a]

We hypothesized that these challenges could be addressed via a mechanistic-based redesign of the catalyst and coupling partners for this reaction. In this chapter, we initially identify fluoroalkyl anhydrides and aryl boronate esters as compatible R$_F$C(O)X and Ar–M' coupling

partners. We then use this pair to interrogate each step of the cycle in Scheme 2.2, B with (SPhos)Pd^0 as the catalyst. These stoichiometric organometallic studies provide key insights into the impact of R_F, X, and M' on each step, ultimately informing the development of a Pd-catalyzed method for the difluoromethylation of aryl boronate esters.

2.2 Identifying Compatible Coupling Partners

As discussed above, our group's previous attempts at Pd-catalyzed decarbonylative aryl fluoroalkylation (Scheme 2.3) were hampered by the uncatalyzed background addition of the diphenyl zinc nucleophile to the trifluoroacetic anhydride electrophile (TFAAn) to form phenyl trifluoromethyl ketone (**A**).[13a] This background reaction proceeds in 77% yield within 1 h at 25 ºC (Table 2.1, entry 1), as determined by ^{19}F NMR spectroscopic analysis. As such, initial studies focused on identifying more compatible coupling partners for the proposed catalytic transformation.

We hypothesized that aryl boron reagents, which are significantly less nucleophilic than their zinc counterparts,[13a,14,22e] would minimize ketone formation. Indeed, none of the ketone **A** was formed upon stirring a $CDCl_3$ solution of trifluoroacetic anhydride (TFAAn) with phenyl boronic acid over 1 h at 25 ºC. However, under these conditions a different undesired reaction, hydrolysis of the anhydride, proceeded to form trifluoroacetic acid (TFA, **B**) in quantitative yield (Table 2.1, entry 2). We next examined phenylboronic acid neopentylglycol ester (PhBneo) as the nucleophile, reasoning that it should minimize this hydrolysis process. Indeed, no detectable side product formation was observed upon stirring stirring a $CDCl_3$ solution of TFAAn with PhBneo over 1 or 3 h at 25 ºC (Table 2.1, entries 3 and 4). Compatibility was also observed when using phenylboronic acid pinacol ester (PhBpin) under otherwise identical conditions (entry 5). Furthermore, compatibility with PhBneo was maintained when moving to other fluoroalkyl anhydrides (e.g., difluoroacetic anhydride) was well as other fluoroalkyl carboxylic acid derivatives (e.g., difluoroacetyl fluoride). The ^{19}F and ^{13}C NMR spectra used to establish these compatibility data and identify the side products formed with each combination of reagents are presented in Figures 2.1-2.6, below.

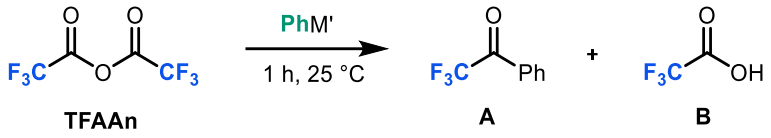

entry	PhM'	yield A	yield B
1	Ph_2Zn	77%	0%
2	$PhB(OH)_2$	<1%	>95%
3	PhBneo	<1%	<1%
4[a]	PhBneo	<1%	<1%
5	PhBpin	<1%	<1%

Table 2.1. Compatibility of TFAAn with different aryl nucleophiles. [a]25 ºC for 3 h.

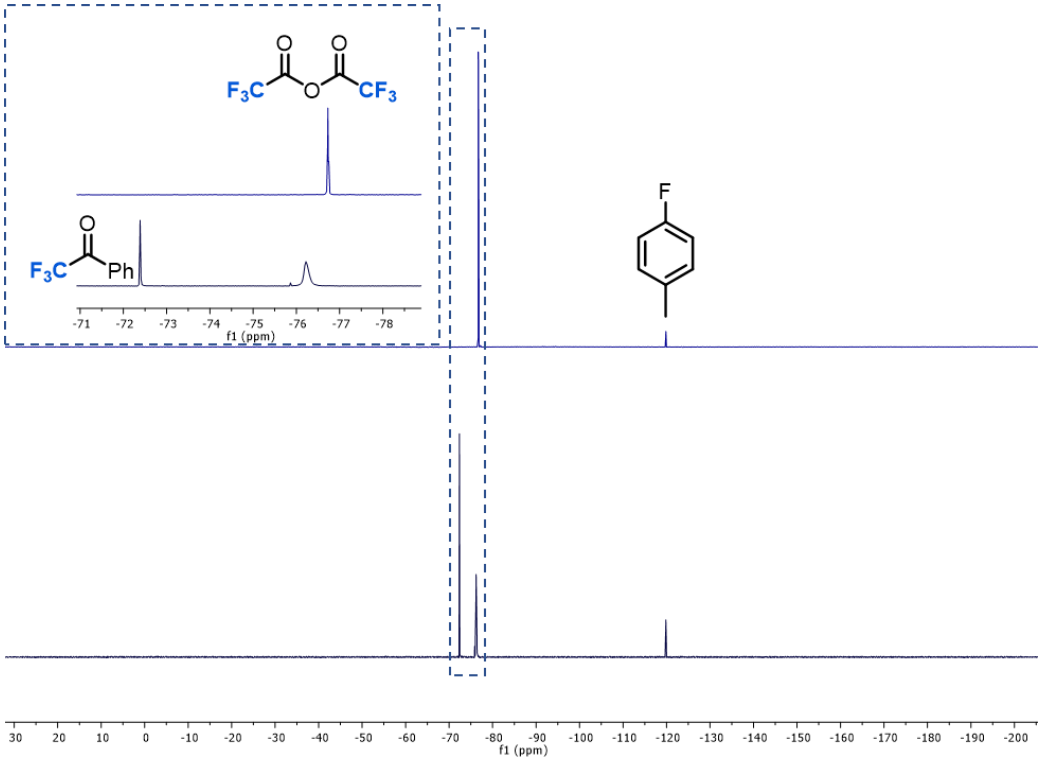

Figure 2.1 Incompatibility of Ph_2Zn with trifluoroacetic anhydride (TFAAn) in THF as shown by (top) ^{19}F NMR spectrum of TFAAn with 4-fluorotoluene internal standard, and (bottom) ^{19}F NMR

spectrum of reaction of TFAAn with diphenyl zinc after 1 h in THF showing formation of ketone **A**.

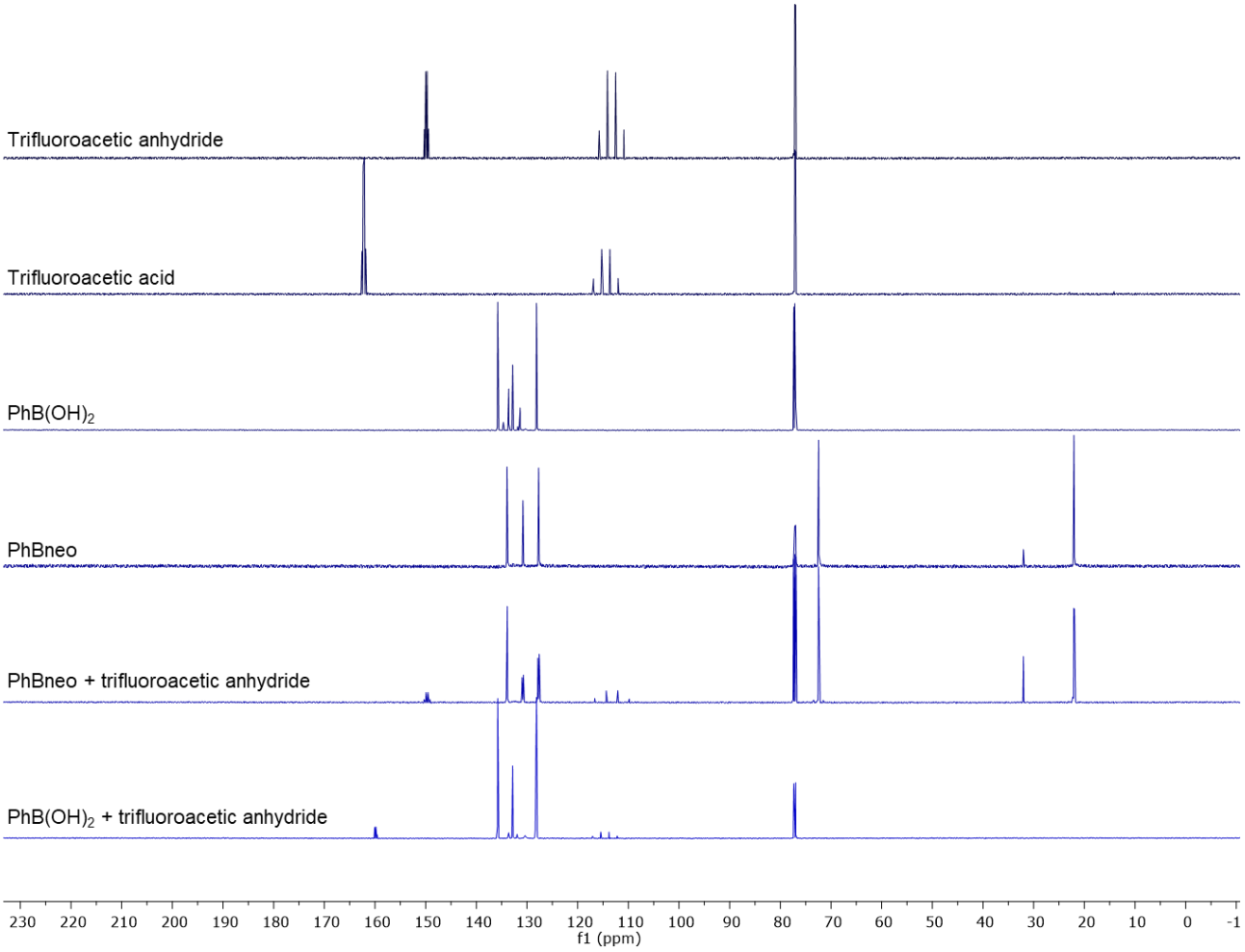

Figure 2.2. Compatibility experiments of organoboron nucleophiles with trifluoroacetic anhydride after 1 h at room temperature in $CDCl_3$ as shown by ^{13}C NMR spectroscopy.

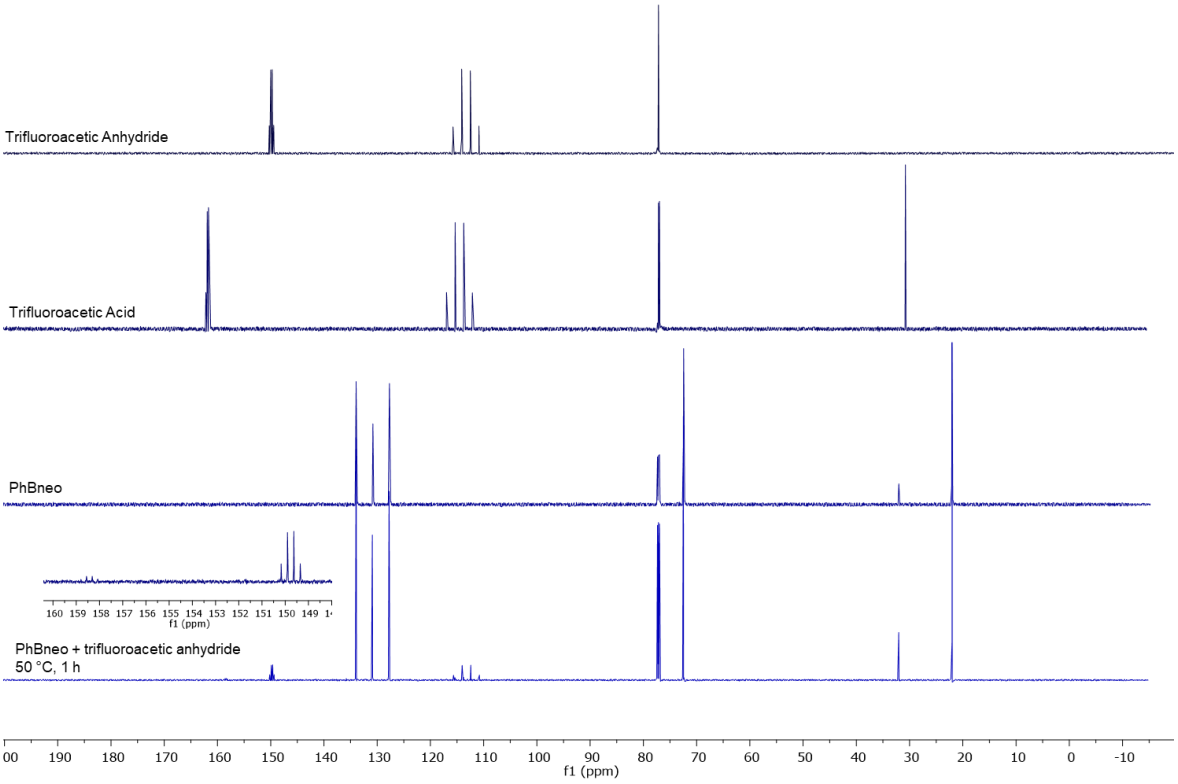

Figure 2.3. ^{13}C NMR spectrum showing minor amount of decomposition of trifluoroacetic anhydride to trifluoroacetic acid in the presence of phenylboronic acid neopentylglycol ester after 1 h at 50 °C in $CDCl_3$.

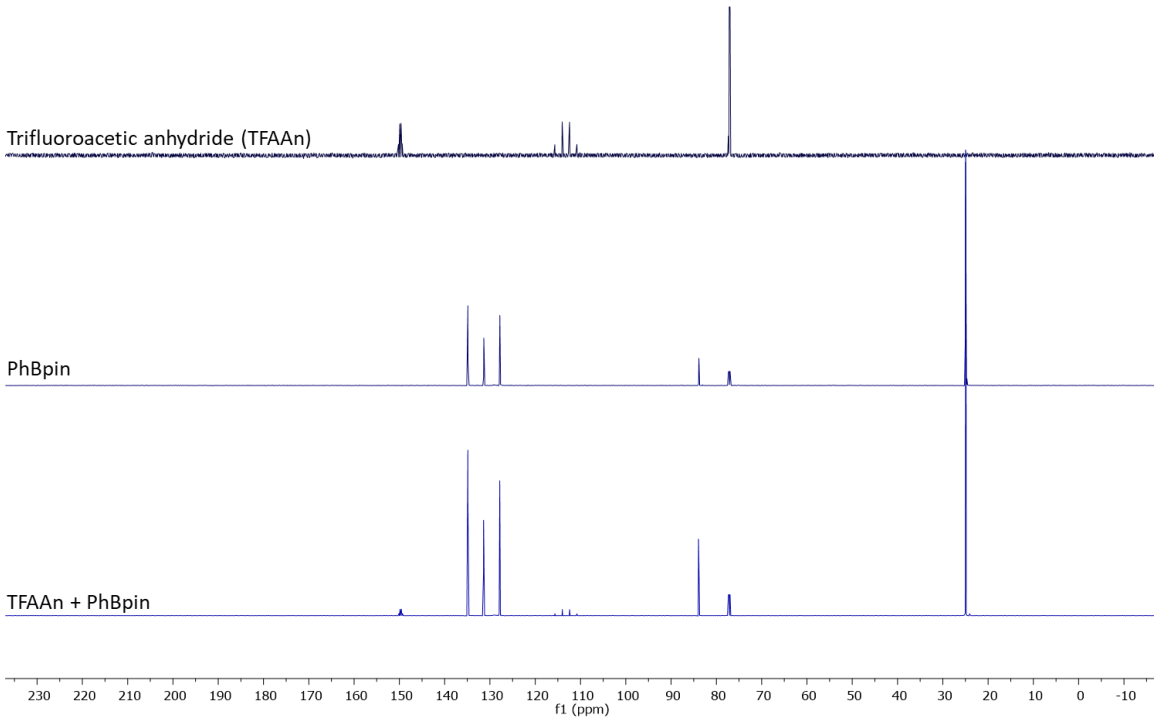

Figure 2.4. Compatibility of phenylboronic acid pinacol ester with trifluoroacetic anhydride after 1 h at room temperature in $CDCl_3$ as shown by ^{13}C NMR spectroscopy.

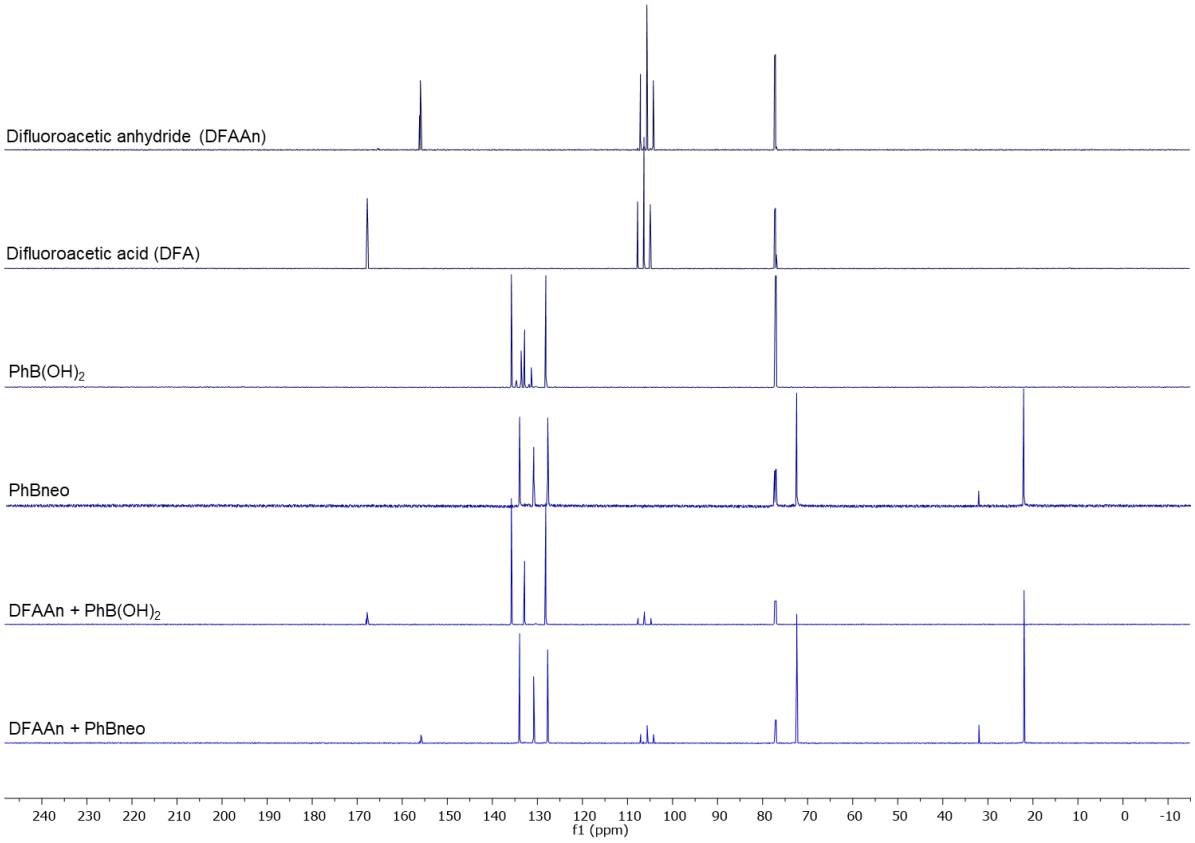

Figure 2.5. Compatibility experiments of organoboron nucleophiles with difluoroacetic anhydride after 1 h at room temperature in $CDCl_3$ as shown by ^{13}C NMR spectroscopy.

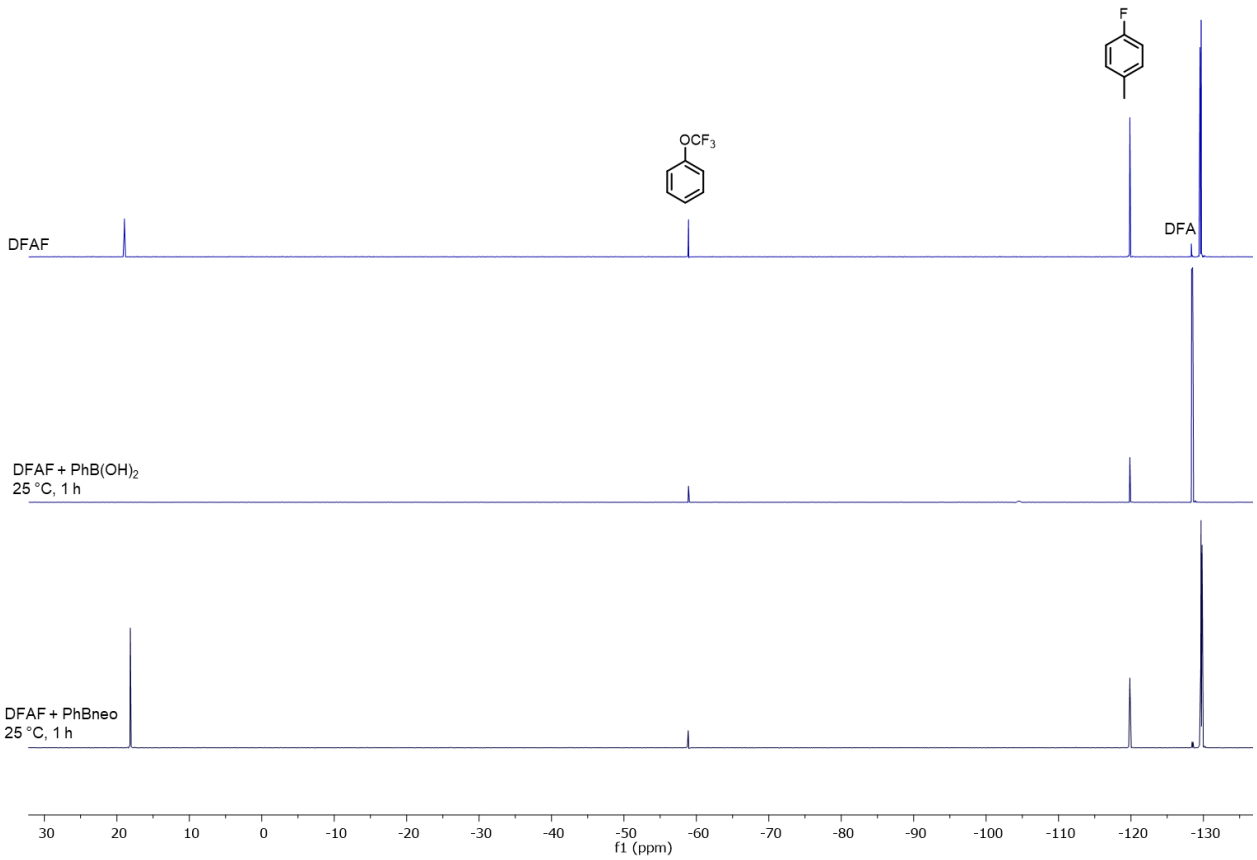

Figure 2.6. Compatibility experiments of organoboron nucleophiles with DFAF after 1 h at room temperature in THF as shown by ^{19}F NMR spectroscopy. NMR spectrum also contains trifluoromethoxybenzene and 4-fluorotoluene as internal standards. Referenced to 4-fluorotoluene as internal standard (-119.85 ppm).

2.3 Catalytic Cycle: Oxidative Addition and Carbonyl De-insertion

With a pair of compatible reagents in hand, we next focused on challenges associated with the individual steps of the catalytic cycle. As described above (Scheme 2.3), previous studies with RuPhos as the ligand accessed the TFAAn oxidative addition product in two discrete steps. First, $Pd(P(o\text{-}Tol)_3)_2$, was treated with TFAAn, and this was followed by a separate ligand exchange with RuPhos.[13a] We hypothesized that replacing the large isopropoxy-substituents of RuPhos with smaller methoxy groups (of SPhos) could accelerate oxidative addition and ligand substitution and

facilitate the single-pot formation of SPhos-ligated trifluoroacetyl intermediate **I-COCF$_3$** (Figure 2.7). Indeed, the reaction of a THF solution of Pd[P(o-Tol)$_3$]$_2$/SPhos with TFAAn yielded **I-COCF$_3$** in 98% yield within 15 min at 25 ºC (Figure 2.7). Complex **I-COCF$_3$** was characterized in situ by ^{19}F and ^{31}P NMR spectroscopy, and the data are in excellent agreement with those for the reported RuPhos analogue.[13a] In particular, this complex can be clearly identified as a trifluoroacyl Pd intermediate (rather than a Pd–CF$_3$ complex) based on the diagnostic chemical shift of the CF$_3$ group (approximately –75 ppm for Pd–C(O)**C**F$_3$ versus –12 ppm for Pd–**CF$_3$**).[3a,13a,14]

While Pd(P(o-Tol)$_3$)$_2$/SPhos proved highly reactive for oxidative addition of TFAAn at room temperature (Scheme 2.2, step *i*), carbonyl de-insertion (Scheme 2.2, step *ii*) at **I-COCF$_3$** remained slow in this system (Figure 2.7, A, B). After 4 h at 25 ºC, no change in the ^{19}F NMR spectrum was observed, and the decarbonylated intermediate, **II-CF$_3$**, was not detected (Figure 2.7, C). CO de-insertion was only observed upon heating the reaction. After 30 min at 90 ºC, **I-COCF$_3$** was nearly fully consumed with concomitant formation of **II-CF$_3$** in 91% yield (Figure 2.7, D). Complex **II-CF$_3$** was characterized in situ (by analogy to the RuPhos analogue) based on its distinct broad Pd–**CF$_3$** ^{19}F NMR resonance at -11.6 ppm. [3a,13a,14]

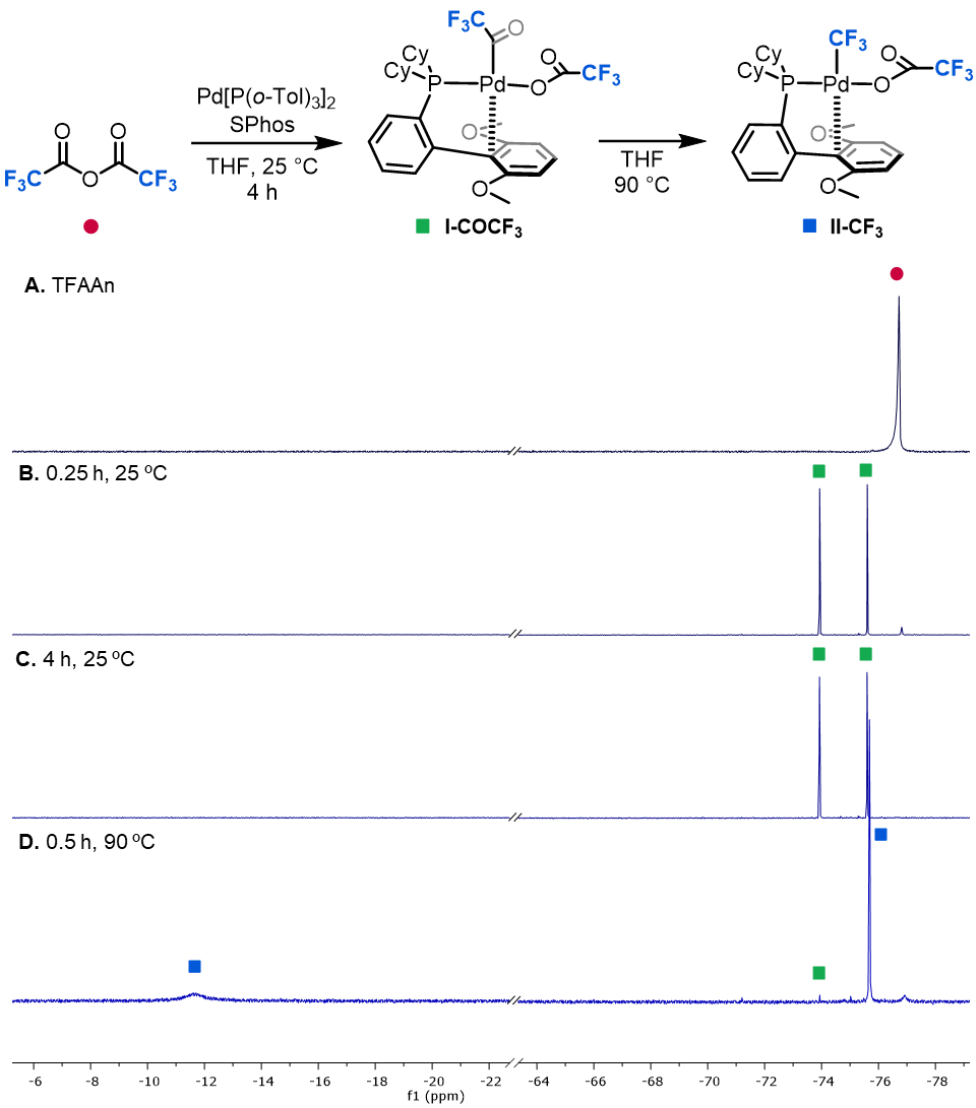

Figure 2.7. Oxidative addition and carbonyl de-insertion of TFAAn at SPhos/Pd^0 in THF. ^{19}F NMR spectra of (A) TFAAn (δ -76.73 (s, 6F)); (B) Reaction of TFAAn with SPhos/Pd^0 in THF after 0.25 h at room temperature forming **I-COCF$_3$** (δ -73.94 (s, 3F), -75.61 (s, 3F)). (C) Reaction of TFAAn with SPhos/Pd^0 in THF after 4 h at room temperature; (D) Reaction heated to 90 °C for 0.5 h forming **II-CF$_3$** (δ -11.60 (bs, 3F), -75.69 (s, 3F)). Spectra are referenced to 4-fluorotoluene (-119.85 ppm).

Similar reactivity to TFAAn was observed when using pentafluoropropionic anhydride (PFPAn) as the fluoroalkyl electrophile (Figures 2.7 and 2.8). The reaction of a THF solution of

Pd[P(o-Tol)$_3$]$_2$/SPhos with a slight excess of PFPAn (Figure 2.8, A, B) yielded **I-COCF$_2$CF$_3$** in >99% yield (characterized in situ by ^{19}F and ^{31}P NMR spectroscopy). Only after heating the reaction to 90 °C for 0.5 h was carbonyl de-insertion observed, forming complex **II-CF$_2$CF$_3$** in 98% yield (Figure 2.8, D). Again, the observation of fast oxidative addition and slow carbonyl de-insertion at room temperature with PFPAn is nearly identical to the reactivity of DFAAn.

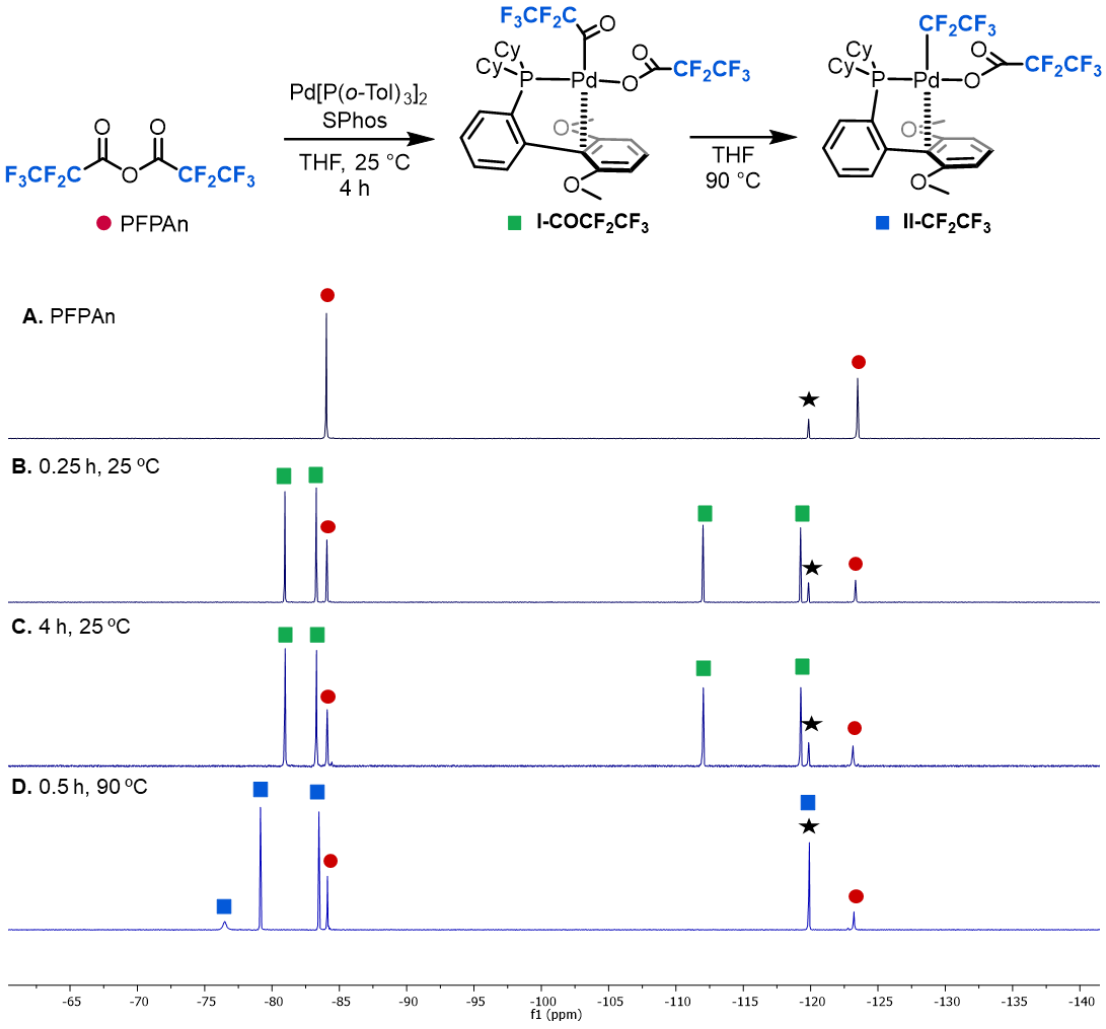

Figure 2.8. ^{19}F NMR spectra associated with oxidative addition and decarbonylation of pentafluoropropionic anhydride at Pd[P(*o*-Tol)$_3$]$_2$/SPhos in THF. (A) PFPAn; (B) 15 min, RT; (C) 4 h, RT; and (D) 0.5 h, 90 °C. Black star represents 4-fluorotoluene internal standard (-119.85 ppm).

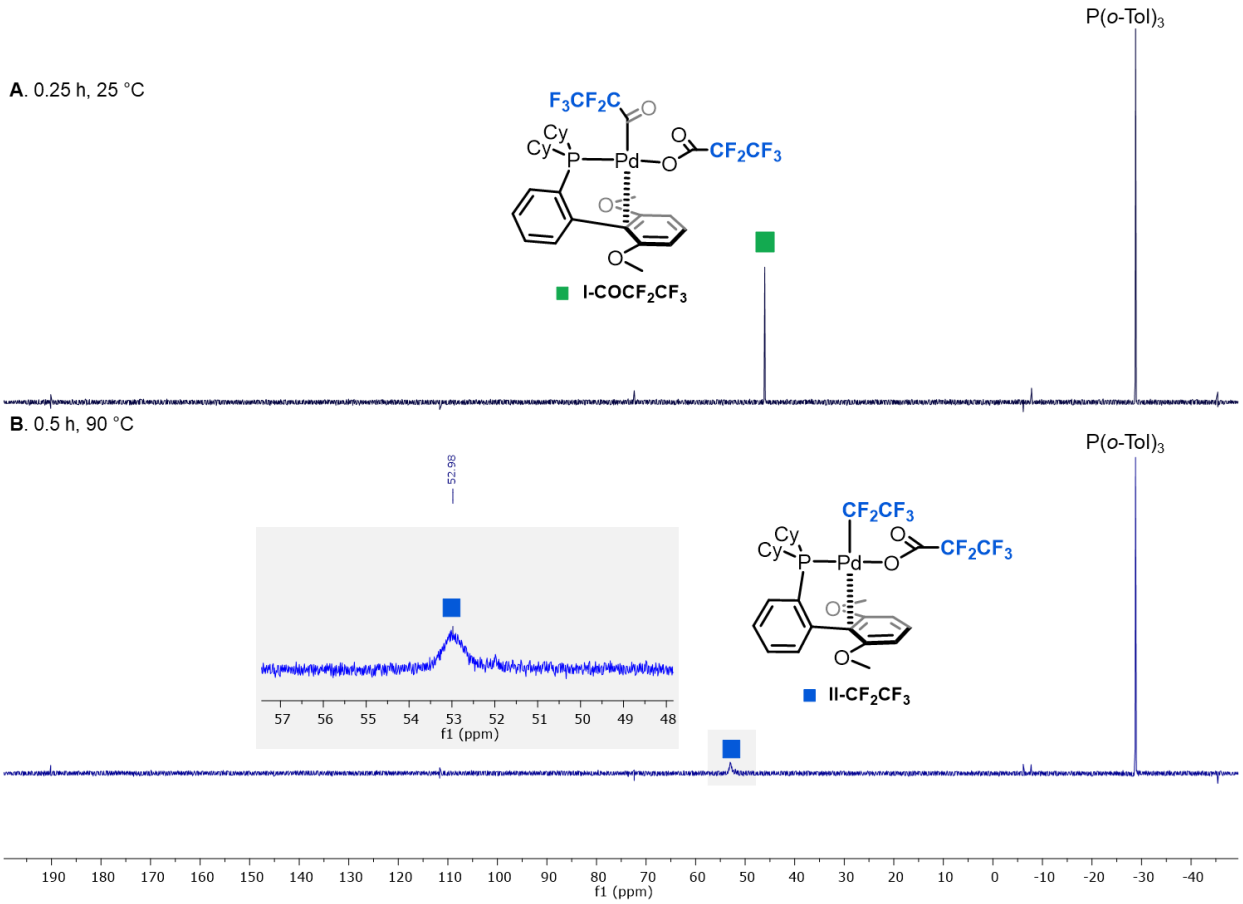

Figure 2.9. ^{31}P NMR spectra associated with oxidative addition and decarbonylation of pentafluoropropionic anhydride at Pd[P(*o*-Tol)$_3$]$_2$/SPhos in THF. (A) 0.25 h, RT; (B) 0.5 h, 90 °C.

We next explored the difluoromethyl analogue, in which a single fluorine atom is replaced by a hydrogen. This dramatically alters the size, nucleophilicity, dipole moment, and H-bond donor ability of the fluoroalkyl group,[2a-d] and all of these factors could potentially impact the carbonyl de-insertion step.[16] Furthermore, it is well-documented that Ar–CHF_2 bond-forming reductive elimination at Pd^{II} centers occurs under much milder conditions than analogous Ar–CF_3 or Ar–CF_2CF_3 couplings.[3,4,9a] As such, this modification should also facilitate the challenging elementary step (*iv*) of the catalytic cycle in Scheme 2.2.

The reaction of a THF solution of Pd[P(*o*-Tol)$_3$]$_2$/SPhos with 1 equiv of difluoroacetic anhydride (DFAAn, Figure 2.10) under otherwise identical conditions afforded >99% conversion of DFAAn within 15 min at room temperature. The oxidative addition product **I-COCHF$_2$** was

formed in 85% yield (Figure 2.10, B) and characterized *in situ* via ^{19}F NMR spectroscopy. This result demonstrates that oxidative addition remains fast in this system, despite the lower electrophilicity of DFAAn relative to that of TFAAn.

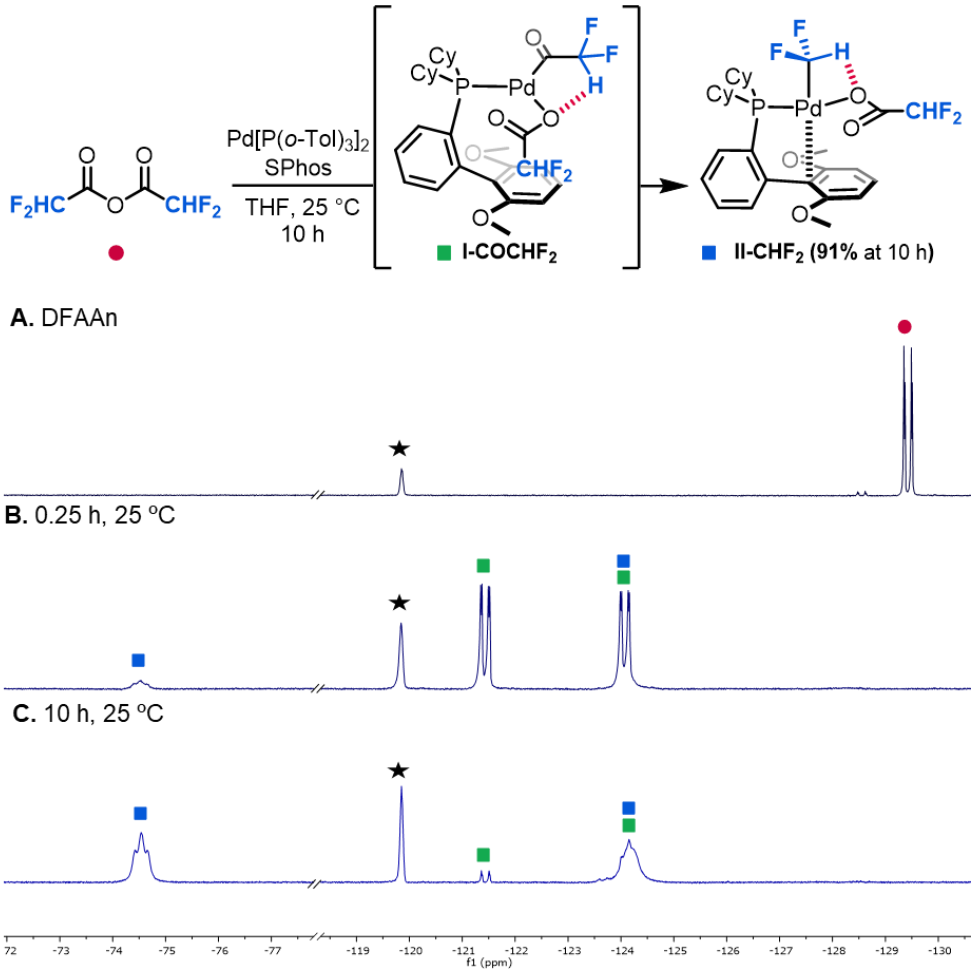

Figure 2.10. Oxidative addition and carbonyl de-insertion of DFAAn at SPhos/Pd^0 in THF. ^{19}F NMR spectrum of (A) DFAAn; (B) Reaction of DFAAn with SPhos/Pd^0 in THF after 15 min at room temperature; (C) Reaction of DFAAn with SPhos/Pd^0 in THF after 10 h at room temperature. Black star represents 4-fluorotoluene (-119.85 ppm, internal standard).

Interestingly, in marked contrast to the trifluoromethyl and pentafluoroethyl analogues, carbonyl de-insertion at **I-COCHF₂** proceeded at room temperature. **II-CHF₂** was formed in 13% yield after 0.25 h (Figure 2.10, B) and the reaction was nearly complete within 10 h at 25 ºC, affording **II-CHF₂** in 91% yield as determined by ^{19}F NMR spectroscopy (Figure 2.10, C)).

Notably, the unstirred reaction of a THF solution of Pd[P(*o*-Tol)$_3$]$_2$/SPhos in an NMR tube with slight excess of difluoroacetic anhydride under otherwise identical conditions afforded much slower carbonyl de-insertion. After 10 h, only 68% of **II-CHF$_2$** was formed (Figure 2.11). We believe this is possibly due to slow mass transport in the unstirred solution.

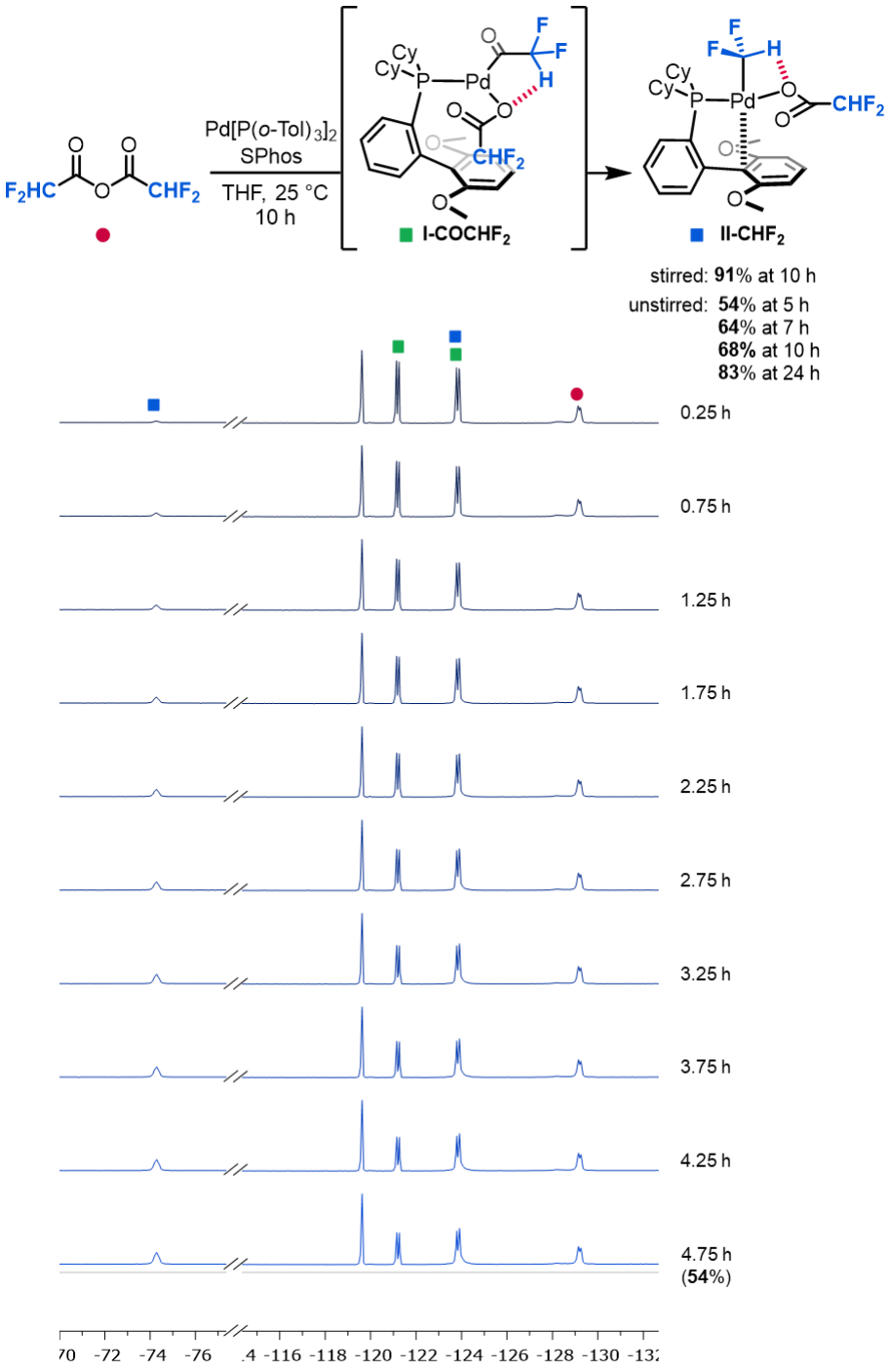

Figure 2.11. Kinetic study for the oxidative addition and carbonyl de-insertion of DFAAn at SPhos/Pd^0 in THF in an NMR tube, unstirred. The associated ^{19}F NMR spectrum are referenced 4-fluorotoluene (-119.85 ppm, internal standard).

Complex **II-CHF$_2$** was isolated in 61% yield and was structurally characterized by X-ray crystallography. An ORTEP diagram of **II-CHF$_2$**, along with representative bond distances and bond angles, are shown in Figure 2.12. A noteworthy feature of this structure is a short (2.38 Å) distance between H29 (from the CHF_2 group) and O3 (of the difluoroacetate ligand). A significantly longer distance (3.60 Å) is observed between H29 and O4. The short (2.38 Å) distance as well as the C29-H29-O3 angle of 96.9º are consistent with the existence of an attractive interaction between H29 and O3.[18]

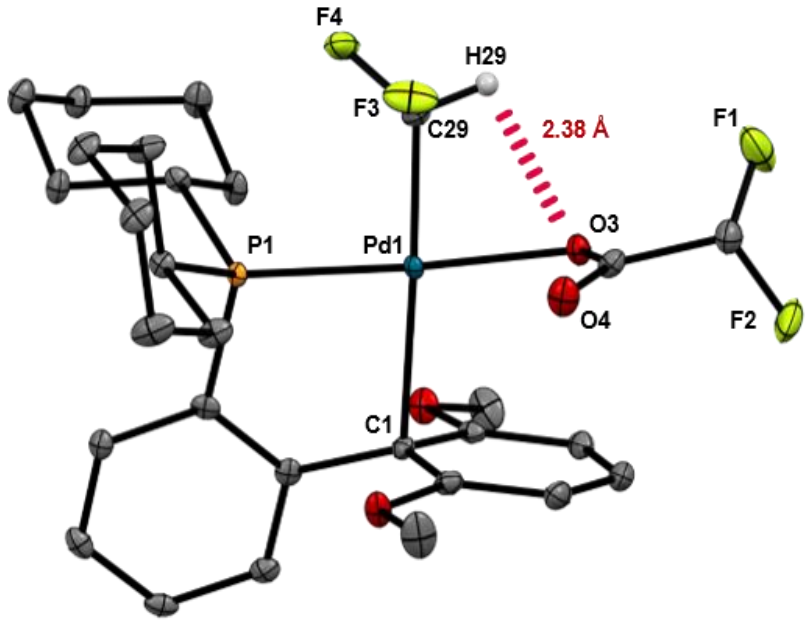

Figure 2.12. ORTEP diagram of **II-CHF$_2$**. Select hydrogen atoms are omitted for clarity. Selected bond lengths (Å) and angle (deg): O3–Pd1 2.11, O4–Pd1 3.09, C29–Pd1 1.99, C1–Pd1 2.46; H29---O3 2.38, H29---O4 3.60; C29–Pd1–O3 81.7, C29–H29---O3 96.9.

Density functional theory (DFT) calculations[18] (M06/ LANL2DZ/6-311G**) were performed by Dr. Nazanin Taimoory to interrogate the origin of the large rate enhancement for carbonyl de-insertion at **I-COCHF$_2$** relative to **I-COCF$_3$**. This difference is counter to commonly accepted trends, where the rate is typically inversely proportional to the nucleophilicity of the migrating R group.[16a] Figure 2.13 shows an energy profile for 1,1-CO de-insertion at **I-COR$_F$** proceeding through **TS1-R$_F$** to initially form CO-bound complex **(CO)Pd-R$_F$**. CO dissociation

then generates the experimentally observed product **II-R$_F$**. Consistent with the experimental observations, the calculations show a large (~16 kcal/mol) difference between the barrier for 1,1-de-insertion at **I-COCHF$_2$** versus **I-COCF$_3$**. In addition, the overall thermodynamics associated with conversion of **I-COCHF$_2$** to **II-CHF$_2$** + CO ($\Delta G = -18.4$ kcal/mol) is significantly more favorable than for the CF_3 analogue ($\Delta G = -3.2$ kcal/mol).

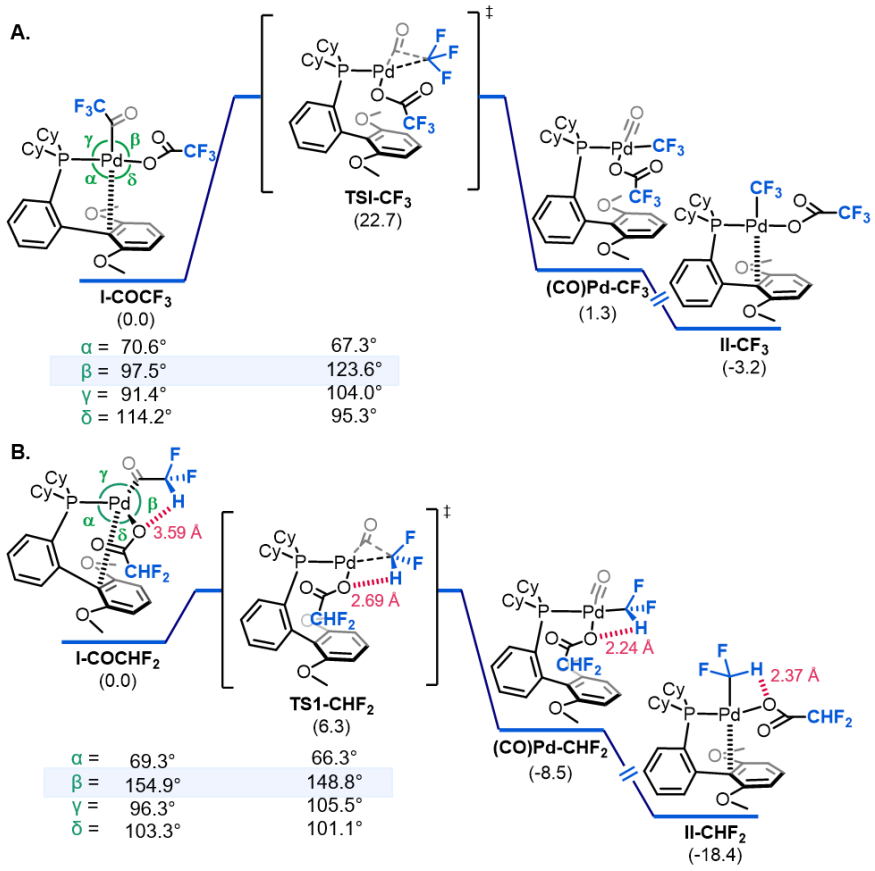

Figure 2.13. Energetics (the preferred binding mode highlighted as conformer A, see SI for details) for the carbonyl de-insertion process at (A) **I-COCF$_3$** and (B) **I-COCHF$_2$** with selected key angles α, β , γ, and δ for **I-COR$_F$** and **TS1-R$_F$**.

The computed structures in Figure 2.13 show the presence of an attractive interaction with electrostatic character between H29 (of the CHF_2 group) and O3 (of the carboxylate ligand). This interaction appears to contribute significantly to both the kinetic and thermodynamic preference for carbonyl deinsertion at the CHF_2 versus CF_3 analogue. In the ground state starting material, **I-**

COCHF₂, a weak H(δ+)−O(δ−) electrostatic contact (3.59 Å) contributes to a distortion of the coordination geometry at Pd away from square planar. For instance, the angle between the acyl and carboxylate ligands (β in Figure 4) is 97.5° in **I-COCF₃** (which cannot engage in this weak contact) versus 154.9° in **I-COCHF₂**. Given that carbonyl de-insertion transition states involve a three-coordinate metal center,[16b] this distortion makes the geometry of **I-COCHF₂** much closer to that of the transition state, **TS1-CHF₂** than in the CF3 analogue. The H−O bond distance becomes significantly shorter moving from **I-COCHF₂** (3.59 Å) to **TS1-CHF₂** (2.69 Å) to **II-CHF₂** (2.37 Å). Notably, the latter closely matches that observed experimentally in the X-ray crystal structure of **II-CHF₂** (2.38 Å). Further analysis of the electrostatic potential surfaces (EPSs) of **I-COCHF₂**, **TS1-CHF₂**, and **II-CHF₂** and of non-covalent interaction (NCI) maps of the **II-R$_F$** adducts reveals the stabilizing role of various attractive interactions.[18p–r] Specifically, orbital donor−acceptor interactions, electrostatic interactions, and a series of weakly attractive non-covalent bonds (dipole−induced dipole) were all observed in the -CHF_2-containing structures, most prominently in **TS1-CHF₂**. In contrast, the electrostatic potential surfaces of the CF_3-analogues show more diffuse dispersive repulsive interactions between the highly electronegative trifluoromethyl groups. These repulsive interactions are most pronounced in **TS1-CF₃**, providing further insights into the relatively high barrier to carbonyl de-insertion at **I-COCF₃**.

2.4 Catalytic Cycle: Transmetalation and Reductive Elimination

We next used complex **II-CHF₂** to interrogate the final two steps of the catalytic cycle: transmetalation and aryl–R_F bond-forming reductive elimination (Figure 2.14). With boronic acid **1a** as the nucleophile, 55% conversion of **II-CHF₂** was observed over 0.25 h at room temperature, with concomitant formation of the difluoromethylated organic product **1** in 40% yield. None of the Pd^{II}-aryl intermediate **III-CHF₂** was detected, indicating that Ar–CHF_2 bond-forming reductive elimination is facile at room temperature. In contrast, the boronate ester nucleophiles **1b** and **1c** showed low reactivity towards transmetalation with **II-CHF₂**. In both cases, >99% of **II-CHF₂** remained after 0.25 h at 25 ºC, and only traces of **1** were detected. These results indicate that transmetalation between the Pd^{II}–difluoroacetate intermediate **II-CHF₂** and aryl boronate esters is likely to be a key bottleneck in catalysis.

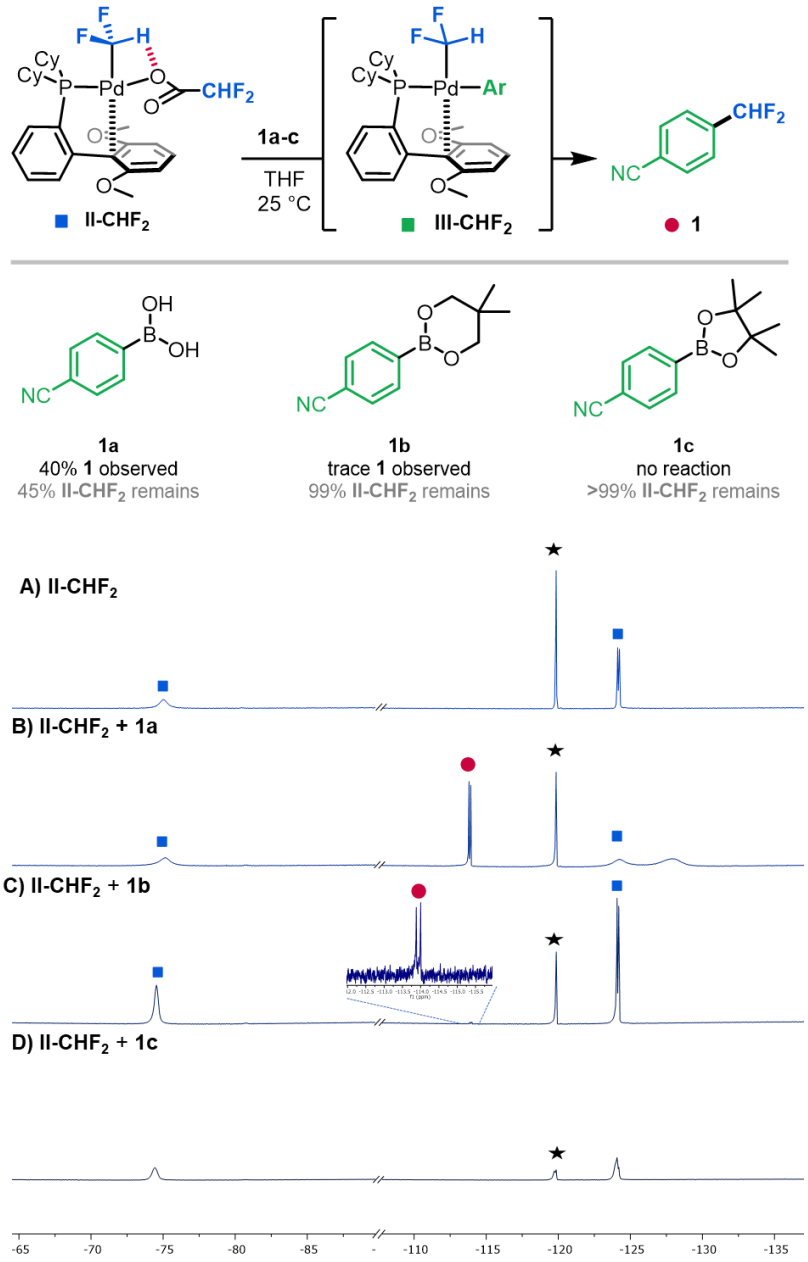

Figure 2.14. ^{19}F NMR spectra associated with transmetalation and reductive elimination sequence of **II-CHF$_2$** with (**B**) boronic acid **1a**, (**C**) boronic ester **1b**, and (**D**) boronic ester **1c.**

We hypothesized that this issue could be addressed by changing the X-type ligand on Pd^{II} from trifluoroacetate to a more reactive fluoride.[19,20] Previous work[20,21] has demonstrated that transition metal fluoride complexes exhibit high transmetalation activity towards various aryl boron nucleophiles. To generate a Pd^{II}–F intermediate, we treated a THF solution of **II-CHF$_2$** with anhydrous tetramethylammonium fluoride[13c] (Me_4NF) for 0.5 h at 25 ºC (Figure 2.15, B). This resulted in complete consumption of **II-CHF$_2$** and the appearance of a broad ^{19}F NMR resonance at –349.5 ppm, which is diagnostic for a metal-fluoride.[19] While this intermediate could not be isolated cleanly, the addition of boronate ester **1b** resulted in consumption of the Pd–F signal within 15 min at 25 ºC and formation of the reductive elimination product **1** in 27% yield (Figure 2.15, C). Again, the putative intermediate **III-CHF$_2$** was not detected. Overall, this sequence demonstrates that a fluoride ligand enables the targeted transmetalation/reductive elimination sequence with **1b**, thus closing the formal catalytic cycle in this system.

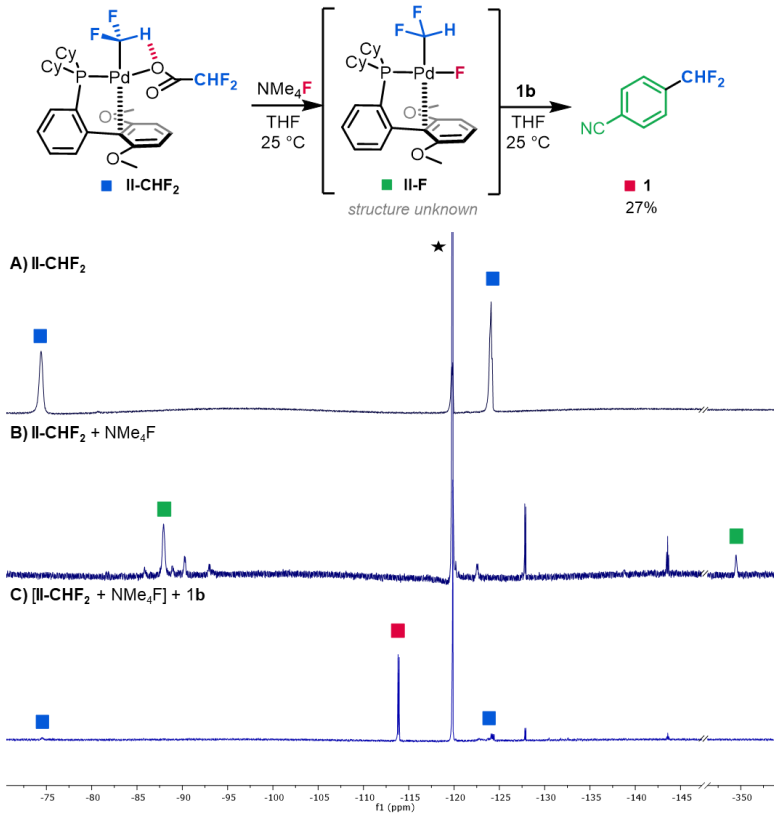

Figure 2.15 Generation of a Pd–F intermediate facilitates transmetalation with organoboron reagent **1b** and subsequent reductive elimination (steps *iii* and *iv* in Scheme 2.2).

2.5 Development of Catalytic Reaction

The organometallic studies described above demonstrate that each individual step of the catalytic cycle (Scheme 2.2) can proceed at room temperature. As such, our initial catalysis attempts focused on the room temperature SPhos/Pd[P(o-Tol)$_3$]$_2$-catalyzed decarbonylative coupling of DFAAn with boronate ester **1b** in the presence of metal fluoride (MF) sources. As summarized in Scheme 2.4, none of these reactions (with Me_4NF, Bu_4NF, or CsF) yielded the target difluoromethylated product **1**. However, in the crude ^{19}F NMR spectra of reactions that used CsF as the fluoride source, difluoroacetyl fluoride (DFAF) was observed as a major by-product.

We noted that acid fluorides are significantly less electrophilic than their anhydride counterparts[8j], which could result in slower oxidative addition. To address this potential issue, we next explored elevated temperatures (Scheme 2.4).

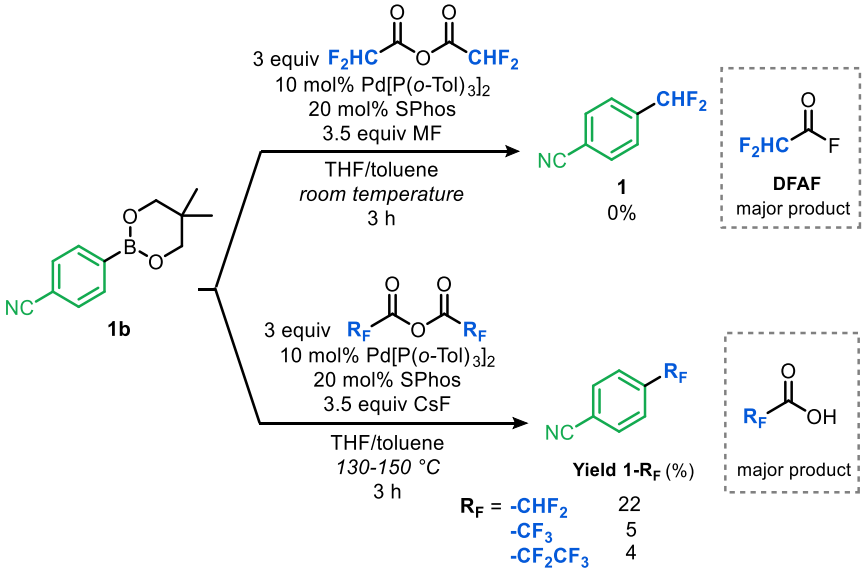

Scheme 2.4 Initial attempts at catalysis using DFAAn and fluoride salts.

Gratifyingly, at 130 ºC using excess CsF relative to DFAAn, the coupling product **1** was observed, albeit in modest (22%) yield (Scheme 2.4). The stoichiometric studies suggest that at 130 ºC carbonyl de-insertion should also be feasible for the -CF_3 and -CF_2CF_3 analogues as well.

As such, we explored the analogous catalytic reactions using TFAAn and PFPAn at 130 ºC. As shown in Figures 2.16 and 2.17, 4-trifluoromethylbenzonitrile and 4-pentafluoroethylbenzonitrile[5b] were formed in these transformations, in modest yields of 5% and 4%, respectively. In all three decarbonylative fluoroalkylation reactions a significant amount of the corresponding fluoroalkyl carboxylic acid was observed in the crude mixture, consistent with competing decomposition of the anhydrides with traces of water in the fluoride salts.

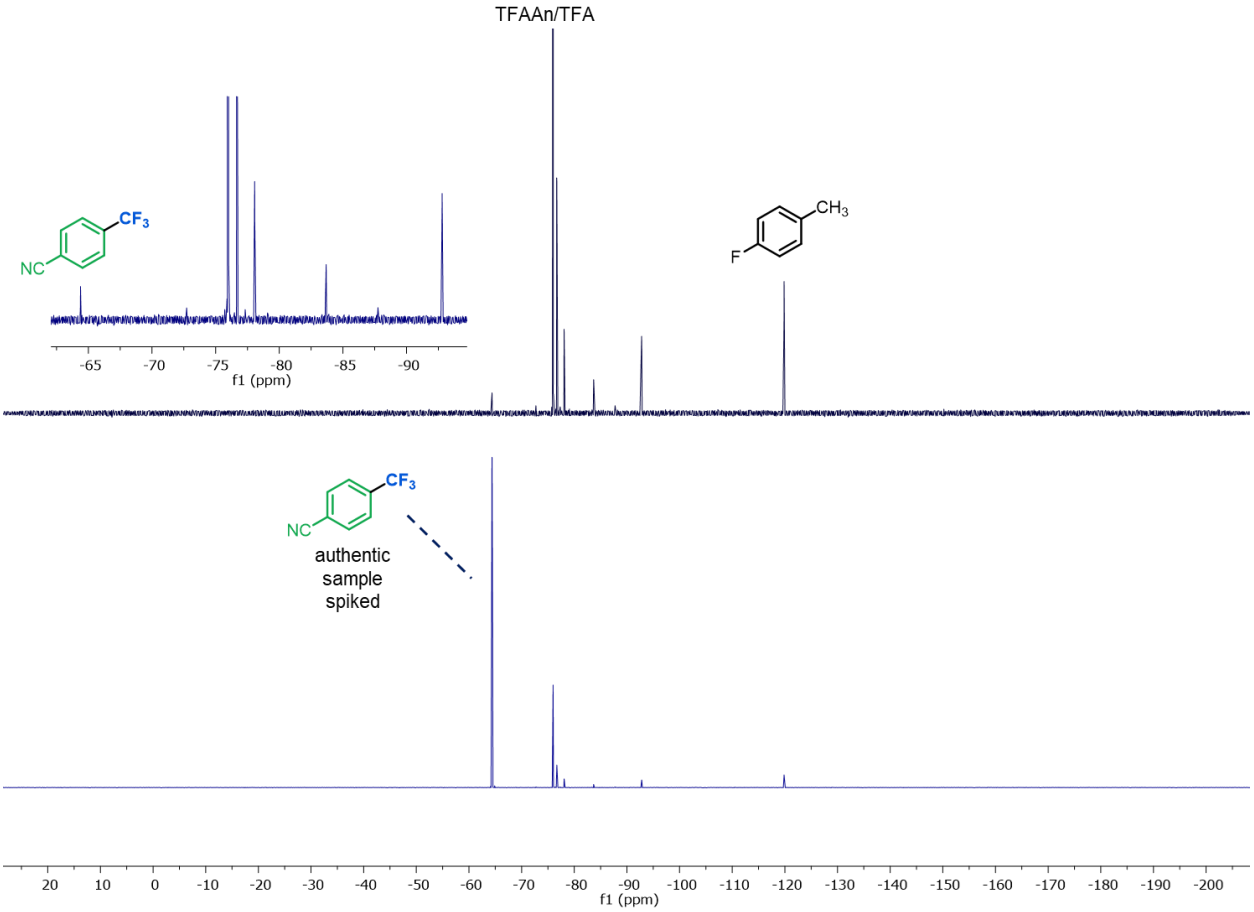

Figure 2.16. (Top) ^{19}F NMR of crude reaction with 4-fluorotoluene internal standard showing 4-trifluoromethylbenzonitrile, **1-CF$_3$** and (bottom) ^{19}F NMR of crude reaction after spiking in an authentic sample of **1-CF$_3$**.

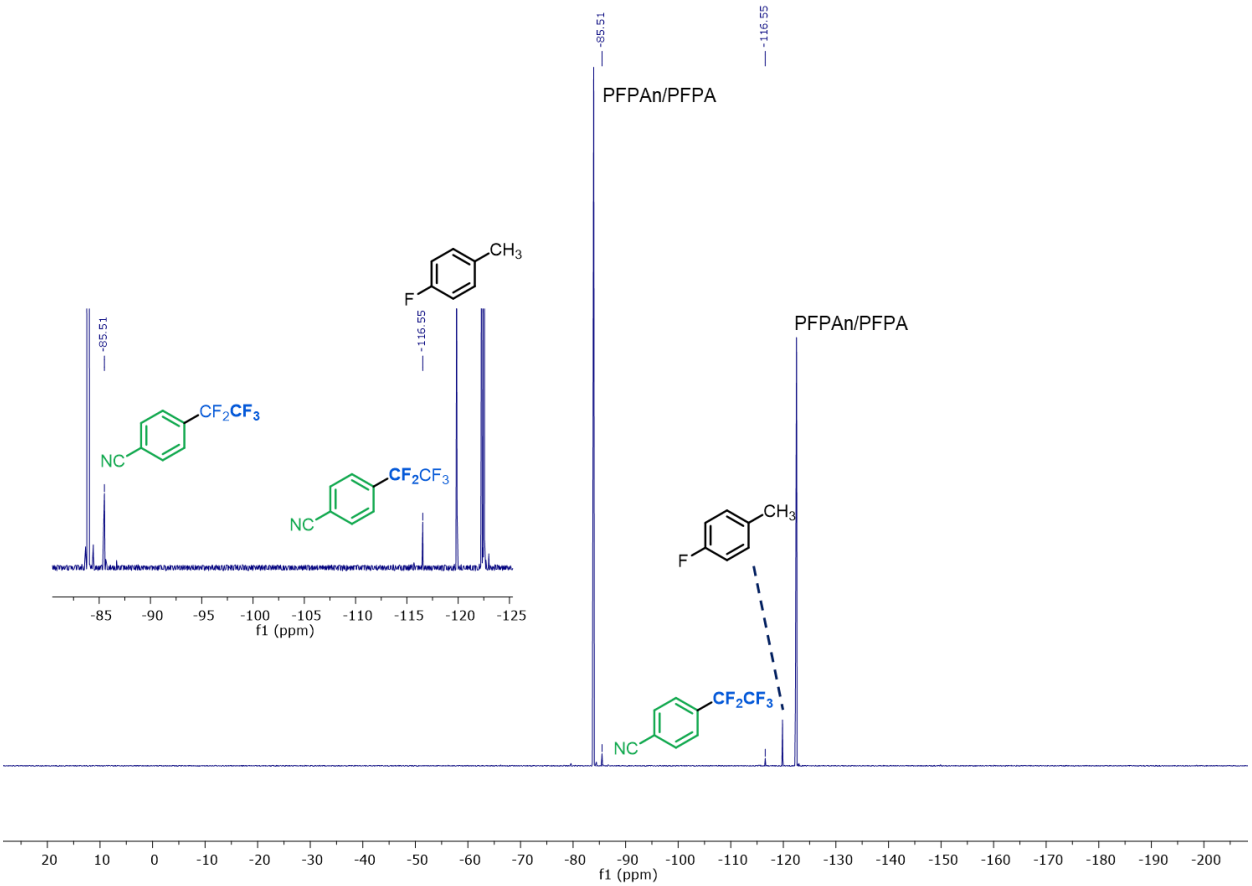

Figure 2.17. ^{19}F NMR of crude reaction with 4-fluorotoluene internal standard indicating formation of **1-CF_2CF_3.**

Moving forward, we focused on optimizing catalytic decarbonylative difluoromethylation, since this was the highest yielding reaction among those in Scheme 2.4. We first synthesized a variety of neopentylglycol boronate esters using two different protocols. If the boronic acid was commercially available, the corresponding ester was synthesized via a condensation reaction with 2,2-dimethyl-1,3-propanediol. If not, the aryl bromide precursor was subjected to a Miyaura borylation reaction with bis(neopentyl glycolato)diboron (see Experimental section for details).

In addition, to eliminate the need for the hygroscopic fluoride additives, we independently synthesized anhydrous DFAF as a concentrated solution in THF and deployed it directly as the electrophile for cross-coupling (Figure 2.18).[23,24] THF was identified to be the most suitable reaction solvent and distillation solvent due to its relatively low boiling point and the high

solubility of CsF in THF. While a higher boiling solvent, such as mesitylene or xylenes, could in principle enable higher temperatures in the catalytic reaction, the poor solubility of CsF in these solvents limited the acid fluoride generation step in these media. Further, there are additional challenges associated the co-distillation of low boiling DFAF in these high boiling aromatic solvents.

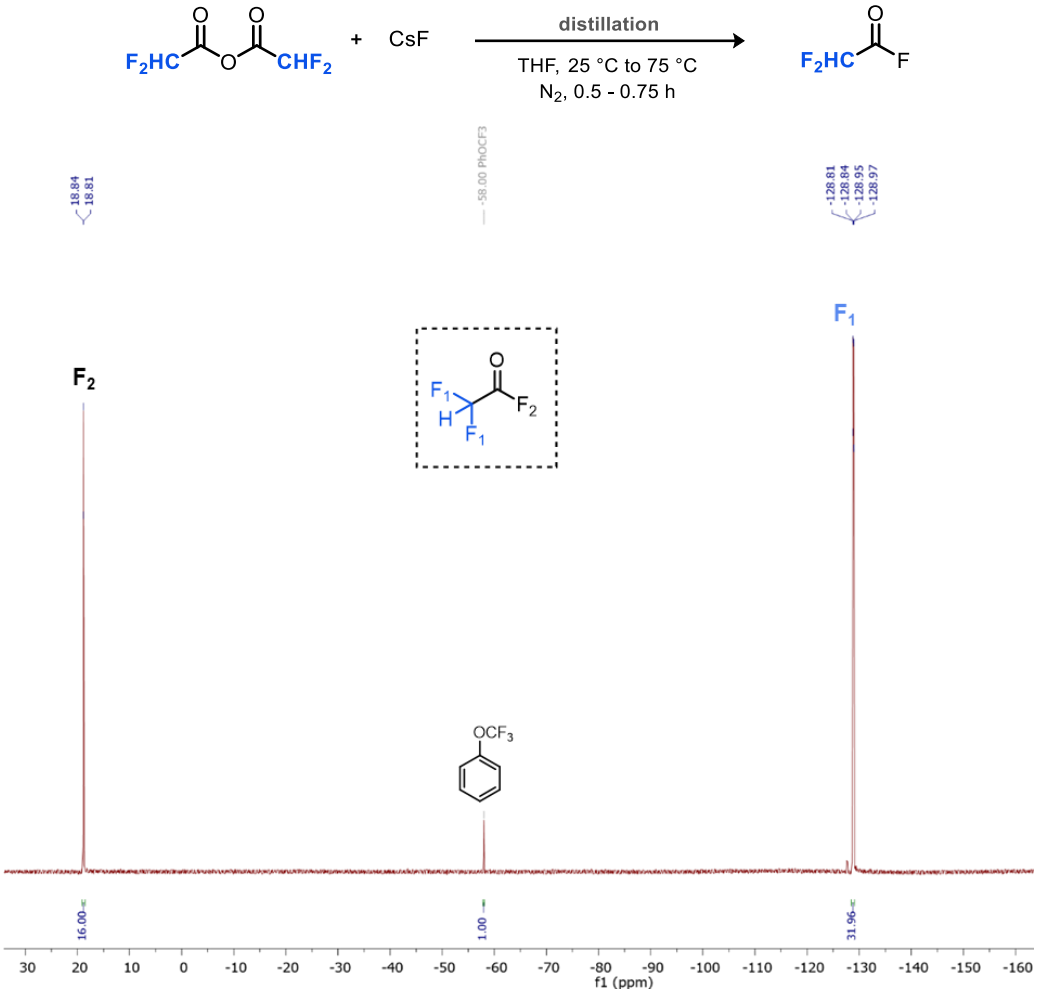

Figure 2.18. Representative ^{19}F NMR spectrum obtained after synthesis and distillation of DFAF containing 0.33 mmol of trifluoromethoxybenzene internal standard.

With the boronate ester and DFAF coupling partners in hand, we began to screen reaction conditions. As shown in Table 2.2, entry 1, none of product **1** was detected at room temperature with DFAF as the electrophile and **1b** as the nucleophile, consistent with slow oxidative addition.

However, upon heating this reaction to 130 °C, **1** was formed in 51% yield (Table 2.2, entry 3). The reaction was further optimized with respect to reagent stoichiometry, temperature, solvent, and reaction time. Under the optimized conditions (10 mol % $Pd[P(o\text{-}Tol)_3]_2$, 20 mol % of SPhos, 5 equiv of DFAF, and 1 equiv of **1b** in a mixture of THF:toluene at 150 ºC for 5 h), **1** was formed in 92-93% yield as determined by ^{19}F NMR spectroscopic analysis and was isolated in 77% yield.

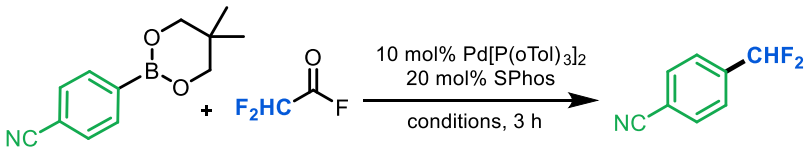

1b (0.05 mmol) **X** equiv **1**

Entry	X	temperature (°C)	solvent(s)	Yield (%)[a]
1	1	25	THF	<1
2	1	100	THF	28
3	1	130	THF:toluene (1:1)	51
4	3	130	THF:toluene (1:1)	58
5	5	130	THF:toluene (1:1)	67
6	5	150	THF:toluene (1:1)	86
7	5	150	THF:dioxane (1:1)	72
8[b]	5	150	THF:toluene (1:1)	93
9[b]	5	150	THF:toluene (1:2)	92

Table 2.2. Optimization of difluoromethylation of **1a** with DFAF. [a]Yields determined by ^{19}F NMR with 4-fluorotoluene internal standard. [b]Reaction was run for 5 h.

Figure 2.18. Reaction solution in tall 10 mL vial before heating in THF/toluene.

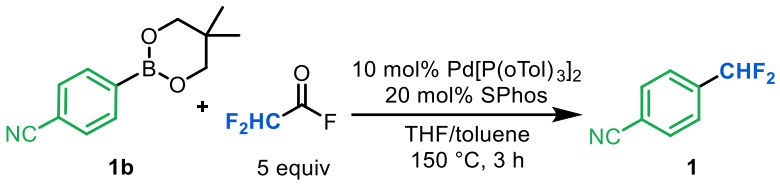

Entry	Change of reaction conditions	Yield (%)[a]
1	none	86
2	RuPhos instead of SPhos	76
3	DavePhos instead of SPhos	78
4	XantPhos instead of SPhos	<1
5	BrettPhos instead of SPhos	36
6	$Pd(dba)_2$ instead of $Pd[P(oTol)_3]_2$	68
7	4-CNPhB$(OH)_2$ instead of **1a**	<1
8	4-CNPhBpin instead of **1a**	29
9	no SPhos	<1
10	no $Pd[P(oTol)_3]_2$	<1

[a]Yields determined by ^{19}F NMR with internal standard

Table 2.3. Impact of catalyst, nucleophile, and ligand loading on reaction yields.

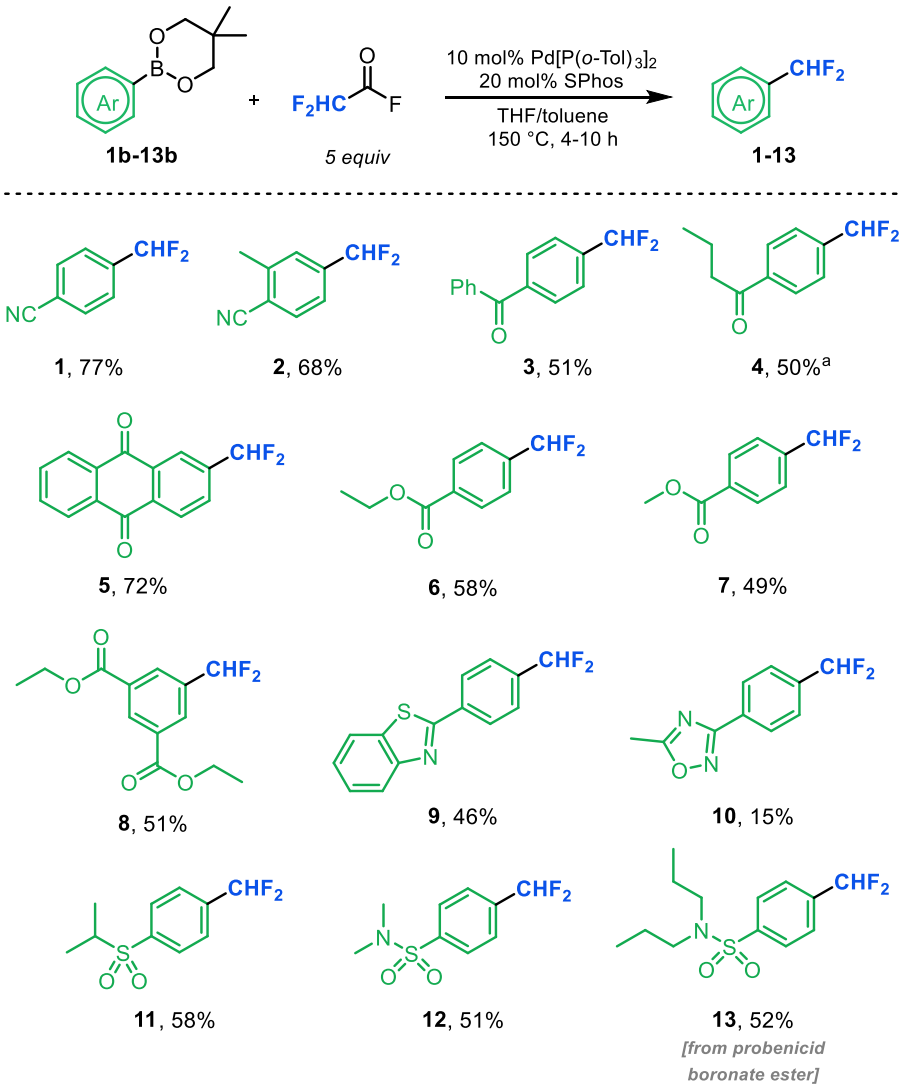

Table 2.4. Scope of aryl boronate esters for the catalytic electrophilic decarbonylative difluoromethylation using difluoroacetyl fluoride. [a]15 mol% Pd[P(*o*-tol)$_3$]$_2$/30 mol% SPhos used for catalysis.

We next evaluated the scope of aryl boronate ester nucleophiles for this transformation. As summarized in Table 2.4, a variety of neopentylglycol boronate esters bearing electron withdrawing substituents (**1-13**) reacted to afford modest to excellent yields of difluoromethylarene products. Nitriles (**1, 2**), ketones (**3-5**), esters (**6-8**), sulfoxides (**11**), sulfonamides (**12, 13**) were well-tolerated under the reaction conditions. In addition, azole derivatives (**9, 10**) reacted in low to modest yields. Boronate esters bearing fluorinated substituents

also underwent difluoromethylation in good to excellent yields but proved too volatile for isolation (Table 2.5).

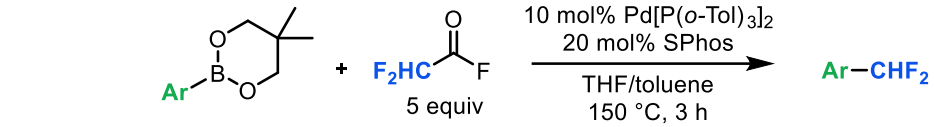

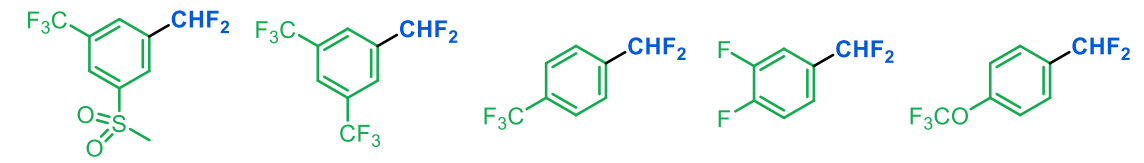

Table 2.5. Scope of difluoromethylated arenes bearing fluorine or fluoroalkyl substituents.

Interestingly, boronate ester derivatives bearing electron donating substituents, such as methyl, phenyl, or benzyl ethers, showed low reactivity under these conditions (typically <5% yield; Table 2.6).

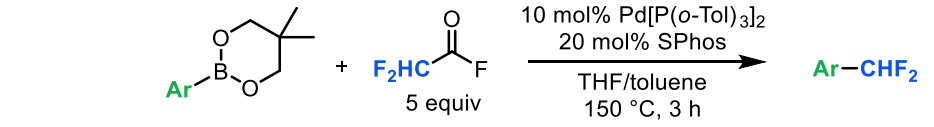

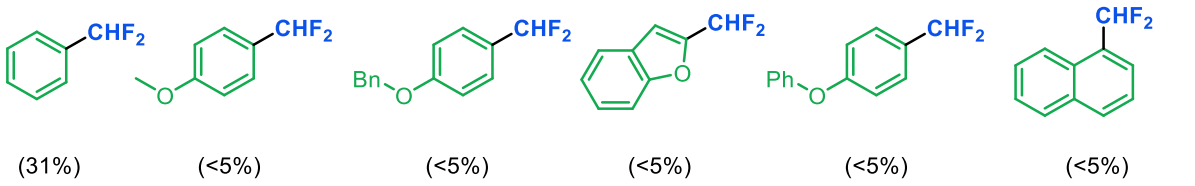

Table 2.6. Other substrates explored for palladium-catalyzed difluoromethylation using difluoroacetyl fluoride.

Given the poor reactivity of electron-rich aryl boronate nucleophiles in the catalytic reaction, we evaluated the fluoride-mediated transmetalation of **II-CHF$_2$** with the p-OCH$_3$ substituted substrate **19b** (Figure 2.19). The difluoromethylated product **19** was formed in 26% yield (nearly identical to the 27% yield of **1** in Figure 2.15), suggesting that the transmetalation step is not the origin of the poor reactivity of electron-rich boronate esters in this system.

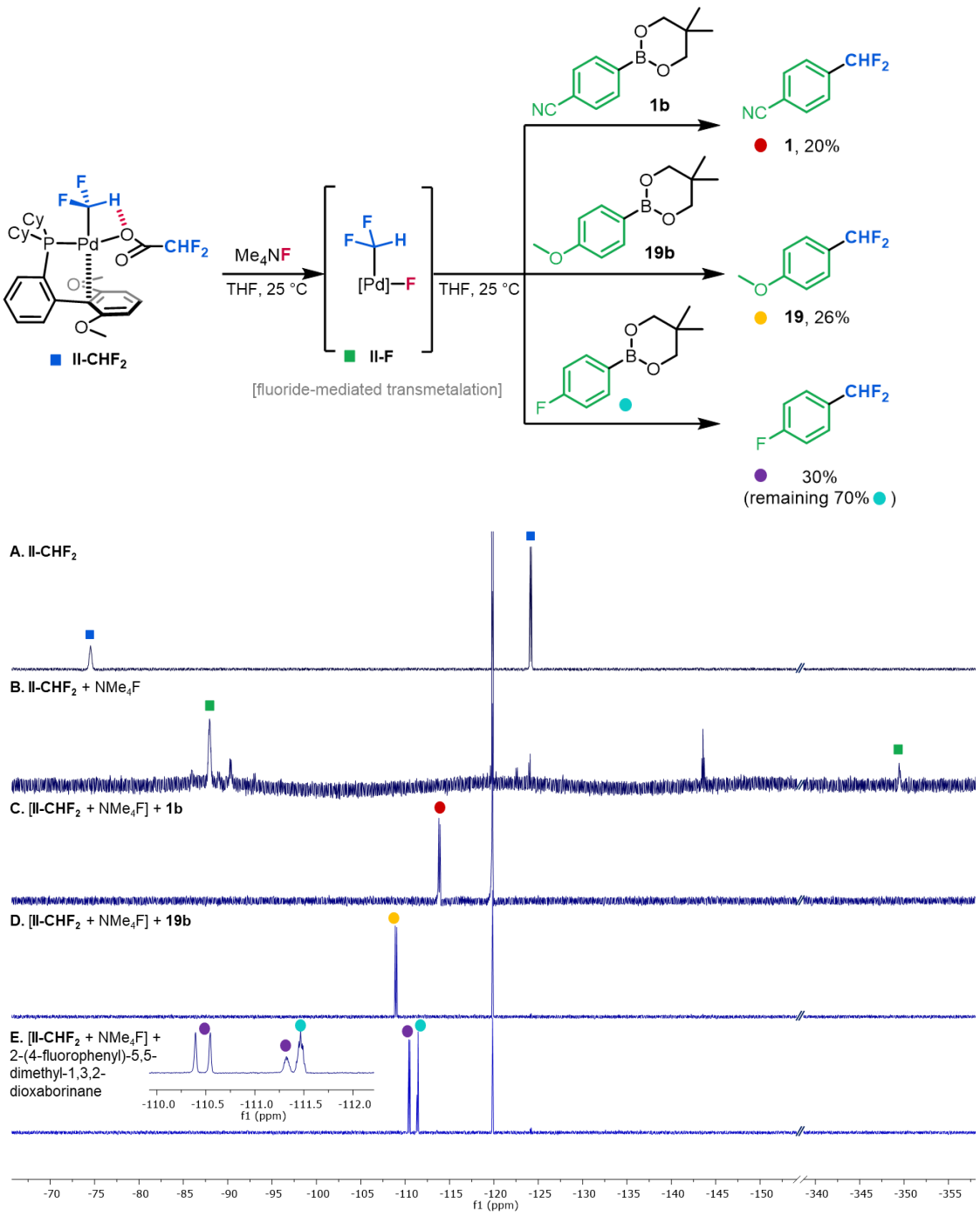

Figure 2.19. Scheme and ^{19}F NMR spectra associated with fluoride-aided transmetalation of **II-CHF2** with substrates **1b**, **19b**, and 2-(4-fluorophenyl)-5,5-dimethyl-1,3,2-dioxaborinane.

^{19}F NMR spectroscopic analysis of the low yielding reactions showed significant quantities of unreacted DFAF and no identifiable organic by-products. The mass balance in the catalytic reaction was evaluated via ^{19}F NMR spectroscopy using 2-(4-fluorophenyl)-5,5-dimethyl-1,3,2-dioxaborinane as the substrate (Figure 2.20). After 3 h, 17% of the difluoromethylated product [1-(difluoromethyl)-4-fluorobenzene], 14% of the protodeboronation product (fluorobenzene), and 43% of the aryl boron starting material were observed, accounting for 74% of the mass balance (Figure 2.21). Similar to the stoichiometric transmetalation experiment using 2-(4-fluorophenyl)-5,5-dimethyl-1,3,2-dioxaborinane, 4-fluorophenyl boronic acid and 4,4'difluorobiphenyl were not observed.

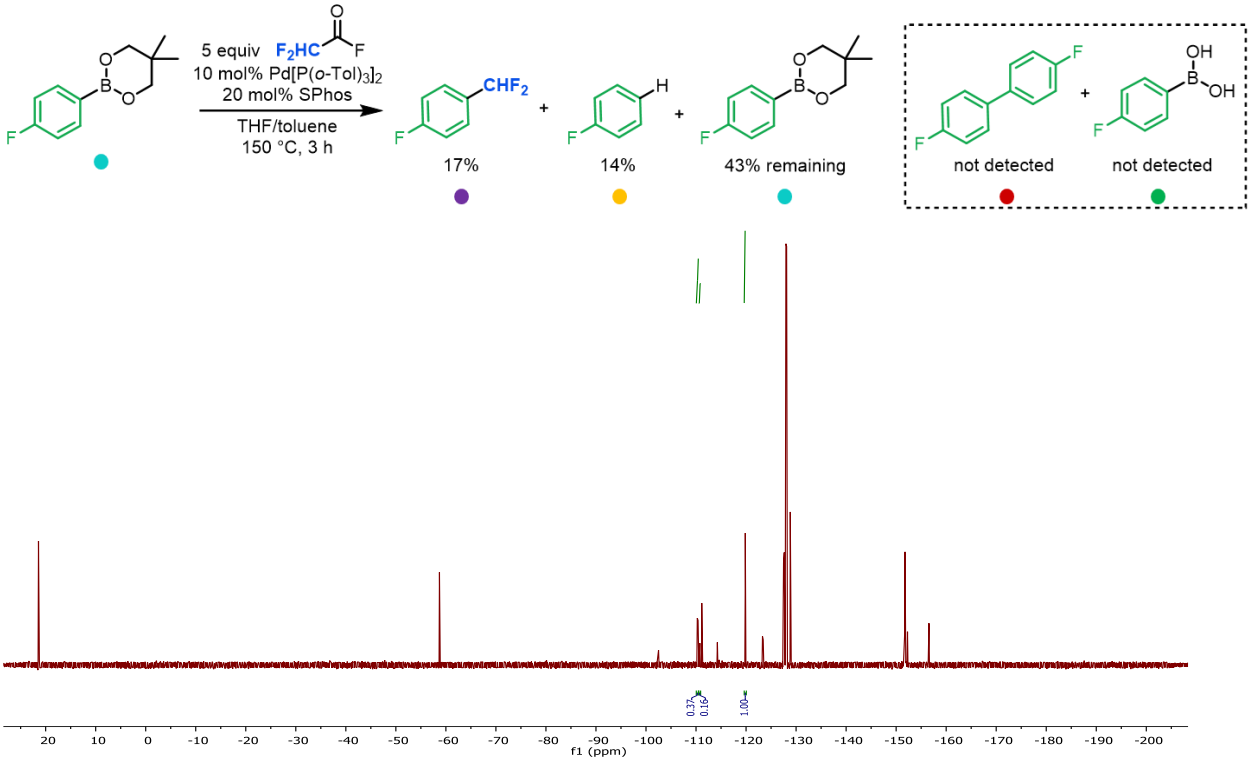

Figure 2.20. ^{19}F NMR spectra obtained from spiking authentic samples into the crude reaction of 2-(4-fluorophenyl)-5,5-dimethyl-1,3,2-dioxaborinane.

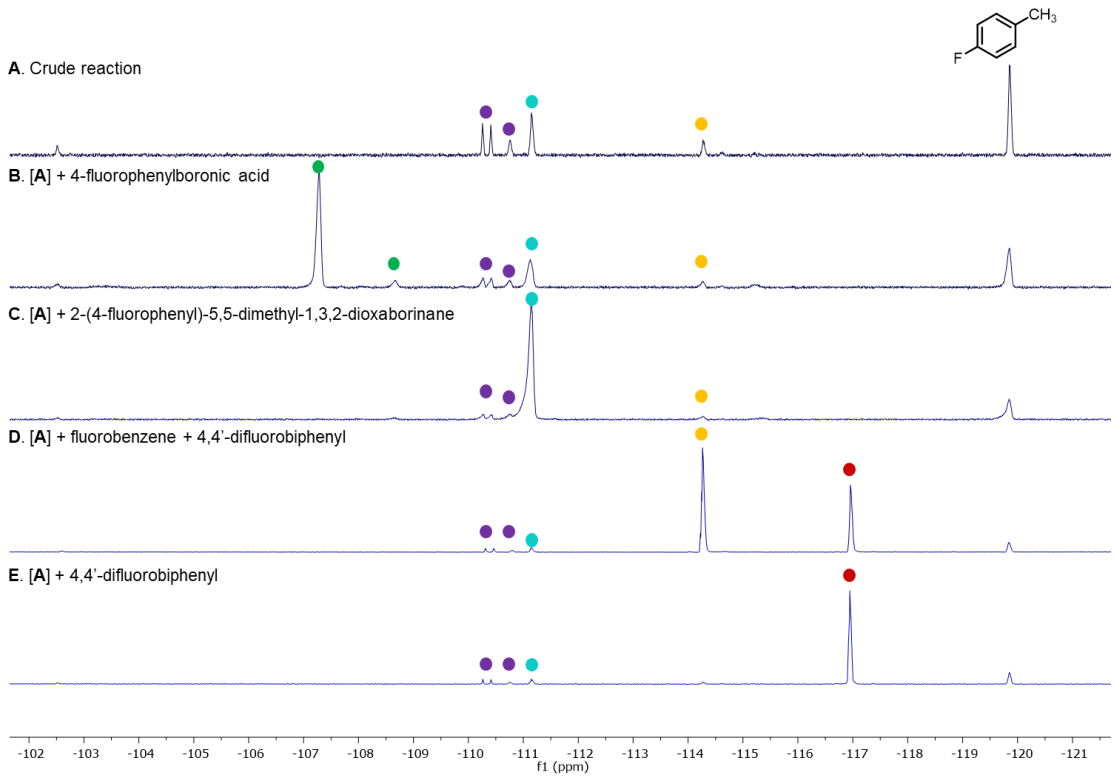

Figure 2.21. ^{19}F NMR spectra obtained from spiking authentic samples into the crude reaction of 2-(4-fluorophenyl)-5,5-dimethyl-1,3,2-dioxaborinane.

2.6. Conclusions

In summary, this chapter presents a detailed investigation of decarbonylative cross-couplings between fluoroalkyl carboxylic acid-derived electrophiles and aryl boron nucleophiles. The combination of stoichiometric organometallic and computational studies unveiled several key findings that ultimately enabled the development of a catalytic difluoromethylation reaction. First, unusually low barriers are observed for the key carbonyl de-insertion step at (SPhos)Pd^{II}($C(O)CHF_2$)(X) complexes relative to their trifluoromethyl and pentafluoroethyl analogues. Several attractive non-covalent interactions involving the acidic CHF_2 hydrogen appear to play a crucial role in lowering this barrier, a finding that could prove more broadly useful in the future development of decarbonylative couplings with these electrophiles.

The generation of a Pd–fluoride intermediate proved critical for promoting the challenging transmetalation step of the sequence. This finding led to the use of difluoroacetyl fluoride as the

electrophile in catalysis to directly access a 'transmetalation-active' Pd-fluoride intermediate in situ and enable base-free transmetalation. While similar effects have been observed at nickel centers, this report is rare example of base-free cross-coupling of an acid fluoride derivative at Pd.[22i] Overall, we expect this study to engender interest in the unique properties of fluoroalkyl groups and the reactivity of metal–fluoroalkyl complexes in the context of catalytic reaction development.

2.7. Experimental Section

General information. All manipulations were performed inside an N_2-filled glovebox unless otherwise noted, and all glassware was oven-dried for a minimum of 24 h in an oven at 150 ºC before use. NMR spectra were obtained on a Varian VNMR 700 (699.76 MHz for 1 H; 175.95 MHz for ^{13}C), Varian VNMR 500 (500.09 MHz for ^{1}H; 470.56 MHz for ^{19}F; 125.75 MHz for ^{13}C), or Varian VNMR 400 (401 MHz for ^{1}H; 376 MHz for ^{19}F; 123 MHz for ^{13}C) spectrometer. ^{1}H and ^{13}C NMR chemical shifts are reported in parts per million (ppm) relative to TMS, with the residual solvent peak used as an internal reference. ^{19}F NMR chemical shifts are reported in ppm and are referenced to 4-fluorotoluene (–119.85 ppm) or trifluoromethoxybenzene (–58.00 ppm). ^{13}C NMR spectra are referenced to the residual $CHCl_3$ peak (77.16 ppm). Abbreviations used in the NMR data are as follows: s, singlet; d, doublet; t, triplet; q, quartet; m, multiplet; br, broad signal. Yields of reactions that generated fluorinated products were determined by ^{19}F NMR spectroscopic analysis using a relaxation delay of 5 s with a 90º pulse angle. Mass spectral data were obtained on a Micromass Magnetic Sector Mass Spectrometer. Automated flash chromatography was performed using a Biotage Isolera One system with cartridges containing high performance silica gel.

Abbreviations: tetrahydrofuran (THF), dichloromethane (DCM), diethyl ether (Et_2O), difluoroacetyl fluoride (DFAF), difluoroacetic anhydride (DFAAn), trifluoroacetic anhydride (TFAAn), difluoroacetic acid (DFA), trifluoroacetic acid (TFA), pentafluoropropionic anhydride (PFPAn), pentafluoropropionic acid (PFPA), tetramethyl ammonium fluoride (TMAF), tetrabutylammonium fluoride (TBAF), room temperature (RT).

Compatibility experiment with trifluoroacetic anhydride and diphenyl zinc. A THF solution (0.5 M) of trifluoroacetic anhydride was prepared, and 0.1 mL of this solution was added to a pre-weighed vial containing a stir bar and Ph_2Zn (11 mg, 0.05 mmol, 1.0 equiv). The solution was diluted to 0.4 mL with THF, sealed with a Teflon-lined cap, and stirred at room temperature for 1 h. 4-Fluorotoluene (0.025 mL, 2.0 M, 0.05 mmol, 1.0 equiv) was added as a ^{19}F NMR standard, the solution was transferred to an NMR tube, and the reaction was analyzed via ^{19}F NMR

spectroscopy. 2,2,2-trifluoromethyl acetophenone **A** was formed in 77% yield (signal at –72.4 ppm) with no remaining anhydride. A broad signal attributed to a zinc trifluoromethyl acetate was also observed at –76.2 ppm as shown in Figure S1.

Compatibility experiment with trifluoroacetic anhydride and phenyl boronic acid. A $CDCl_3$ solution (1.0 M) of trifluoroacetic anhydride was prepared, and 0.3 mL was added to a pre-weighed vial containing a stir bar and $PhB(OH)_2$ (36 mg, 0.30 mmol, 1.0 equiv). The solution was diluted to 0.4 mL with $CDCl_3$, sealed with a Teflon-lined cap, and stirred at room temperature for 1 h. The reaction solution was transferred to an NMR tube and analyzed by ^{13}C NMR spectroscopy. (^{13}C rather than ^{19}F NMR was used, because the former allows more clear differentiation of the CF_3-containing products, *vide infra*.) As shown in Figure S2, trifluoroacetic acid (**B**) is the major CF_3-containing product formed under these conditions. Conducting the experiment in THF or toluene with analysis by ^{19}F NMR spectroscopy led to inconclusive results due to the poor resolution between TFAAn and TFA in the ^{19}F NMR spectra.

Compatibility experiment with trifluoroacetic anhydride and phenylboronic acid neopentylglycol ester. A $CDCl_3$ solution (1.0 M) of trifluoroacetic anhydride was prepared, and 0.3 mL was added to a pre-weighed vial containing a stir bar and phenylboronic acid neopentylglycol ester (54 mg, 0.30 mmol). The solution was diluted to 0.4 mL with $CDCl_3$, sealed with a Teflon-lined cap, and stirred at room temperature for 1 h. The solution was transferred to an NMR tube, and ^{13}C NMR analysis was conducted. After 1 h or 3 h, ^{13}C NMR spectroscopic analysis showed that neither **A** nor **B** was formed (Figure S2). Conducting the experiment in THF or toluene followed by analysis via ^{19}F NMR spectroscopy led to inconclusive results due to the poor resolution between TFAAn and TFA in the ^{19}F NMR spectra.

Compatibility experiment with trifluoroacetic anhydride and phenylboronic acid neopentylglycol ester at 50 ºC. A $CDCl_3$ solution (1.0 M) of trifluoroacetic anhydride was prepared, and 0.3 mL was added to a pre-weighed vial containing a stir bar and phenylboronic acid neopentylglycol ester (54 mg, 0.30 mmol). The solution was diluted to 0.4 mL with $CDCl_3$, sealed with a Teflon-lined cap, and stirred at 50 ºC for 1 h. The reaction was cooled to room temperature. The solution was transferred to an NMR tube and ^{13}C NMR analysis was conducted, showing a small amount of trifluoroacetic acid **B** (Figure S3).

Compatibility experiment with trifluoroacetic anhydride and phenylboronic acid pinacol ester. A $CDCl_3$ solution (1.0 M) of trifluoroacetic anhydride was prepared, and 0.3 mL was added to a pre-weighed vial containing a stir bar and phenylboronic acid pinacol ester (61 mg, 0.30 mmol). The solution was diluted to 0.4 mL with $CDCl_3$, sealed with a Teflon-lined cap, and stirred at room temperature for 1 h. The mixture was transferred to an NMR tube and ^{13}C NMR spectroscopic analysis was conducted. Neither **A** nor **B** was detected.

Compatibility experiment with difluoroacetic anhydride and phenyl boronic acid. A $CDCl_3$ solution (1.0 M) of difluoroacetic anhydride was prepared, and 0.15 mL was added to a pre-weighed vial containing a stir bar and $PhB(OH)_2$ (18 mg, 0.15 mmol, 1.0 equiv). The solution was diluted to 0.4 mL with $CDCl_3$, sealed with a Teflon-lined cap, and stirred at room temperature for 1 h at room temperature. The solution was transferred to an NMR tube and ^{13}C NMR analysis was conducted, which showed complete hydrolysis of DFAAn to form difluoroacetic acid (DFA).

Compatibility experiment with difluoroacetic anhydride and phenylboronic acid neopentylglycol ester. A $CDCl_3$ solution (1.0 M) of difluoroacetic anhydride was prepared, and 0.15 mL was added to a pre-weighed vial containing a stir bar and phenyl boronate ester **1b** (26 mg, 0.15 mmol). The solution was diluted to 0.4 mL with $CDCl_3$, sealed with a Teflon-lined cap, and stirred at room temperature for 1 h at room temperature. The solution was transferred to an NMR tube, and ^{13}C NMR analysis was conducted, which showed no detectable DFA.

Compatibility experiment with difluoroacetyl fluoride and phenyl boronic acid. A solution of $PhB(OH)_2$ (12 mg, 0.10 mmol, 1.0 equiv) in 0.4 mL THF was prepared. To this was added a THF solution of DFAF (0.035 mL, 2.85 M, 0.10 mmol, 1.0 equiv), and the reaction was sealed with a Teflon-lined cap and stirred at room temperature for 1 h. 4-fluorotoluene (0.05 mL, 2.0 M, 0.10 mmol, 1.0 equiv) was added as an internal standard, the solution was transferred to an NMR tube, and ^{19}F NMR analysis was conducted. No DFAF was detected in solution; instead, a doublet at –128.45 ppm appeared, which corresponds to the hydrolysis product DFA.

Compatibility experiment with difluoroacetyl fluoride and phenylboronic acid neopentylglycol ester. A solution of PhBneo (19 mg, 0.10 mmol, 1.0 equiv) in 0.4 mL THF was prepared. To this was added a THF solution of DFAF (0.035 mL, 2.85 M, 0.10 mmol, 1.0 equiv), and the reaction was sealed with a Teflon-lined cap and stirred at room temperature for 1 h. 4-

fluorotoluene (0.05 mL, 2.0 M, 0.10 mmol, 1.0 equiv) was added as an internal standard, the solution was transferred to an NMR tube, and ^{19}F NMR analysis was conducted. Less than 3% DFA was observed in solution.

Stoichiometric reaction oxidative addition and carbonyl-deinsertion experiment of trifluoroacetic anhydride with Pd/SPhos. A solution of trifluoroacetic anhydride (0.4 mL, 0.04 mmol, 0.1 M, 4 equiv) in anhydrous tetrahydrofuran was prepared. To this was added a THF-solution of 4-fluorotoluene (0.4 mL, 0.04 mmol, 0.1 M, 4.0 equiv). Pd[P(*o*-Tol)$_3$]$_2$ (21.3 mg, 0.03 mmol, 3 equiv) and SPhos (12.3 mg, 0.03 mmol, 3 equiv) were suspended in anhydrous THF (0.3 mL), and this mixture was stirred vigorously for 5 min. To the THF-suspension of Pd and SPhos was added 0.6 mL of the anhydride solution to generate a solution with 0.9 mL of total volume. The remaining 0.2 mL of anhydride solution was diluted and used as a ^{19}F NMR reference. The reaction mixture was stirred briefly to ensure homogeneity and was then portioned evenly into three vials (*i, ii, iii*). A ^{19}F NMR spectrum of sample *i* was acquired after 15 min and showed 98% yield of **I-COCF$_3$**. A ^{19}F NMR spectrum of sample *ii* was acquired after 4 h and lacked the minor TFAAn peak still observed in the spectrum collected after 15 min, with no detectable **II-CF$_3$**. Sample *iii* was heated to 90 ºC for 30 min and then analyzed by ^{19}F NMR spectroscopy, which showed the formation of **II-CF$_3$** in 90% yield. The complexes were identified by ^{19}F NMR spectroscopy based on the diagnostic locations of the observed peaks, which are in excellent agreement with our previous report[1a] of an analogous transformation at (RuPhos)Pd(0). *In situ NMR characterization:* TFAAn: **^{19}F NMR** (376 MHz) δ -76.73 (s, 6F). **I-COCF$_3$: ^{19}F NMR** (376 MHz) δ -73.94 (s, 3F), -75.61 (s, 3F). **II-CF$_3$: ^{19}F NMR** (376 MHz) δ -11.60 (bs, 3F), -75.69 (s, 3F).

Stoichiometric oxidative addition and carbonyl de-insertion experiment of difluoroacetic anhydride with Pd/SPhos. A solution of difluoroacetic anhydride (0.4 mL, 0.04 mmol, 0.1 M, 4 equiv) in anhydrous tetrahydrofuran was prepared. To this was added a THF solution of 4-fluorotoluene (0.4 mL, 0.04 mmol, 0.1 M, 4.0 equiv). Pd[P(*o*-Tol)$_3$]$_2$ (21.3 mg, 0.03 mmol, 3 equiv) and SPhos (12.3 mg, 0.03 mmol, 3 equiv) were suspended in anhydrous THF (0.3 mL), and this mixture stirred vigorously for 5 min. To the THF suspension of Pd and SPhos was added 0.6 mL of the anhydride solution. The remaining 0.2 mL of anhydride solution was diluted and used

as a ^{19}F NMR reference (spectrum A in Figure S8). The Pd solution containing internal standard, ligand, and anhydride was stirred briefly to ensure homogeneity and then portioned evenly into three vials (*i, ii, iii*). A ^{19}F NMR spectrum was acquired of sample *i* after 15 min at room temperature and showed 85% yield of **I-COCHF$_2$** and 13% yield of **II-CF$_3$**. A ^{19}F NMR spectrum was acquired of sample *iii* after 10 h at room temperature and showed 91% yield of **II-CHF$_2$** and 6% remaining **I-COCHF$_2$**. The spectra show a dramatically lower barrier for carbonyl de-insertion at **I-COCHF$_2$** compared to **I-COCF$_3$**. After 10 h stirring at room temperature, **II-CHF$_2$** is obtained in 91% yield with 6% acyl complex remaining based on the ^{19}F NMR spectrum. This is in sharp contrast to the temperature requirement for carbonyl de-insertion of **I-COCF$_3$**. Notably, reacting Pd[P(*o*-Tol)$_3$]$_2$/SPhos with difluoroacetic anhydride in an NMR tube without stirring led to significantly lower rates of carbonyl de-insertion.

Stoichiometric oxidative addition and carbonyl de-insertion experiment of pentafluoropropionic anhydride (PFPAn) with Pd/SPhos. A THF-solution of pentafluoropropionic anhydride (0.4 mL, 0.05 mmol, 0.125 M, 5 equiv) was prepared. To this was added a THF-solution of 4-fluorotoluene (0.4 mL, 0.04 mmol, 0.1 M, 4 equiv). Pd[P(*o*-Tol)$_3$]$_2$ (21.3 mg, 0.03 mmol, 3 equiv) and SPhos (12.3 mg, 0.03 mmol, 3 equiv) were weighed in a separate 4-mL vial with a stirbar, 0.6 mL THF were added, and the mixture was stirred. To the stirred mixture of Pd and SPhos in THF was added 0.6 mL of the anhydride/4-fluorotoluene solution to generate a solution with a total volume of 1.2 mL. The remaining 0.2 mL of anhydride/4-fluorotoluene solution was diluted with THF and used as a ^{19}F NMR reference (spectrum A in Figure S9). The reaction mixture was stirred briefly to ensure homogeneity and was then portioned evenly (0.4 mL) into three vials (*i, ii, iii*). A ^{19}F NMR spectrum of sample *i* was acquired after 0.25 h and shows conversion of PFPAn to **I-COCF$_2$CF$_3$** (Figure S9, B). Sample *ii* was also analyzed by ^{31}P NMR spectroscopy. A ^{19}F NMR spectrum of sample *ii* was acquired after 4 h and showed no significant change to the ^{19}F NMR spectrum obtained from sample *i*. Sample *iii* was heated to 90 ºC for 30 min and then analyzed by ^{19}F NMR spectroscopy (Figure S9, D) and ^{31}P spectroscopy, which support the quantitative conversion of **I-COCF$_2$CF$_3$** to **II-CF$_2$CF$_3$**. The complexes were characterized in situ by ^{19}F NMR and ^{31}P NMR spectroscopy based on the diagnostic locations of the observed peaks[1a]. *In situ NMR characterization:* PFPAn: **^{19}F**

NMR (376 MHz) δ -84.07 (s, 6F), -123.33 (s, 4F). **I-COCF$_2$CF$_3$: ^{19}F NMR** (376 MHz) δ -80.96 (s, 3F), -83.28 (s, 3F), -112.00 (s, 2F), -119.25 (s, 2F). **^{31}P NMR** (162 MHz) δ 46.04 (s, 1P). **II-CF$_2$CF$_3$: ^{19}F NMR** (376 MHz) δ -76.49 (bs, 2F), -79.14 (s, 3F), -88.48 (s, 3F), -119.91* (s, 2F). **^{31}P NMR** (162 MHz) δ 52.98 (bs, 1P). The data in Figures S9 and S10 show that the reactivity of PFPAn nearly identical to that observed for TFAAn (i.e., fast oxidative addition and slow carbonyl de-insertion at room temperature). Notably, both TFAAn and PFPAn lack the acidic hydrogen found in DFAAn and thus require high temperatures for carbonyl de-insertion.

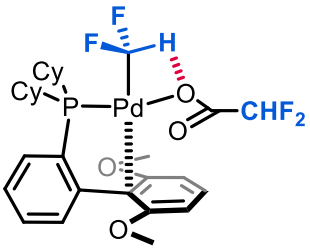

Synthesis and analytical data for complex II-CHF$_2$. A 20 mL vial equipped with a stir bar was charged with Pd[P(*o*-Tol)$_3$]$_2$ (340 mg, 0.48 mmol, 1.0 equiv), SPhos (195 mg, 0.48 mmol, 1.0 equiv), and THF (4 mL). To this stirring suspension was added difluoroacetic anhydride (87 mg, 0.5 mmol, 1.05 equiv). The reaction was stirred for 18 h at room temperature, then concentrated to ca. 1 mL *in vacuo* to yield a dark yellow oil. The oil was loaded onto a 2 cm tall celite plug in a disposable fritted funnel and eluted with THF (8-10 mL). The yellow filtrate was concentrated *in vacuo*, yielding a yellow, oily residue. After addition of pentanes, a pale-yellow precipitate formed. The yellow suspension was loaded onto a 2 cm tall celite plug in a disposable fritted funnel, and the solid was washed with diisopropyl ether (10 mL), then a minimal amount of cold anhydrous Et$_2$O. The pale solid was eluted with tetrahydrofuran, and the resultant yellow filtrate was concentrated *in vacuo*, yielding **II-CHF$_2$** as an off-white solid (195 mg, 0.29 mmol, 61% yield) containing about 0.2 equiv of tetrahydrofuran, as determined by ^{1}H NMR spectroscopy. **^{19}F NMR** (470 MHz, Methylene Chloride-d$_2$) δ –75.29 (t, *J* = 46.1 Hz), –124.38 (d, *J* = 57.0 Hz). **^{31}P NMR** (202 MHz, Methylene Chloride-d$_2$) δ 46.05 (t, *J* = 37.6 Hz). **^{1}H NMR** (700 MHz, Methylene Chloride-*d*$_2$) δ 7.73 (t, *J* = 7.1 Hz, 1H), 7.58-7.38 (*multiple peaks*, 3H), 6.78 (ddd, *J* = 7.6, 3.0, 1.4 Hz, 1H), 6.57 (d, *J* = 8.5 Hz, 2H), 6.26 (td, *J* = 53.0, 5.1 Hz, 1H), 5.60 (t, *J* = 55.7 Hz, 1H), 3.80 (s, 6H), 2.33-2.23 (m, 2H), 2.13 (d, *J* = 8.1 Hz, 2H), 1.95-1.76 (*multiple peaks*, 6H), 1.74-1.55 (*multiple peaks*, 4H), 1.41-1.16 (*multiple peaks*, 6H). **^{13}C NMR** (176 MHz, Methylene Chloride-d$_2$) δ 167.24 (t, *J* = 24.4 Hz), 161.94, 144.06 (d, *J* = 17.5 Hz), 137.15, 135.32 (d, *J* = 42.3 Hz), 132.58, 132.08, 132.01 (d, J = 3.0 Hz), 127.49 (d, *J* = 6.0 Hz), 119.50 (td, *J* = 314.1, 14.1 Hz), 110.20 (t, *J* = 249.6 Hz), 56.38, 35.85 (d, *J* = 26.9 Hz),

29.50, 29.16 (d, *J* = 1.8 Hz), 27.87 (dd, *J* = 29.1, 12.8 Hz), 26.62 (d, *J* = 1.7 Hz). **HRMS** (ESI+) calcd. for $C_{29}H_{37}F_4O_4PPd$ [M+H] *m/z* 662.1400. Parent – $OCOCHF_2$ *m/z* 567.1456. Found 567.1470. **X-ray** quality crystals of **II-CHF$_2$** were obtained by vapor diffusion of Et_2O /pentanes into a THF solution of **II-CHF$_2$** at room temperature. An ORTEP diagram of **II-CHF$_2$** is shown with select hydrogen atoms are omitted for clarity. Selected bond lengths (Å) and angle (deg): O3–Pd1 2.11, O4–Pd1 3.09, C29–Pd1 1.99, C1–Pd1 2.46; H29---O3 2.38; C29–Pd1–O3 81.7, C29–H29---O3 96.9.

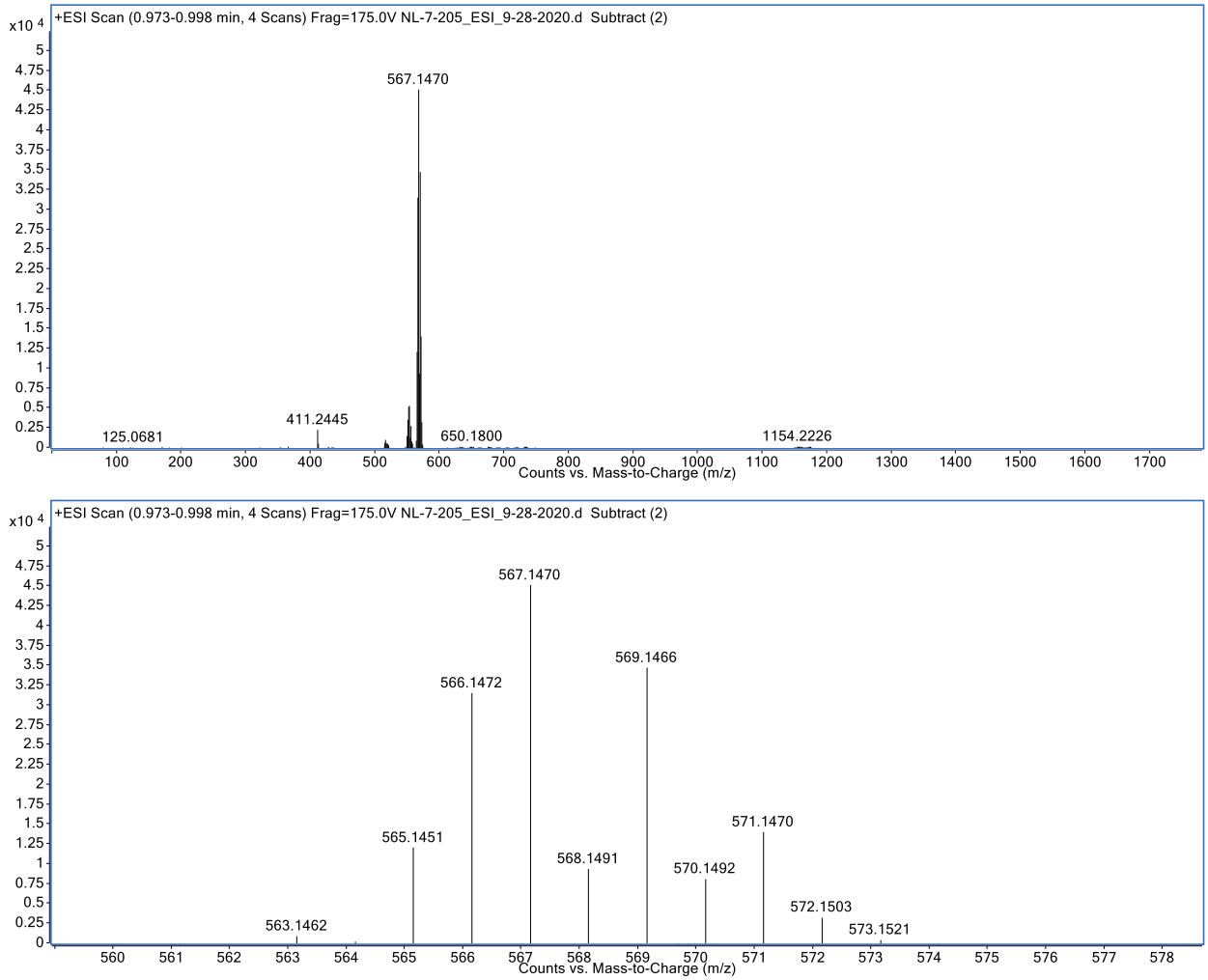

Figure 2.22 ESI+ Scans for HRMS analysis of **II-CHF$_2$**–$OCOCHF_2$.

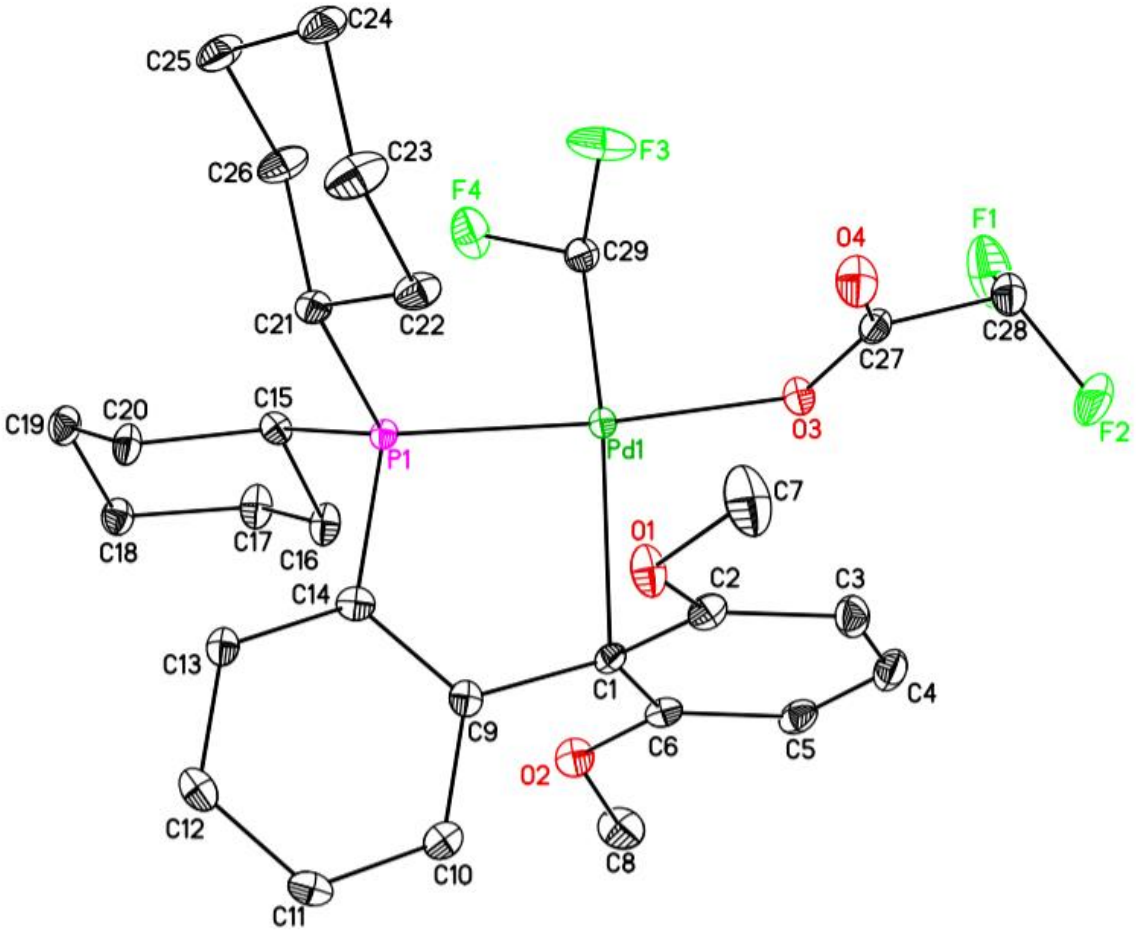

Structure determination of II-CHF2. Yellow blocks of II-CHF_2 were grown via vapor diffusion of pentane/diethyl ether solution into tetrahydrofuran solution of the compound at 22 °C. A crystal of dimensions 0.22 x 0.20 x 0.16 mm was mounted on a Rigaku AFC10K Saturn 944+ CCD-based X-ray diffractometer equipped with a low temperature device and Micromax-007HF Cu-target micro-focus rotating anode (l = 1.54187 A) operated at 1.2 kW power (40 kV, 30 mA). The X-ray intensities were measured at 85(1) K with the detector placed at a distance 42.00 mm from the crystal. A total of 2028 images were collected with an oscillation width of 1.0° in w. The exposure times were 1 sec. for the low angle images, 3 sec. for high angle. Rigaku d*trek images were exported to CrysAlisPro for processing and corrected for absorption. The integration of the data yielded a total of 42225 reflections to a maximum 2q value of 138.80° of which 5201 were independent and 5166 were greater than 2s(I). The final cell constants (Table S4) were based

on the xyz centroids of 29274 reflections above 10s(I). Analysis of the data showed negligible decay during data collection. The structure was solved and refined with the Bruker SHELXTL (version 2018/3) software package, using the space group P2(1)/c with Z = 4 for the formula C29H37O4F4PPd. All non-hydrogen atoms were refined anisotropically with the hydrogen atoms placed in idealized positions. The difluoroacetato group is rotationally disordered. Full matrix least-squares refinement based on F2 converged at R1 = 0.0317 and wR2 = 0.0851 [based on I > 2sigma(I)], R1 = 0.0319 and wR2 = 0.0853 for all data. Additional details are presented in Table 4 and are given as Supporting Information in a CIF file. Acknowledgement is made for funding from NSF grant CHE-0840456 for X-ray instrumentation.

G.M. Sheldrick (2015) "Crystal structure refinement with SHELXL", Acta Cryst., C71, 3-8 (Open Access).

CrystalClear Expert 2.0 r16, Rigaku Americas and Rigaku Corporation (2014), Rigaku Americas, 9009, TX, USA 77381-5209, Rigaku Tokyo, 196-8666, Japan.

CrysAlisPro 1.171.38.41 (Rigaku Oxford Diffraction, 2015).

Empirical formula	$C_{29}H_{37}F_4O_4PPd$	
Formula weight	662.95	
Temperature	85(2) K	
Wavelength	1.54184 A	
Crystal system	Monoclinic	
space group	P2(1)/c	
Unit cell dimensions	a = 9.68570(10) A	α = 90 °
	b = 18.93400(10) A	ß = 91.4640(10)°
	c = 15.37910(10) A	γ = 90 °
Volume	2819.44(4) A^3	
Z	4	
Calculated density	1.562 Mg/m^3	
Absorption coefficient	6.373 mm^-1	

F(000)	1360
Crystal size	0.220 x 0.200 x 0.160 mm
Theta range for data collection	3.703 to 69.400 deg.
Limiting indices	-11<=h<=11, -22<=k<=22, -17<=l<=18
Reflections collected / unique	42225 / 5201 [R(int) = 0.0734]
Completeness to theta	67.684 (99.0 %)
Absorption correction	Semi-empirical from equivalents
Max. and min. transmission	1.00000 and 0.64949
Refinement method	Full-matrix least-squares on F^2
Data / restraints / parameters	5201 / 6 / 366
Goodness-of-fit on F^2	1.054
Final R indices [I>2σ(I)]	R1 = 0.0317, wR2 = 0.0851
R indices (all data)	R1 = 0.0319, wR2 = 0.0853
Largest diff. peak and hole	0.799 and -0.744 $e.A^{-3}$

Table 2.7. Addition details regarding crystals of **II-CHF_2**.

	x	y	z	U(eq)
Pd(1)	7311(1)	3028(1)	3624(1)	8(1)
P(1)	7388(1)	2039(1)	4429(1)	8(1)
C(28)	5771(2)	4882(1)	2276(2)	16(1)
F(1)	6121(2)	4680(1)	1465(1)	35(1)
F(2)	6549(2)	5452(1)	2513(2)	29(1)
C(28A)	5771(2)	4882(1)	2276(2)	16(1)
F(1A)	6121(2)	4680(1)	1465(1)	35(1)
F(2A)	4496(7)	5092(4)	2254(5)	41(3)
F(3)	4813(1)	2651(1)	2780(1)	27(1)
F(4)	6393(2)	1893(1)	2465(1)	24(1)
O(1)	7084(2)	3752(1)	5572(1)	14(1)
O(2)	11039(2)	3195(1)	4036(1)	15(1)
O(3)	7094(2)	3928(1)	2821(1)	12(1)
O(4)	5151(2)	4229(1)	3515(1)	18(1)

C(1)	8980(2)	3458(1)	4735(1)	9(1)
C(2)	7952(2)	3961(1)	4945(2)	12(1)
C(3)	7932(2)	4634(1)	4570(2)	15(1)
C(4)	8958(3)	4812(1)	4006(2)	16(1)
C(5)	10016(2)	4349(1)	3797(2)	14(1)
C(6)	10032(2)	3677(1)	4164(2)	11(1)
C(7)	5933(3)	4204(1)	5754(2)	23(1)
C(8)	12257(2)	3432(2)	3609(2)	21(1)
C(9)	9254(2)	2863(1)	5366(2)	9(1)
C(10)	10231(3)	2987(1)	6034(2)	12(1)
C(11)	10433(2)	2503(1)	6703(2)	12(1)
C(12)	9645(2)	1892(1)	6722(2)	12(1)
C(13)	8699(2)	1752(1)	6054(2)	10(1)
C(14)	8517(2)	2228(1)	5360(1)	10(1)
C(15)	8127(2)	1265(1)	3887(1)	10(1)
C(16)	9514(2)	1472(1)	3493(2)	13(1)
C(17)	10062(3)	870(1)	2934(2)	16(1)
C(18)	10177(2)	180(1)	3446(2)	14(1)
C(19)	8803(2)	-12(1)	3854(2)	15(1)
C(20)	8289(2)	589(1)	4429(2)	13(1)
C(21)	5768(2)	1750(1)	4915(2)	10(1)
C(22)	5028(2)	2390(1)	5298(2)	14(1)
C(23)	3699(3)	2168(2)	5742(2)	20(1)
C(24)	2745(2)	1758(1)	5123(2)	16(1)
C(25)	3488(2)	1120(1)	4752(2)	16(1)
C(26)	4802(2)	1337(1)	4293(2)	16(1)
C(27)	6002(2)	4288(1)	2941(2)	12(1)
C(29)	6200(2)	2589(1)	2656(2)	13(1)

Table 2.8 Atomic coordinates (x 10^4) and equivalent isotropic displacement parameters (A^2 x 10^3) for **II-CHF2**. U(eq) is defined as one third of the trace of the orthogonalized Uij tensor.

Pd(1)-C(29)	1.995(2)
Pd(1)-O(3)	2.1124(16)
Pd(1)-P(1)	2.2440(6)
Pd(1)-C(1)	2.461(2)
P(1)-C(14)	1.816(2)
P(1)-C(15)	1.839(2)
P(1)-C(21)	1.839(2)
C(28)-F(1)	1.355(3)
C(28)-F(2)	1.361(3)
C(28)-C(27)	1.532(3)
C(28)-H(28)	1.0000

C(28A)-F(2A)	1.297(7)
C(28A)-F(1A)	1.355(3)
C(28A)-C(27)	1.532(3)
C(28A)-H(28A)	1.0000
F(3)-C(29)	1.367(3)
F(4)-C(29)	1.365(3)
O(1)-C(2)	1.355(3)
O(1)-C(7)	1.439(3)
O(2)-C(6)	1.354(3)
O(2)-C(8)	1.437(3)
O(3)-C(27)	1.276(3)
O(4)-C(27)	1.228(3)
C(1)-C(2)	1.421(3)
C(1)-C(6)	1.424(3)
C(1)-C(9)	1.506(3)
C(2)-C(3)	1.398(3)
C(3)-C(4)	1.378(3)
C(3)-H(3)	0.9500
C(4)-C(5)	1.393(4)
C(4)-H(4)	0.9500
C(5)-C(6)	1.391(3)
C(5)-H(5)	0.9500
C(7)-H(7A)	0.9800
C(7)-H(7B)	0.9800
C(7)-H(7C)	0.9800
C(8)-H(8A)	0.9800
C(8)-H(8B)	0.9800
C(8)-H(8C)	0.9800
C(9)-C(14)	1.397(3)
C(9)-C(10)	1.399(4)
C(10)-C(11)	1.386(3)
C(10)-H(10)	0.9500
C(11)-C(12)	1.387(3)
C(11)-H(11)	0.9500
C(12)-C(13)	1.385(3)
C(12)-H(12)	0.9500
C(13)-C(14)	1.405(3)
C(13)-H(13)	0.9500
C(15)-C(20)	1.534(3)
C(15)-C(16)	1.539(3)
C(15)-H(15)	1.0000
C(16)-C(17)	1.531(3)
C(16)-H(16A)	0.9900
C(16)-H(16B)	0.9900

C(17)-C(18)	1.528(3)
C(17)-H(17A)	0.9900
C(17)-H(17B)	0.9900
C(18)-C(19)	1.529(3)
C(18)-H(18A)	0.9900
C(18)-H(18B)	0.9900
C(19)-C(20)	1.530(3)
C(19)-H(19A)	0.9900
C(19)-H(19B)	0.9900
C(20)-H(20A)	0.9900
C(20)-H(20B)	0.9900
C(21)-C(22)	1.535(3)
C(21)-C(26)	1.535(3)
C(21)-H(21)	1.0000
C(22)-C(23)	1.531(3)
C(22)-H(22A)	0.9900
C(22)-H(22B)	0.9900
C(23)-C(24)	1.523(3)
C(23)-H(23A)	0.9900
C(23)-H(23B)	0.9900
C(24)-C(25)	1.525(3)
C(24)-H(24A)	0.9900
C(24)-H(24B)	0.9900
C(25)-C(26)	1.528(3)
C(25)-H(25A)	0.9900
C(25)-H(25B)	0.9900
C(26)-H(26A)	0.9900
C(26)-H(26B)	0.9900
C(29)-H(29)	1.0000

C(29)-Pd(1)-O(3)	81.69(8)
C(29)-Pd(1)-P(1)	94.23(7)
O(3)-Pd(1)-P(1)	175.49(5)
C(29)-Pd(1)-C(1)	171.11(8)
O(3)-Pd(1)-C(1)	101.09(7)
P(1)-Pd(1)-C(1)	83.23(5)
C(14)-P(1)-C(15)	106.35(10)
C(14)-P(1)-C(21)	103.93(10)
C(15)-P(1)-C(21)	107.06(10)
C(14)-P(1)-Pd(1)	106.28(8)
C(15)-P(1)-Pd(1)	115.02(7)
C(21)-P(1)-Pd(1)	117.13(8)
F(1)-C(28)-F(2)	108.7(2)
F(1)-C(28)-C(27)	111.84(19)

F(2)-C(28)-C(27)	109.5(2)
F(1)-C(28)-H(28)	108.9
F(2)-C(28)-H(28)	108.9
C(27)-C(28)-H(28)	108.9
F(2A)-C(28A)-F(1A)	108.9(4)
F(2A)-C(28A)-C(27)	111.4(4)
F(1A)-C(28A)-C(27)	111.84(19)
F(2A)-C(28A)-H(28A)	108.2
F(1A)-C(28A)-H(28A)	108.2
C(27)-C(28A)-H(28A)	108.2
C(2)-O(1)-C(7)	117.50(18)
C(6)-O(2)-C(8)	117.26(19)
C(27)-O(3)-Pd(1)	114.68(14)
C(2)-C(1)-C(6)	117.5(2)
C(2)-C(1)-C(9)	117.91(19)
C(6)-C(1)-C(9)	119.91(19)
C(2)-C(1)-Pd(1)	85.87(13)
C(6)-C(1)-Pd(1)	97.81(14)
C(9)-C(1)-Pd(1)	107.52(14)
O(1)-C(2)-C(3)	123.9(2)
O(1)-C(2)-C(1)	114.6(2)
C(3)-C(2)-C(1)	121.3(2)
C(4)-C(3)-C(2)	118.7(2)
C(4)-C(3)-H(3)	120.6
C(2)-C(3)-H(3)	120.6
C(3)-C(4)-C(5)	122.5(2)
C(3)-C(4)-H(4)	118.7
C(5)-C(4)-H(4)	118.7
C(6)-C(5)-C(4)	118.8(2)
C(6)-C(5)-H(5)	120.6
C(4)-C(5)-H(5)	120.6
O(2)-C(6)-C(5)	123.9(2)
O(2)-C(6)-C(1)	115.0(2)
C(5)-C(6)-C(1)	121.1(2)
O(1)-C(7)-H(7A)	109.5
O(1)-C(7)-H(7B)	109.5
H(7A)-C(7)-H(7B)	109.5
O(1)-C(7)-H(7C)	109.5
H(7A)-C(7)-H(7C)	109.5
H(7B)-C(7)-H(7C)	109.5
O(2)-C(8)-H(8A)	109.5
O(2)-C(8)-H(8B)	109.5
H(8A)-C(8)-H(8B)	109.5
O(2)-C(8)-H(8C)	109.5

H(8A)-C(8)-H(8C)	109.5
H(8B)-C(8)-H(8C)	109.5
C(14)-C(9)-C(10)	119.0(2)
C(14)-C(9)-C(1)	123.9(2)
C(10)-C(9)-C(1)	116.9(2)
C(11)-C(10)-C(9)	120.9(2)
C(11)-C(10)-H(10)	119.5
C(9)-C(10)-H(10)	119.5
C(10)-C(11)-C(12)	120.0(2)
C(10)-C(11)-H(11)	120.0
C(12)-C(11)-H(11)	120.0
C(13)-C(12)-C(11)	119.8(2)
C(13)-C(12)-H(12)	120.1
C(11)-C(12)-H(12)	120.1
C(12)-C(13)-C(14)	120.6(2)
C(12)-C(13)-H(13)	119.7
C(14)-C(13)-H(13)	119.7
C(9)-C(14)-C(13)	119.5(2)
C(9)-C(14)-P(1)	118.22(17)
C(13)-C(14)-P(1)	122.25(17)
C(20)-C(15)-C(16)	110.35(18)
C(20)-C(15)-P(1)	117.05(15)
C(16)-C(15)-P(1)	109.21(15)
C(20)-C(15)-H(15)	106.5
C(16)-C(15)-H(15)	106.5
P(1)-C(15)-H(15)	106.5
C(17)-C(16)-C(15)	110.47(19)
C(17)-C(16)-H(16A)	109.6
C(15)-C(16)-H(16A)	109.6
C(17)-C(16)-H(16B)	109.6
C(15)-C(16)-H(16B)	109.6
H(16A)-C(16)-H(16B)	108.1
C(18)-C(17)-C(16)	111.67(19)
C(18)-C(17)-H(17A)	109.3
C(16)-C(17)-H(17A)	109.3
C(18)-C(17)-H(17B)	109.3
C(16)-C(17)-H(17B)	109.3
H(17A)-C(17)-H(17B)	107.9
C(17)-C(18)-C(19)	111.15(19)
C(17)-C(18)-H(18A)	109.4
C(19)-C(18)-H(18A)	109.4
C(17)-C(18)-H(18B)	109.4
C(19)-C(18)-H(18B)	109.4
H(18A)-C(18)-H(18B)	108.0

C(18)-C(19)-C(20)	111.12(19)
C(18)-C(19)-H(19A)	109.4
C(20)-C(19)-H(19A)	109.4
C(18)-C(19)-H(19B)	109.4
C(20)-C(19)-H(19B)	109.4
H(19A)-C(19)-H(19B)	108.0
C(19)-C(20)-C(15)	109.68(19)
C(19)-C(20)-H(20A)	109.7
C(15)-C(20)-H(20A)	109.7
C(19)-C(20)-H(20B)	109.7
C(15)-C(20)-H(20B)	109.7
H(20A)-C(20)-H(20B)	108.2
C(22)-C(21)-C(26)	110.99(19)
C(22)-C(21)-P(1)	109.45(15)
C(26)-C(21)-P(1)	114.22(16)
C(22)-C(21)-H(21)	107.3
C(26)-C(21)-H(21)	107.3
P(1)-C(21)-H(21)	107.3
C(23)-C(22)-C(21)	111.12(19)
C(23)-C(22)-H(22A)	109.4
C(21)-C(22)-H(22A)	109.4
C(23)-C(22)-H(22B)	109.4
C(21)-C(22)-H(22B)	109.4
H(22A)-C(22)-H(22B)	108.0
C(24)-C(23)-C(22)	111.4(2)
C(24)-C(23)-H(23A)	109.4
C(22)-C(23)-H(23A)	109.4
C(24)-C(23)-H(23B)	109.4
C(22)-C(23)-H(23B)	109.4
H(23A)-C(23)-H(23B)	108.0
C(23)-C(24)-C(25)	110.7(2)
C(23)-C(24)-H(24A)	109.5
C(25)-C(24)-H(24A)	109.5
C(23)-C(24)-H(24B)	109.5
C(25)-C(24)-H(24B)	109.5
H(24A)-C(24)-H(24B)	108.1
C(24)-C(25)-C(26)	111.44(19)
C(24)-C(25)-H(25A)	109.3
C(26)-C(25)-H(25A)	109.3
C(24)-C(25)-H(25B)	109.3
C(26)-C(25)-H(25B)	109.3
H(25A)-C(25)-H(25B)	108.0
C(25)-C(26)-C(21)	110.50(19)
C(25)-C(26)-H(26A)	109.5

C(21)-C(26)-H(26A)	109.5
C(25)-C(26)-H(26B)	109.5
C(21)-C(26)-H(26B)	109.5
H(26A)-C(26)-H(26B)	108.1
O(4)-C(27)-O(3)	129.0(2)
O(4)-C(27)-C(28)	117.2(2)
O(3)-C(27)-C(28)	113.78(19)
O(4)-C(27)-C(28A)	117.2(2)
O(3)-C(27)-C(28A)	113.78(19)
F(4)-C(29)-F(3)	104.67(19)
F(4)-C(29)-Pd(1)	119.26(16)
F(3)-C(29)-Pd(1)	111.95(15)
F(4)-C(29)-H(29)	106.8
F(3)-C(29)-H(29)	106.8
Pd(1)-C(29)-H(29)	106.8

Table 2.9. Bond lengths [Å] and angles [deg] for II-CHF_2.

General procedure A for the stoichiometric transmetalation of complex II-CHF_2 with various aryl boron-based nucleophiles. A 4 mL vial equipped with a stir bar was charged with **II-CHF_2** (19.9 mg, 0.03 mmol, 3.0 equiv) and anhydrous tetrahydrofuran (0.6 mL). To the stirred solution, a THF solution of 4-fluorotoluene (0.3 mL, 0.1 M, 0.03 mmol, 3 equiv) was added. The solution was divided into three separate solutions (0.3 mL each), each in a 4 mL vial equipped with a stir bar. The first solution was transferred to a screw-cap NMR tube and used for ^{19}F NMR analysis (t = 0). To each of the remaining solutions was added one of the following nucleophiles: 4-phenyl boronic acid **1a**, 4-(5,5-dimethyl-1,3,2-dioxaborinan-2-yl)benzonitrile, **1b** (2.2 mg, 0.01 mmol, 1.0 equiv) or 4-(4,4,5,5-tetramethyl-1,3,2-dioxaborolan-2-yl)benzonitrile, **1c** (2.3 mg, 0.01 mmol, 1.0 equiv). Each solution was stirred for 0.25 h, transferred to a screw cap NMR tube, and analyzed via ^{19}F NMR spectroscopy. The spectra are shown in Figure S12. After 0.25 h, 40% of product **1** was observed with the reaction with 45% of **II-CHF_2** remaining. Trace product **1** was observed using neopentyl boronate ester **1b**, whereas no detectable product was observed in the reaction between **II-CHF_2** and pinacol boronate ester **1c.** Notably, the Pd–aryl intermediate is not observed, only the organic product **1** was observed at -114.2 ppm (d, J = 56.4 Hz) by ^{19}F NMR spectroscopy as result of transmetalation and reductive elimination at room temperature.

General procedure B for the stoichiometric transmetalation at II-CHF_2 with added NMe_4F. A 4 mL vial equipped with a stir bar was charged with **II-CHF_2** (6.6 mg, 0.01 mmol, 0.5 equiv) and anhydrous tetrahydrofuran (0.2 mL). To this was added a THF solution of 4-fluorotoluene (0.1 mL, 0.1 M, 0.01 mmol, 1.0 equiv) then solid NMe_4F•^{t}AmylOH (3.6 mg, 0.02 mmol, 2.0 equiv).[13c] The suspension was stirred for 0.5 h, filtered through a syringe filter, then transferred to a screw cap NMR tube, sealed with a Teflon-lined cap, and analyzed by ^{19}F NMR spectroscopy. The formation of a distinct Pd-F intermediate in 12% yield is observed, based on a diagnostic resonance at –349.5 ppm.[19] Moreover, several new peaks appear in the Pd-CHF_2 region (–86 to –93 ppm). Upon addition of substrate **1b** (2.2 mg, 0.01 mmol, 1.0 equiv) to this sample, the Pd–F intermediate disappears, and organic product **1** was formed in 27% yield

Procedure for transmetalation of II-CHF_2 with 19b. The general procedure B was followed resulting in 4% of Pd–F observed by ^{19}F NMR with 4-fluorotoluene internal standard. After addition of substrate **19b** (2.2 mg, 0.01 mmol, 1.0 equiv) to this sample, the Pd–F signal was consumed and organic product **19** was formed in 26% yield by ^{19}F NMR (Figure S14, D). Characterized product **19** in situ: **^{19}F NMR** (376 MHz) δ -108.96 (d, *J* = 56.7 Hz, 2F).

Procedure for transmetalation with 2-(4-fluorophenyl)-5,5-dimethyl-1,3,2-dioxaborinane. The general procedure B was followed resulting in 4% of Pd–F observed by ^{19}F NMR with 4-fluorotoluene internal standard. After addition of 2-(4-fluorophenyl)-5,5-dimethyl-1,3,2-dioxaborinane (2.0 mg, 0.01 mmol, 1.0 equiv) to this sample, the Pd–F signal was consumed and 1-(difluoromethyl)-4-fluorobenzene was formed in 30% yield by ^{19}F NMR. The remaining mass balance is 2-(4-fluorophenyl)-5,5-dimethyl-1,3,2-dioxaborinane (70%) observed at -111.47 ppm in the ^{19}F NMR. Characterized 1-(difluoromethyl)-4-fluorobenzene in situ: **^{19}F NMR** (376 MHz) δ -110.47 (d, *J* = 56.4 Hz, 2F), -111.35 (m, 1F).

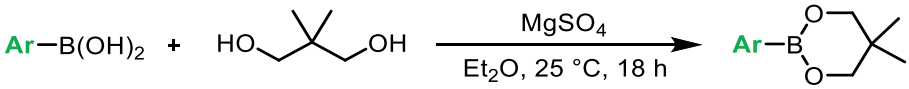

General procedure for the synthesis of aryl neopentyl boronate esters from aryl boronic acids (Method A)[16b]: Under ambient conditions, the respective aryl boronic acid (2.0 mmol, 1.0 equiv), 2,2-dimethyl-1,3-propanediol (208 mg, 2.0 mmol, 1.0 equiv), and anhydrous magnesium

sulfate (240 mg, 2.0 mmol, 1.0 equiv) were weighed into a 20 mL vial. The vial was equipped with a magnetic stirbar, and Et_2O (10 mL) was added. The vial was sealed with a Teflon-lined screw cap, and the resulting suspension was stirred under ambient conditions for 18 h. The reaction mixture was then filtered through a 3 cm x 3 cm x 3 cm celite plug set with Et_2O. The celite plug was washed with Et_2O (100 mL). Solvent was removed *in vacuo* to afford the corresponding aryl neopentyl boronate ester as a white solid for use in catalysis without further purification, unless stated otherwise.[16b]

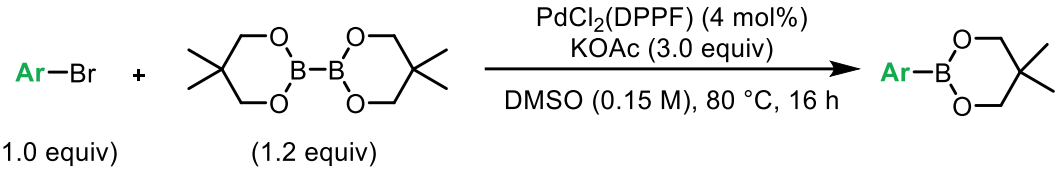

General procedure for synthesis of aryl neopentyl boronate esters from aryl bromides (Method B) [16c]**:** To a 20 mL vial equipped with a magnetic stirbar was added $PdCl_2$(DPPF) (58 mg, 0.08 mmol, 0.04 equiv), anhydrous potassium acetate (589 mg, 6.0 mmol, 3.0 equiv), bis(neopentyl glycolato)diboron (542 mg, 2.4 mmol, 1.2 equiv), and aryl bromide (2.0 mmol, 1.0 equiv). To these solids was added anhydrous dimethyl sulfoxide (14 mL), forming a red-orange suspension. The reaction was sealed with a Telfon-lined cap, removed from the glovebox, and heated at 80 ºC for 18 h. The reaction mixture was allowed to cool to room temperature, then poured into ice-cold deionized water (75 mL). The mixture was extracted with ethyl acetate (3 x 40 mL), and the combined organic extracts were washed with saturated solution of aqueous NaCl (50 mL), dried over anhydrous sodium sulfate, and concenrated *in vacuo*. The crude residue was dissolved in minimal dichloromethane and purified via flash chromatography on silica gel using ethyl acetate/hexanes gradient elution (5-50%). Removal of solvent afforded the aryl neopentyl boronate ester as a white solid to be used in catalysis without further purification, unless otherwise stated.[16c]

The ^{13}C NMR signal corresponding to the carbon of the C–B bond for all boronate esters below is not observed due to broadening.[16d]

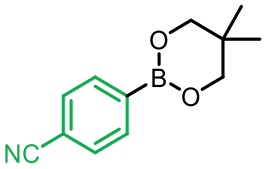

Preparation of 5,5-dimethyl-1,3,2-dioxaborinan-2-yl)benzonitrile (1b). Method A was followed and yielded a white solid (427 mg, 99% yield). **^{1}H NMR** (700 MHz, $CDCl_3$) δ 7.87 (d, *J* = 7.7 Hz, 2H), 7.62 (d, *J* = 7.7 Hz, 2H), 3.78 (s, 4H), 1.03 (s, 6H). **^{13}C NMR** (176 MHz, $CDCl_3$) δ 134.36, 131.16, 119.26, 114.07, 72.57, 32.05, 21.98. **HRMS** (positive ion GC-APCI) calcd. for $C_{12}H_{14}BNO_2$ [M+H] *m/z* 216.1190. Found 216.1194.

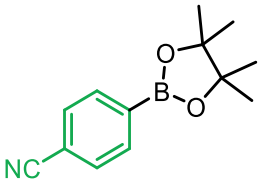

Preparation of 4-(4,4,5,5-tetramethyl-1,3,2-dioxaborolan-2-yl)benzonitrile (1c). Method A was followed, except 2,3-dimethylbutane-2,3-diol (1.0 equiv) was used instead of 2,2-dimethyl-1,3-propanediol. The aryl pinacol boronate ester was obtained as white solid (455 mg, 99% yield). **^{1}H NMR** (700 MHz, $CDCl_3$) δ 7.88 (d, *J* = 7.9 Hz, 2H), 7.63 (d, *J* = 7.9 Hz, 2H), 1.35 (s, 12H). **^{13}C NMR** (176 MHz, $CDCl_3$) δ 135.22, 131.25, 118.99, 114.67, 84.62, 25.00. **HRMS** (positive ion GC-APCI) calcd. for $C_{13}H_{16}BNO_2$ [M+H] *m/z* 230.1347. Found 230.1354.

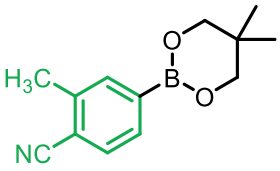

Preparation of 4-(5,5-dimethyl-1,3,2-dioxaborinan-2-yl)-2-methylbenzonitrile (2b). Method B was followed and yielded a white solid (302 mg, 66% yield). **^{1}H NMR** (401 MHz, $CDCl_3$) δ 7.73 (s, 1H), 7.66 (d, *J* = 7.7 Hz, 1H), 7.56 (d, *J* = 7.7 Hz, 1H), 3.78 (s, 4H), 2.54 (s, 3H), 1.02 (s, 6H). **^{13}C NMR** (176 MHz, $CDCl_3$) δ 140.73, 135.52, 131.60, 131.44, 118.55, 114.49, 72.57, 32.05, 21.99, 20.49. **HRMS** (positive ion GC-APCI) calcd. for $C_{13}H_{16}BNO_2$ [M+H] *m/z* 230.1374. Found 230.1352.

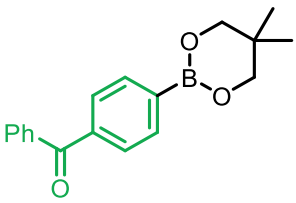

Preparation of (4-(5,5-dimethyl-1,3,2-dioxaborinan-2-yl)phenyl)(phenyl)methanone (3b). Method A was followed and yielded a white solid (560 mg, 95% yield). **^{1}H NMR** (401 MHz, $CDCl_3$) δ 7.91 (d, *J* = 8.2 Hz, 2H), 7.85-7.72 *(multiple peaks*, 4H), 7.62-7.55 (m, 1H), 7.48 (t, *J* = 7.6 Hz, 2H), 3.80 (s, 4H), 1.05 (s, 6H). **^{13}C NMR** (176 MHz, $CDCl_3$) δ 197.22,

139.42, 137.83, 133.80, 132.54, 130.25, 129.12, 128.39, 72.56, 32.07, 22.05. **HRMS** (ESI+) calcd. for $C_{18}H_{19}BO_3$ [M+H] *m/z* 295.1500. Found 295.1503.

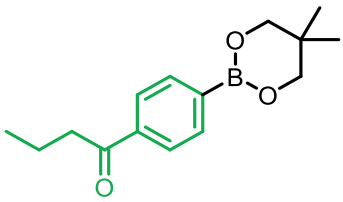

Preparation of 1-(4-(5,5-dimethyl-1,3,2-dioxaborinan-2-yl)phenyl)butan-1-one (4b). Method B was followed and yielded a white solid (422.6 mg, 81% yield). **^{1}H NMR** (500 MHz, $CDCl_3$) δ 8.13-7.76 (*multiple peaks*, 4H), 3.78 (s, 4H), 2.95 (t, *J* = 7.3 Hz, 2H), 1.81-1.72 (m, 2H), 1.08-0.98 *(multiple peaks*, 9H). **^{13}C NMR** (126 MHz, $CDCl_3$) δ 201.00, 138.77, 134.13, 127.09, 72.53, 40.84, 32.05, 22.03, 17.93, 14.04. **HRMS** (positive ion GC-APCI) calcd. for $C_{15}H_{21}BO_3$ [M+H] *m/z* 261.1657. Found 261.1661.

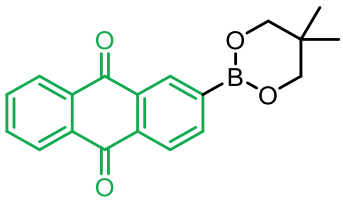

Preparation of 2-(5,5-dimethyl-1,3,2-dioxaborinan-2-yl)anthracene-9,10-dione (5b). Method B was followed and yielded a yellow solid (419 mg, 65% yield). **^{1}H NMR** (500 MHz, $CDCl_3$) δ 8.77-8.71 (m, 1H), 8.37-8.28 (*multiple peaks*, 2H), 8.27 (d, *J* = 7.6 Hz, 1H), 8.20 (dd, *J* = 7.7, 1.3 Hz, 1H), 7.83-7.75 (*multiple peaks*, 2H), 3.83 (s, 4H), 1.05 (s, 6H). **^{13}C NMR** (176 MHz, $CDCl_3$) δ 183.71, 183.51, 139.44, 134.91, 134.20, 134.07, 133.82, 133.78, 133.06, 132.54, 127.38, 127.29, 126.20, 72.62, 32.10, 22.04. **HRMS** (ESI+) calcd. for $C_{19}H_{17}BO_4$ [M+H] *m/z* 321.1293. Found 321.1306.

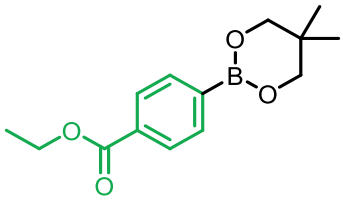

Preparation of ethyl 4-(5,5-dimethyl-1,3,2-dioxaborinan-2-yl)benzoate (6b). Method A was followed and yielded a white solid (471 mg, 90% yield). **^{1}H NMR** (401 MHz, $CDCl_3$) δ 8.01 (d, *J* = 8.2 Hz, 2H), 7.86 (d, *J* = 8.2 Hz, 2H), 4.38 (q, *J* = 7.1 Hz, 2H), 3.78 (s, 4H), 1.40 (t, *J* = 7.1 Hz, 3H), 1.03 (s, 6H). **^{13}C NMR** (176 MHz, $CDCl_3$) δ 166.99, 133.86, 132.32, 128.60, 72.53, 61.08, 32.05, 22.05, 14.49. **HRMS** (positive ion GC-APCI) calcd. for $C_{14}H_{19}BO_4$ [M+] *m/z* 263.1449. Found 263.1454.

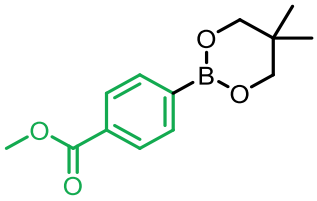

Preparation of methyl 4-(5,5-dimethyl-1,3,2-dioxaborinan-2-yl)benzoate (7b). Method A was followed and yielded a white solid (468 mg, 94% yield). **^{1}H NMR** (401 MHz, $CDCl_3$) δ 8.01 (d, *J* = 8.2 Hz, 2H), 7.86 (d, *J* = 8.2 Hz, 2H), 3.91 (s, 3H), 3.78 (s, 4H), 1.03 (s, 6H). **^{13}C NMR** (126 MHz, $CDCl_3$) δ 167.46, 133.90, 131.95, 128.64, 72.53, 52.22, 32.04, 22.04. **HRMS** (positive ion GC-APCI) calcd. for $C_{13}H_{17}BO_4$ [M+H] *m/z* 249.1293. Found 249.1298.

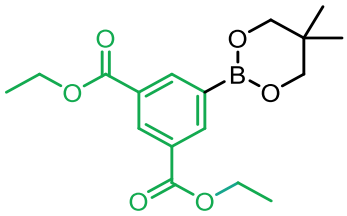

Preparation of diethyl 5-(5,5-dimethyl-1,3,2-dioxaborinan-2-yl)isophthalate (8b). Method A was followed and yielded a white solid (662 mg, 99% yield). **^{1}H NMR** (500 MHz, $CDCl_3$) δ 8.73 (s, 1H), 8.62 (s, 2H), 4.41 (q, *J* = 7.4 Hz, 4H), 3.80 (s, 4H), 1.41 (t, *J* = 7.5 Hz, 6H), 1.03 (s, 6H). **^{13}C NMR** (176 MHz, $CDCl_3$) δ 166.27, 139.11, 132.89, 130.33, 72.54, 61.31, 32.08, 22.01, 14.52. **HRMS** (positive ion GC-APCI) calcd. for $C_{17}H_{23}BO_6$ [M+H] *m/z* 335.166. Found 335.1164.

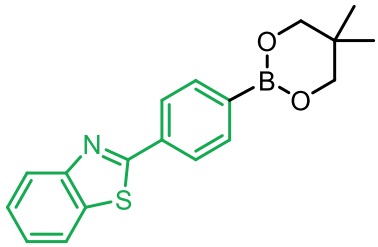

Preparation of 2-(4-(5,5-dimethyl-1,3,2-dioxaborinan-2-yl)phenyl)benzo[d]thiazole (9b). Method B was followed and yielded a white solid (595 mg, 91% yield). **^{1}H NMR** (500 MHz, $CDCl_3$) δ 8.08-7.90 (*multiple peaks*, 3H), 7.95-7.87 (*multiple peaks*, 3H), 7.49 (m, *J* = 7.7 Hz, 1H), 7.39 (t, *J* = 8.1 Hz, 1H), 3.80 (s, 4H), 1.05 (s, 6H). **^{13}C NMR** (126 MHz, $CDCl_3$) δ 168.42, 154.33, 135.48, 135.27, 134.62, 126.75, 126.45, 125.36, 123.43, 121.77, 72.55, 32.08, 22.08. **HRMS** (positive ion GC-APCI) calcd. for $C_{18}H_{18}BNO_2S$ [M+H] *m/z* 324.1224. Found 324.1234.

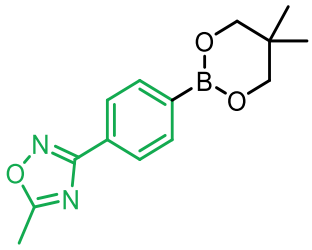

Preparation of 3-(4-(5,5-dimethyl-1,3,2-dioxaborinan-2-yl)phenyl)-5-methyl-1,2,4-oxadiazole (10b). Method B was followed and yielded a white solid (418 mg, 77% yield). **^{1}H NMR** (401 MHz, $CDCl_3$) δ 8.04 (d, *J* = 8.1 Hz, 2H), 7.90 (d, *J* = 8.1 Hz, 2H), 3.79 (s, 4H), 2.65 (s, 3H), 1.04 (s, 6H). **^{13}C NMR** (176 MHz, $CDCl_3$) δ 176.63, 168.68, 134.42, 128.71, 126.51, 72.52, 32.06, 22.06, 12.56. **HRMS** (positive ion GC-APCI) calcd. for $C_{14}H_{17}BN_2O_3$ [M+H] *m/z* 273.1405. Found 273.1408.

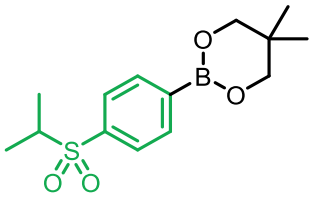

Preparation of 2-(4-(isopropylsulfonyl)phenyl)-5,5-dimethyl-1,3,2-dioxaborinane (11b). Method A was followed and yielded a white solid (569 mg, 96% yield). **^{1}H NMR** (401 MHz, $CDCl_3$) δ 7.96 (d, *J* = 8.3 Hz, 2H), 7.82 (d, *J* = 8.3 Hz, 2H), 3.78 (s, 4H), 3.17 (hept, *J* = 6.9 Hz, 1H), 1.26 (d, *J* = 6.9 Hz, 6H), 1.02 (s, 6H). **^{13}C NMR** (176 MHz, $CDCl_3$) δ 138.59, 134.42, 127.97, 72.54, 55.61, 32.01, 21.95, 15.78. **HRMS** (positive ion GC-APCI) calcd. for $C_{14}H_{21}BO_4S$ [M+NH_4] *m/z* 342.1592. Found 342.1909.

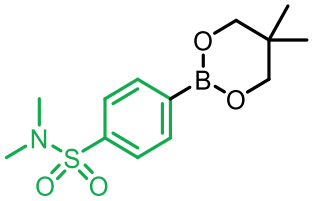

Preparation of 4-(5,5-dimethyl-1,3,2-dioxaborinan-2-yl)-N,N-dimethylbenzenesulfonamide (12b). Method A was followed and yielded a white solid (517 mg, 87% yield). **^{1}H NMR** (500 MHz, $CDCl_3$) δ 7.95 (d, *J* = 8.1 Hz, 2H), 7.81-7.69 (m, 2H), 3.79 (s, 4H), 2.68 (s, 6H), 1.03 (s, 6H). **^{13}C NMR** (176 MHz, $CDCl_3$) δ 137.09, 134.46, 126.75, 72.57, 38.08, 32.05, 21.99. **HRMS** (positive ion GC-APCI) calcd. for $C_{13}H_{20}BNO_4S$ [M+H] *m/z* 298.1279. Found 298.1292.

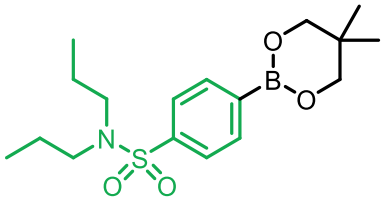

Preparation of 4-(5,5-dimethyl-1,3,2-dioxaborinan-2-yl)-N,N-dipropylbenzenesulfonamide (13b). Substrate was synthesized and isolated according to a previously reported procedure[20e] and yielded a white solid (80.5 mg, 76% yield). **^{1}H NMR** (401 MHz, $CDCl_3$) δ 7.90 (d, *J* = 8.3 Hz, 2H), 7.76 (d, *J* = 8.3 Hz, 2H), 3.78 (s, 4H), 3.10-3.03 (m, 4H), 1.58-1.48 (m, 4H), 1.03 (s, 6H), 0.86 (t, *J* = 7.4 Hz, 6H). **^{13}C NMR** (176 MHz, $CDCl_3$) δ 141.92, 134.46, 126.08, 72.57, 50.12, 32.06, 22.11, 22.03, 11.34. **HRMS** (positive ion GC-APCI) calcd. for $C_{17}H_{28}BNO_4S$ [M+H] *m/z* 354.1905. Found 354.1905.

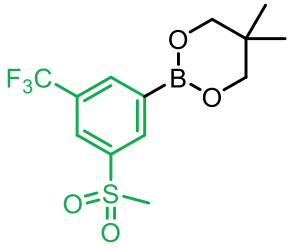

Preparation of 5,5-dimethyl-2-(3-(methylsulfonyl)-5-(trifluoromethyl)phenyl)-1,3,2-dioxaborinane (14b). Method B was followed and yielded a white solid (544 mg, 81% yield). **^{1}H NMR** (500 MHz, $CDCl_3$) δ 8.54 (s, 1H), 8.31 (s, 1H), 8.25 (s, 1H), 3.81 (s, 4H), 3.09 (s, 3H), 1.04 (s, 6H). **^{19}F NMR** (377 MHz, $CDCl_3$) δ –62.90. **^{13}C NMR** (176 MHz, $CDCl_3$) δ 140.98, 135.97, 135.69 (q, *J* = 3.3 Hz), 131.40 (q, *J* = 33.3 Hz), 126.35 (q, *J*

= 3.7 Hz), 123.50 (q, *J* = 273.0 Hz), 72.66, 44.55, 32.14, 21.95. **HRMS** (positive ion GC-APCI) calcd. for $C_{13}H_{16}BF_3O_4S$ [M+H] *m/z* 337.0887. Found 337.0898.

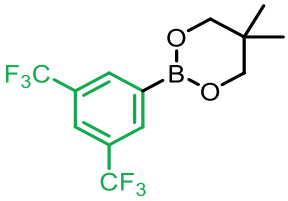

Preparation of 2-(3,5-bis(trifluoromethyl)phenyl)-5,5-dimethyl-1,3,2-dioxaborinane (15b). Method A was followed and yielded a white solid (639 mg, 98% yield). **^{1}H NMR** (500 MHz, $CDCl_3$) δ 8.24 (s, 2H), 7.91 (s, 1H), 3.81 (s, 4H), 1.04 (s, 6H). **^{19}F NMR** (377 MHz, $CDCl_3$) δ –62.87. **^{13}C NMR** (176 MHz, $CDCl_3$) δ 133.99, 130.79 (q, *J* = 32.9 Hz), 124.30, 123.82 (q, *J* = 272.5 Hz), 72.64, 32.13, 21.96. **HRMS** (positive ion GC-APCI) calcd. for $C_{13}H_{13}BF_6O_2$ [M+H] *m/z* 327.0986. Found 327.0985.

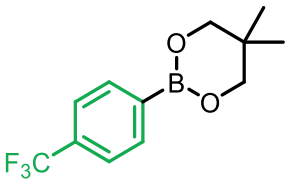

Preparation of 5,5-dimethyl-2-(4-(trifluoromethyl)phenyl)-1,3,2-dioxaborinane (16b). Method A was followed and yielded a white solid (485 mg, 94% yield). **^{1}H NMR** (500 MHz, $CDCl_3$) δ 7.90 (d, *J* = 7.7 Hz, 2H), 7.60 (d, *J* = 7.6 Hz, 2H), 3.79 (s, 4H), 1.03 (s, 6H). **^{19}F NMR** (377 MHz, $CDCl_3$) δ –62.93. **^{13}C NMR** (176 MHz, $CDCl_3$) δ 134.24, 132.41 (q, *J* = 31.9 Hz), 124.44 (q, *J* = 272.2 Hz), 124.31 (q, *J* = 3.7 Hz), 72.54, 32.05, 22.00. **HRMS** (positive ion GC-APCI) calcd. for $C_{12}H_{14}BF_3O_2$ [M+H] *m/z* 259.1112. Found 259.1120.

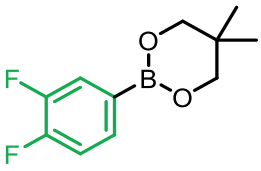

Preparation of 2-(3,4-difluorophenyl)-5,5-dimethyl-1,3,2-dioxaborinane (17b). Method A was followed and yielded a yellow solid (408 mg, 90% yield). **^{1}H NMR** (500 MHz, $CDCl_3$) δ 7.62-7.49 (*multiple peaks*, 2H), 7.12 (dt, *J* = 10.5, 7.9 Hz, 1H), 3.76 (s, 4H), 1.02 (s, 6H). **^{19}F NMR** (471 MHz, $CDCl_3$) δ –135.53 (dtd, *J* = 20.0, 9.5, 4.8 Hz), –140.35 (ddd, *J* = 19.8, 11.1, 7.7 Hz). **^{13}C NMR** (176 MHz, $CDCl_3$) δ 152.43 (dd, *J* = 251.1, 12.7 Hz), 150.31 (dd, *J* = 248.0, 11.9 Hz), 130.45 (dd, *J* = 6.6, 3.7 Hz), 122.54 (d, *J* = 15.2 Hz), 116.76 (d, *J* = 16.2 Hz), 72.50, 32.04, 22.00. **HRMS** (positive ion GC-APCI) calcd. for $C_{11}H_{13}BF_2O_2$ [M+H] *m/z* 227.1049. Found 227.1043.

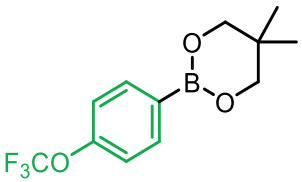

Preparation of 5,5-dimethyl-2-(4-(trifluoromethoxy)phenyl)-1,3,2-dioxaborinane (18b). Method A was followed and yielded a white solid (521 mg, 95% yield). **^{1}H NMR** (500 MHz, $CDCl_3$) δ 7.83 (d, *J* = 8.5 Hz, 2H), 7.18 (d, *J* = 7.9 Hz, 2H), 3.77 (s, 4H), 1.02 (s, 6H). **^{19}F NMR** (471

MHz, $CDCl_3$) δ –57.84. **^{13}C NMR** (176 MHz, $CDCl_3$) δ 151.46, 135.71, 120.62 (q, *J* = 257.1 Hz), 119.86, 72.49, 32.03, 21.99. **HRMS** (positive ion GC-APCI) calcd. for $C_{12}H_{14}BF_3O_3$ [M+H] *m/z* 275.1061. Found 275.1066.

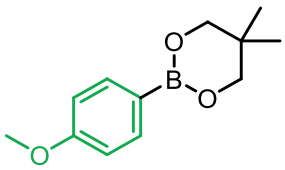

Preparation of 2-(4-methoxyphenyl)-5,5-dimethyl-1,3,2-dioxaborinane (19b). Method A was followed and yielded a white solid (406 mg, 93%). **^{1}H NMR** (500 MHz, $CDCl_3$) δ 7.74 (d, *J* = 8.5 Hz, 2H), 6.89 (d, *J* = 8.6 Hz, 2H), 3.82 (s, 3H), 3.75 (s, 4H), 1.02 (s, 6H). **^{13}C NMR** (126 MHz, $CDCl_3$) δ 161.89, 135.65, 113.29, 72.41, 55.20, 32.05, 22.08. **HRMS** (positive ion GC-APCI) calcd. for $C_{12}H_{17}BO_3$ [M+] *m/z* 220.1271. Found 220.1277.

General procedure for the catalytic reaction with DFAAn and fluoride salts. Pd[P(*o*-Tol)$_3$]$_2$ (4.1 mg, 0.005 mmol, 0.1 equiv, 3.6 mg) and SPhos (4.1 mg, 0.01 mmol, 0.2 equiv) were combined in THF (0.15 mL). The yellow suspension was stirred vigorously in a tall 10 mL vial for 15 min. To this solution was added a toluene-solution of DFAAn (0.2 mL, 0.75 M, 0.15 mmol, 3 equiv), then **1b** (10.8 mg, 0.05 mmol, 1 equiv), and finally CsF, NMe_4F, or NBu_4F (0.175 mmol, 3.5 equiv). The vial was sealed with a Teflon-lined screw cap with a septum, removed from the glovebox, and heated to the appropriate temperature for 3 h. After 3 h, the reaction mixture was allowed to cool to room temperature, and then 4-fluorotoluene (25 µL, 2.0 M in DCM, 1.0 equiv) was added as an internal standard, followed by dichloromethane (1.0 mL). The mixture was filtered through a plug of celite, and an aliquot of the solution was transferred to an NMR tube and analyzed by ^{19}F NMR spectroscopy to determine the yield of **1** as well as the identity of major by-products. Conducting the reaction at room temperature with 3 equiv of DFAAn and 3.6 equiv of CsF produced no observable quantity of **1**. However, in the crude ^{19}F NMR spectra of these reactions, DFAF was observed as a major side product. In the reactions with NMe_4F or NBu_4F, DFAF was not observed, and DFA was a major side product.

Reactions conducted at 130 ºC using 3 equiv of DFAAn and 3.6 equiv CsF produced modest but variable yields of **1** (17-31%). The range of 17-31% represents four reactions set up under identical conditions, with yields of 15%, 17%, 24%, and 31%, respectively, emphasizing the poor

reproducibility of this transformation. Using equimolar amounts of CsF to DFAAn under otherwise analogous conditions resulted in significantly lower yields of **1** (4-9%). Reactions conducted using NMe_4F or NBu_4F produced no observable quantity of **1** or DFAF in these experiments, as determined by ^{19}F NMR spectroscopy.

General procedure for the catalytic reaction with TFAAn and CsF. $Pd[P(o\text{-}Tol)_3]_2$ (4.1 mg, 0.005 mmol, 0.1 equiv, 3.6 mg) and SPhos (4.1 mg, 0.01 mmol, 0.2 equiv) were combined in THF (0.15 mL). The yellow suspension was stirred vigorously in a tall 10 mL vial for 15 min. To this solution was added a toluene-solution of TFAAn (0.2 mL, 0.75 M, 0.15 mmol, 3 equiv), then **1b** (10.8 mg, 0.05 mmol, 1 equiv), and finally CsF, (26.6 mg, 0.175 mmol, 3.5 equiv). The vial was sealed with a Teflon-lined screw cap with a septum, removed from the glovebox, and heated to the appropriate temperature for 3 h. After 3 h, the reaction mixture was allowed to cool to room temperature, and then 4-fluorotoluene (25 µL, 2.0 M in DCM, 1.0 equiv) was added as an internal standard, followed by dichloromethane (1.0 mL). The mixture was filtered through a plug of celite, and an aliquot of the solution was transferred to an NMR tube and analyzed by ^{19}F NMR spectroscopy to determine the yield of 4-trifluoromethylbenzonitrile, **1-CF₃**. Spiking in an authentic sample of **1-CF₃** to the crude reaction mixture confirmed its presence in the crude reaction mixture. The associated ^{19}F NMR spectra are shown below in Figure S15.

General procedure for the catalytic reaction with PFPAn and CsF. $Pd[P(o\text{-}Tol)_3]_2$ (4.1 mg, 0.005 mmol, 0.1 equiv, 3.6 mg) and SPhos (4.1 mg, 0.01 mmol, 0.2 equiv) were combined in THF (0.15 mL) and toluene (0.2 mL). The yellow suspension was stirred vigorously in a tall 10 mL vial for 15 min. To this solution was added a PFPAn (46.5 mg, 0.15 mmol, 3 equiv), then **1b** (10.8 mg, 0.05 mmol, 1 equiv), and finally CsF, (26.6 mg, 0.175 mmol, 3.5 equiv). The vial was sealed with a Teflon-lined screw cap with a septum, removed from the glovebox, and heated to the appropriate temperature for 3 h. After 3 h, the reaction mixture was allowed to cool to room temperature, and then 4-fluorotoluene (25 µL, 2.0 M in DCM, 1.0 equiv) was added as an internal standard, followed by dichloromethane (1.0 mL). The mixture was filtered through a plug of celite, and an aliquot of the solution was transferred to an NMR tube and analyzed by ^{19}F NMR spectroscopy (Figure S16) to determine the yield of **1-CF_2CF_3**. Spectral data for this product in this reaction (^{19}F NMR: -

85.51 ppm (s, 3F), -116.55 ppm (s, 2F)) are consistent with our previous report[5b] and other reports[5c] in the literature. Pentafluoropropionic acid (PFPA) was observed (55%) in the crude reaction.

General procedure for the distillation of difluoroacetyl fluoride. A 20 mL vial containing THF (7 mL) was placed in the freezer at –36 ºC and cooled for 15 min. In a 4 mL vial, a solution of difluoroacetic anhydride (4.35 g, 25 mmol, 1.0 equiv) in tetrahydrofuran (1 mL) was prepared and cooled to –36 ºC in the glovebox freezer for 15 min. While cooling, solid cesium fluoride (5.32 g, 35 mmol, 1.4 equiv) was added to a 25 mL round bottom flask equipped with a medium-sized stirbar. Cooled THF (5 mL) was added to the reaction flask. The cooled solution of anhydride in THF was then added to the flask containing CsF. The flask was quickly sealed with a rubber septum, removed from the glovebox, and allowed to stir at room temperature for 15 min. A short-path distillation apparatus equipped with nitrogen flow, water circulation, and a thermoprobe was fitted to a 25 mL round bottom collection flask cooled to 0 ºC in an ice water bath. The reaction flask was quickly connected to the distillation apparatus and heated from 25 ºC to 80 ºC in a water bath over a period of 30-45 min. The distillation was determined complete when minimal solvent remained in the reaction flask, the temperature of the gas in the apparatus as determined by the thermoprobe dropped below 45 ºC, and condensation into the collection flask slowed dramatically. Once complete, the collection flask containing the product in tetrahydrofuran was quickly sealed with a rubber septum, wrapped securely with black electrical tape, and short-cycled into the glovebox. In a 20 mL vial, trifluoromethoxybenzene (54 mg, 0.33 mmol, 1 equiv in F) was weighed as an internal standard, and a portion of the DFAF solution was added via syringe to the vial with total volume recorded. The trifluoromethoxybenzene was treated as approximately 0.05 mL in volume. After determining the total volume to be 5.4 mL and ensuring homogeneity, a sample of this solution was transferred to a screw cap NMR tube, diluted with 0.5 mL tetrahydrofuran, and analyzed via ^{19}F NMR spectroscopy. The bulk solution was sealed with a Teflon-lined screw cap and stored in the glovebox freezer. The spectrum is shown in Figure S19 with DFAF characterized *in situ*. Trace difluoroacetic acid is observed in all cases. The concentration of DFAF was calculated as mmol DFAF divided by the volume (mL) of solution as determined by ^{19}F NMR spectroscopy (Figure S17). A sample calculation is shown under Figure S12. In some cases, 4-fluorotoluene (110 mg, 1 mmol, treated as 0.11 mL in volume) or

fluorobenzene (96 mg, 1 mmol, treated at 0.095 mL in volume) was used as the internal standard to assess the yield from DFAF synthesis. *Characterized in situ:* **^{19}F NMR** (377 MHz, THF) δ 18.82 (m), –128.89 (dd, J = 51.9, 8.9 Hz).

General procedure for the optimization of catalytic decarbonylative aryl difluoromethylation. A Pd^0 source (0.005 mmol, 0.1 equiv) was dissolved with a phosphine ligand (0.01 mmol, 0.2 equiv) in 0.2 mL of anhydrous co-solvent and 0.05 mL THF. The yellow suspension was stirred in a tall 10 mL vial until homogenous, then **1b** (10.8 mg, 0.05 mmol, 1 equiv) was added. To the resulting mixture was added a cold (–36 °C) solution of DFAF (0.085 mL, 0.25 mmol, 2.96 M) in anhydrous THF. The reaction mixture was then diluted with THF to a total volume of 0.35 mL. The vial was sealed with a Teflon-lined screw cap with a septum (Figure S18), removed from the glovebox, and heated to a given temperature for 3 h. After 3 h, the reaction mixture was allowed to cool to room temperature. To it was added 4-fluorotoluene (25 µL, 2.0 M in DCM, 1.0 equiv) as an internal standard, followed by dichloromethane (1.0 mL). An aliquot of the solution was transferred to an NMR tube and analyzed by ^{19}F NMR spectroscopy.

Procedure for determining mass balance of catalytic reaction using 2-(4-fluorophenyl)-5,5-dimethyl-1,3,2-dioxaborinane. In a 4-mL vial with stirbar, $Pd[P(o\text{-}Tol)_3]_2$ (21.5 mg, 0.03 mmol, 0.6 equiv) and SPhos (24.6 mg, 0.06 mmol, 1.2 equiv) were combined with 1.2 mL toluene and 0.3 mL THF. The mixture was stirred for fifteen minutes. In each of five tall 10 mL vials equipped with a stir bar, 2-(4-fluorophenyl)-5,5-dimethyl-1,3,2-dioxaborinane (10 mg, 0.05 mmol, 1.0 equiv) was added. To each vial containing substrate was added an aliquot (0.25 mL) of the Pd/SPhos mixture. A THF solution of difluoroacetyl fluoride (0.095 mL, 0.25 mmol, 5 equiv) was added via syringe to each vial, and the vials were sealed with Teflon-lined screw caps. The vials were removed from the glovebox and heated at 150 ºC for 3 h. The reaction mixtures were allowed to cool to room temperature and then were combined. To the combined reaction mixture was added 4-fluorotoluene (125 µL, 2.0 M in DCM, 5.0 equiv) as an internal standard. An aliquot (0.4 mL) of the solution was transferred to an NMR tube and analyzed via ^{19}F NMR spectroscopy (Figure S19). The crude NMR yield of 1-(difluoromethyl)-4-fluorobenzene after 3 h was 17% as determined by ^{19}F NMR. After initial analysis, five additional NMR samples were prepared (0.4 mL each), and the following authentic standards were spiked in: 4-fluorophenyl boronic acid, 2-

(4-fluorophenyl)-5,5-dimethyl-1,3,2-dioxaborinane, 4-fluorobenzene and 4,4'difluorobiphenyl. Then, ^{19}F NMR analysis was conducted.

General procedure for the Pd-catalyzed decarbonylative difluoromethylation of aryl neopentyl boronate esters with difluoroacetyl fluoride. In a tall 10 mL vial equipped with a stir bar, $Pd[P(o\text{-}Tol)_3]_2$ (3.6 mg, 0.005 mmol, 0.1 equiv) and SPhos (4.2 mg, 0.01 mmol, 0.2 equiv) were combined in toluene (~0.2 mL) and THF (0.05 mL), and the resulting mixture was stirred vigorously for fifteen minutes at room temperature. A THF solution of difluoroacetyl fluoride (0.25 mmol, 5 equiv) was added via syringe, and the vial was sealed with a Teflon-lined screw cap and shaken gently to ensure homogeneity (total 0.35 mL volume). To this solution was added aryl neopentyl boronate ester **1b-19b** (0.05 mmol, 1.0 equiv). The vial was sealed with a Teflon-lined screw cap, removed from the glovebox, and heated at 150 ºC for 4-10 h. The reaction mixture was allowed to cool to room temperature. To it was added 4-fluorotoluene (25 µL, 2.0 M in DCM, 1.0 equiv) as an internal standard, followed by dichloromethane (1.0 mL). An aliquot of the solution was transferred to an NMR tube and analyzed via ^{19}F NMR spectroscopy. These reactions were observed to be highly sensitive to the purity of all components as well as the reaction vessel used. Efforts to scale the reaction using reaction vials, Schlenk glassware, pressure tubes, and microwave tubes of various volumes resulted in significantly diminished yields. For isolation of products **1-13**, six reactions were conducted in parallel to total 0.3 mmol scale. After the reaction time, the reaction mixtures were allowed to cool to room temperature and diluted with DCM and Et_2O. The mixture was filtered through a pad of silica and concentrated *in vacuo*. The crude material was then purified via silica gel chromatography using a gradient elution with solvent mixture A/B (%); A = 15% chloroform in diethyl ether and B = hexanes, unless otherwise stated. Fractions containing product were collected and carefully concentrated *in vacuo* to yield pure difluoromethyl arene product.

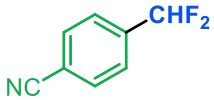

Preparation of 4-(difluoromethyl)benzonitrile (1). Reaction was conducted for isolation scale (6 reactions in parallel, 0.05 mmol scale each) using substrate **1b**. Reactions were run for 5 h. Reactions were carefully concentrated to due to the volatity of the product. Purification by flash chromatography on silica gel (0-10% A/B; B = pentanes) afforded

the product as a low-melting white solid (35 mg, 77% yield). **^{1}H NMR** (500 MHz, $CDCl_3$) δ 7.77 (d, *J* = 7.9 Hz, 2H), 7.64 (d, *J* = 7.9 Hz, 2H), 6.69 (t, *J* = 55.8 Hz, 1H). **^{19}F NMR** (471 MHz, $CDCl_3$) δ –113.26 (d, *J* = 55.8 Hz). **^{13}C NMR** (176 MHz, $CDCl_3$) δ 138.69 (t, *J* = 22.9 Hz), 132.73, 126.54 (t, *J* = 6.1 Hz), 118.02, 114.93 (t, *J* = 2.0 Hz), 113.45 (t, *J* = 240.7 Hz). **HRMS** (positive ion GC-APCI) calcd. for $C_8H_5F_2N$ [M+H] *m/z* 154.0463. Found 154.0457.

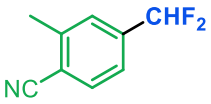

Preparation of 4-(difluoromethyl)-2-methylbenzonitrile (2). Reaction was conducted for isolation scale (6 reactions in parallel, 0.05 mmol scale each) using substrate **2b**. Reactions were run for 5 h. Purification by flash chromatography on silica gel (0-10% A/B; B = pentanes) afforded the purified product as a colorless oil (34 mg, 68% yield). **^{1}H NMR** (500 MHz, $CDCl_3$) δ 7.69 (d, *J* = 8.0 Hz, 1H), 7.47 (s, 1H), 7.42 (d, *J* = 8.0 Hz, 1H), 6.64 (t, *J* = 55.9 Hz, 1H), 2.60 (s, 3H). **^{19}F NMR** (377 MHz, $CDCl_3$) δ –113.12 (d, *J* = 55.9 Hz). **^{13}C NMR** (126 MHz, $CDCl_3$) δ 142.90, 138.48 (t, *J* = 22.6 Hz), 133.09, 127.46 (t, *J* = 6.1 Hz), 123.59 (t, *J* = 6.1 Hz), 117.36, 115.26 (t, *J* = 2.1 Hz), 113.58 (t, *J* = 240.3 Hz), 20.65. **HRMS** (positive ion GC-APCI) calcd. for $C_9H_7F_2N$ [M+H] *m/z* 168.0619. Found 168.0623.

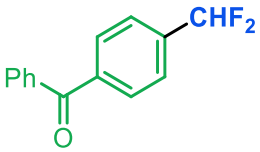

Preparation of (4-(difluoromethyl)phenyl)(phenyl)methanone (3). Reaction was conducted for isolation scale (6 reactions in parallel, 0.05 mmol scale each) using substrate **3b**. Reactions were run for 8 h. Purification by flash chromatography on silica gel (0-10% A/B) afforded the purified product as a white solid (36 mg, 51% yield). **^{1}H NMR** (500 MHz, $CDCl_3$) δ 7.88 (d, *J* = 7.0 Hz, 2H), 7.81 (d, *J* = 7.7 Hz, 2H), 7.71-7.59 *(multiple peaks*, 3H), 7.51 (t, *J* = 6.9 Hz, 2H), 6.73 (t, *J* = 56.1 Hz, 1H). **^{19}F NMR** (471 MHz, $CDCl_3$) δ –112.12 (d, *J* = 56.1 Hz). **^{13}C NMR** (176 MHz, $CDCl_3$) δ 196.04, 139.88, 137.95 (t, *J* = 22.5 Hz), 137.17, 133.02, 130.37, 130.23, 114.18 (t, *J* = 239.7 Hz). **HRMS** (positive ion GC-APCI) calcd. for $C_{14}H_{10}F_2O$ [M+H] *m/z* 233.0772. Found 233.0777.

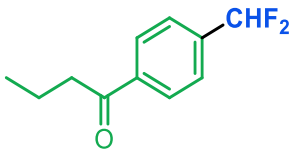

Preparation of 1-(4-(difluoromethyl)phenyl)butan-1-one (4). Reaction was conducted for isolation scale (6 reactions in parallel, 0.05 mmol scale each) using substrate **4b** and 15 mol % $Pd[P(o\text{-}Tol)_3]_2$ and 30

mol % SPhos. Reactions were run for 10 h. Purification by flash chromatography on silica gel (0-10% A/B) afforded the purified product as a white solid (30 mg, 50% yield). Small amounts of grease were present in the purified product but could not be successfully removed via washing with HPLC-grade hexanes. Under the optimized conditions (Entry 1, Table S2), the ^{19}F NMR yield of product **4** as determined with 4-fluorotoluene internal standard is 37% after 3 h. **^{1}H NMR** (500 MHz, $CDCl_3$) δ 8.03 (d, *J* = 8.2 Hz, 2H), 7.60 (d, *J* = 8.1 Hz, 2H), 6.69 (t, *J* = 56.1 Hz, 1H), 2.96 (t, *J* = 7.3 Hz, 2H), 1.78 (m, 2H), 1.01 (t, *J* = 7.4 Hz, 3H). **^{19}F NMR** (471 MHz, $CDCl_3$) δ –112.52 (d, *J* = 56.1 Hz). **^{13}C NMR** (176 MHz, $CDCl_3$) δ 199.79, 139.05, 138.41 (t, *J* = 22.4 Hz), 128.50, 126.00 (t, *J* = 6.0 Hz), 114.14 (t, *J* = 239.7 Hz), 40.88, 17.77, 13.97. **HRMS** (positive ion GC-APCI) calcd. for $C_{11}H_{12}F_2O$ [M+H] *m/z* 199.0929. Found 199.0931.

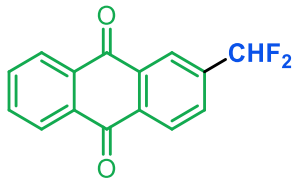

Preparation of 2-(difluoromethyl)anthracene-9,10-dione (5). Reaction was conducted for isolation scale (6 reactions in parallel, 0.05 mmol scale each) using substrate **5b**. Reactions were run for 6 h. Purification by flash chromatography on silica gel (0-10% A/B) afforded the purified product as a pale yellow solid (55 mg, 72% yield). Small amounts of grease were present in the purified product but could not be successfully removed via washing with HPLC-grade hexanes. **^{1}H NMR** (500 MHz, $CDCl_3$) δ 8.46-8.37 (*multiple peaks*, 2H), 8.32 (dt, *J* = 6.0, 3.1 Hz, 2H), 7.94 (d, *J* = 8.0 Hz, 1H), 7.83 (dt, *J* = 5.7, 2.4 Hz, 2H), 6.79 (t, *J* = 55.8 Hz, 1H). **^{19}F NMR** (377 MHz, $CDCl_3$) δ –112.97 (d, *J* = 55.8 Hz). **^{13}C NMR** (176 MHz, $CDCl_3$) δ 182.51, 182.38, 139.87 (t, *J* = 23.0 Hz), 135.04 (t, *J* = 1.7 Hz), 134.60, 133.94, 133.45, 133.44, 130.90 (t, *J* = 5.6 Hz), 128.12, 127.57, 127.55, 124.97 (t, *J* = 6.4 Hz), 113.60 (t, *J* = 240.8 Hz). **HRMS** (positive ion GC-APCI) calcd. for $C_{15}H_8F_2O_2$ [M+H] *m/z* 259.0565. Found 259.0571.

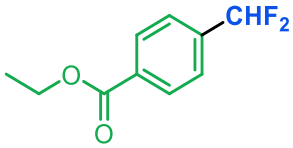

Preparation of ethyl 4-(difluoromethyl)benzoate (6). Reaction was conducted for isolation scale (6 reactions in parallel, 0.05 mmol scale each) using substrate **6b**. Reactions were run for 6 h. Reaction was carefully concentrated to due to volatity of product. Purification by flash chromatography on silica gel (0-20% A/B; B = pentanes) afforded the purified product as a white solid (35 mg, 58% yield).

^{1}H NMR (500 MHz, $CDCl_3$) δ 8.13 (d, *J* = 7.9 Hz, 2H), 7.59 (d, *J* = 7.9 Hz, 2H), 6.69 (t, *J* = 55.8 Hz, 1H), 4.41 (q, *J* = 7.1, 2H), 1.41 (t *J* = 7.1, 3H). **^{19}F NMR** (471 MHz, $CDCl_3$) δ –112.27 (d, *J* = 55.8 Hz). **^{13}C NMR** (176 MHz, $CDCl_3$) δ 165.88, 138.47 (t, *J* = 22.4 Hz), 132.81 (t, *J* = 2.0 Hz), 130.03, 125.71 (t, *J* = 6.0 Hz), 114.16 (t, *J* = 239.6 Hz), 61.47, 14.39. **HRMS** (positive ion GC-APCI) calcd. for $C_{10}H_{10}F_2O_2$ [M+H] *m/z* 201.0722. Found 201.0727.

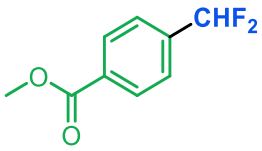

Preparation of methyl 4-(difluoromethyl)benzoate (7). Reaction was conducted for isolation scale (6 reactions in parallel, 0.05 mmol scale each) using substrate **7b.** Reactions were run for 6 h. Reactions were carefully concentrated to due to the volatity of the product. Purification by flash chromatography on silica gel (0-20% A/B; B = pentanes) afforded the purified product as a white solid (27 mg, 49% yield). **^{1}H NMR** (500 MHz, $CDCl_3$) δ 8.13 (d, *J* = 7.9 Hz, 2H), 7.59 (d, *J* = 7.9 Hz, 2H), 6.69 (t, *J* = 56.1 Hz, 1H), 3.95 (s, 3H). **^{19}F NMR** (471 MHz, $CDCl_3$) δ –112.36 (d, *J* = 56.1 Hz). **^{13}C NMR** (176 MHz, $CDCl_3$) δ 166.37, 138.59 (t, *J* = 22.4 Hz), 132.46, 130.09, 125.77 (t, *J* = 6.0 Hz), 114.14 (t, *J* = 239.8 Hz), 52.52. **HRMS** (positive ion GC-APCI) calcd. for $C_9H_8F_2O_2$ [M+H] *m/z* 187.0565. Found 187.0569.

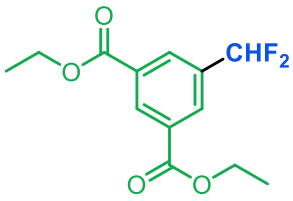

Preparation of diethyl 5-(difluoromethyl)isophthalate (8). Reaction was conducted for isolation scale (6 reactions in parallel, 0.05 mmol scale each) using substrate **8b**. Reactions were run for 6 h. Purification by flash chromatography on silica gel (0-10% A/B) afforded the purified product as a white solid (41 mg, 51% yield). **^{1}H NMR** (401 MHz, $CDCl_3$) δ 8.78 (s, 1H), 8.48-8.07 (*multiple peaks*, 2H), 6.73 (t, *J* = 55.4 Hz, 1H), 4.43 (q, *J* = 7.1 Hz, 4H), 1.42 (t, *J* = 7.1 Hz, 6H). **^{19}F NMR** (377 MHz, $CDCl_3$) δ –111.73 (d, *J* = 55.4 Hz). **^{13}C NMR** (176 MHz, $CDCl_3$) δ 165.05, 135.34 (t, *J* = 23.3 Hz), 132.77 (t, *J* = 1.7 Hz), 131.89, 130.86 (t, *J* = 6.0 Hz), 113.69 (t, *J* = 240.3 Hz), 61.89, 14.43. **HRMS** (positive ion GC-APCI) calcd. for $C_{13}H_{14}F_2O_4$ [M+H] *m/z* 273.0933. Found 273.0935.

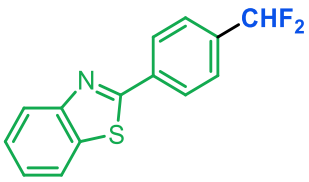

Preparation of 2-(4-(difluoromethyl)phenyl)benzo[d]thiazole (9). Reaction was conducted for isolation scale (6 reactions in parallel, 0.05 mmol scale each) using substrate **9b**. Reactions were run for 8 h. Purification by flash chromatography on silica gel (0-10% A/B) afforded the purified product as a white solid (36 mg, 46% yield). Small amounts of grease were present in the purified product but could not be successfully removed via washing with HPLC-grade hexanes. **^{1}H NMR** (401 MHz, $CDCl_3$) δ 8.19 (d, *J* = 8.2 Hz, 2H), 8.10 (d, *J* = 8.2 Hz, 1H), 7.93 (d, *J* = 7.9 Hz, 1H), 7.65 (d, *J* = 8.2 Hz, 2H), 7.52 (ddd, *J* = 8.4, 7.2, 1.3 Hz, 1H), 7.42 (ddd, *J* = 8.3, 7.2, 1.2 Hz, 1H), 6.72 (t, *J* = 56.2 Hz, 1H). **^{19}F NMR** (377 MHz, $CDCl_3$) δ –111.85 (d, *J* = 56.2 Hz). **^{13}C NMR** (176 MHz, $CDCl_3$) δ 166.80, 154.22, 136.68 (t, *J* = 22.5 Hz), 135.94, 135.31, 127.97, 126.71, 126.45 (t, *J* = 6.1 Hz), 125.76, 123.66, 121.86, 114.32 (t, *J* = 239.4 Hz). **HRMS** (positive ion GC-APCI) calcd. for $C_{14}H_9F_2NS$ [M+H] *m/z* 262.0497. Found 262.0503.

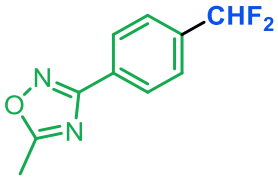

Preparation of 3-(4-(difluoromethyl)phenyl)-5-methyl-1,2,4-oxadiazole (10). Reaction was conducted for isolation scale (6 reactions in parallel, 0.05 mmol scale each) using substrate **10b**. Reactions were run for 10 h. Purification by flash chromatography on silica gel (0-10% A/B) afforded the purified product as a white solid (10 mg, 15% yield). **^{1}H NMR** (500 MHz, $CDCl_3$) δ 8.16 (d, *J* = 8.0 Hz, 2H), 7.63 (d, *J* = 8.1 Hz, 2H), 6.70 (t, *J* = 56.2 Hz, 1H), 2.67 (s, 3H). **^{19}F NMR** (471 MHz, $CDCl_3$) δ –111.78 (d, *J* = 56.2 Hz). **^{13}C NMR** (176 MHz, $CDCl_3$) δ 177.02, 167.85, 136.96 (t, *J* = 22.5 Hz), 129.30 (t, *J* = 1.8 Hz), 127.83, 126.27 (t, *J* = 6.1 Hz), 114.30 (t, *J* = 239.5 Hz), 12.56. **HRMS** (positive ion GC-APCI) calcd. for $C_{10}H_8F_2N_2O$ [M+H] *m/z* 211.0677. Found 211.0680.

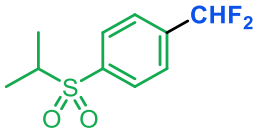

Preparation of 1-(difluoromethyl)-4-(isopropylsulfonyl)benzene (11). Reaction was conducted for isolation scale (6 reactions in parallel, 0.05 mmol scale each) using substrate **11b**. Reactions were run for 6 h. Purification by flash chromatography on silica gel (0-20% A/B) afforded the purified product as a

white solid (41 mg, 58% yield). **^{1}H NMR** (500 MHz, $CDCl_3$) δ 7.99 (d, J = 8.1, 2H), 7.72 (d, *J* = 8.1 Hz, 2H), 6.73 (t, *J* = 55.9 Hz, 1H), 3.21 (hept, *J* = 6.8 Hz, 1H), 1.31 (d, *J* = 6.8 Hz, 6H). **^{19}F NMR** (471 MHz, $CDCl_3$) δ –113.19 (d, *J* = 55.9 Hz). **^{13}C NMR** (176 MHz, $CDCl_3$) δ 139.57 (t, *J* = 1.7 Hz), 139.53 (t, *J* = 22.7 Hz), 129.75, 126.55 (t, *J* = 6.0 Hz), 113.56 (t, *J* = 240.6 Hz), 55.81, 15.80. **HRMS** (positive ion GC-APCI) calcd. for $C_{10}H_{12}F_2O_2S$ [M+H] *m/z* 235.0599. Found 235.0607.

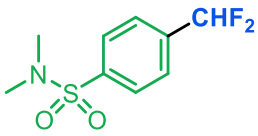

Preparation of 4-(difluoromethyl)-N,N-dimethylbenzenesulfonamide (12). Reaction was conducted for isolation scale (6 reactions in parallel, 0.05 mmol scale each) using substrate **12b**. Reactions were run for 6 h. Purification by flash chromatography on silica gel (0-50% A/B) afforded the purified product as a colorless oil (36 mg, 51% yield). **^{1}H NMR** (500 MHz, $CDCl_3$) δ 7.88 (d, *J* = 8.0 Hz, 2H), 7.70 (d, *J* = 8.0 Hz, 2H), 6.72 (t, *J* = 55.9 Hz, 1H), 2.74 (s, 6H). **^{19}F NMR** (471 MHz, $CDCl_3$) δ –112.68 (d, J = 55.9 Hz). **^{13}C NMR** (176 MHz, $CDCl_3$) δ 138.54 (t, *J* = 22.8 Hz), 138.21 (t, *J* = 2.0 Hz), 128.24, 126.53 (t, *J* = 6.0 Hz), 113.67 (t, *J* = 240.3 Hz), 37.97. **HRMS** (positive ion GC-APCI) calcd. for $C_9H_{11}F_2NO_2S$ [M+H] *m/z* 236.0551. Found 236.0556.

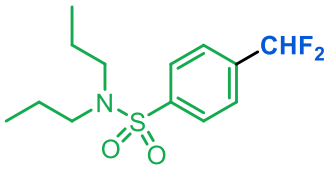

Preparation of 4-(difluoromethyl)-N,N-dipropylbenzenesulfonamide (13). Reaction was conducted for isolation scale (6 reactions in parallel, 0.05 mmol scale each) using substrate **13b**. Reactions were run for 6 h. Purification by flash chromatography on silica gel (0-20% A/B) afforded the purified product as a white solid (45 mg, 52% yield). **^{1}H NMR** (500 MHz, $CDCl_3$) δ 7.90 (d, *J* = 7.9 Hz, 2H), 7.65 (d, *J* = 7.9 Hz, 2H), 6.70 (t, *J* = 56.0 Hz, 1H), 3.10 (t *J* = 7.6, 4H), 1.61-1.51 (m, 4H), 0.88 (t, *J* = 7.4, 6H).**^{19}F NMR** (471 MHz, $CDCl_3$) δ –112.51 (d, *J* = 56.0 Hz). **^{13}C NMR** (176 MHz, $CDCl_3$) δ 142.60, 137.90 (t, *J* = 22.7 Hz), 127.40, 126.29 (t, *J* = 6.0 Hz), 113.57 (t, *J* = 240.2 Hz), 49.98, 21.97, 11.12. **HRMS** (positive ion GC-APCI) calcd. for $C_{13}H_{19}F_2NO_2S$ [M+H] *m/z* 292.1177. Found 292.1182.

Fluorine- and fluoroalky-substituted ArBneo substrates **14b-18b** were also explored. ^{19}F NMR spectroscopic analysis of the crude reaction mixtures implicates the formation of the $ArCHF_2$ products **14-18**. The ^{19}F NMR chemical shifts that are assigned as **-CHF_2** resonance for each product are listed below, along with a ^{19}F NMR yields (versus 4-fluorotoluene as an internal standard). None of these products were isolated due to their volatility.

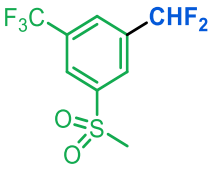

Preparation of 1-(difluoromethyl)-3-(methylsulfonyl)-5-(trifluoromethyl)benzene (14). The reaction was conducted as a single run using **14b**, and the yield of **14** was determined by ^{19}F NMR spectroscopy with 4-fluorotoluene as an internal standard. Reaction time: 4 h; yield: 65%. **^{19}F NMR** (377 MHz) δ –113.77 (d, *J* = 56.4 Hz).

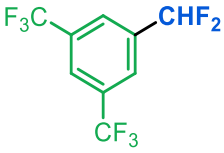

Preparation of 1-(difluoromethyl)-3,5-bis(trifluoromethyl)benzene (15). The reaction was conducted as a single run using **15b**, and the yield of **15** was determined by ^{19}F NMR spectroscopy with 4-fluorotoluene as an internal standard. Reaction time: 4 h; yield: 94%. A second trial using substrate **15b** yielded 86% of **15**.**^{19}F NMR** (471 MHz) δ –113.64 (d, *J* = 55.5 Hz).

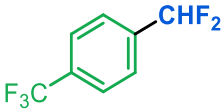

Preparation of 1-(difluoromethyl)-4-(trifluoromethyl)benzene (16). The reaction was conducted as a single run using **16b**, and the yield of **16** was determined by ^{19}F NMR spectroscopy with trifluoromethoxybenzene as an internal standard. Reaction time: 4 h; yield: 58%. A second trial using substrate **16b** yielded 50% of **16**. **^{19}F NMR** (471 MHz) δ –113.13 (d, *J* = 56.1 Hz).

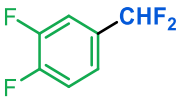

Preparation of 1-(difluoromethyl)-4-(trifluoromethyl)benzene (17). The reaction was conducted as a single run using **17b**, and the yield of **17** was determined by ^{19}F NMR trifluoromethoxybenzene as an internal standard. Reaction time: 4 h; yield: 60%. **^{19}F NMR** (377 MHz) δ –110.39 (d, *J* = 55.9 Hz).

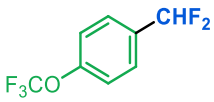

Preparation of 1-(difluoromethyl)-4-(trifluoromethyl)benzene (18). The reaction was conducted as a single run using **18b**, and the yield of **18** was determined ^{19}F NMR spectroscopy with 4-fluorotoluene as an internal standard. Reaction time: 4 h; yield: 69%. **^{19}F NMR** (471 MHz) δ –117.08 (d, *J* = 55.6 Hz).

2.8 References

(1) On fluorine in molecules: (a) Müller, K.; Faeh, C.; Diederich, F. Fluorine in pharmaceuticals: looking beyond intuition. *Science* **2007**, *317*, 1881−1886. (b) Purser, S.; Moore, P. R.; Swallow, S.; Gouverneur, V. Fluorine in medicinal chemistry. *Chem. Soc. Rev.* **2008**, *37*, 320−330. (c) Hagmann, W. K. The many roles for fluorine in medicinal chemistry. *J. Med. Chem.* **2008**, *51*, 4359−4369. (d) Wang, J.; Sanchez-Roselló, M.; Acená , J. L.; del Pozo, C.; Sorochinsky, A. E.; Fustero, S.; Soloshonok, V. A.; Liu, H. Fluorine in pharmaceutical industry: fluorine-containing drugs introduced to the market in the last decade (2001−2011). *Chem. Rev.* **2014**, *114*, 2432− 2506. (e) Liang, T.; Neumann, C. N.; Ritter, T. Introduction of fluorine and fluorine-containing functional groups. *Angew. Chem., Int. Ed.* **2013**, *52*, 8214−8264. (f) Caron, S. Where does fluorine come from? A review on the challenges associated with the synthesis of organofluorine compounds. *Org. Process Res. Dev.* **2020**, *24*, 470−480. (g) Shah, P.; Westwell, A. D. The role of fluorine in medicinal chemistry. *J. Enzyme Inhib. Med. Chem.* **2007**, *22*, 527−540. (h) O'Hagan, D. Fluorine in health care: organofluorine containing blockbuster drugs. *J. Fluorine Chem.* **2010**, 131, 1071−1081. (i) Jackel, C.; Salwiczek, M.; Koksch, B. Fluorine in native protein environment - how the spatial demand and polarity of fluoroalkyl groups affect protein folding. *Angew. Chem., Int. Ed.* **2006**, 45, 4198−4203.

(2) On the properties and synthesis of difluoromethylarenes: (a) Zafrani, Y.; Yeffet, D.; Sod-Moriah, G.; Berliner, A.; Amir, D.; Marciano, D.; Gershonov, E.; Saphier, S. Difluoromethyl ioisostere: examining the "lipophilic hydrogen bond donor" concept. *J. Med. Chem.* **2017**, *60*, 797−804. (b) Zafrani, Y.; Saphier, S.; Gershonov, E. Utilizing the CF2H moiety as a H-bond-donated group in drug discovery. *Future Med. Chem.* **2020**, *12*, 361−365. (c) Erickson, J. A.; McLoughlin, J. I. Hydrogen bond donor properties of the difluoromethyl group. *J. Org. Chem.* **1995**, *60*, 1626−1631. (d) Sessler, C. D.; Rahm, M.; Becker, S.; Goldberg, J. M.; Wang, F.; Lippard, S. J. CHF2, a hydrogen bond donor. *J. Am. Chem. Soc.* **2017**, *139*, 9325− 9332. (e) Rageot, D.; Beaufils, F.; Borsari, C.; Dall'Asen, A.; Neuburger, M.; Hebeisen, P.; Wymann, M. P. Scalable, economical, and practical synthesis of 4-(difluoromethyl)pyridine-2-amine, a fey intermediate for lipid kinase inhibitors. *Org. Process Res. Dev.* **2019**, *23*, 2416−2424.

(3) Metal-catalyzed nucleophilic trifluoromethylation via cross-coupling: (a) Cho, E. J.; Senecal, T. D.; Kinzel, T.; Zhang, Y.; Watson, D. A.; Buchwald, S. L. The palladium-catalyzed trifluoromethylation of aryl chlorides. *Science* **2010**, *328*, 1679−1681. (b) Morimoto, H.; Tsubogo, T.; Litvinas, N. D.; Hartwig, J. F. A broadly applicable copper reagent for trifluoromethylations and perfluoroalkylations of aryl iodides and bromides. *Angew. Chem., Int. Ed.* **2011**, *50*, 3793−3798.

(4) Metal-catalyzed nucleophilic fluoroalkylation: (a) Fier, P. S.; Hartwig, J. F. Copper-mediated difluoromethylation of aryl and vinyl iodides. *J. Am. Chem. Soc.* **2012**, *134*, 5524−5527. (b) Jiang, X.-L.; Chen, Z.-H.; Xu, X.-H.; Qing, F.-L. Copper-mediated difluoromethylation of electron-poor aryl iodides at room temperature. *Org. Chem. Front.* **2014**, *1*, 774−776. (c) Prakash, G. K. S.; Ganesh, S. K.; Jones, J.-P.; Kulkarni, A.; Masood, K.; Swabeck, J. K.; Olah, G. A. Coppermediated difluoromethylation of (hetero)aryl iodides and β-styryl halides with tributyl(difluoromethyl)stannane. *Angew. Chem., Int. Ed*. **2012**, *51*, 12090−12094. (d) Gu, Y.; Leng, X.; Shen, Q. Cooperative dual palladium/silver catalyst for direct difluoromethylation of aryl bromides and iodides. *Nat. Commun*. **2014**, *5*, 5405. (e) Chang, D.; Gu, Y.; Shen, Q. Pd-Catalyzed difluoromethylation of vinyl bromides, triflates, tosylates, and nonaflates. *Chem. - Eur. J.* **2015**, *21*, 6074− 6078. (f) Nakamura, Y.; Fujiu, M.; Murase, T.; Itoh, Y.; Serizawa, H.; Aikawa, K.; Mikami, K. Cu-catalyzed trifluoromethylation of aryl iodides with trifluoromethylzinc reagent prepared in situ from trifluoromethyl iodide. *Beilstein J. Org. Chem*. **2013**, *9*, 2404−2409. (g) Aikawa, K.; Nakamura, Y.; Yokota, Y.; Toya, W.; Mikami, K. Stable but reactive perfluoroalkylzinc reagents: application in ligand-free copper-catalyzed perfluoroalkylation of aryl iodides. *Chem. - Eur. J.* **2015,** *21*, 96−100. (h) Aikawa, K.; Toya, W.; Nakamura, Y.; Mikami, K. Development of (trifluoromethyl)zinc reagent as trifluoromethyl anion and difluorocarbene sources. *Org. Lett.* **2015**, *17*, 4996−4999. (i) Xu, L.; Vicic, D. A. Direct difluoromethylation of aryl halides via base metal catalysis at room temperature. *J. Am. Chem. Soc.* **2016**, *138*, 2536−2539. (j) Serizawa, H.; Ishii, K.; Aikawa, K.; Mikami, K. Copper-Catalyzed difluoromethylation of aryl iodides with (difluoromethyl)zinc reagent. *Org. Lett.* **2016**, *18*, 3686−3689.

(5) (a) Furuya, T.; Kamlet, A. S.; Ritter, T. Catalysis for fluorination and trifluoromethylation. Nature 2011, 473, 470−477. (b) Ferguson, D. M.; Bour, J. R.; Canty, A. J. Kampf, J. W. Sanford, M. S. Stoichiometric and catalytic aryl-perfluoroalkyl coupling at tri-*tert*-butylphosphine palladium(II) complexes. *J. Am. Chem. Soc.* **2017**, *139*, 11662–11665. (c) Lishchynskyi, A.; Grushin, V. V. Cupration of C_2F_5H: Isolation, structure, and synthetic applications of $[K(DMF)_2][(t\text{-BuO})Cu(C_2F_5)]$. Highly efficient pentafluoroethylation of unactivated aryl bromides. *J. Am. Chem. Soc*. **2013**, *135*, 12584.

(6) On the reagent TMSCF3: (a) Liu, X.; Xu, C.; Wang, M.; Liu, Q. Trifluoromethyltrimethylsilane: nucleophilic trifluoromethylation and beyond. *Chem. Rev.* **2015**, *115*, 683−730. (b) Krishnamoorthy, S.; Kothandaraman, J.; Saldana, J.; Prakash, G. K. S. Direct difluoromethylation of carbonyl compounds by using TMSCF3: the right conditions. *Eur. J. Chem.* **2016**, 4965−4969. (c) Xie, Q.; Li, L.; Zhu, Z.; Zhang, R.; Ni, C.; Hu, J. From C1 to C2: $TMSCF_3$ as a precursor to pentafluoroethylation. *Angew. Chem., Int. Ed*. **2018**, *57*, 13211−13215. (d) Johnston, C. P.; West, T. H.; Dooley, R. E.; Reid, M.; Jones, A. B.; King, E. J.; Leach, A. G.; Lloyd-Jones, G. C. Anion-initiated trifluoromethylation by $TMSCF_3$: deconvolution of the siliconate-carbonanion dichotomy by stopped-flow NMR/IR. *J. Am. Chem. Soc*. **2018**, *140*, 11112−11124.

(7) Mudarra, A. L.; Martinez de Salinas, S.; Perez-Temprano, M. H. Beyond the traditional roles of Ag in catalysis: the transmetalating ability of organosilver(i) species in Pd-catalysed reactions. *Org. Biomol. Chem.* **2019,** *17*, 1655−1667.

(8) For reviews on carboxylic acids and their derivatives as electrophiles in cross-coupling: (a) Baudoin, O. New approaches for decarboxylative biaryl coupling. *Angew. Chem., Int. Ed.* **2007**, *46*, 1373−1375. (b) Gooßen, K.; Rodriguez, N.; Gooßen, L. J. Carboxylic acids as substrates in homogenous catalysis. *Angew. Chem., Int. Ed.* **2008**, *47*, 3100−3120. (c) Yu, D. G.; Li, B. J.; Shi, Z. J. Exploration of new C−O electrophiles in cross-coupling reactions. *Acc. Chem. Res.* **2010**, *43*, 1486−1495. (d) Rodriguez, N.; Gooßen, L. J. Decarboxylative coupling reactions: a modern strategy for C−C bond formation. *Chem. Soc. Rev.* **2011**, *40*, 5030−5048. (e) Cornella, J.; Larrosa, I. Decarboxylative carbon-carbon bond-forming transformations of (hetero)aromatic carboxylic acids. *Synthesis* **2012**, *44*, 653−656. (f) Hoover, J. M. Mechanistic aspects of copper-catalyzed

decarboxylative coupling reactions of (hetero)aryl carboxylic acids. *Inorg. Chem.* **2017**, *37*, 169−200. (g) Takise, R.; Muto, K.; Yamaguchi, J. Cross-coupling of aromatic esters and amides. *Chem. Soc. Rev.* **2017**, 46, 5864−5888. (h) Guo, L.; Rueping, M. Decarbonylative cross-couplings: Nickel catalyzed functional group interconversion strategies for the construction of complex organic molecules. *Acc. Chem. Res.* **2018**, *51*, 1185−1195. (i) Meng, G.; Szostak, M. N-Acyl-glutarimides: Privileged scaffolds in amide N−C bond cross-coupling. *Eur. J. Org. Chem* **2018**, 2352−2365. (j) Zhao, Q.; Szostak, M. Redox-neutral decarbonylative cross-couplings coming of age. *Chem. Sus. Chem* **2019**, *12*, 2983−2987. (k) Blanchard, N.; Bizet, V. Acid fluorides in transition-metal catalysis: a good balance between stability and reactivity. *Angew. Chem., Int. Ed.* **2019**, *58*, 6814−6187. (l) Ogiwara, Y.; Sakai, N. Acyl fluorides in late transition-metal catalysis. *Angew. Chem., Int. Ed.* **2020**, *59*, 574−594. (m) Wang, Z.; Wang, X.; Nishihara, Y. Nickel or palladium-catalyzed decarbonylative transformations of carboxylic acid derivatives. *Chem. Asian J.* **2020**, *15*, 1234−1247. (n) Zheng, Y.-L.; Newman, S. G. Cross-coupling reactions with esters, aldehydes, and alcohols. *Chem. Commun.* **2021**, *57*, 2591−2604. (o) Fahandej-Sadi, A.; Lundgren, R. J. Copper-mediated synthesis of monofluoro aryl acetates via decarboxylative cross-coupling. *Synlett* **2017**, *28*, 2886− 2890. (p) Moon, P. J.; Yin, S.; Lundgren, R. J. Ambient decarboxylative arylation of malonate half-esters via oxidative catalysis. *J. Am. Chem. Soc.* **2016**, *138*, 13826−13829.

(9) For relevant difluoromethylation examples: (a) Pan, F.; Boursalian, G. B.; Ritter, T. Palladium-catalyzed decarbonylative difluoromethylation of acid chlorides at room temperature. *Angew. Chem., Int. Ed.* **2018**, *57*, 16871−16876. (b) Feng, Z.; Min, Q.; Fu, X.; An, L.; Zhang, X. Chlorodifluoromethane-triggered formation of difluoromethylated arenes catalysed by palladium. *Nat. Chem.* **2017**, *9*, 918−923. (c) Hori, K.; Motohashi, H.; Saito, D.; Mikami, K. Precatalyst effects of Pd-catalyzed cross-coupling difluoromethylation of aryl boronic acids. *ACS Catal*., 9, 417−421.

(10) Fluorinated carboxylic acids in decarboxylative coupling: (a) Beatty, J. W.; Douglas, J. J.; Cole, K. P.; Stephenson, C. R. J. A Scalable and operationally simple radical trifluoromethylation. *Nat. Commun*. **2015**, *6*, 7919−7925. (b) Matsui, K.; Tobita, E.; Ando, M.; Kondo, K. A convenient trifluoromethylation of aromatic halides with sodium trifluoroacetate. *Chem. Lett*. **1981**, *10*,

1719−1720. (c) Chen, M.; Buchwald, S. L. Rapid and efficient trifluoromethylation of aromatic and heteroaromatic compounds using potassium trifluoroacetate enabled by a flow system. *Angew. Chem., Int. Ed.* **2013**, *52*, 11628−11631. (d) Ambler, B. R.; Zhu, L.; Altman, R. A. Coppercatalyzed synthesis of trifluoroethylarenes from benzylic bromodifluoroacetates. *J. Org. Chem.* **2015**, *80*, 8449−8457. (e) Ambler, B. R.; Peddi, S.; Altman, R. A. Ligand-controlled regioselective copper-catalyzed trifluoromethylation to generate (trifluoromethyl)allenes. *Org. Lett.* **2015**, *17*, 2506−2509. (f) Carr, G. E.; Chambers, R. D.; Holmes, T. F.; Parker, D. G. Sodium perfluoroalkane carboxylates as sources of perfluoroalkyl groups. *J. Chem. Soc., Perkin Trans. 1* **1988**, *1*, 921−926. (g) Johansen, M. B.; Lindhardt, A. T. Copper-catalyzed and additive free decarboxylative trifluoromethylation of aromatic and heteroaromatic iodides. *Org. Biomol. Chem.* **2020**, *18*, 1417−1425. (h) Zapf, A.; Beller, M. Fine chemical synthesis with homogeneous palladium catalysts: examples, status, and trends. Top. Catal. **2002**, *19*, 101−109.

(11) (a) Sun, A. C.; McClain, E. J.; Beatty, J. W.; Stephenson, C. R. J. Visible light-mediated decarboxylative alkylation of pharmaceutically relevant heterocycles. *Org. Lett.* **2018**, *20*, 3487−3490. (b) Tung, T. T.; Christensen, S. B.; Nielsen, J. Difluoroacetic acid as a new reagent for direct C−H difluoromethylation of heteroaromatic compounds. *Chem. Eur. J.* **2017**, *23*, 18125−18128.

(12) For other examples of fluoroalkyl carboxylic acid derivatives being used as fluoroalkyl sources, see: (a) Yang, M.-H.; Orsi, D. L.; Altman, R. A. Ligand-controlled regiodivergent palladium-catalyzed decarboxylative allylation reaction to access α-difluoroketones. *Angew. Chem., Int. Ed.* **2015**, *54*, 2361−2365. (b) Yang, M.-H.; Hunt, J. R.; Sharifi, N.; Altman, R. A. Palladium catalysis enables benzylation of α,α-difluoroketone enolates. *Angew. Chem., Int. Ed.* **2016**, *55*, 9080−9083. (c) Ambler, B. R.; Yang, M.-H.; Altman, R. A. Metal-catalyzed decarboxylative fluoroalkylation reactions. *Synlett* **2016**, *27*, 2747−2755.

(13) (a) Maleckis, A.; Sanford, M. S. Catalytic cycle for palladium-catalyzed decarbonylative trifluoromethylation using trifluoroacetic esters as the CF3 source. *Organometallics* **2014**, *33*, 2653−2660. (b) Brigham, C. E.; Malapit, C. A.; Lalloo, N.; Sanford, M. S. Nickel-catalyzed decarbonylative synthesis of fluoroalkyl thioethers. *ACS Catal.* **2020**, *10*, 8315−8320. (c) See, Y.

Y., Morales-Colon, M. T.; Bland, D. C.; Sanford, M. S. Development of S_NAr nucleophilic fluorination: a fruitful academia-industry collaboration. *Acc. Chem. Res.* **2020**, *53*, 2372–2383.
(14) Bakhmutov, V. I.; Bozoglian, F.; Gomez, K.; Gonzalez, G.; Grushin, V. V.; Macgregor, S. A.; Martin, E.; Miloserdov, F. M.; Novikov, M. A.; Panetier, J. A.; Romashov, L. V. CF3−Ph reductive elimination from [(XantPhos}Pd(CF3)(Ph)]. *Organometallics* **2012**, *31*, 1315−1328.
(15) (a) Lennox, A. J. J.; Lloyd-Jones, G. C. Selection of boron reagents for Suzuki−Miyaura coupling. *Chem. Soc. Rev.* **2014**, *43*, 412−443. (b) Fang, H.; Kaur, G.; Yan, J.; Wang, B. An efficient synthesis of sterically hindered arylboronic acids. *Tet. Lett.* **2005**, *46*, 1671–1674. (c) Matthew, C. S.; Glasspoosle, B. W.; Eisenberger, P.; Crudden, C. M. Synthesis of enantiomerically enriched triarylmethanes by enantiospecific Suzuki-Miyaura cross coupling reactions. *J. Am. Chem. Soc.* **2014**, *136*, 5828–5831. (d) Wrackmeyer, B. Carbon-13 NMR spectroscopy of boron compounds. *Progress in NMR spectroscopy* **1978**, *12*, 227–259.
(16) For relative rates in carbonylation reactions, see: (a) Shusterman, A. J.; Tamir, I.; Pross, A. The mechanism of organometallic migration reactions. A configuration mixing approach. *J. Organomet. Chem.* **1988**, *340*, 203−222. (b) Ortuno, M. A.; Dereli, B.; Cramer, C. J. Mechanism of Pd-catalyzed decarbonylation of biomass-derived hydrocinnamic acid to styrene following activation as an anhydride. *Inorg. Chem.* **2016**, *55*, 4124−4131.
(17) (a) Johnston, R. C.; Cheong, H. Y. C-H---O non-classical hydrogen bonding in the stereomechanics of organic transformations: theory ad recognition. *Org. Biomol. Chem.* **2013**, *11*, 5057−5064. (b) Gilli, P.; Pretto, L.; Bertolasi, V.; Gilli, G. Predicting hydrogen-bond strengths from acid-base molecular properties. The pKa slide rule: toward the solution of a long-lasting problem. *Acc. Chem. Res.* **2009**, *42*, 33−44.
(18) For DFT methods, see: (a) Schrödinger Release 2019-2: MacroModel; Schrödinger, LLC, New York, NY, 2019. (b) Schrödinger Release 2019-2: Maestro; Schrödinger, LLC, New York, NY, 2019. (c) Frisch, M. J.; Trucks, G. W.; Schlegel, H. B.; Scuseria, G. E.; Robb, M. A.; Cheeseman, J. R.; Scalmani, G.; Barone, V.; Mennucci, B.; Petersson, G. A.; Nakatsuji, H.; Caricato, M.; Li, X.; Hratchian, H. P.; Izmaylov, A. F.; Bloino, J.; Zhang, G.; Sonnenberg, J. L.; Hada, M.; Ehara, M.; Toyota, K.; Fukuda, R.; Hasegawa, J.; Ishida, M.; Journal of the American Chemical Society pubs.acs.org/JACS Article https://doi.org/10.1021/jacs.1c08551 J. Am. Chem.

Soc. 2021, 143, 18617−18625 18624 Nakajima, T.; Honda, Y.; Kitao, O.; Nakai, H.; Vreven, T.; Montgomery, J. A., Jr.; Peralta, J. E.; Ogliaro, F.; Bearpark, M.; Heyd, J. J.; Brothers, E.; Kudin, K. N.; Staroverov, V. N.; Kobayashi, R.; Normand, J.; Raghavachari, K.; Rendell, A.; Burant, J. C.; Iyengar, S. S.; Tomasi, J.; Cossi, M.; Rega, N.; Millam, J. M.; Klene, M.; Knox, J. E.; Cross, J. B.; Bakken, V.; Adamo, C.; Jaramillo, J.; Gomperts, R.; Stratmann, R. E.; Yazyev, O.; Austin, A. J.; Cammi, A. R.; Pomelli, C.; Ochterski, J. W.; Martin, R. L.; Morokuma, K.; Zakrzewski, V. G.; Voth, G. A.; Salvador, P.; Dannenberg, J. J.; Dapprich, S.; Daniels, A. D.; Farkas, Ö .; Foresman, J. B.; Ortiz, J. V.; Cioslowski, J.; Fox, D. J. Gaussian 09, Revision C.02; Gaussian, Inc.: Wallingford, CT, 2009. (d) Roy, L. E.; Hay, P. J.; Martin, R. L. Revised Basis Sets for the LANL Effective Core Potentials. *J. Chem. Theory Comput.* **2008**, *4*, 1029−1031. (e) Zhao, Y.; Truhlar, D. G. Density Functionals with Broad Applicability in Chemistry. *Acc. Chem. Res.* **2008**, 41, 157−167. (f) Huzinaga, S. Gaussian Basis Sets for Molecular Calculations; Elsevier Science Pub. Co.: Amsterdam, 1984; p 15. (g) Hay, P. J.; Wadt, W. R. Ab initio effective core potentials for molecular calculations. Potentials for K to Au including the outermost core orbitals. J. Chem. Phys. 1985, 82, 299−310. (h) Hay, P. J.; Wadt, W. R. Ab initio effective core potentials for molecular calculations. Potentials for the transition metal atoms Sc to Hg. *J. Chem. Phys.* **1985**, *82*, 270−283. (i) Gonzalez, C.; Schlegel, H. B. An improved algorithm for reaction path following. *J. Chem. Phys*. 1989, 90, 2154−2161. (j) Gonzalez, C.; Schlegel, H. B. Reaction Path Following in Mass-Weighted Internal Coordinates. *J. Phys. Chem*. **1990**, *94*, 5523−5527. (k) Barone, V.; Cossi, M. Quantum Calculation of Molecular Energies and Energy Gradients in Solution by a Conductor Solvent Model. *J. Phys. Chem. A* **1998**, *102*, 1995−2001. (l) Cossi, M.; Rega, N.; Scalmani, G.; Barone, V. J. Energies, structures, and electronic properties of molecules in solution with the C-PCM solvation model. *J. Comput. Chem*. **2003**, *24*, 669−681. (m) Reed, A. E.; Weinstock, R. B.; Weinhold, F. Natural population analysis. *J. Chem. Phys.* **1985**, *83*, 735−746. (n) Reed, A. E.; Weinhold, F. Natural localized molecular orbitals. *J. Chem. Phys*. **1985**, *83*, 1736−1740. (o) Reed, A. E.; Curtiss, L. A.; Weinhold, F. Intermolecular interactions from a natural bond orbital, donor acceptor viewpoint. *Chem. Rev.* **1988**, *88*, 899−926. (p) Glendening, E. D.; Reed, A. E.; Carpenter, J. E.; Weinhold, F. NBO, Version 3.1;. (q) Contreras-García, J.; Johnson, E. R.; Keinan, S.; Chaudret, R.; Piquemal, J.-P.; Beratan, D. N.; Yang, W. NCIPLOT: A program for plotting

noncovalent regions. *J. Chem. Theory Comput*. **2011**, 7, 625− 632. (r) Shakourian-Fard, M.; Kamath, G.; Jamshidi, Z. Trends in physisorption of ionic liquids on boron-nitride sheets. *J. Phys. Chem. C* **2014**, *118*, 26003−26016.

(19) (a) Fraser, S. L.; Antipin, M. Yu.; Khroustalyov, V. N.; Grushin, V. V. Molecular fluoro palladium complexes. *J. Am. Chem. Soc.* **1997**, *119*, 4769s−4770. (b) Beweries, T.; Brammer, L.; Jasim, N. A.; McGrady, J. E.; Perutz, R. N.; Whitwood, A. C. Energetics of halogen bonding of group 10 metal fluoride complexes. *J. Am. Chem. Soc*. **2011**, *133*, 14338−14348.

(20) For recent examples of studies on transmetalation-active organometallic complexes with organoboron and silicon, see: (a) Carrow, B. P.; Hartwig, J. F. Distinguishing between pathways for transmetalation in Suzuki-Miyaura reactions. *J. Am. Chem. Soc.* **2011**, *133*, 2116−2119. (b) Amatore, C.; Jutand, A.; Le Duc, G. The triple role of fluoride ions in palladium-catalyzed Suzuki−Miyaura reactions: unprecedented transmetalation from [ArPdFL2] complexes. *Angew. Chem., Int. Ed.* **2012**, *51*, 1379−1382. (c) Thomas, A. A.; Denmark, S. E. Pre-transmetalation intermediates in the Suzuki− Miyaura reaction revealed: the missing link. *Science* **2016**, *352*, 329−332. (d) Malapit, C. A.; Bour, J. R.; Brigham, C. E.; Sanford, M. S. Base-free nickel-catalysed decarbonylative Suzuki-Miyaura coupling of acid fluorides. *Nature* **2018**, *563*, 100−104. (e) Malapit, C. A.; Bour, J. R.; Laursen, S. R.; Sanford, M. S. Mechanism and scope of nickel-catalyzed decarbonylative borylation of carboxylic acid fluorides. *J. Am. Chem. Soc.* **2019**, *141*, 17322−17330. (f) Malapit, C. A.; Borrell, M.; Milbauer, M. W.; Brigham, C. E.; Sanford, M. S. Nickel-catalyzed decarbonylative amination of carboxylic acid esters. *J. Am. Chem. Soc.* **2020**, *142*, 5918−5923.

(21) For reviews on the utility of acid fluorides in decarbonylative cross-coupling, see refs 8k and m.

(22) For examples of the utility of acid fluorides in decarbonylative cross-coupling, see refs 22d, f, and the following: (a) Keaveney, S. T.; Schoenebeck, F. Palladium-catalyzed decarbonylative trifluoromethylation of acid fluorides. *Angew. Chem., Int. Ed.* **2018**, *57*, 4073−4077. (b) Wang, Z.; Wang, X.; Nishihara, Y. Nickel-catalysed decarbonylative borylation of aroyl fluorides. *Chem. Commun.* **2018**, *54*, 13969−13972. (c) Ogiwara, Y.; Sakurai, Y.; Hattori, H.; Sakai, N. Palladium-catalyzed reductive conversion of acyl fluorides via ligandcontrolled decarbonylation. *Org. Lett.*

2018, *20*, 4204−4208. (d) Okuda, Y.; Xu, J.; Ishida, T.; Wang, C.-a.; Nishihara, Y. Nickelcatalyzed decarbonylative alkylation of aroyl fluorides assisted by Lewis-acidic organoboranes. *ACS Omega* **2018**, *3*, 13129−13140. (e) Sakurai, S.; Yoshida, T.; Tobisu, M. Iridium-catalyzed decarbonylative coupling of acyl fluorides with arenes and heteroarenes via CH activation. *Chem. Lett*. **2019**, *48*, 94−97. (f) Ogiwara, Y.; Iino, Y.; Sakai, N. Catalytic C−H/C−F coupling of azoles and acyl fluorides. *Chem. - Eur. J.* 2019, *25*, 6513−6516. (g) Wang, X.; Wang, Z.; Liu, L.; Asanuma, Y.; Nishihara, Y. Nickel-catalyzed decarbonylative stannylation of acyl fluorides under ligand-free conditions. *Molecules* **2019**, *24*, 1671−1682. (h) Wang, X.; Wang, Z.; Nishihara, Y. Nickel/ copper-cocatalyzed decarbonylative silylation of acyl fluorides. *Chem. Commun.* **2019**, *55*, 10507−10510. (i) Kayumov, M.; Zhao, J.-N.; Mirzaakhmedov, S.; Wang, D.-Y.; Zhang, A. Synthesis of arylstannanes via palladium-catalyzed decarbonylative coupling of aroyl fluorides. *Adv. Synth. Catal.* **2020**, *362*, 776−781. (j) Chen, Q.; Fu, L.; Nishihara, Y. Palladium/copper-cocatalyzed decarbonylative alkynylation of acyl fluorides with alkynylsilanes: synthesis of unsymmetrical diarylethynes. *Chem. Commun*. **2020**, *56*, 7977− 7980. (k) Wang, Z.; Wang, X.; Ura, Y.; Nishihara, Y. Nickel-catalyzed decarbonylative cyanation of acyl chlorides. *Org. Lett.* **2019**, *21*, 6779−6784. (l) Sakurai, Y.; Ogiwara, Y.; Sakai, N. Palladium-catalyzed annulation of acyl fluorides with norbornene via decarbonylation and CO reinsertion. *Chem. - Eur. J*. **2020**, *26*, 12972−12977. (m) He, B.; Liu, X.; Li, H.; Zhang, X.; Ren, Y.; Su, W. Rh-Catalyzed general method for directed C−H functionalization via decarbonylation of in-situ-generated acid fluorides from carboxylic acids. *Org. Lett.* **2021**, *23*, 4191−4196.

Chapter 3 – Further Developments in Fluoroalkylation Catalysis at Palladium

3.1 Introduction

Chapter 2 focused on the development of a palladium-catalyzed decarbonylative difluoromethylation reaction involving cross-coupling between difluoroacetyl fluoride and aryl boronate neopentylglycol esters (Scheme 3.1).[1a]

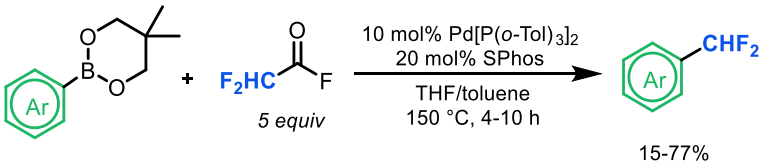

Scheme 3.1. Reaction scheme for decarbonylative difluoromethylation using DFAF.[1a]

The proposed catalytic cycle for this transformation is shown in Figure 3.1 and involves (i) oxidative addition of gaseous DFAF into Pd^0, (ii) carbonyl de-insertion at the Pd^{II}-acyl intermediate, (iii) transmetalation between the $Pd^{II}(CF_2H)(F)$ and an aryl boronate ester, and (iv) Ar–CHF_2 bond-forming reductive elimination to release the product and regenerate the Pd^0 catalyst.

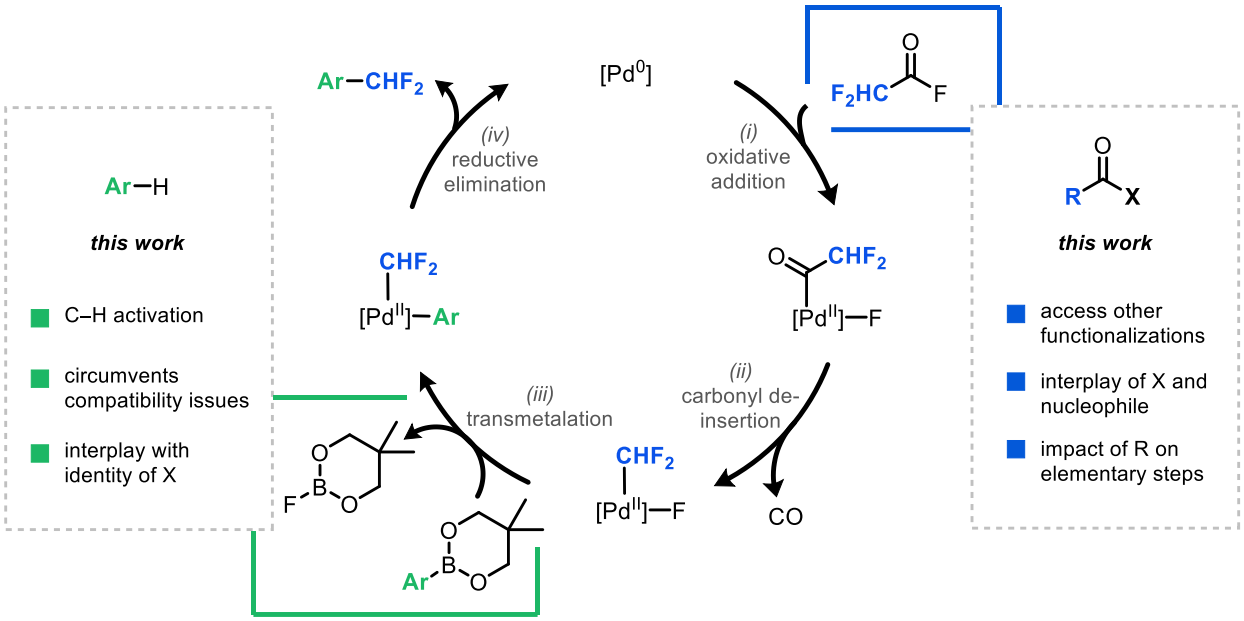

Figure 3.1. Catalytic cycle proposed from ref. 1a with focus on the coupling partners.

A key limitation of the developed cross-coupling reaction is that it has a limited substrate scope: it requires gaseous DFAF as the electrophile and only works with electron-deficient aryl boronate neopentylglycol esters.[1a] Moving forward, we aimed to expand the scope of this transformation by changing the identity of the electrophile and the nucleophile. This chapter presents our efforts to achieve this goal through the development of two new transformations: (1) a Pd-catalyzed decarbonylative aryl difluoromethylation of C–H substrates and (2) a Pd-catalyzed decarbonylative difluorobenzylation of aryl boron organometallics.

3.2 Motivations Towards Decarbonylative C–H Difluoromethylation

In our Chapter 2,[1a] we studied the room temperature oxidative addition and carbonyl de-insertion reactions of **DFAAn** that led to the formation of complex **II-CHF2**. However, this Pd^{II} intermediate was not transmetalation-active with aryl boronate esters. Utilization of DFAF as an electrophile enabled transmetalation with these nucleophiles because it generates a reactive Pd^{II}-fluoride (rather than a Pd^{II}-carboxylate) intermediate. However, the developed cross-coupling reaction[1a] is only effective using DFAF and with a limited a subset of electron-deficient aryl

boronate neopentylglycol esters (despite the compatibility between both electron-rich and -deficient organoboronate esters with DFAF).[1a] To expand the scope of the reaction while circumventing issues related to the compatibility of the organometallic and electrophile, we first focused on developing a Pd-catalyzed decarbonylative C–H difluoromethylation reaction of arenes. Compared to other C–H activation methods[2c], this strategy would be advantageous, as pre-functionalization of the arene nucleophile should not be required. Instead, simple arenes, activated arenes, and arenes with directing groups could be leveraged in this process.

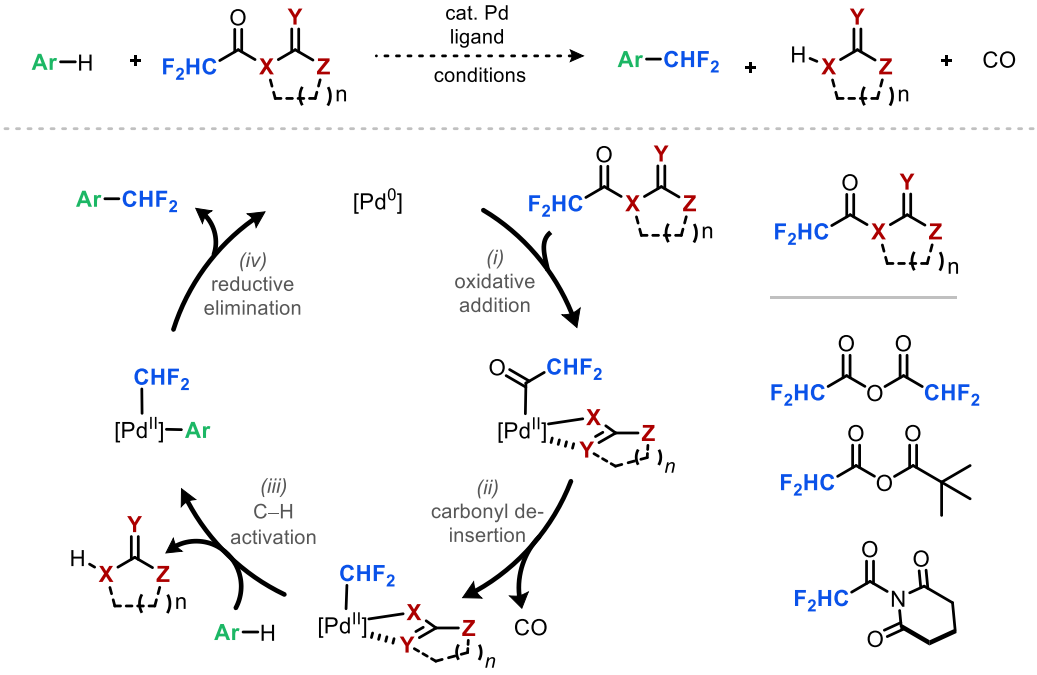

Scheme 3.2. Proposed reaction and catalytic cycle for decarbonylative C–H difluoromethylation.

The general reaction scheme and proposed catalytic for this reaction is shown in Scheme 3.2. It involves initial oxidative addition of a difluoroacyl electrophile ($CHF_2C(O)X$) at Pd^0 to form a $(X)Pd^{II}–COCHF_2$ intermediate (step *i*). Subsequent carbonyl de-insertion (step *ii*) forms a $(X)Pd^{II}–CHF_2$ complex, which that could undergo C–H activation (step *iii*) and then reductive elimination (step *iv*) to afford the $ArCHF_2$ product

This reaction would involve replacing the pre-functionalized aryl boronate ester in our previous system[1a] with an unfunctionalized arene, Ar–H. However, we also posited that this change in arene may require a concomitant change in the identity of the difluoroacyl electrophile

in order to facilitate the C–H activation step (Figure 3.2). A variety of mixed anhydrides, amides, and other similar structures could be tested for their efficacy in the proposed C–H activation.

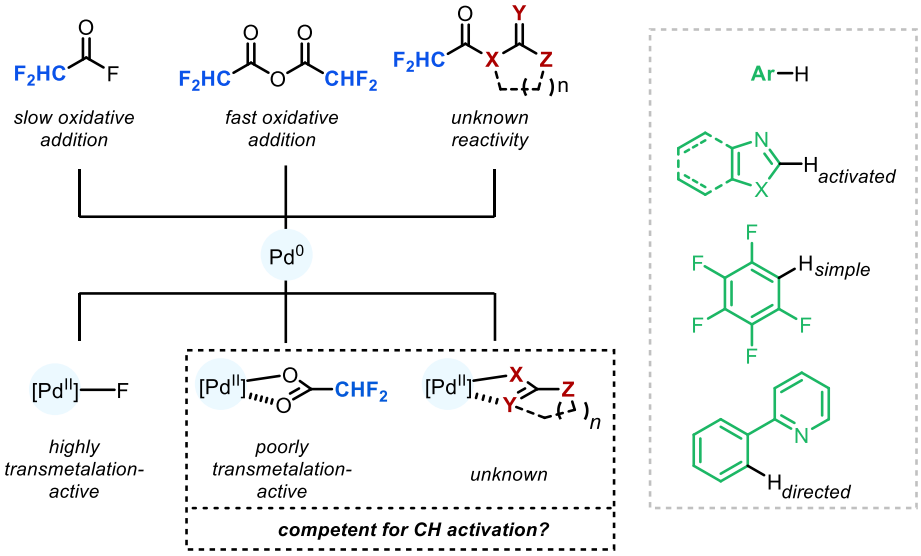

Figure 3.2. Potential structures for difluoroacyl electrophiles and arenes in C–H activation.

We first investigated the difluoroacetate intermediate $(CHF_2)Pd–OCOCHF_2$ (which is analogous to complex **II-CHF$_2$** in ref. 1a). We reasoned that the difluoroacetate could plausibly serve as a base to facilitate a C–H activation of arenes via a concerted-metalation-deprotonation (CMD-type) mechanism.

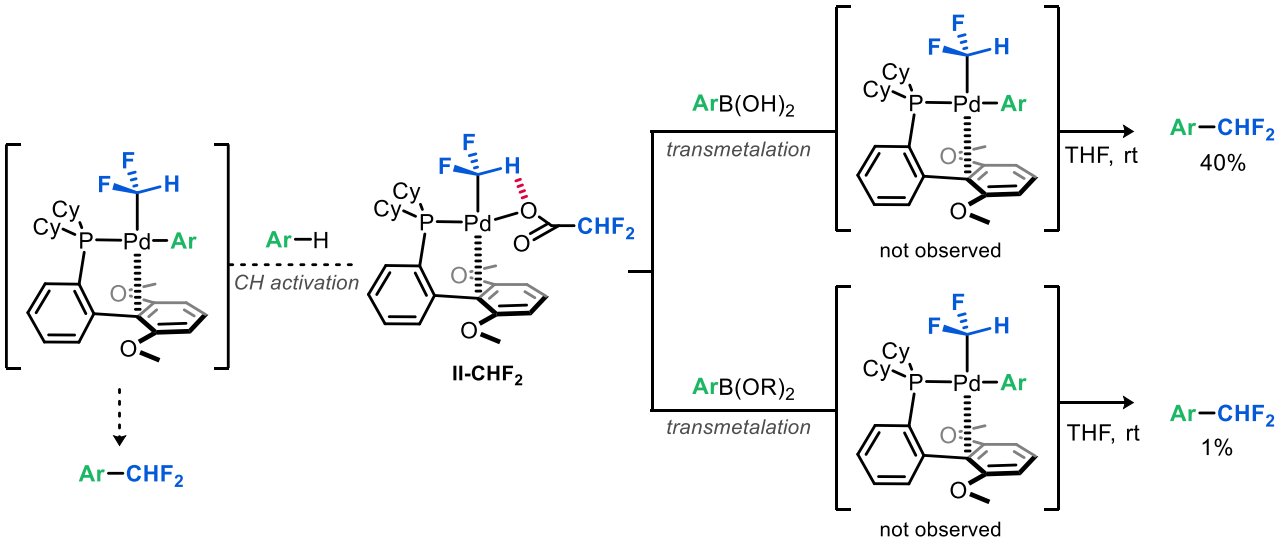

Scheme 3.3. Proposed C–H activation utilizing complex **II-CHF$_2$** from ref. 1a.

There are several examples of decarbonylative processes that use a C–H substrate as a nucleophile, although most feature Rh or Ir complexes as catalysts.[2] A recent report from the Tobisu lab demonstrates an Ir-catalyzed decarbonylative coupling reaction of acyl fluorides and arenes via C–H activation.[2a] In this report (Scheme 3.4), solvent quantities of benzene are required to promote its C–H activation and obtain a modest yield of 40%.[2a]

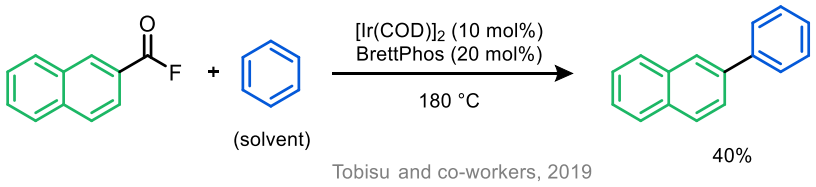

Scheme 3.4. Reaction scheme for Ir-catalyzed decarbonylative arylation using solvent quantities of benzene.

In general, these systems often require solvent quantities of arene, high temperature, high catalyst loadings, and exogenous base to promote reactivity.[2c] As such, the activation of simple arenes, such as benzene, remains challenging and ineffecient.[2c]

Moving forward, we selected benzoxazole as a model substrate for our C–H activation due to its novel biological activity[3a] and precedent in C–H activation reactions[3b-k]. Benzoxazole, a planar heterocycle, is found in biologically-active compounds and organic materials (Figure 3.3). As such, a variety of methods exist for the preparation of these compounds, and there has been large increase in the number of 2-substituted benzoxazoles that have been pharmacologically characterized from 1990 to 2014.[3l]

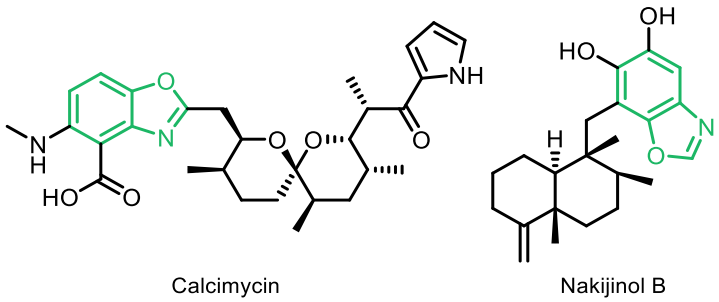

Figure 3.3. Examples of benzoxazole-containing pharmaceuticals.[3]

3.3 Optimization of Decarbonylative C–H Difluoromethylation of Arenes

To get a baseline for the desired reactivity, we first evaluated the efficacy of DFAF as the electrophile in a C–H difluoromethylation reaction of benzoxazole under the optimized conditions from our previous report (using Pd^0/SPhos as the catalyst).[1a] Under these preliminary conditions, only 6% of the desired product was observed and characterized in situ by ^{19}F NMR spectroscopic analysis (Scheme 3.5). The mass balance of the fluorinated by-products showed a significant amount of DFAF remaining and minor amounts of difluoroacetic acid as a by-product.

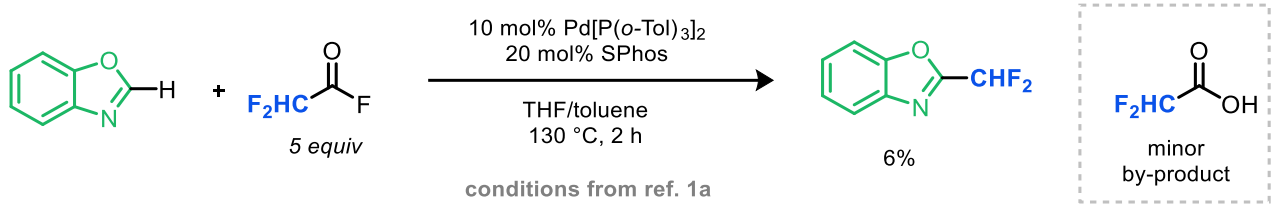

Scheme 3.5. Initial attempt at decarbonylative C–H difluoromethylation of benzoxazole under conditions from ref. 1a.

We next attempted the reaction between excess DFAAn and benzoxazole catalyzed by our Pd^0/SPhos system. Under similar conditions to our previous report[1a] (albeit with 20 mol% Pd[P(*o*-Tol)$_3$]$_2$ and 40 mol% SPhos), we were pleased to see 23% of the C–H difluoromethylation product, as determined by ^{19}F NMR spectroscopy with trifluoromethoxybenzene as an internal standard. Conducting the same experiment with $Pd(OAc)_2$, which is a common palladium precatalyst used in C–H activation reactions resulted in a lower yield of 12%. Overall, the results in Scheme 3.6 suggest that the X-type ligand that derives from the electrophile (F for DFAF vs difluoroacetate for DFAAn) plays a key role in the reaction.

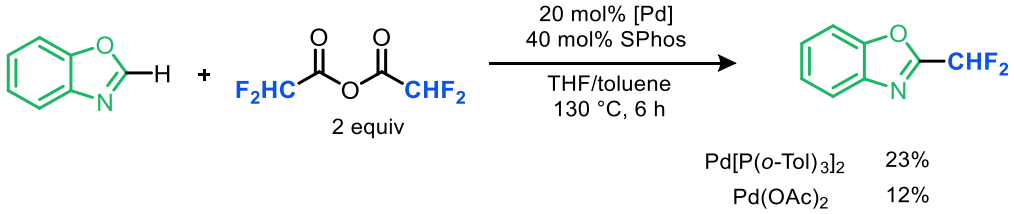

Scheme 3.6. Viability of DFAAn as an electrophile for decarbonylative C–H difluoromethylation under preliminary conditions from ref. 1a.

After demonstrating the feasibility of the decarbonylative difluoromethylation of benzoxazole, we moved to optimize the reaction conditions. Working with a first-year rotation student (Emily Wearing), the catalyst, solvent, and temperature were optimized (Table 3.1). By changing the ligand from the hemilabile bidentate SPhos to symmetrical wide bite angle bidentate ligand XantPhos[4], we observed a significant improvement in reactivity. Under optimized conditions using a Pd^0/Xantphos as the catalyst in toluene, we observed nearly quantitative yield of 2-difluoromethylbenzoxazole (see Experimental Section for full details).

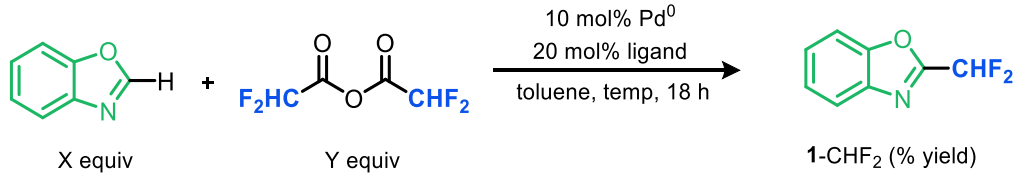

Entry	X equiv	Y equiv	Pd^0	ligand	solvent, temp, time	1-CHF_2 (% yield)
1	1	1	$Pd[P(o\text{-}Tol)_3]_2$	SPhos	toluene, 140 °C	13
2	3	1	$Pd[P(o\text{-}Tol)_3]_2$	SPhos	toluene, 140 °C	35
3	1	3	$Pd[P(o\text{-}Tol)_3]_2$	SPhos	toluene, 140 °C	34
4	1	3	$Pd[P(o\text{-}Tol)_3]_2$	SPhos	toluene:THF 2:1, 140 °C	23
5	1	3	$Pd[P(o\text{-}Tol)_3]_2$	SPhos	1,4-dioxane, 140 °C	24
6	1	3	$Pd[P(o\text{-}Tol)_3]_2$	SPhos	DMSO, 140 °C	0
7	1	3	$Pd[P(o\text{-}Tol)_3]_2$	SPhos	toluene, 150 °C	42
8	1	3	$Pd[P(o\text{-}Tol)_3]_2$	RuPhos	toluene, 150 °C	47
9	1	3	$Pd[P(o\text{-}Tol)_3]_2$	BrettPhos	toluene, 150 °C	47
10	1	3	$Pd[P(o\text{-}Tol)_3]_2$	XPhos	toluene, 150 °C	61
11	1	3	$Pd[P(o\text{-}Tol)_3]_2$	DPEPhos	toluene, 150 °C	70
12	1	3	$Pd[P(o\text{-}Tol)_3]_2$	*t*-BuXantPhos	toluene, 150 °C	45
13	**1**	**3**	**$Pd[P(o\text{-}Tol)_3]_2$**	**XantPhos**	**toluene, 150 °C**	**>99**
14	**1**	**3**	**$Pd(dba)_2$**	**XantPhos**	**toluene, 150 °C**	**>99**

Yields determined by ^{19}F NMR with C_6F_6 internal standard

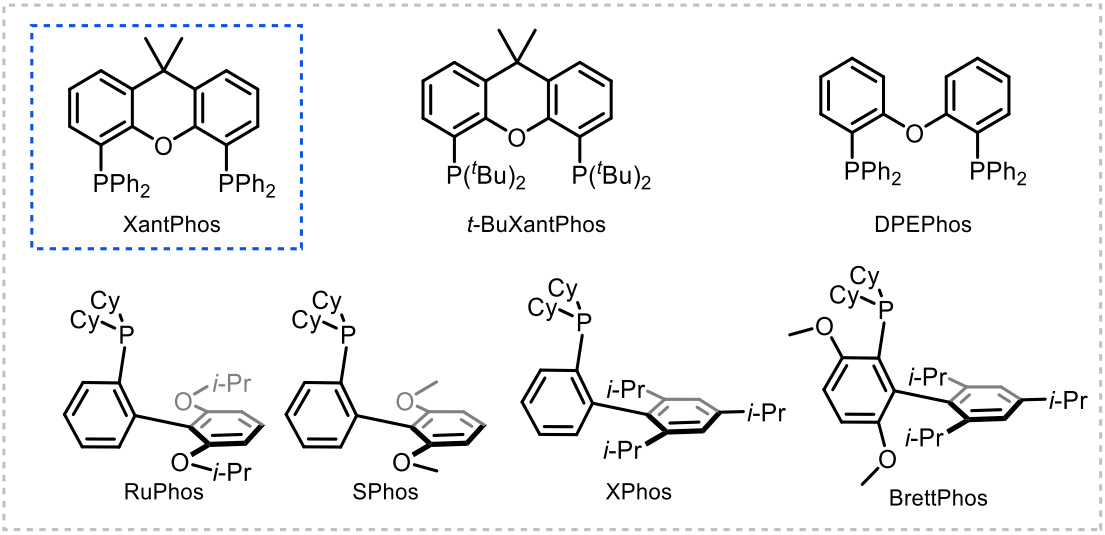

Table 3.1. Optimization of decarbonylative C–H difluoromethylation of benzoxazole using DFAAn.

As shown in Table 3.1, increasing the equivalents of either DFAAn or benzoxazole resulted in improved yields (entries 2 and 3 compared to entry 1). Solvent screening using SPhos showed that the reaction works comparably in toluene, mixture of THF and toluene, and in 1,4-dioxane. In contrast, DMSO was not a viable solvent (entry 6). Selecting toluene moving forward, we screened a variety of Buchwald-type phosphine ligands (RuPhos – entry 8, BrettPhos – entry 9, XPhos – entry 10) in addition to other ligands commonly used in palladium catalysis.[4] These screens uncovered XantPhos as a uniquely effective ligand for this transformation (entry 13 and 14). XantPhos, a bidentate phosphine ligand, is known[4] for having a particularly wide bite angle of 108°; a variety of cis-chelated Xantphos derivatives synthesized by the van Leeuwen group have natural bite angles ranging from 102° to 123°.[4] Additionally, XantPhos has been demonstrated in a trans configuration at palladium (Figure 3.3).[4g] There is extensive precedent for XantPhos as the ligand in a variety of carbonylative processes, including Rh-catalyzed hydroformylation, Pt-catalyzed alkene hydroformylation, and Pd-catalyzed CO/ethene polymerization.[4a] The efficacy of Xantphos in C–H activation reactions is supported by previous work by Blackmond and co-workers.[4e] However, in this report, a mono-oxidized XantPhos is reported to form in situ and act as the active catalyst for C–H functionalization (Figure 3.4).[4e]

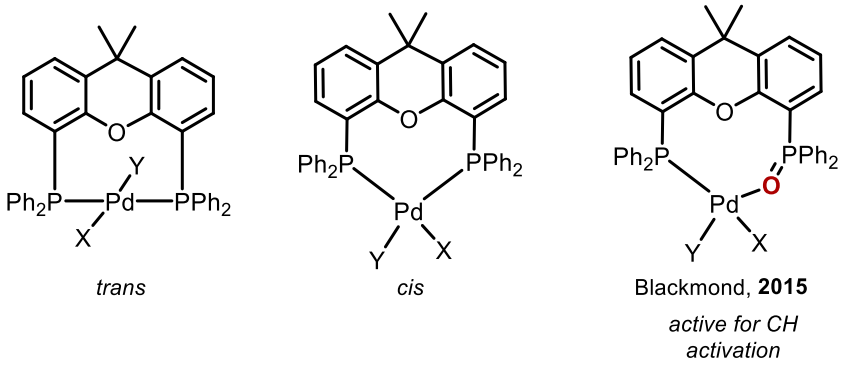

Figure 3.4. Potential binding modes for XantPhos at Pd.[4]

Having identified a reactive $Pd(dba)_2$/Xantphos catalyst system, we moved to screen other azoles and (hetero)arenes in the C–H activation reaction. Ultimately, we targeted a C–H activation reaction that could functionalize a variety of arenes and was not limited to a particular class of arene (azoles). We tested a small subset of azoles and other arenes using the Pd^0/XantPhos catalyst.

However, as shown in Scheme 3.7, only benzoxazole and its sulfur analogue, benzathiazole, afforded detectable yields under these conditions, giving 99% and 70% of the difluoromethylated product, respectively.

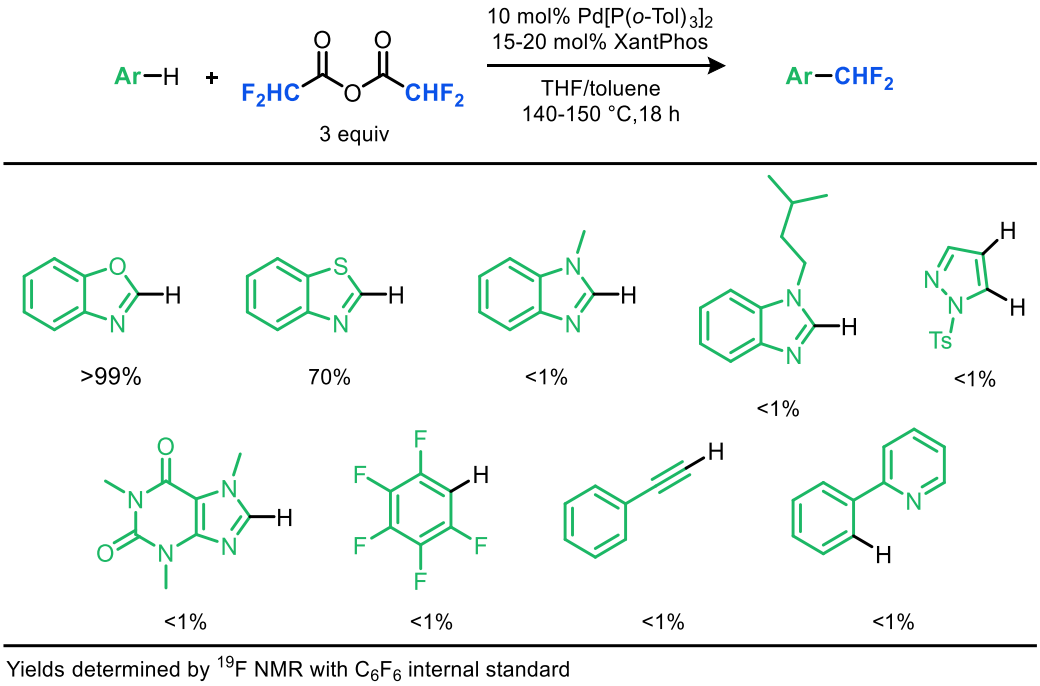

Scheme 3.7. Substrate screen for C–H difluoromethylation under preliminary Pd/XantPhos conditions

We hypothesized that the (XantPhos)Pd^{II}–difluoroacetate intermediate that formed after oxidative addition and carbonyl de-insertion with DFAAn might not be sufficiently basic to participate in a CMD-type C–H activation with substrates that are less acidic than benzoxazole. We hypothesized that the incorporation of a more basic carboxylate into the electrophile (such that it ultimately ended up as the X-type ligand at Pd^{II}) could have a beneficial impact on reactivity and substrate scope (Scheme 3.8).

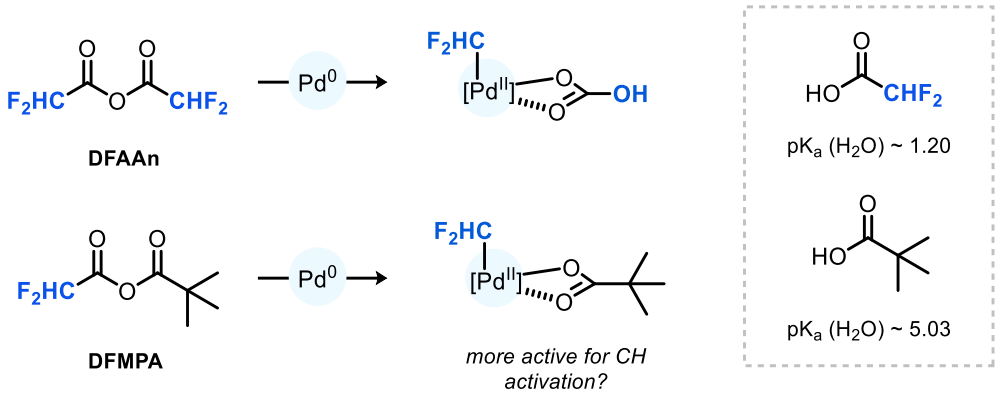

Scheme 3.8. Potential for more basic endogenous base incorporated into structure of the difluoroacyl electrophile.

To test this hypothesis, Frances Gu (a graduate student under my mentorship) synthesized the mixed difluoromethyl pivalyl anhydride DFMPA. Below in Scheme 3/9, a small summary of this work is presented that compares the efficacy of DFAF, DFAAn, and DFMPA as electrophiles for our C–H activation system. The full extent of this work will be described in her thesis. Overall, these studies demonstrate the impact of electrophile structure on product yield, with notable effectiveness of DFMPA for imidazole substrates (entries 3, 6, 9, and 12) that did not show any reactivity with the symmetric anhydride DFAAn. Frances was also able to functionalize not only fused azoles but also aryl substituted azoles. Ongoing work in this area is focused on expanding the arene scope beyond fused and substituted azoles to simple arenes.

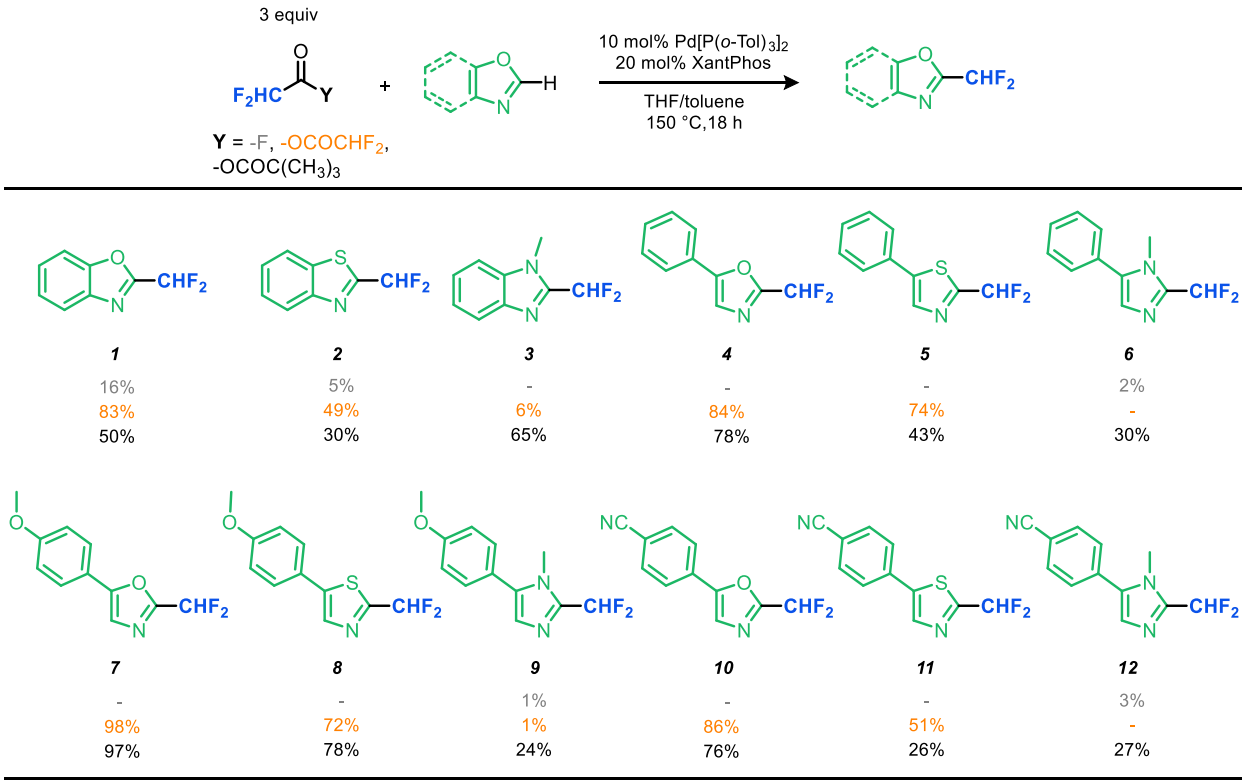

Yields determined by ^{19}F NMR with C_6F_6 internal standard

Scheme 3.9. Substrate scope for C–H difluoromethylation obtained by Frances Gu using three different difluoroacyl electrophiles.

In addition to the entries above, we conducted a small set of catalytic reactions using DFAAn and $Ni(COD)_2$ as the precatalyst. The inspiration for this work was based on related work from Itami and co-workers from 2012 in which they demonstrated the feasibility of a decarbonylative C–H arylation of benzoxazole with *O*-aryl esters using $Ni^0(COD)_2$/dcype as the catalyst.[5]

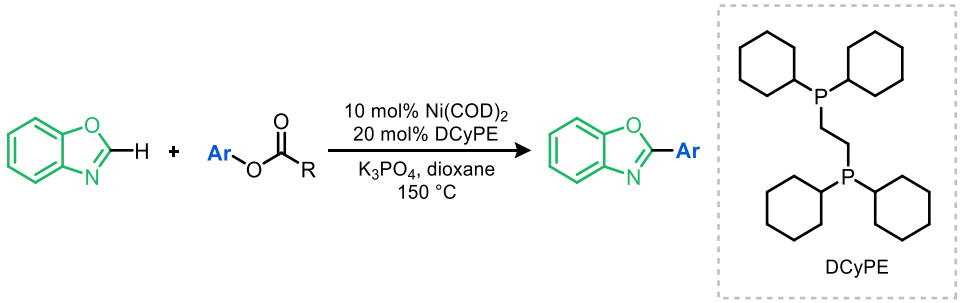

Scheme 3.10. Decarbonylative C–H arylation of benzoxazole conducted by Itami and co-workers.[5]

We initially tested the reactivity of DCyPE in our reaction and observed very little of the C–H difluoromethylated product (entry 1, 5%). Moving forward, we screened a variety of other ligands and found that XantPhos was still the most effective ligand under these conditions. Key differences between our conditions and those reported by Itami[5] are the presence of base for an *arylation* reaction rather than a difluoromethylation reaction.

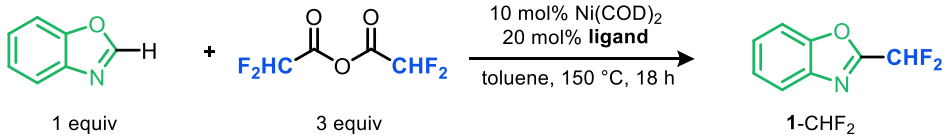

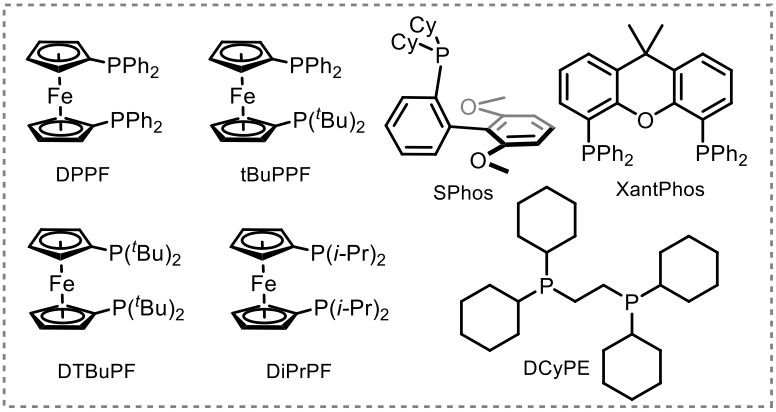

Entry	ligand	**1**-CHF_2 (% yield)
1	DCyPE	5
2	SPhos	15
3	DPPF	4
4	tBuPPF	4
5	DTBuPF	5
6	DiPrPF	3
7	**XantPhos**	**18**
8	none	0

Yields determined via ^{19}F NMR with C_6F_6 int. std.

Scheme 3.11. Screen of Ni-catalyzed conditions for decarbonylative C–H difluoromethylation showing XantPhos as the most effective ligand.

3.4 Synthesis of (XantPhos)Pd(CHF_2)($OCOCHF_2$) [Xant-II-CHF_2]

To better understand the substrate effects and mechanistic impacts of a (XantPhos)Pd catalyst, we aimed to synthesize one of the proposed catalytic intermediates in the reaction, **Xant-II-CHF_2** (Scheme 3.12) Due to the unique ability of Xantphos to bind the metal in a cis or trans configuration[4], we were interested in characterizing the coordination geometry of this proposed intermediate. In addition, we sought to test its stoichiometric reactions with a variety of arenes to assess the feasibility, mechanism, and relative rates of the C–H activation step as a function of

carboxylate ligand structure. This could then inform the design of news electrophiles that are even more effective in this transformation.

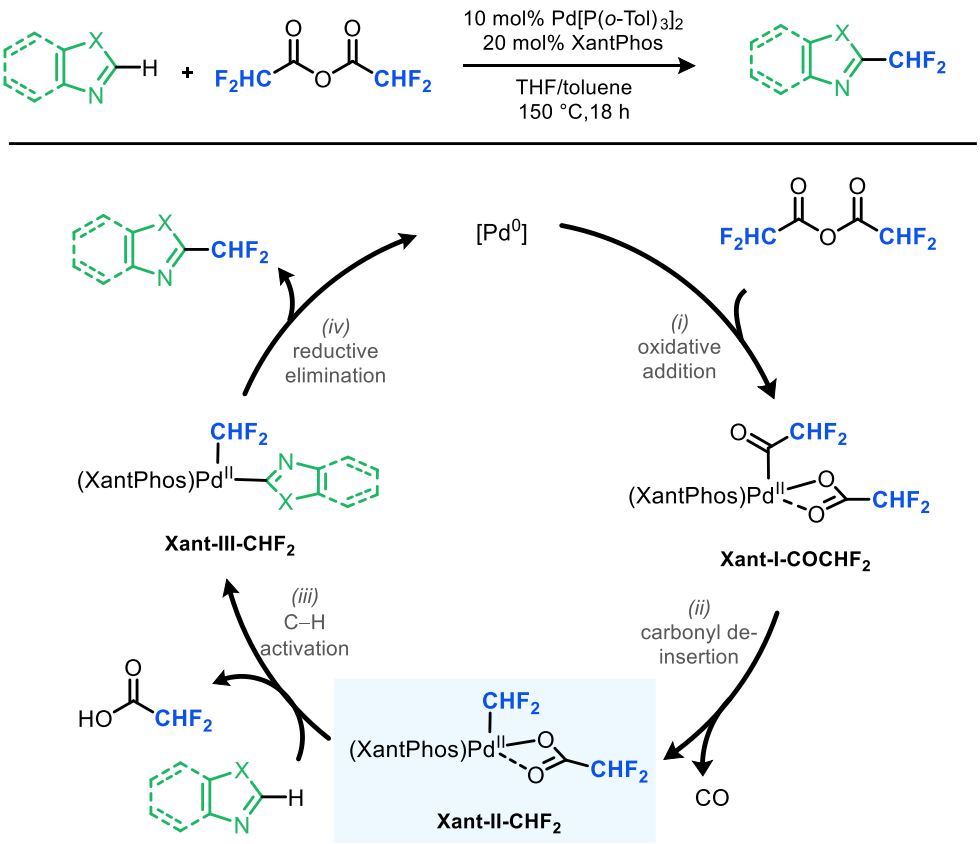

Scheme 3.12. Proposed catalytic cycle for decarbonylative C–H difluoromethylation with targeted complex **Xant-II-CHF$_2$**.

To begin, we took inspiration from our previous work synthesizing an analogous (SPhos)Pd complex[1a] and reacted DFAAn with 1 equiv of Pd^0 and 1 equiv of Xantphos in THF at room temperature (see Experimental Section for complete details). We anticipated that oxidative addition and subsequent carbonyl de-insertion would generate the target complex **Xant-II-CHF$_2$**. Purification of the crude reaction via precipitation and subsequent recrystallization afforded a crystalline orange solid. Subsequent ^{19}F NMR spectroscopy however showed only one resonance (d, -124.8 ppm, J = 54.1 Hz, unreferenced), which is indicative of a single type of CF_2H group within the molecule. Only one phosphorus signal was observed in the 31P NMR (s, 6.78 ppm) and

one difluoromethyl signal was observed in the ^{1}H NMR (t, 4.92 ppm, J = 55.2 Hz, 2H). This is inconsistent with the proposed catalytic intermediate, which should have two unique -CHF_2 signals. Based on our previous work[1a], we hypothesized that this complex was likely the symmetrical (XantPhos)Pd($OCOCHF_2$)$_2$ complex **Xant-sym** (Scheme 3.13).

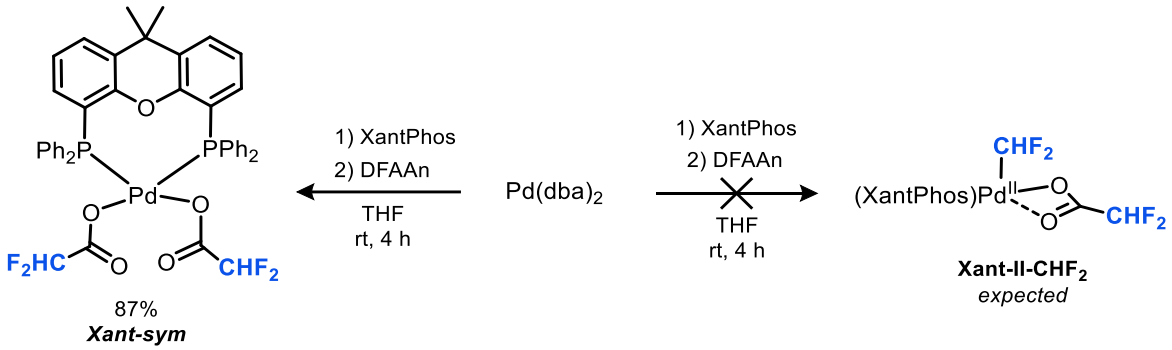

Scheme 3.13. Attempted one-step synthesis of **Xant-II-CHF_2**.

Single crystal growth of the isolated solid was attempted via vapor diffusion using a mixture of DCM and THF in a jacket solution of diisopropylether (see Experimental Section for details). Structure elucidation via X-ray diffraction of this single crystal was conducted by Dr. Jeff W. Kampf and an ORTEP diagram is shown below in Figure 3.5.

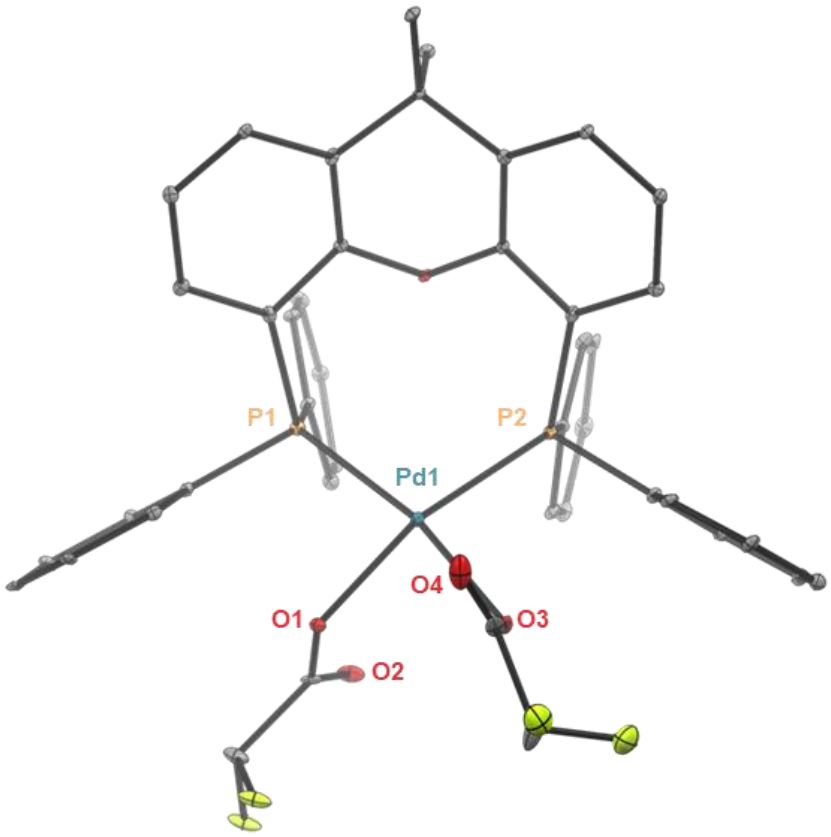

Figure 3.5. ORTEP diagram of **Xant-sym**. Hydrogen atoms are omitted for clarity. Selected bond lengths (Å) and angles (deg): Pd1–P1 2.32, Pd1–P2 2.30, Pd1–O1 2.09, Pd1–O3 2.09, Pd1---O2 2.97, P1–Pd1–P2 103.0.

Complex **Xant-sym** features XantPhos in a cis geometry with a P–Pd–P bite angle of 103°. This complex was characterized via NMR spectroscopy ^{19}F, ^{31}P, and ^{1}H NMR spectroscopy. Complex **Xant-sym** has similar Pd–P bond lengths (2.32, 2.30 Å) to other (XantPhos)Pd complexes[4f] that feature a cis-chelated XantPhos (2.44, 2.40 Å). The calculated bite angle of this complex (103°) is slightly smaller than that of reported (XantPhos)Pd complexes (111°).[4f]

We were surprised to find that the one-step synthesis attempted above was not effective for generating the proposed catalytically-relevant metal intermediate **Xant-II-CHF$_2$**. Based on precedents from our lab[6], we proposed an alternative, two-step synthesis to obtain the desired complex (Scheme 3.14). We first reacted Pd[P(*o*-Tol)$_3$]$_2$ with excess DFAAn in THF at room temperature for 24 h to afford the *trans*-[P(*o*-Tol)$_3$]$_2$Pd(CHF$_2$)(OCOCHF$_2$) complex **1** via oxidative addition and carbonyl de-insertion. Complex **1** was not isolated but was characterized *in*

situ based on its diagnostic broad ^{19}F NMR resonances for the difluoromethyl (bs, -86.10 ppm, 2F) and difluoroacetate (d, -124.0 ppm, J = 48.5 Hz) ligands.

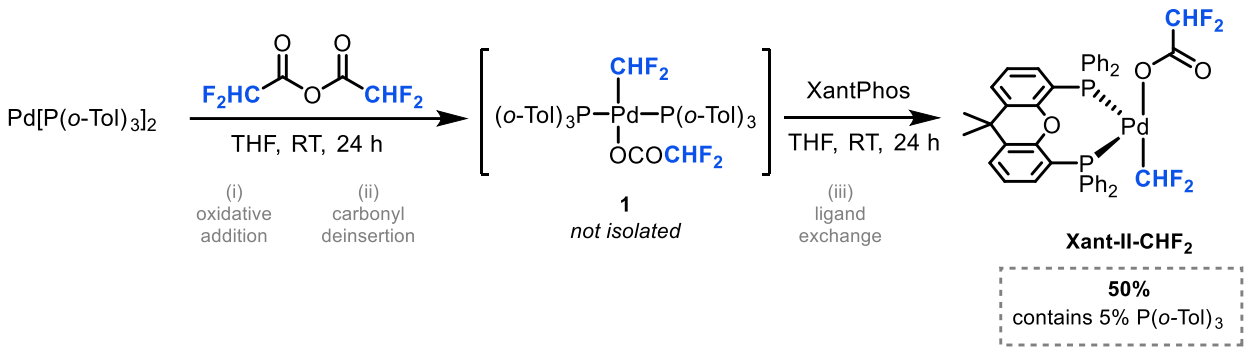

Scheme 3.14. Two-step synthesis of **Xant-II-CHF$_2$**.

The subsequent addition of XantPhos to this crude residue led to the formation of a yellow solid that was isolated via precipitation and subsequent recrystallization (Scheme 3.14). Subsequent ^{1}NMR spectroscopy of this yellow solid showed two distinct signals in the ^{19}F NMR (q, -71.8 ppm, J = 48.7 Hz and d, -124.0, J = 56.2 Hz) and an associated signal in the ^{31}P NMR (t, 12.89, J = 50.4 Hz). This information suggested that two unique CH**F**$_2$ signals existed for the complex with only one associated phosphorus signal of XantPhos. Single crystal growth of the yellow solid was attempted via vapor diffusion using a mixture of DCM and THF in a jacket solution of diisopropylether. We obtained the crystal structure of **Xant-II-CHF$_2$** and isolated the complex in 50% yield from this recrystallization. The ORTEP diagram for **Xant-II-CHF$_2$** is shown in **Figure 3.6**.

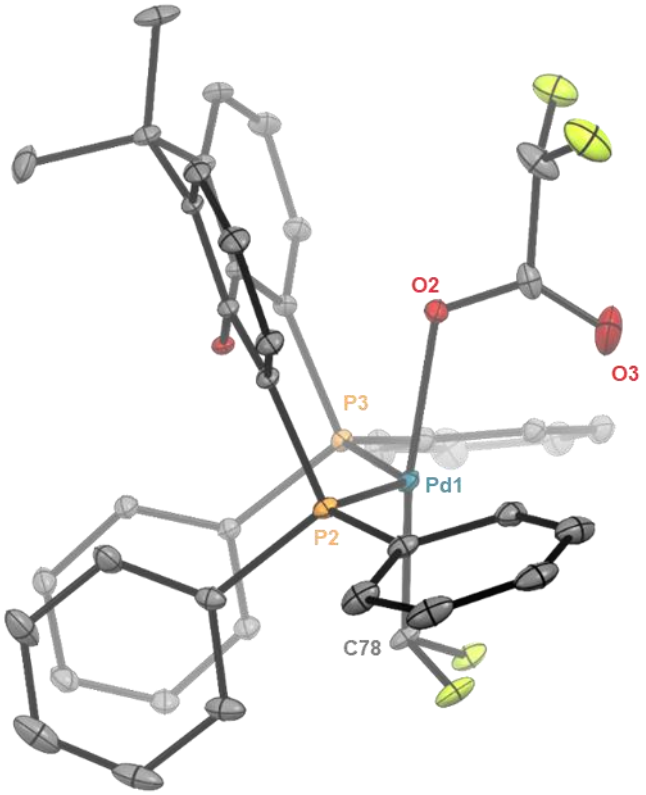

Figure 3.6. ORTEP diagram of **Xant-II-CHF$_2$**. Hydrogen atoms are omitted for clarity. Selected bond lengths (Å) and angles (deg): Pd1–P2 2.32, Pd1–P2 2.32, Pd1–O2 2.16, Pd1---O3 3.12, Pd1–C78 1.98, P2–Pd1–P3 132.6, O2–Pd1–C78 171.6.

As shown in in Figure 3.6, the geometry of this complex is a four-coordinate "see-saw" featuring XantPhos with a 132.6° bite angle. Notably, the -CFH_2 and -$OCOCHF_2$ ligands are trans to one other, with an O2–Pd1–C78 angle of 171.6°. The 4-coordinate see-saw geometry of **Xant-II-CHF$_2$** is most closely related to the 5-coordinate trigonal bipyramidal geometry, except with one of the equatorial ligands removed. Notably, this complex has a unique geometry relative to other (XantPhos)Pd^{II} complexes that are known in the literature.[4] In complexes that feature a cis-ligated XantPhos (and related bisphosphines, including DPEPhos) on Pd^{II}, the P–Pd–Pd bite angles range from 102 to 120.6°.[4] Indeed, the bite angle in **Xant-sym** (Figure 3.5) is 103°. Known complexes that feature trans-chelated Xantphos at Pd^{II} have bite angles of 150.7° in a report by Buchwald[4g] and 153° in a report by van Leeuwen.[4f] In contrast, **Xant-II-CHF$_2$** has a significantly

contracted P–Pd–P bite angle of 132.6°, which lies between the observed ranges for cis and trans-chelated (XantPhos)Pd^{II} complexes.[4] We hypothesize that the open coordination site of **Xant-II-CHF$_2$** could be ligated by an arene to form a catalytically-relevant intermediate to undergoes C–H activation. The reactivity of these complexes is currently being studied by Frances Gu and will be detailed in her thesis.

3.5 Future Directions for Decarbonylative C–H Difluoromethylation of Arenes

The initial goal in this area will be to isolate complex **Xant-II-CHF$_2$** in high purity and yield. With this complex in hand, we can study its reactivity with a variety of arene substrates to understand the mechanism, chemoselectivity, and regioselectivity of C–H activation. Further, kinetic data could be generated that would elucidate on the possible mechanistic pathways for the C–H activation process.

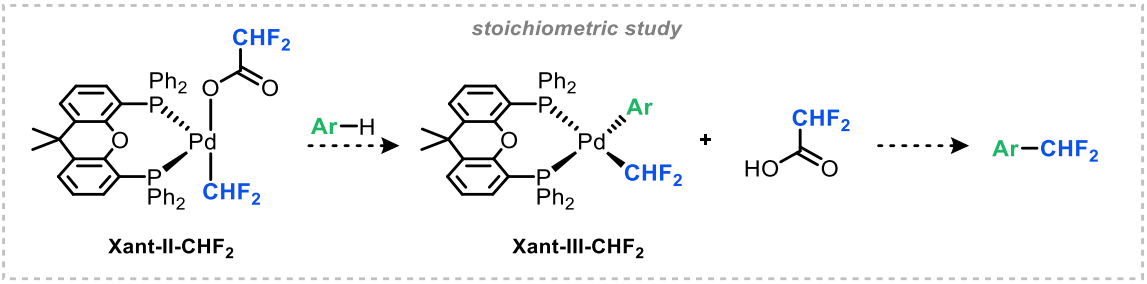

Scheme 3.15. Proposed stoichiometric C–H activation study conducted with complex **Xant-II-CHF$_2$**.

Our ultimate goal is to develop a decarbonylative C–H difluoromethylation that has a broad scope with respect to the C–H substrate. We propose that we can synthesize a variety of a complexes via the exchange of different basic X-type ligands (**Y**, shown in Scheme 3.16). This will then enable the identification of a palladium complex that is sufficiently activated to react with C–H bonds of a more diverse array of arenes.

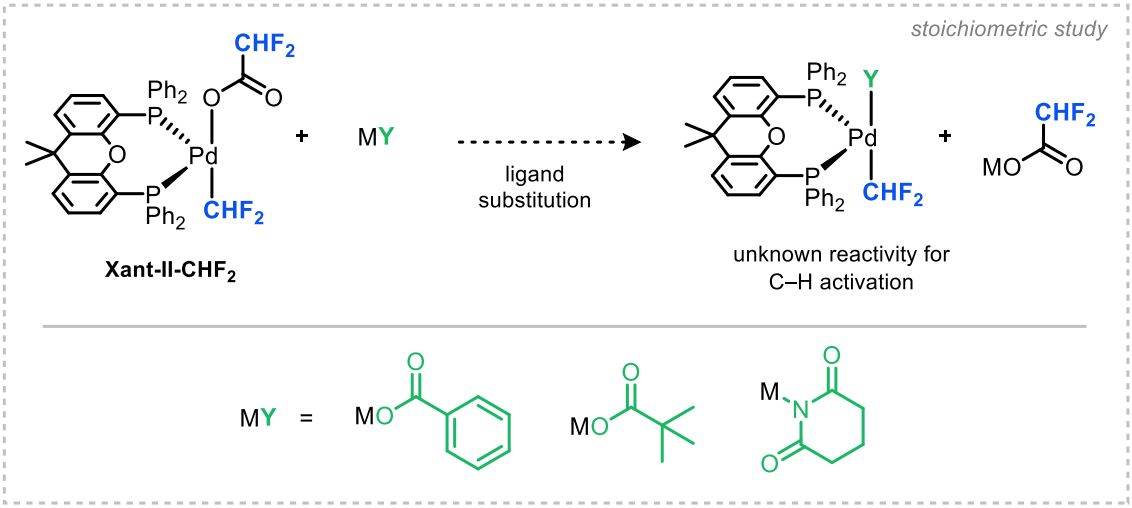

Scheme 3.16. Stoichiometric identification of other reactive X-type ligands (Y) for decarbonylative C–H difluoromethylation.

In addition to the above stoichiometric experiments, we aim to assess the efficiency of the isolated **Xant-II-CHF2** as a catalyst (Scheme 3.17) for this decarbonylative C–H activation reaction. In many cases, the utilization of an on-cycle catalytic intermediate as the catalyst leads to improved catalytic efficiency and product yield.

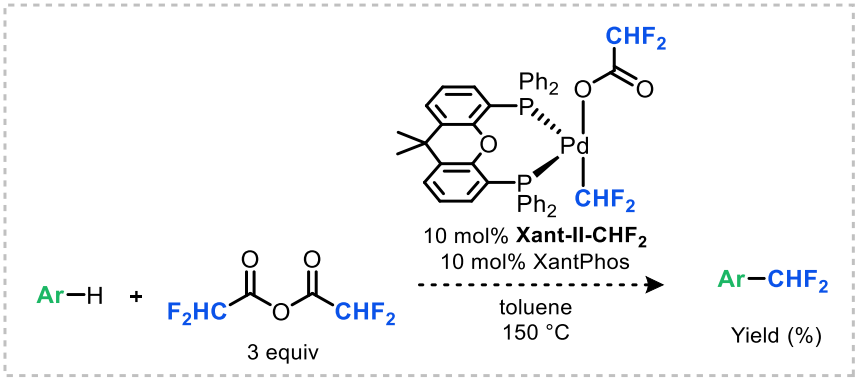

Scheme 3.17. Proposed utilization of **Xant-II-CHF2** as a precatalyst for decarbonylative C–H difluoromethylation.

3.6 Decarbonylative Cross-Coupling of Chiral Acid Derivatives

In the studies in Section 2.5 and in Section 3.3, we developed two different catalytic decarbonylative difluoromethylation reactions that utilized difluoromethyl-containing electrophiles (Scheme 3.18). We observed significant ligand effects in both systems, with the optimized ligands displayed unique activity for the desired reaction.

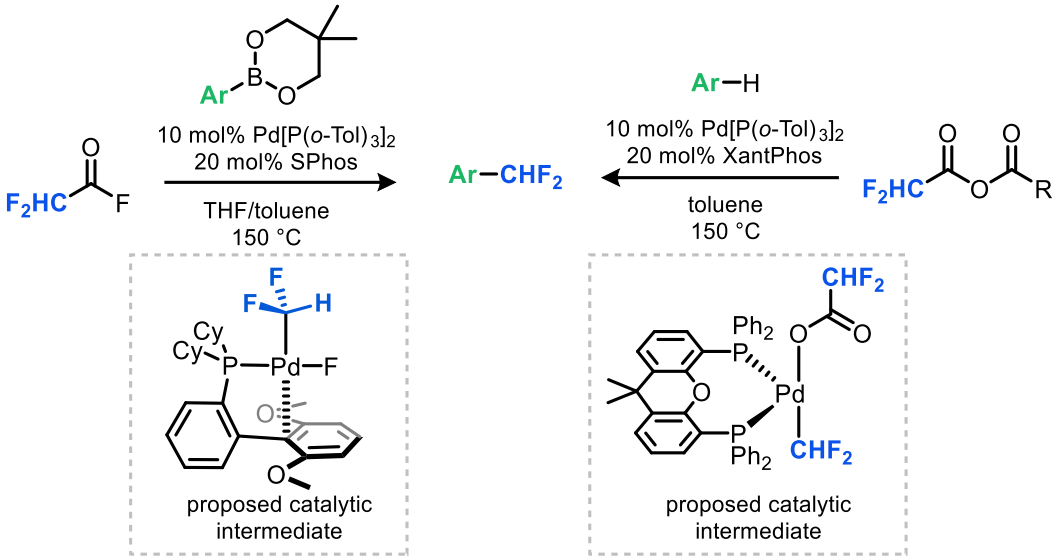

Scheme 3.18. Developed methods for decarbonylative difluoromethylation catalyzed by Pd.[1a]

Our first system Pd-catalyzed system (described in Chapter 2) generated the difluoromethylated product via cross-coupling using aryl boronate esters and DFAF.[1a] This system was uniquely effective with SPhos and other Buchwald ligands, including RuPhos and DavePhos. When initially attempting the C–H difluoromethylation of benzoxazole under similar conditions, we found that SPhos was largely ineffective for promoting the desired transformation. We also found that alternative electrophiles (DFAAn, DFMPA) generally displayed superior reactivity to DFAF in these C–H activation reactions. The system was uniquely enabled by wide bite angle bis-phosphines, such as DPEPhos and particularly XantPhos.

One of the ultimate goals in our work is to develop the decarbonylative cross-coupling of chiral acid derivatives. This approach would enable the coupling of the chiral alkyl groups of the electrophile with organometallic reagents to form chiral products, thereby leveraging these

abundant chiral pool reagents. The proposed catalytic cycle for this process is shown in Scheme 3.19.

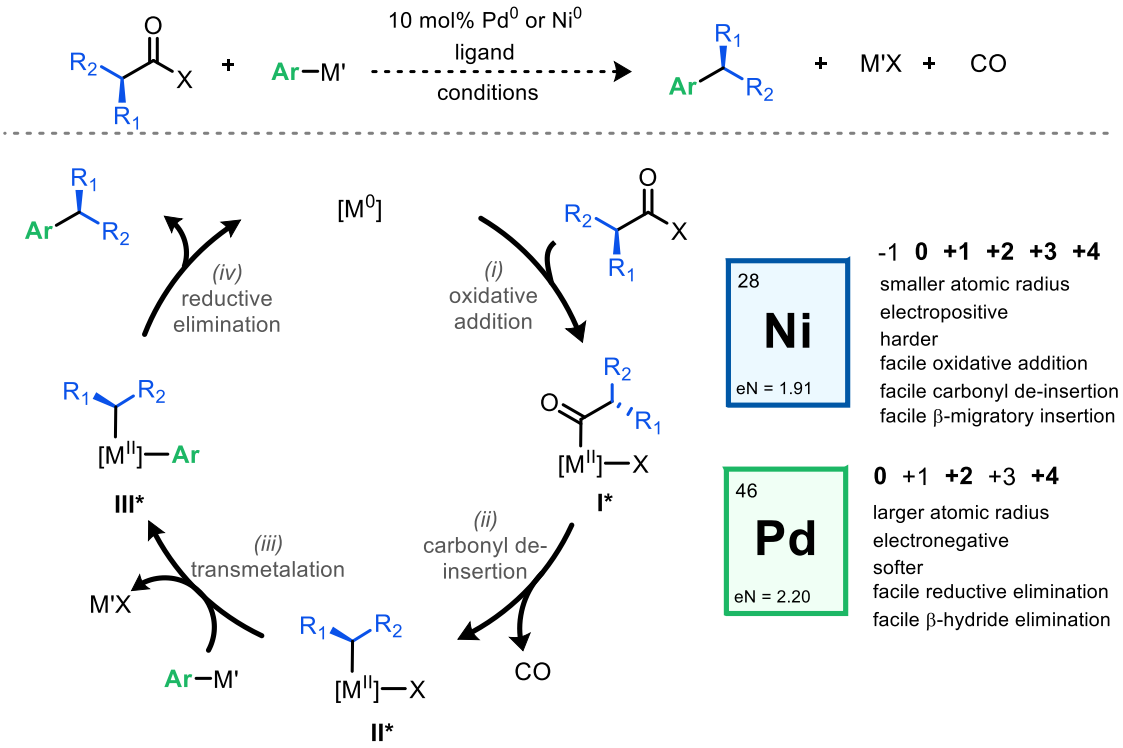

Scheme 3.19. Proposed catalytic cycle for decarbonylative chiral acid coupling.

However, this proposed system presents many challenges regarding the individual steps of the catalytic cycle. These challenges include:

(1) The oxidative addition of an acid derivative to form **complex I*** may be challenging. As such, we anticipated that Ni-based catalysts might be preferable to then Pd analogues[7].

(2) The rate of carbonyl de-insertion of a bulky, chiral alkyl group to generate complex **II*** and extrude CO will be likely be slow[7].

(3) If carbonyl de-insertion is slow relative to transmetalation, transmetalation could occur at intermediate **I***. The subsequent C(sp^2)-C(sp^2) reductive elimination to form a ketone product will likely to be faster than the desired C(sp^2)–C(sp^3) reductive elimination,

(4) C(sp^2)–C(sp^3) reductive elimination, which has been demonstrated from Ni(III) complexes, would likely be challenging from more electron-rich Ni(II)[7],

(5) The organometallic intermediates **II*** and **III*** are likely susceptible to ß-hydride elimination, leading to decomposition of substrate and catalyst. This is expected to be be particularly problematic at Pd^{II}.[7]

We initially sought to assess the feasibility of the target transformation using a commercially available chiral acid derivative. We selected Mosher's acid[8] as a starting material due to its commercial availability and the -CF_3 substituent it contains. Generally, the presence of fluorine and fluoroalkyl groups enables a fast and highly sensitive method for chemical analysis in ^{19}F NMR spectroscopy. This technique allowed us to readily analyze the difluoromethylation reactions in Section 2.3 (and detect the room temperature carbonyl de-insertion of difluoroacetic anhydride at a (SPhos)Pd complex[1a]) via diagnostic resonances in the ^{19}F NMR spectrum. Accordingly, the decarbonylative coupling of acid derivatives that are absent of fluorine atoms presents a challenge regarding rapid and sensitive chemical analysis of intermediates related to oxidative addition, carbonyl de-insertion, subsequent reaction pathways, and/or decomposition modes. We synthesized the phenyl ester of Mosher's acid via reaction of the acid chloride and phenol. This reaction was afforded ester **1** in 69% yield.

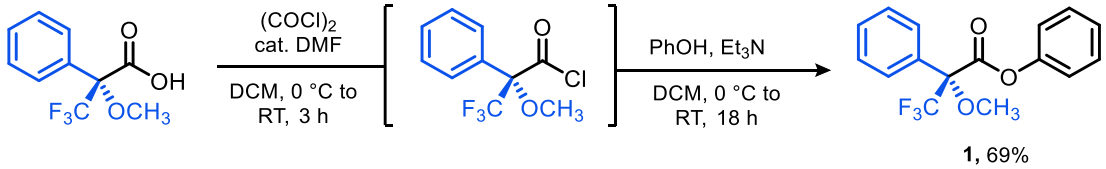

Scheme 3.20. Synthesis of Mosher's ester **1** via the acyl chloride intermediate.

A ^{19}F NMR-scale stoichiometric reaction was conducted to probe the reaction of ester **1** with 1 equiv of $Ni^0(COD)_2$ and 2 equiv of P(^{n}Bu)$_3$. We reasoned that Ni would be a good strating point because it undergoes more facile oxidative additon and CO de-insertion compared to the Pd analogues. Further, the metal intermediates of this acid may be susceptible to ß-fluoride elimination, a process that is generally slower at Ni.[7] Tri-*n*-butylphosphine, P(^{n}Bu)$_3$, was selected based on preliminary results from our lab that suggested its efficacy in decarbonylative processes.[1] As shown in Scheme 3.21, after 2.5 h at 80 °C, we observed oxidative addition of **1** to form a new species tentatively assigned as Ni^{II}-acyl complex **A** in 38% yield. This complex shows a singlet at

-71.7 ppm by ^{19}F NMR spectroscopy (referenced to 4-fluorotoluene) and a singlet at 13.87 ppm in the ^{31}P NMR. Minimal changes to the NMR spectrum were observed after heating the reaction mixture at 80 °C for a total of 18 h.

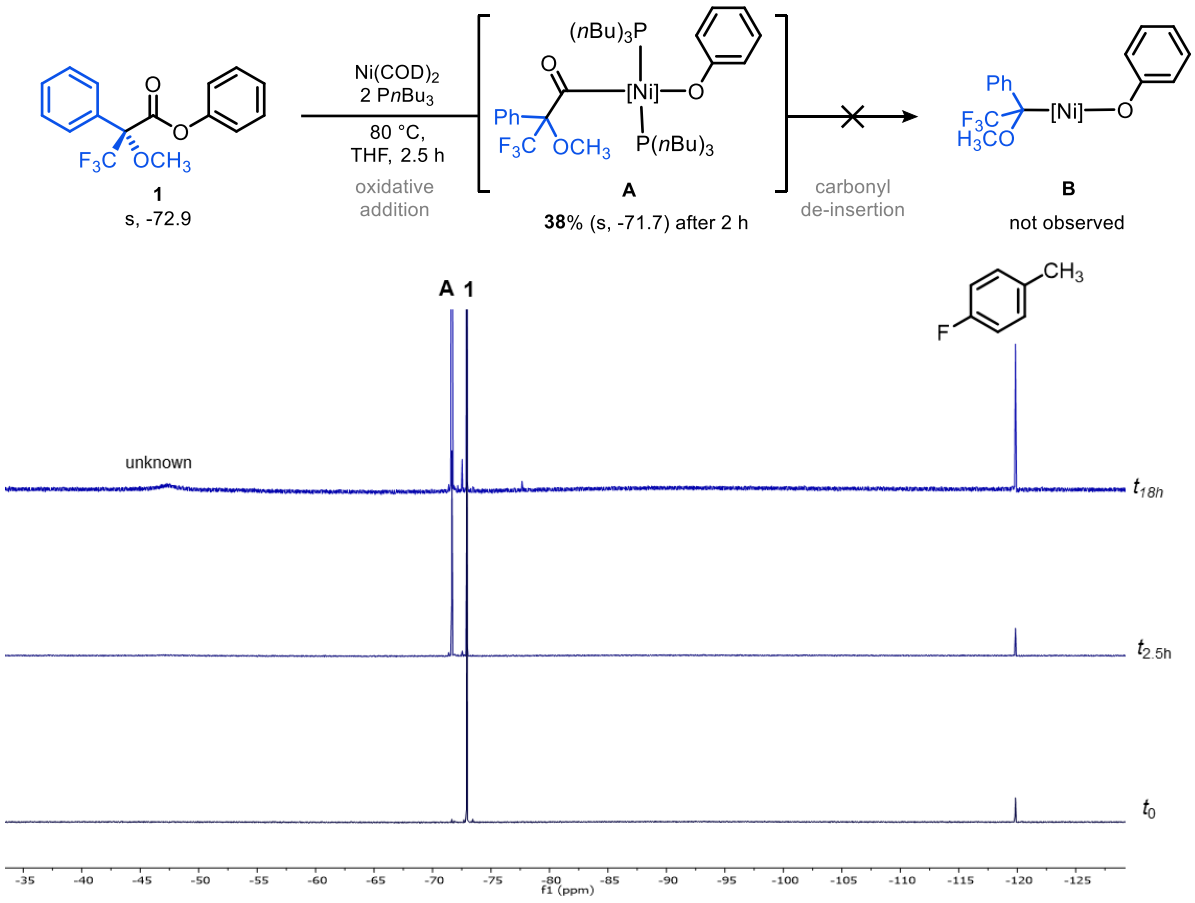

Scheme 3.21. Oxidative addition and carbonyl de-insertion study of Mosher's ester **1**.

Having observed oxidative addition of **1** at 80 °C in THF, our next goal was to observe the carbonyl de-insertion event that follows in the proposed catalytic cycle (Scheme 3.19). Therefore, we conducted a related experiment reacting **1** with Ni(^{0}COD)$_2$/P(*n*Bu)$_3$ at higher temperature (120 °C) in THF. After 18 h, we did not observe either complex **A** or **B** by ^{19}F NMR sectroscopy. Instead, the ^{19}F NMR spectrum showed remaining ester **1** along the formation of a single by-product with a pair of doublets at -100.4 ppm and -110.3 ppm (J = 60 Hz in both cases). The chemical shift and coupling constants are consistent with the difluorinated alkene product (2,2-

difluoro-1-methoxyvinyl)benzene (**X**), which could form by ß-fluoride elimination from Ni^{II} complex **B** (Scheme 3.22).[9]

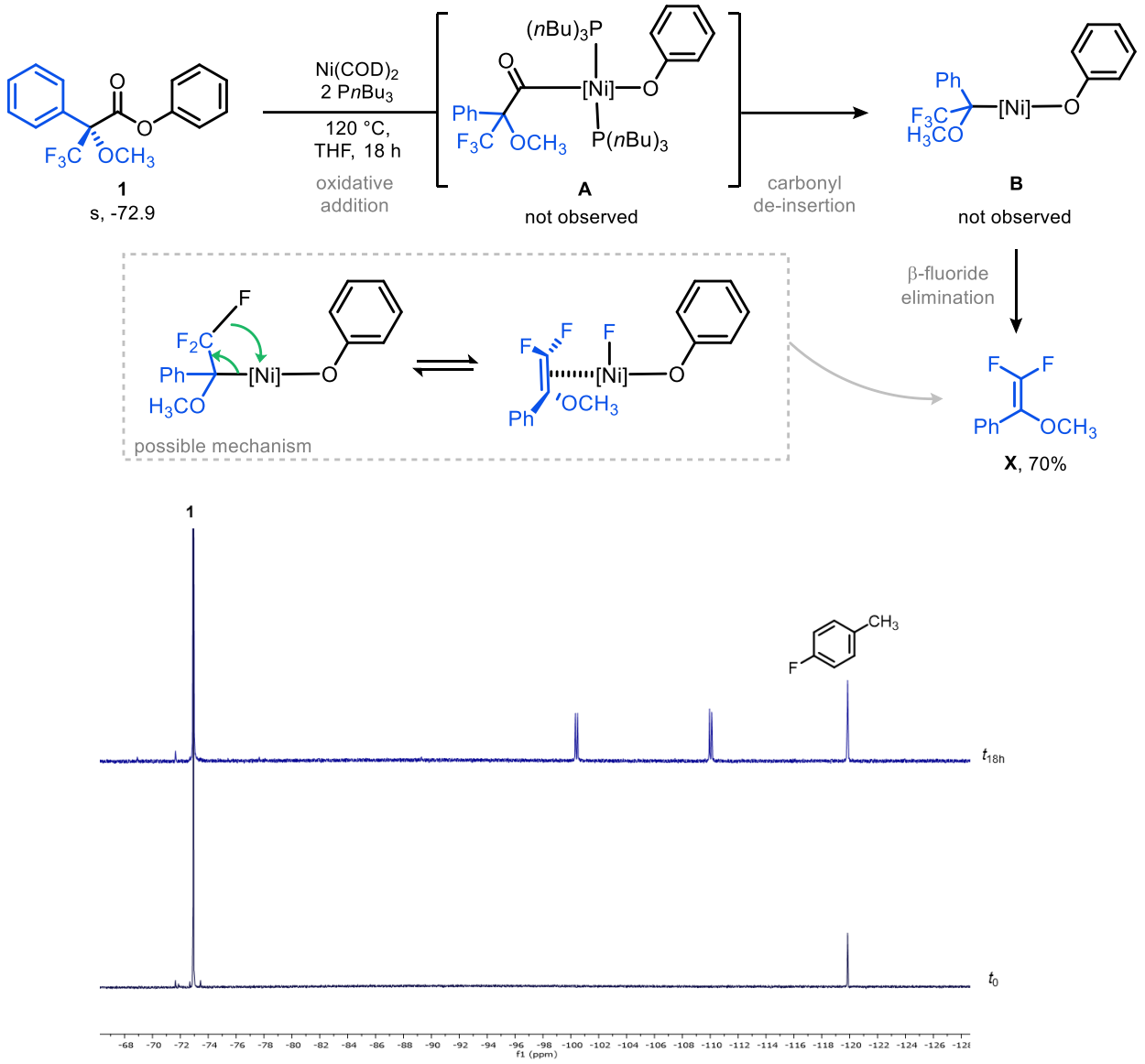

Scheme 3.22. Observation of alkene **X** in the crude NMR spectrum after heated reaction of **1** with Ni catalyst.

Given that neither **A** or **B** were observed after 18 h, we concluded that under these conditions, ß-fluoride elimination consumes **B** and drives the reaction to form (2,2-difluoro-1-

methoxyvinyl)benzene, **X**. Indeed, the literature values for the ^{19}F spectrum of this fluorinated alkene[9] are nearly identical to what we observed in the experiment shown in Scheme 3.22.

Due to these challenges, we re-evaluated our transition from decarbonylative difluoromethylation to decarbonylative chiral acid coupling. We posited that a systematic set of decarbonylative transformations increasing in complexity and similarity to chiral acids could be informative about the relationship between electrophile structure and reactivity in our decarbonylative coupling reactions.

3.7 Preliminary Results in Decarbonylative Difluorobenzylation of Arenes

Having already developed a variety of difluoromethylation reactions (continued in Chapter 4) we selected the set of electrophiles shown in Figure 3.7 in order to iteratively change one atom or group at a time. We posited that this systematic study would inform us about the span of decarbonylative reactivity over a set of comparable electrophiles. Ultimately, the data collected would inform on the variety of challenges posed by our targeted decarbonylative chiral acid coupling.

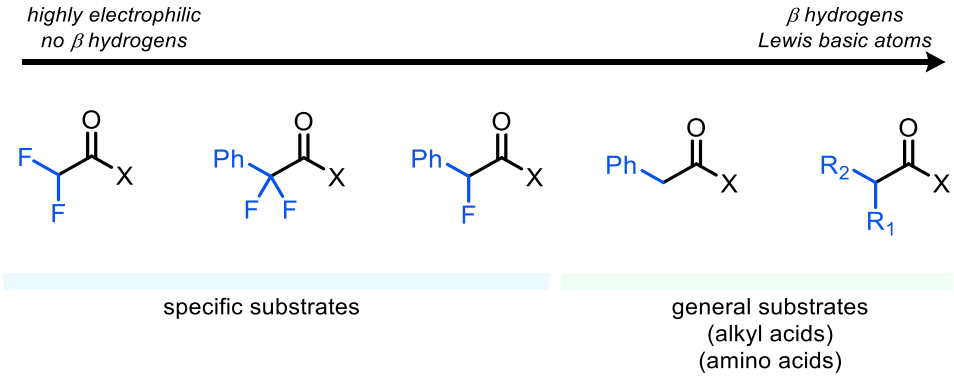

Figure 3.7. Proposed systematic study for bridging previous studies with targeted chiral acid coupling.

Moving from difluoromethyl (-CHF_2), we noted that the difluorobenzyl (-CF_2Ph) group would be of interest, as it replaces the proton of the difluoromethyl group with a phenyl substituent. As we previously reported[1a], the acidic hydrogen of the difluoromethyl group participates in a stabilizing C–$H^{\delta+}$---$O^{\delta-}$ interaction that facilitates the carbonyl de-insertion reaction at Pd^{II}, both thermodynamically and kinetically. The trifluoromethyl group, which lacks this acidic proton and

has a third fluorine atom, showed a significantly higher barrier to carbonyl de-insertion at Pd^{II}.[1a] Shown in Figure 3.8 are the electrostatic potential maps associated transition states for the carbonyl de-insertion.[1a]

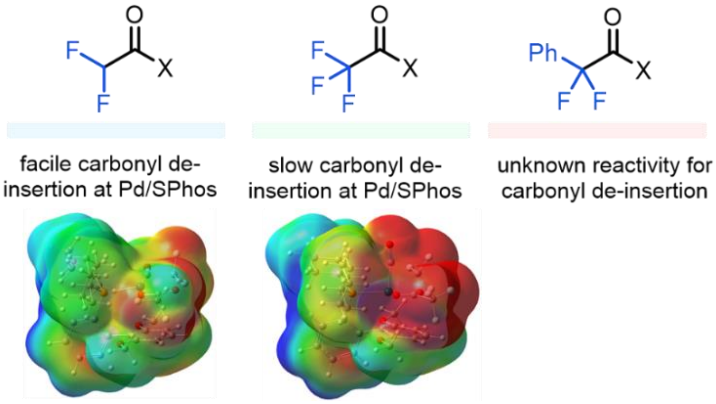

Figure 3.8. Electrostatic potential surfaces associated with the transition states for the carbonyl de-insertion process.[1a]

Due to the large impact of this change on carbonyl de-insertion, we were interested in the impact of a phenyl substituent in $-CF_2Ph$, compared to $-CF_2H$ and $-CF_3$ on the catalytic process. Overall, we hoped to learn about the differences in reactivity moving from decarbonylative difluoromethylation to decarbonylative difluorobenzylation, the impact of the change on the relative barriers of the elementary steps of the catalytic cycle, and the impact of the change on the ligand and conditions.

We desired to develop a palladium-catalyzed decarbonylative difluorobenzylation using a difluorobenzyl acid derivative and an aryl organometallic to form difluorodiarylmethane ($Ar–CF_2–Ar$) products.

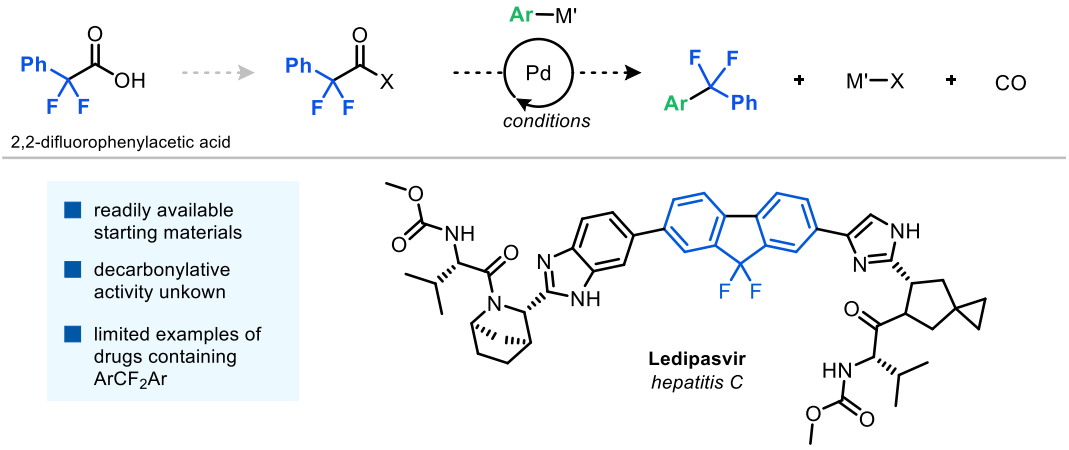

Scheme 3.23. Reaction scheme for the proposed decarbonylative difluorobenzylation reaction using a difluorobenzyl acid derivative.

While benzylic methylene linkages (Ar–CH_2–R) are common structural motifs in a variety of molecules, doubly benylic Ar–CH_2–Ar linkages are less stable and only found in a small number of drugs.[9,10] Replacement of the methylene protons in these linkages (Ar–C**F_2**–Ar) is expected to impart unique properties, such as enhanced metabolic stability and lipophilicity.[11-13] At present, limited examples of this linkage exist in pharmaceuticals.[9,10] As such, the development of an efficient reaction to form this Ar–CF_2–Ar linkage would likely promote the inclusion of this motif into pharmaceuticals, agrochemicals, and materials.[13]

Given the commercial availability of α,α-difluorophenyl acetic acid, we posited that we could synthesize the Ar–CF_2–Ar motif via a decarbonylative cross-coupling reaction between an α,α-difluoroacetic acid derivative and suitable organometallic nucleophile. We propose that this reaction could occur via an analogous catalytic cycle to those previously reported herein (Scheme 3.24). Oxidative addition into a Pd^0 species (step *i*) would generate acyl complex **I-COCF_2Ph**. Carbonyl de-insertion (step *ii*) to extrude CO would generate Pd–CF_2Ph complex **II-CF_2Ph**. Subsequent transmetalation with a compatible organometallic Ar–M' (step *iii*) would generate intermediate **III-CF_2Ph** that undergoes reductive elimination (step *iv*) to give the desired difluorobenzylated product.

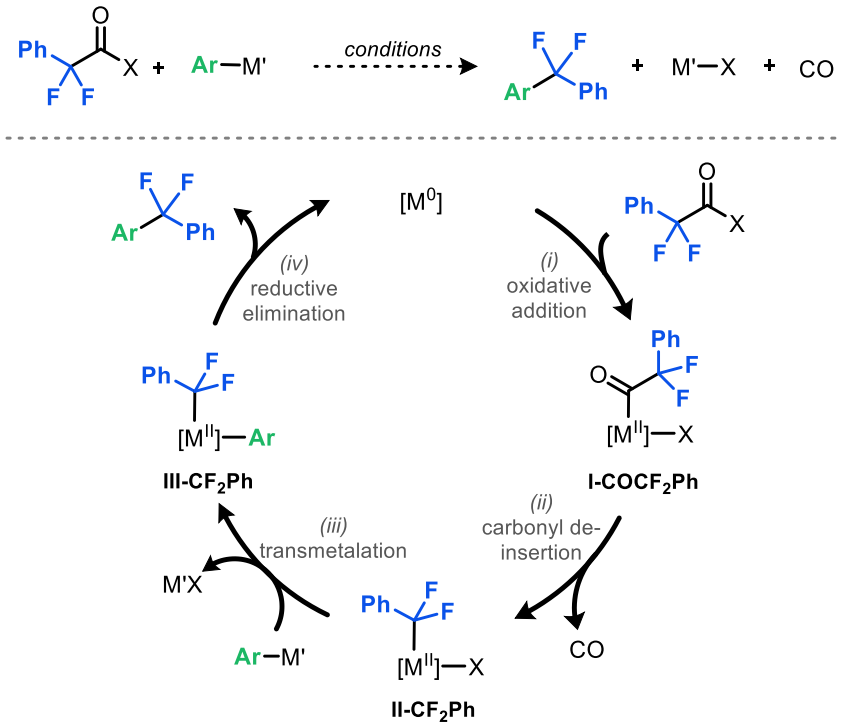

Scheme 3.24. Catalytic cycle for the proposed decarbonylative difluorobenzylation reaction using a difluorobenzyl acid derivative.

We sought to identify a suitable α,α-difluorophenyl carboxylic acid derivative to serve as the electrophile for the process. We were excited to find precedent for the cross-coupling of a α,α-difluorophenyl acyl electrophile with aryl boronic acids catalyzed by Pd.[14] In this report by Amgoune and co-workers, the authors conducted a base-free Suzuki-Miyaura cross-coupling reaction between the 2,2-difluorophenyl acetamide **glut-COCF$_2$Ph** with aryl boronic acids to form ketone products, as shown in Scheme 3.X.

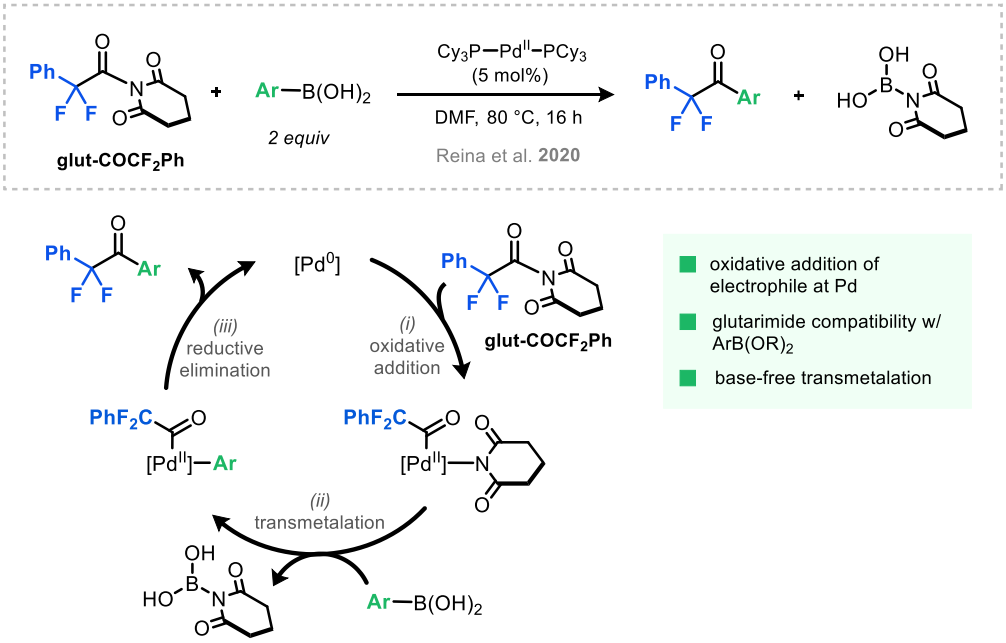

Scheme 3.25. Proposed catalytic cycle for synthesis of difluorophenyl ketones reported by Amgoune and co-workers.[14]

The proposed catalytic cycle of the process involves initial oxidative addition of **glut-COCF2Ph** into a $Pd(PCy_3)_2$ catalyst to form a Pd–$COCF_2Ph$ complex (step *i*).[14] This intermediate then undergoes transmetalation with an aryl boronic acid (step *ii*) and subsequent reductive elimination (step *iii*) to yield the α,α-difluorobenzyl ketone product. The above reaction[14] establishes precedent for a number of steps in our proposed catalytic cycle.

First, the authors are able to readily synthesize compound **glut-COCF2Ph**, which is reactive towards oxidative addition at Pd. Notably, this imide electrophile is reactive at Pd^0 due to ground-state destabilization because of its twisted amide bond.[15] Seminal work by Szostak has elucidated the properties and reactivity of these twisted amides (Scheme 3.26).[15] It is generally concluded that the distortion of planarity in the twisted amides labilizes the C–N bond towards oxidative addition.[15] In addition to this, Szostak has previously demonstrated the efficacy of glutarimide electrophiles in decarbonylative transformations (Scheme 3.26).[15d] This was particularly exciting as there were no known reports of a catalytic transformation involving carbonyl de-insertion of a M–$COCF_2Ph$.

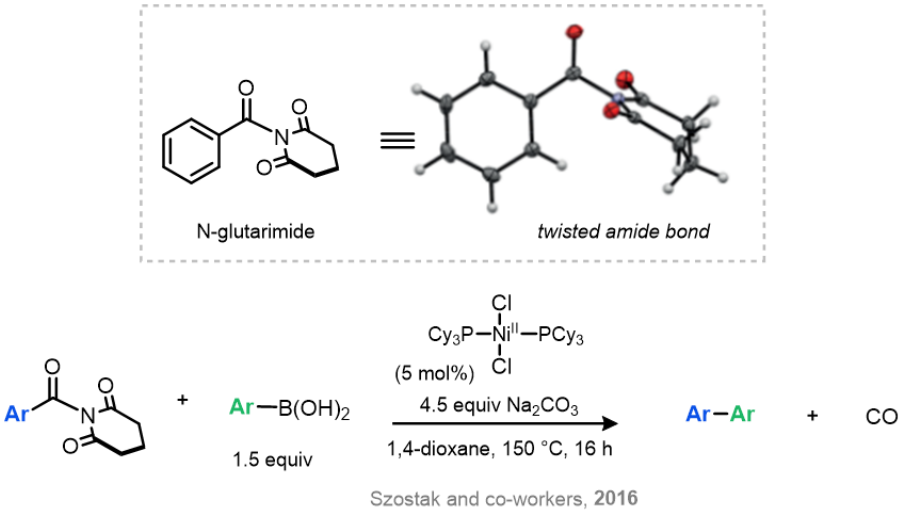

Scheme 3.26. Twisted glutarimide-based amides and decarbonylative arylation reaction catalyzed by palladium.[15d]

The report by Amgoune and co-workers[14] (Scheme 3.25) also demonstrates the compatibility of organoboronic acids and esters with **glut-COCF$_2$Ph**. Great effort was spent in our previous work optimizing the pair of electrophile and nucleophile to be compatible and selectively reactive with the metal catalyst.[1a] Thus, we were excited to have a set of compatible reagents in hand that are also reactive with the Pd catalyst towards cross-coupling.

We began our studies with the synthesis of compound **glut-COCF$_2$Ph**. The literature protocol was generally followed,[14] although the material obtained after chromatographic purification was a yellow oil (literature report suggests that this should be a colorless crystalline solid). Thus, we developed a recrystallization method for the obtained oil using a two-solvent system of diethyl ether and heptanes to afford colorless crystalline **glut-COCF$_2$Ph** in 72% yield and purity (Scheme 3.27).

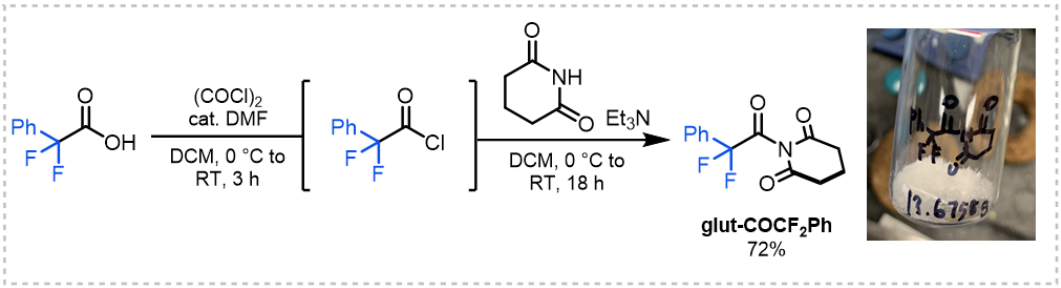

Scheme 3.27. Synthesis of glut-$COCF_2Ph$ and colorless crystalline product shown.

With **glut-$COCF_2Ph$** in hand, we sought to optimize the reaction for the desired decarbonylative transformation. We initially attempted the reaction of our glutarimide electrophile with 4-cyanophenylboronic acid using $Pd[P(o\text{-}Tol)_3]_2$ in combination with either PCy_3 (the ligand used by Amgoune and co-workers)[14] and SPhos (the ligand used in our decarbonylative difluoromethylation).[1a] As expected based on the literature report,[14] the PCy_3 reaction formed ketone in 53% yield in high selectivity over the decarbonylated product $ArCF_2Ph$ (entry 1). In contrast with SPhos, very little reactivity was observed, with 2% of $ArCOCF_2Ph$ and no detectable $ArCF_2Ph$ (entry 3).

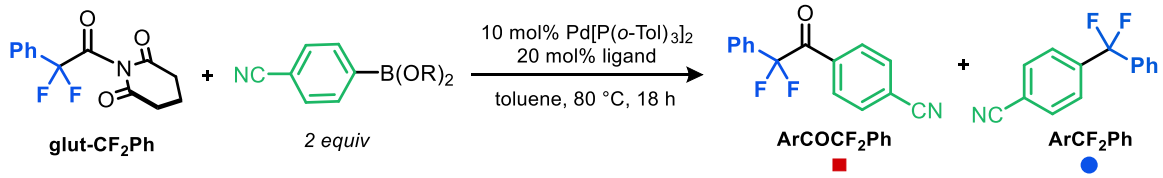

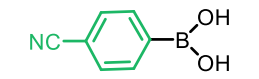

4-CNPhB(OH)$_2$

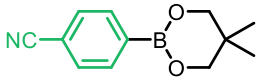

4-CNPhBneo

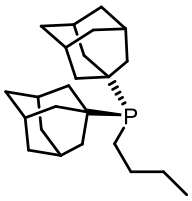

CataXCium A

Entry	ligand	4-CNPhB(OR)$_2$	$ArCOCF_2Ph$ (% yield) ■	$ArCF_2Ph$ (% yield) ●
1	PCy_3	4-CNPhB(OH)$_2$	53	0
2	PCy_3	4-CNPhBneo	trace	8
3	SPhos	4-CNPhB(OH)$_2$	2	0
4	SPhos	4-CNPhBneo	0	7
5	CataCXium A	4-CNPhB(OH)$_2$	25	0
6	**CataCXium A**	**4-CNPhBneo**	**4**	**25**
7	DavePhos	4-CNPhBneo	0	3
8	BrettPhos	4-CNPhBneo	0	0
9	AlPhos	4-CNPhBneo	0	0
10	JosiPhos 009	4-CNPhBneo	0	0
11	PAd_3	4-CNPhBneo	0	4
12	CataCXium B	4-CNPhBneo	0	3
13	morDalPhos	4-CNPhBneo	0	0

Yields determined via ^{19}F NMR with 4-fluorotoluene internal standard

Table 3.2. Ligand and nucleophile optimization of decarbonylative difluorobenzylation reaction.

We next changed the organoboron reagent from the boronic acid to the neopentyl boronate ester. With PCy_3 as the ligand this resulted in a change in selectivity, affording selective formation

of the decarbonylative coupling product, albeit in low (8%) yield. Changing the from PCy_3 to SPhos resulted in similar selectivity for the decarbonylation product, but similarly low yield (7%, entry 4). We next tested a variety of Buchwald ligands (DavePhos, BrettPhos, AlPhos, moreDalPhos) but did not observe significant reactivity. Out of many ligand tried under these conditions, ultimately, it was observed that a bulky monophosphine in CataCXium A was uniquely effective for the desired decarbonylative difluorobenzylation reaction. This ligand in combination with neopentyl boronate esters (entry 6) yielded the highest yield (25% of $ArCF_2Ph$) and selectivity against the ketone by-product (4%). The utilization of the analogous boronic acid under these conditions (entry 5) yielded the opposite selectivity (25% $ArCOCF_2Ph$ and 4% of $ArCF_2Ph$).

Using the Pd^0/CataCXium catalyst identified in the ligand screen, we next explored a small scope of boronate ester and tributyltin nucleophiles. Under these conditions, we observed a range in yields of the desired product (2-45%), as well as varying amounts of undesired ketone product (0-25%) depending on the organometallic used. The results are summarized in **Scheme 3.28**.

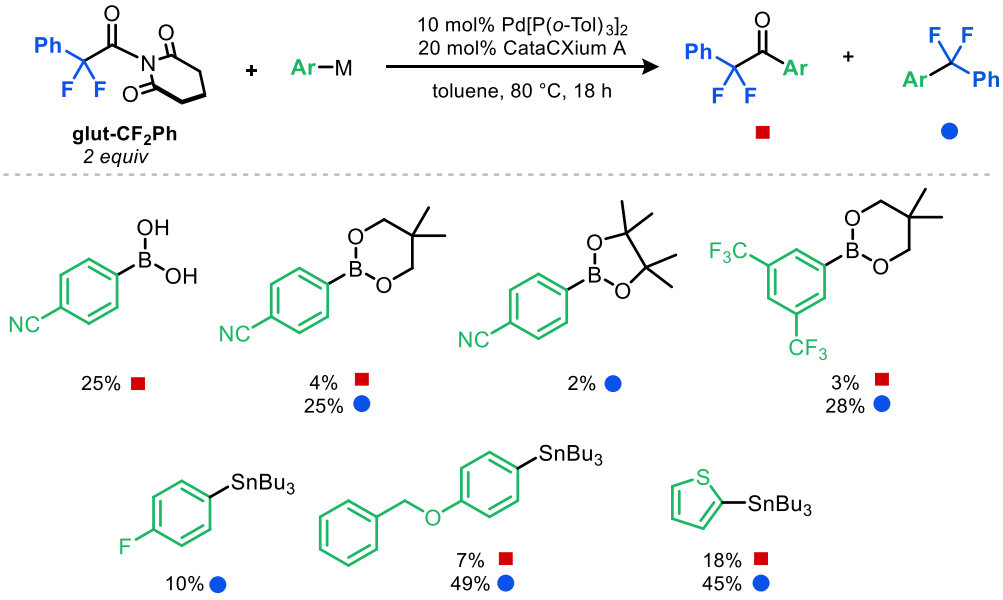

Scheme 3.28. Initial substrate screen of boron and tin nucleophiles under Pd/CataCXium A difluorobenzylation conditions.

The data in Scheme 3.28 shows that both boron and tin organometallics are effective in the reaction. As shown in Table 3.3, 2-tributylstannylthiophene displayed superior reactivity with

lower loadings of catalyst. For instance, with this substrate and 1 mol% of Pd and 4 mol% of ligand, we observed a 28% yield of ketone and 65% yield of the desired decarbonylated product (entry 3). This compares favorably to the 18% and 44% respectively obtained when using 10 mol % of Pd^0 and 40 mol % of phosphine (entry 2). However, unfortunately this result was not general for other nucleophiles.

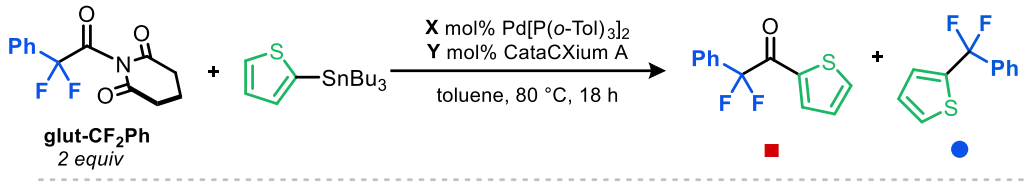

Entry	X	Y	Yield ■ (%)	Yield ● (%)	TON
1	10	20	18	45	6.3
2	10	40	18	44	6.2
2	5	20	18	47	13
3	**1**	**4**	**28**	**65**	**93**
4	0	0	0	0	0

Yields determined by ^{19}F NMR

Table 3.3. Superior reactivity of tributyl(2-thiophenyl)stannane with low loadings of catalyst and ligand.

With the reaction working in modest yields under preliminary conditions (2 equiv **A**, **1** equivalent of organometallic reagent, 10 mol% $Pd[P(o\text{-}Tol)_3]_2$, 40 mol% CataCXium A, toluene (c = 0.17 M), 80 °C, 18 h), the project was turned over to a first-year student in the lab, Alexander Bunnell. Under my mentorship, Alex optimized the reaction conditions further, expanded the scope of organometallics used in the reaction, and isolated the Ar–CF_2–Ar products. This work will be detailed in full in his thesis, but a small summary of his work is presented in Scheme 3.29, below.

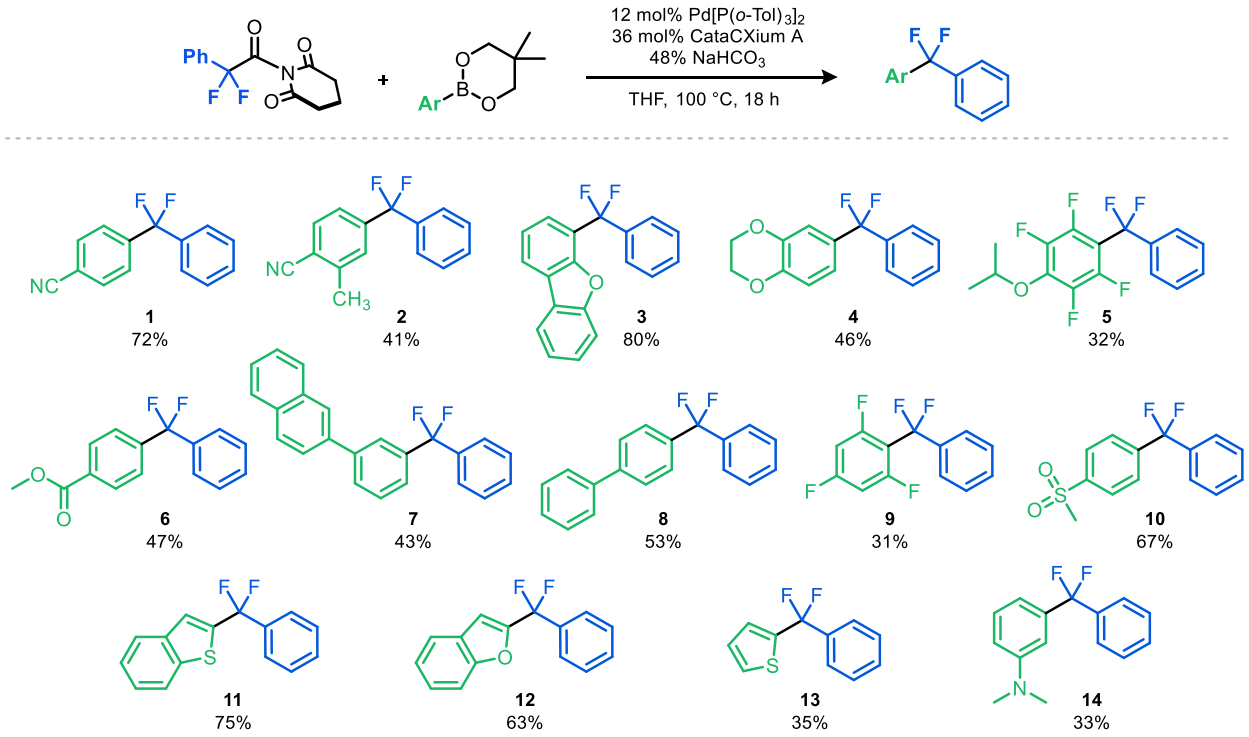

Scheme 3.29. Substrate scope for decarbonylative difluorobenzylation obtained by Alexander W. Bunnell.

As Alex demonstrated, the decarbonylative difluorobenzylation reaction is effective for a variety of aryl boronate ester substrates. All yields above are isolated yields of pure product. Notably, this system works for both electron-rich (e.g., **14**) and electron-deficient aryl boronate esters (e.g., **1**), whereas our decarbonylative difluoromethylation reaction was only effective for electron-poor aryl boronate esters.[1a] Alex will be working to understand these substrate effects through a systematic assessment of compatible organometallics.

3.8 Conclusions and Future Directions

This chapter delineates our preliminary results regarding the development of a Pd-catalyzed decarbonylative C–H difluoromethylation reaction. We observed that a variety of difluoroacyl electrophiles are in reactive towards the C–H functionalization of azole derivatives using a (XantPhos)Pd catalyst system. Preliminary stoichiometric investigations in this area were conducted and led to the synthesis of catalytically-relevant complex **Xant-II-CHF2**. This complex features a unique P–Pd–P bite angle that is not included in the known ranges for (XantPhos)Pd

complexes. Further investigation to be conducted by Frances Gu will elucidate the reactivity of this complex towards stoichiometric C–H activation and as a precatalyst in the catalytic reaction.

We also observed ß–F elimination in our attempts to develop the Ni-catalyzed decarbonylative coupling of a chiral, -CF_3-bearing ester derivative. Future work will focus on quelling this undesired reactivity through the design of a model chiral substrate. Possible chiral acids include (1S)-(+)-ketopinic acid, which should not be as susceptible to such decomposition modes. We also proposed a systematic set of decarbonylative transformations that would enable us to slowly build in complexity, ultimately reaching chiral acid derivatives absent of fluorine atoms. Based on a recent report by Amgoune and co-workers[14], we developed the Pd-catalyzed decarbonylative difluorobenzylation reaction of aryl boron and tin organometallics. This project is being continued by Alexander W. Bunnell and will focus on the comparison of different organometallics in the reaction and the subsequent impact on product selectivity.

3.9 Experimental Section

General information. All manipulations were performed inside an N_2-filled glovebox unless otherwise noted, and all glassware was oven-dried for a minimum of 24 h in an oven at 150 ºC before use. NMR spectra were obtained on a Varian VNMR 700 (699.76 MHz for 1 H; 175.95 MHz for ^{13}C), Varian VNMR 500 (500.09 MHz for ^{1}H; 470.56 MHz for ^{19}F; 125.75 MHz for ^{13}C), or Varian VNMR 400 (401 MHz for ^{1}H; 376 MHz for ^{19}F; 123 MHz for ^{13}C) spectrometer. ^{1}H and ^{13}C NMR chemical shifts are reported in parts per million (ppm) relative to TMS, with the residual solvent peak used as an internal reference. ^{19}F NMR chemical shifts are reported in ppm and are referenced to 4-fluorotoluene (–119.85 ppm) or trifluoromethoxybenzene (–58.00 ppm). ^{13}C NMR spectra are referenced to the residual $CHCl_3$ peak (77.16 ppm). Abbreviations used in the NMR data are as follows: s, singlet; d, doublet; t, triplet; q, quartet; m, multiplet; br, broad signal. Yields of reactions that generated fluorinated products were determined by ^{19}F NMR spectroscopic analysis. Mass spectral data were obtained on a Micromass Magnetic Sector Mass Spectrometer. Automated flash chromatography was performed using a Biotage Isolera One system with cartridges containing high performance silica gel.

Abbreviations: tetrahydrofuran (THF), dichloromethane (DCM), diethyl ether (Et_2O), difluoroacetyl fluoride (DFAF), difluoroacetic anhydride (DFAAn), trifluoroacetic anhydride (TFAAn), difluoroacetic acid (DFA), trifluoroacetic acid (TFA), room temperature (RT).

General procedure for the catalytic optimization of C–H difluoromethylation using DFAAn. A Pd^0 source (0.005 mmol, 0.1 equiv) was dissolved with a phosphine ligand (0.01 mmol, 0.2 equiv) in 0.3 mL of anhydrous solvent and pre-stirred for five minutes in a tall 10 mL vial. DFAAn was added as a toluene-solution (0.15 mmol, 3 equiv, 1.5 M, 0.1 mL) and the solution was stirred. To the solution was added arene substrate (0.05 mmol, 1 equiv). The vial was sealed with a Teflon-lined screw cap with a septum, removed from the glovebox, and heated to a given temperature for 18 h. After the reaction time, the reaction mixture was allowed to cool to room temperature. To it was added hexafluorobenzene (25 µL, 2.0 M in DCM, 1.0 equiv) as an internal standard, followed by dichloromethane (1.0 mL). An aliquot of the solution was transferred to an

NMR tube and analyzed by ^{19}F NMR spectroscopy. The results of a selection of these optimization reactions are shown in Table 3.X.

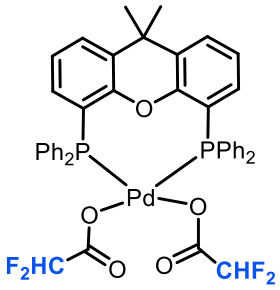

Synthesis of complex Xant-sym. A 20 mL vial equipped with a stir bar was charged with $Pd(dba)_2$ (288 mg, 0.5 mmol, 1.0 equiv), XantPhos (295 mg, 0.51 mmol, 1.02 equiv), and THF (8 mL). To this stirring suspension was added difluoroacetic anhydride (180 mg, 1.02 mmol, 2.04 equiv). The dark red suspension was stirred for 18 h at room temperature. After 18 h, a greenish solid was observed to precipitate out of the dark red reaction mixture. The mixture was filtered through a 2 cm tall celite plug (set with Et_2O) in a disposable fritted funnel the solid was washed with a mixture of Et_2O/pentanes. The red/orange filtrate was collected as an initial fraction. The green solid was eluted through with DCM (15 mL) into a second, orange fraction, leaving Pd^0 remaining on the celite. The orange solution was concentrated en vacuo to yield a crude orange solid (363 mg, 0.42 mmol, 83%). This solid was not fully characterized by NMR but was structurally elucidated via X-ray crystallography. **^{19}F NMR** (470 MHz, CD_2Cl_2) δ -124.8 ppm, (d, *J* = 54.1 Hz). **^{31}P NMR** (202 MHz, CD_2Cl_2) δ 6.78 (s). **^{1}H NMR** (500 MHz, Methylene Chloride-*d*$_2$) δ 7.71 (d, *J* = 7.7 Hz, 2H), 7.47 – 7.35 (*multiple peaks*, 12H), 7.25 (td, *J* = 7.7, 2.2 Hz, 8H), 7.15 (tt, *J* = 7.9, 1.9 Hz, 2H), 6.58 (t, *J* = 8.4 Hz, 2H), 4.92 (t, *J* = 55.2 Hz, 2H), 1.73 (s, 6H).

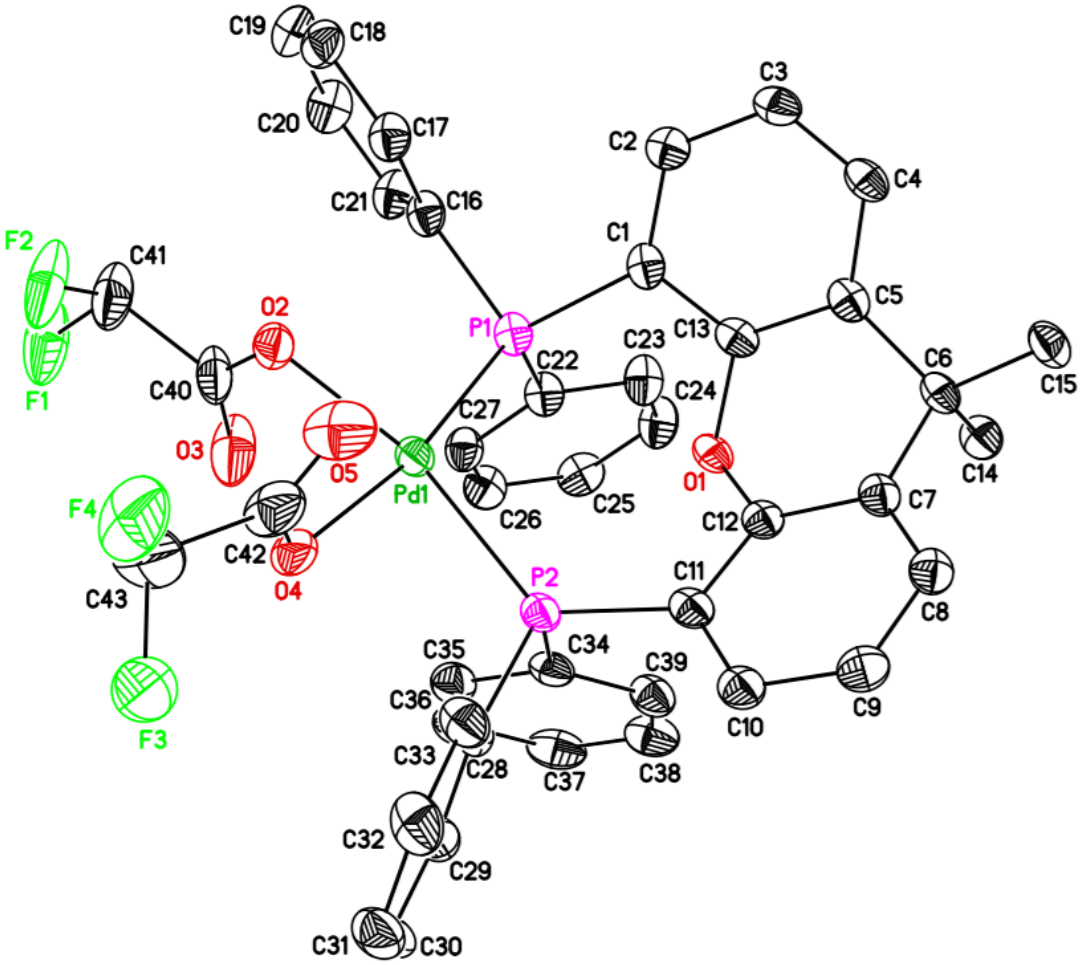

Structure Determination of Xant-sym. Orange prisms of **Xant-sym** were grown from a tetrahydrofuran/di-isopropyl ether/pentane solution of the compound at 25 deg. C. A crystal of dimensions 0.22 x 0.20 x 0.20 mm was mounted on a Rigaku AFC10K Saturn 944+ CCD-based X-ray diffractometer equipped with a low temperature device and Micromax-007HF Cu-target micro-focus rotating anode (l = 1.54187 A) operated at 1.2 kW power (40 kV, 30 mA). The X-ray intensities were measured at 225(1) K with the detector placed at a distance 42.00 mm from the crystal. A destructive phase change precluded collection at lower temperature. A total of 2028 images were collected with an oscillation width of 1.0° in w. The exposure times were 1 sec. for the low angle images, 3 sec. for high angle. Rigaku d*trek images were exported to CrysAlisPro for processing and corrected for absorption. The integration of the data yielded a total of 35047 reflections to a maximum 2q value of 138.81° of which 8464 were independent and 8334 were

greater than 2s(I). The final cell constants (Table 1) were based on the xyz centroids of 24891 reflections above 10s(I). Analysis of the data showed negligible decay during data collection. The structure was solved and refined with the Bruker SHELXTL (version 2018/3) software package, using the space group P-1 with Z = 2 for the formula $C_{48.5}H_{45}O_6F_4Cl_3Pd$. All non-hydrogen atoms were refined anisotropically with the hydrogen atoms placed in idealized positions. The difluoroacetato ligand is disordered over two rotationally related orientations. Full matrix least-squares refinement based on F^2 converged at R1 = 0.0618 and wR2 = 0.1728 [based on I > 2sigma(I)], R1 = 0.0629 and wR2 = 0.1735 for all data. Additional details are presented in Table 1 and are given as Supporting Information in a CIF file. Acknowledgement is made for funding from NSF grant CHE-0840456 for X-ray instrumentation.

G.M. Sheldrick (2015) "Crystal structure refinement with SHELXL", Acta Cryst., C71, 3-8 (Open Access).

CrystalClear Expert 2.0 r16, Rigaku Americas and Rigaku Corporation (2014), Rigaku Americas, 9009, TX, USA 77381-5209, Rigaku Tokyo, 196-8666, Japan.

CrysAlisPro 1.171.40.53 (Rigaku Oxford Diffraction, 2019).

Empirical formula	$C_{43}H_{34}F_4O_5P_2Pd$	
Formula weight	875.09	
Temperature	85(2) K	
Wavelength	1.54184 A	
Crystal system	Triclinic	
space group	P-1	
Unit cell dimensions	a = 11.8332(2) Å	α = 91.0831(13)°
	b = 12.1836(2) Å	ß = 107.8232(14)°
	c = 17.8663(2) Å	γ = 105.8668(16)°
Volume	2343.89(7) $Å^3$	
Z	2	
Calculated density	1.523 Mg/m^3	
Absorption coefficient	5.963 mm^{-1}	

F(000)	1094
Crystal size	0.220 x 0.200 x 0.200 mm
Theta range for data collection	2.614 to 69.403°
Limiting indices	-14<=h<=14, -14<=k<=14, -21<=l<=21
Reflections collected / unique	35047 / 8468 [R(int) = 0.0481]
Completeness to theta	67.684 97.5 %
Absorption correction	Semi-empirical from equivalents
Max. and min. transmission	1.00000 and 0.66585
Refinement method	Full-matrix least-squares on F^2
Data / restraints / parameters	8468 / 504 / 661
Goodness-of-fit on F^2	1.059
Final R indices [I>2σ(I)]	R1 = 0.0618, wR2 = 0.1728
R indices (all data)	R1 = 0.0629, wR2 = 0.1735
Largest diff. peak and hole	1.766 and -1.801 e.A^-3

Table 3.4. Addition details regarding crystals of **Xant-sym.**

	x	y	z	U(eq)
Pd(1)	3352(1)	2722(1)	2672(1)	24(1)
P(1)	3922(1)	1498(1)	3598(1)	22(1)
P(2)	1876(1)	1485(1)	1623(1)	22(1)
O(1)	1629(3)	-115(3)	2745(2)	21(1)
O(2)	4797(3)	4040(3)	3418(2)	29(1)
O(3)	6004(4)	3584(3)	2783(3)	56(1)
O(6)	9201(8)	6604(7)	5319(4)	106(3)
F(1)	7851(3)	5385(3)	3549(3)	66(1)
F(2)	6508(3)	6110(3)	3809(3)	64(1)
C(1)	2821(4)	670(4)	4045(3)	22(1)
C(2)	2994(4)	684(4)	4858(3)	25(1)
C(3)	2066(4)	-6(4)	5118(3)	26(1)
C(4)	972(4)	-706(4)	4583(3)	24(1)
C(5)	776(4)	-773(4)	3772(3)	22(1)
C(6)	-350(4)	-1529(4)	3132(3)	22(1)

C(7)	-578(4)	-859(4)	2417(3)	22(1)
C(8)	-1740(4)	-872(4)	1891(3)	24(1)
C(9)	-1822(4)	-223(4)	1256(3)	28(1)
C(10)	-765(4)	481(4)	1129(3)	26(1)
C(11)	409(4)	530(4)	1655(3)	23(1)
C(12)	452(4)	-157(4)	2261(2)	21(1)
C(13)	1731(4)	-80(4)	3538(2)	21(1)
C(14)	-51(4)	-2622(4)	2897(3)	26(1)
C(15)	-1482(4)	-1892(4)	3409(3)	27(1)
C(16)	5161(4)	2334(4)	4463(3)	25(1)
C(17)	4939(4)	3182(4)	4895(3)	27(1)
C(18)	5867(5)	3831(4)	5554(3)	31(1)
C(19)	7038(5)	3657(4)	5790(3)	34(1)
C(20)	7258(5)	2821(4)	5364(3)	34(1)
C(21)	6339(4)	2167(4)	4709(3)	28(1)
C(22)	4544(4)	441(4)	3267(3)	23(1)
C(23)	4188(4)	-710(4)	3410(3)	29(1)
C(24)	4704(4)	-1482(4)	3158(3)	32(1)
C(25)	5575(4)	-1123(4)	2783(3)	30(1)
C(26)	5946(4)	22(4)	2651(3)	30(1)
C(27)	5433(4)	799(4)	2886(3)	27(1)
C(28)	1336(4)	2295(4)	808(3)	26(1)
C(29)	1602(4)	2229(4)	104(3)	28(1)
C(30)	1121(5)	2825(4)	-510(3)	34(1)
C(31)	354(5)	3480(4)	-436(3)	36(1)
C(32)	81(5)	3542(4)	263(3)	36(1)
C(33)	577(5)	2962(4)	887(3)	30(1)
C(34)	2628(4)	595(4)	1252(2)	25(1)
C(35)	3770(5)	1139(4)	1145(3)	31(1)
C(36)	4373(5)	508(5)	846(3)	35(1)
C(37)	3864(5)	-676(5)	665(3)	36(1)
C(38)	2749(5)	-1233(5)	779(3)	34(1)
C(39)	2122(5)	-590(4)	1071(3)	29(1)
C(40)	5803(5)	4163(4)	3268(3)	38(1)
C(41)	6860(5)	5151(5)	3815(4)	49(2)
O(4)	3093(8)	4059(6)	1983(4)	35(2)
C(42)	2610(15)	4688(11)	2230(8)	43(2)
O(5)	2028(8)	4485(6)	2708(4)	48(2)
C(43)	2818(11)	5878(9)	1905(6)	57(2)
F(3)	2447(7)	5729(6)	1072(4)	66(2)
F(4)	2120(6)	6468(5)	2097(4)	64(2)
O(4A)	3500(19)	3911(12)	1898(9)	47(3)
C(42A)	3120(20)	4715(15)	1980(11)	52(3)
O(5A)	2520(20)	4810(20)	2444(12)	57(4)

C(43A)	3310(20)	5607(15)	1405(12)	66(4)
F(3A)	3450(30)	5680(30)	633(13)	79(7)
F(4A)	2585(18)	6289(15)	1427(12)	97(5)
O(4B)	3500(19)	3911(12)	1898(9)	47(3)
C(42B)	3120(20)	4715(15)	1980(11)	52(3)
O(5B)	2520(20)	4810(20)	2444(12)	57(4)
C(43B)	3310(20)	5607(15)	1405(12)	66(4)
F(4B)	2585(18)	6289(15)	1427(12)	97(5)
F(3B)	4494(19)	6279(13)	1696(9)	61(4)
C(44)	10101(9)	6282(7)	5678(6)	68(2)
C(45)	11031(7)	7289(7)	6264(5)	64(2)
C(46)	10228(9)	7980(9)	6530(5)	78(2)
C(47)	8918(8)	7212(10)	5896(7)	92(3)
C(48)	7903(9)	4090(8)	1739(7)	89(3)
Cl(2)	9468(2)	4561(2)	2120(1)	77(1)
Cl(1)	7447(3)	2612(3)	1311(3)	141(2)
C(49)	4920(20)	4760(20)	933(13)	112(8)
Cl(3)	5941(6)	6113(6)	1382(5)	116(2)
Cl(4)	5050(8)	4058(9)	110(5)	155(3)

Table 3.5 Atomic coordinates (x 10^4) and equivalent isotropic displacement parameters (A^2 x 10^3) for **Xant-sym**. U(eq) is defined as one third of the trace of the orthogonalized Uij tensor.

Pd(1)-C(40)	1.979(3)
Pd(1)-O(2A)	2.129(11)
Pd(1)-O(2)	2.164(7)
Pd(1)-P(2)	2.3177(7)
Pd(1)-P(1)	2.3245(7)
P(1)-C(22)	1.813(4)
P(1)-C(16)	1.818(3)
P(1)-C(1)	1.825(3)
P(2)-C(34)	1.815(3)
P(2)-C(28)	1.816(3)
P(2)-C(12)	1.829(3)
O(1)-C(13)	1.385(3)
O(1)-C(6)	1.388(3)
F(1)-C(40)	1.377(4)
F(2)-C(40)	1.374(4)
C(1)-C(6)	1.388(4)
C(1)-C(2)	1.398(4)
C(2)-C(3)	1.381(5)
C(2)-H(2)	0.9400

C(3)-C(4)	1.376(6)
C(3)-H(3)	0.9400
C(4)-C(5)	1.389(5)
C(4)-H(4)	0.9400
C(5)-C(6)	1.399(3)
C(5)-C(7)	1.511(6)
C(7)-C(8)	1.525(5)
C(7)-C(15)	1.526(5)
C(7)-C(14)	1.568(6)
C(8)-C(9)	1.386(5)
C(8)-C(13)	1.394(4)
C(9)-C(10)	1.370(6)
C(9)-H(9)	0.9400
C(10)-C(11)	1.382(5)
C(10)-H(10)	0.9400
C(11)-C(12)	1.393(4)
C(11)-H(11)	0.9400
C(12)-C(13)	1.403(4)
C(14)-H(14A)	0.9700
C(14)-H(14B)	0.9700
C(14)-H(14C)	0.9700
C(15)-H(15A)	0.9700
C(15)-H(15B)	0.9700
C(15)-H(15C)	0.9700
C(16)-C(17)	1.378(6)
C(16)-C(21)	1.382(5)
C(17)-C(18)	1.386(6)
C(17)-H(17)	0.9400
C(18)-C(19)	1.336(10)
C(18)-H(18)	0.9400
C(19)-C(20)	1.362(10)
C(19)-H(19)	0.9400
C(20)-C(21)	1.401(8)
C(20)-H(20)	0.9400
C(21)-H(21)	0.9400
C(22)-C(23)	1.380(6)
C(22)-C(27)	1.389(5)
C(23)-C(24)	1.433(8)
C(23)-H(23)	0.9400
C(24)-C(25)	1.387(8)
C(24)-H(24)	0.9400
C(25)-C(26)	1.299(8)
C(25)-H(25)	0.9400
C(26)-C(27)	1.366(6)

C(26)-H(26)	0.9400
C(27)-H(27)	0.9400
C(28)-C(29)	1.389(4)
C(28)-C(33)	1.391(4)
C(29)-C(30)	1.380(4)
C(29)-H(29)	0.9400
C(30)-C(31)	1.371(5)
C(30)-H(30)	0.9400
C(31)-C(32)	1.371(5)
C(31)-H(31)	0.9400
C(32)-C(33)	1.381(5)
C(32)-H(32)	0.9400
C(33)-H(33)	0.9400
C(34)-C(39)	1.381(4)
C(34)-C(35)	1.385(5)
C(35)-C(36)	1.394(6)
C(35)-H(35)	0.9400
C(36)-C(37)	1.375(7)
C(36)-H(36)	0.9400
C(37)-C(38)	1.349(6)
C(37)-H(37)	0.9400
C(38)-C(39)	1.389(4)
C(38)-H(38)	0.9400
C(39)-H(39)	0.9400
C(40)-H(40)	0.9900
O(2)-C(41)	1.221(11)
C(41)-O(3)	1.170(11)
C(41)-C(42)	1.540(11)
C(42)-F(3)	1.154(11)
C(42)-F(4)	1.239(11)
C(42)-H(42)	0.9900
O(2A)-C(41A)	1.232(12)
C(41A)-O(3A)	1.204(11)
C(41A)-C(42A)	1.563(10)
C(42A)-F(3A)	1.194(15)
C(42A)-F(4A)	1.229(14)
C(42A)-H(42A)	0.9900
F(3A)-F(4A)	1.824(13)

C(40)-Pd(1)-O(2A)	165.8(4)
C(40)-Pd(1)-O(2)	171.6(3)
C(40)-Pd(1)-P(2)	90.99(9)
O(2A)-Pd(1)-P(2)	101.3(4)
O(2)-Pd(1)-P(2)	89.7(3)

C(40)-Pd(1)-P(1)	91.93(9)
O(2A)-Pd(1)-P(1)	84.9(3)
O(2)-Pd(1)-P(1)	93.7(2)
P(2)-Pd(1)-P(1)	132.67(3)
C(22)-P(1)-C(16)	108.09(16)
C(22)-P(1)-C(1)	103.61(13)
C(16)-P(1)-C(1)	104.95(14)
C(22)-P(1)-Pd(1)	120.80(12)
C(16)-P(1)-Pd(1)	112.05(10)
C(1)-P(1)-Pd(1)	105.85(10)
C(34)-P(2)-C(28)	105.69(13)
C(34)-P(2)-C(12)	106.29(14)
C(28)-P(2)-C(12)	105.86(12)
C(34)-P(2)-Pd(1)	123.84(10)
C(28)-P(2)-Pd(1)	108.85(9)
C(12)-P(2)-Pd(1)	105.06(10)
C(13)-O(1)-C(6)	117.2(2)
C(6)-C(1)-C(2)	118.2(3)
C(6)-C(1)-P(1)	120.8(2)
C(2)-C(1)-P(1)	120.9(3)
C(3)-C(2)-C(1)	120.3(4)
C(3)-C(2)-H(2)	119.8
C(1)-C(2)-H(2)	119.8
C(4)-C(3)-C(2)	120.1(3)
C(4)-C(3)-H(3)	119.9
C(2)-C(3)-H(3)	119.9
C(3)-C(4)-C(5)	121.8(3)
C(3)-C(4)-H(4)	119.1
C(5)-C(4)-H(4)	119.1
C(4)-C(5)-C(6)	117.0(3)
C(4)-C(5)-C(7)	124.1(3)
C(6)-C(5)-C(7)	118.8(3)
C(1)-C(6)-O(1)	117.8(2)
C(1)-C(6)-C(5)	122.6(3)
O(1)-C(6)-C(5)	119.6(3)
C(5)-C(7)-C(8)	109.1(3)
C(5)-C(7)-C(15)	110.7(4)
C(8)-C(7)-C(15)	112.3(4)
C(5)-C(7)-C(14)	107.8(3)
C(8)-C(7)-C(14)	107.6(3)
C(15)-C(7)-C(14)	109.2(4)
C(9)-C(8)-C(13)	116.9(3)
C(9)-C(8)-C(7)	124.1(3)
C(13)-C(8)-C(7)	118.9(3)

C(10)-C(9)-C(8)	121.7(3)
C(10)-C(9)-H(9)	119.2
C(8)-C(9)-H(9)	119.2
C(9)-C(10)-C(11)	120.6(4)
C(9)-C(10)-H(10)	119.7
C(11)-C(10)-H(10)	119.7
C(10)-C(11)-C(12)	120.5(4)
C(10)-C(11)-H(11)	119.7
C(12)-C(11)-H(11)	119.7
C(11)-C(12)-C(13)	117.2(3)
C(11)-C(12)-P(2)	120.9(3)
C(13)-C(12)-P(2)	121.5(2)
O(1)-C(13)-C(8)	119.5(3)
O(1)-C(13)-C(12)	117.4(2)
C(8)-C(13)-C(12)	123.1(3)
C(7)-C(14)-H(14A)	109.5
C(7)-C(14)-H(14B)	109.5
H(14A)-C(14)-H(14B)	109.5
C(7)-C(14)-H(14C)	109.5
H(14A)-C(14)-H(14C)	109.5
H(14B)-C(14)-H(14C)	109.5
C(7)-C(15)-H(15A)	109.5
C(7)-C(15)-H(15B)	109.5
H(15A)-C(15)-H(15B)	109.5
C(7)-C(15)-H(15C)	109.5
H(15A)-C(15)-H(15C)	109.5
H(15B)-C(15)-H(15C)	109.5
C(17)-C(16)-C(21)	118.0(4)
C(17)-C(16)-P(1)	120.9(3)
C(21)-C(16)-P(1)	120.7(3)
C(16)-C(17)-C(18)	121.1(5)
C(16)-C(17)-H(17)	119.5
C(18)-C(17)-H(17)	119.5
C(19)-C(18)-C(17)	120.6(6)
C(19)-C(18)-H(18)	119.7
C(17)-C(18)-H(18)	119.7
C(18)-C(19)-C(20)	120.2(5)
C(18)-C(19)-H(19)	119.9
C(20)-C(19)-H(19)	119.9
C(19)-C(20)-C(21)	120.3(5)
C(19)-C(20)-H(20)	119.9
C(21)-C(20)-H(20)	119.9
C(16)-C(21)-C(20)	119.9(6)
C(16)-C(21)-H(21)	120.1

C(20)-C(21)-H(21)	120.1
C(23)-C(22)-C(27)	120.0(4)
C(23)-C(22)-P(1)	123.8(3)
C(27)-C(22)-P(1)	116.0(3)
C(22)-C(23)-C(24)	117.0(5)
C(22)-C(23)-H(23)	121.5
C(24)-C(23)-H(23)	121.5
C(25)-C(24)-C(23)	119.5(5)
C(25)-C(24)-H(24)	120.3
C(23)-C(24)-H(24)	120.3
C(26)-C(25)-C(24)	121.9(5)
C(26)-C(25)-H(25)	119.0
C(24)-C(25)-H(25)	119.0
C(25)-C(26)-C(27)	120.5(6)
C(25)-C(26)-H(26)	119.8
C(27)-C(26)-H(26)	119.8
C(26)-C(27)-C(22)	121.0(5)
C(26)-C(27)-H(27)	119.5
C(22)-C(27)-H(27)	119.5
C(29)-C(28)-C(33)	118.6(3)
C(29)-C(28)-P(2)	121.1(2)
C(33)-C(28)-P(2)	119.7(2)
C(30)-C(29)-C(28)	120.7(3)
C(30)-C(29)-H(29)	119.7
C(28)-C(29)-H(29)	119.7
C(31)-C(30)-C(29)	119.8(3)
C(31)-C(30)-H(30)	120.1
C(29)-C(30)-H(30)	120.1
C(32)-C(31)-C(30)	120.4(3)
C(32)-C(31)-H(31)	119.8
C(30)-C(31)-H(31)	119.8
C(31)-C(32)-C(33)	120.2(3)
C(31)-C(32)-H(32)	119.9
C(33)-C(32)-H(32)	119.9
C(32)-C(33)-C(28)	120.2(3)
C(32)-C(33)-H(33)	119.9
C(28)-C(33)-H(33)	119.9
C(39)-C(34)-C(35)	119.4(3)
C(39)-C(34)-P(2)	117.8(2)
C(35)-C(34)-P(2)	122.8(3)
C(34)-C(35)-C(36)	119.1(4)
C(34)-C(35)-H(35)	120.4
C(36)-C(35)-H(35)	120.4
C(37)-C(36)-C(35)	120.5(4)

C(37)-C(36)-H(36)	119.7
C(35)-C(36)-H(36)	119.7
C(38)-C(37)-C(36)	120.3(4)
C(38)-C(37)-H(37)	119.8
C(36)-C(37)-H(37)	119.8
C(37)-C(38)-C(39)	120.2(4)
C(37)-C(38)-H(38)	119.9
C(39)-C(38)-H(38)	119.9
C(34)-C(39)-C(38)	120.4(3)
C(34)-C(39)-H(39)	119.8
C(38)-C(39)-H(39)	119.8
F(2)-C(40)-F(1)	104.0(3)
F(2)-C(40)-Pd(1)	109.0(2)
F(1)-C(40)-Pd(1)	108.8(2)
F(2)-C(40)-H(40)	111.5
F(1)-C(40)-H(40)	111.5
Pd(1)-C(40)-H(40)	111.5
C(41)-O(2)-Pd(1)	118.1(8)
O(3)-C(41)-O(2)	127.9(11)
O(3)-C(41)-C(42)	118.9(12)
O(2)-C(41)-C(42)	113.2(11)
F(3)-C(42)-F(4)	107.9(11)
F(3)-C(42)-C(41)	117.7(12)
F(4)-C(42)-C(41)	121.3(10)
F(3)-C(42)-H(42)	102.2
F(4)-C(42)-H(42)	102.2
C(41)-C(42)-H(42)	102.2
C(41A)-O(2A)-Pd(1)	121.2(10)
O(3A)-C(41A)-O(2A)	128.6(11)
O(3A)-C(41A)-C(42A)	120.0(11)
O(2A)-C(41A)-C(42A)	111.3(11)
F(3A)-C(42A)-F(4A)	97.7(13)
F(3A)-C(42A)-C(41A)	117.5(13)
F(4A)-C(42A)-C(41A)	111.5(13)
F(3A)-C(42A)-H(42A)	109.8
F(4A)-C(42A)-H(42A)	109.8
C(41A)-C(42A)-H(42A)	109.8
C(42A)-F(3A)-F(4A)	41.9(7)
C(42A)-F(4A)-F(3A)	40.4(8)

Table 3.6 Bond lengths [Å] and angles [deg] for **Xant-sym**.

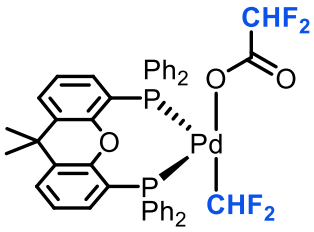

Two-step synthesis of complex Xant-II-CHF$_2$. A 20 mL vial equipped with a stir bar was charged with Pd[P(*o*-Tol)$_3$]$_2$ (358 mg, 0.5 mmol, 1.0 equiv) in THF (5 mL). To this stirring suspension was added difluoroacetic anhydride (96 mg, 0.55 mmol, 1.1 equiv). The dark suspension was stirred for 18 h at room temperature. After 18 h, XantPhos was added (0.55 equiv, 1.1 equiv) and the reaction was stirred for 15 minutes at room temperature. After this, the dark colored solution was concentrated to ca. 1 mL in THF. After sitting for five minutes, a green solid has precipitated. The suspension was filtered through 2 cm tall celite plug (set with pentanes)

in a disposable fritted funnel. The solid was washed with pentanes/diisopropyl ether. However, during this wash, a green band eluted through the plug and was collected as F1. An orange band remained adsorbed to the celite and some green solid remained on top. The orange band was eluted through with diisopropyl ether to give a strongly orange colored solution (F2). Attempts to elute the green solid through with THF and Et$_2$O were unsuccessful. Interestingly, upon addition of DCM, the green solid eluted through as an orange band (F3). F2 was concentrated and NMR was taken in CD_2Cl_2, which confirmed the presence of the desired complex **Xant-II-CHF$_2$**. Single crystal growth was attempted and was successful. Due to the issues related to the unusual solubility and precipitation of the components in the reaction mixture, this complex was not isolated as a pure complex but was subjected to X-ray crystallography. **^{19}F NMR** (471 MHz, Methylene Chloride-d$_2$) δ –71.79 (q, *J* = 48.7 Hz, 2F), –123.96 (d, *J* = 56.2 Hz). Minor impurity observed at -79.68 (dd, *J* = 50.4 Hz). **^{31}P NMR** (202 MHz, Methylene Chloride-d$_2$) δ 12.89 (t, *J* = 50.4 Hz, 2P). Minor impurity (P(*o*-Tol)$_3$) observed at -29.06 (s). **^{1}H NMR** (500 MHz, Methylene Chloride-*d*$_2$) δ 7.71 (dd, *J* = 7.8 Hz, 1.5 Hz, 2H), 7.68-7.58 (*multiple peaks*, 8H), 7.51 (t, *J* = 7.4, 4H), 7.44 (*multiple peaks*, 8H), 7.24 (t, *J* = 7.8 2H), 5.86 (tt, *J* = 52.1 Hz, 13.3 Hz, 1H), 4.85 (t, *J* = 55.9 Hz, 1H), 1.78 (s, 6H).

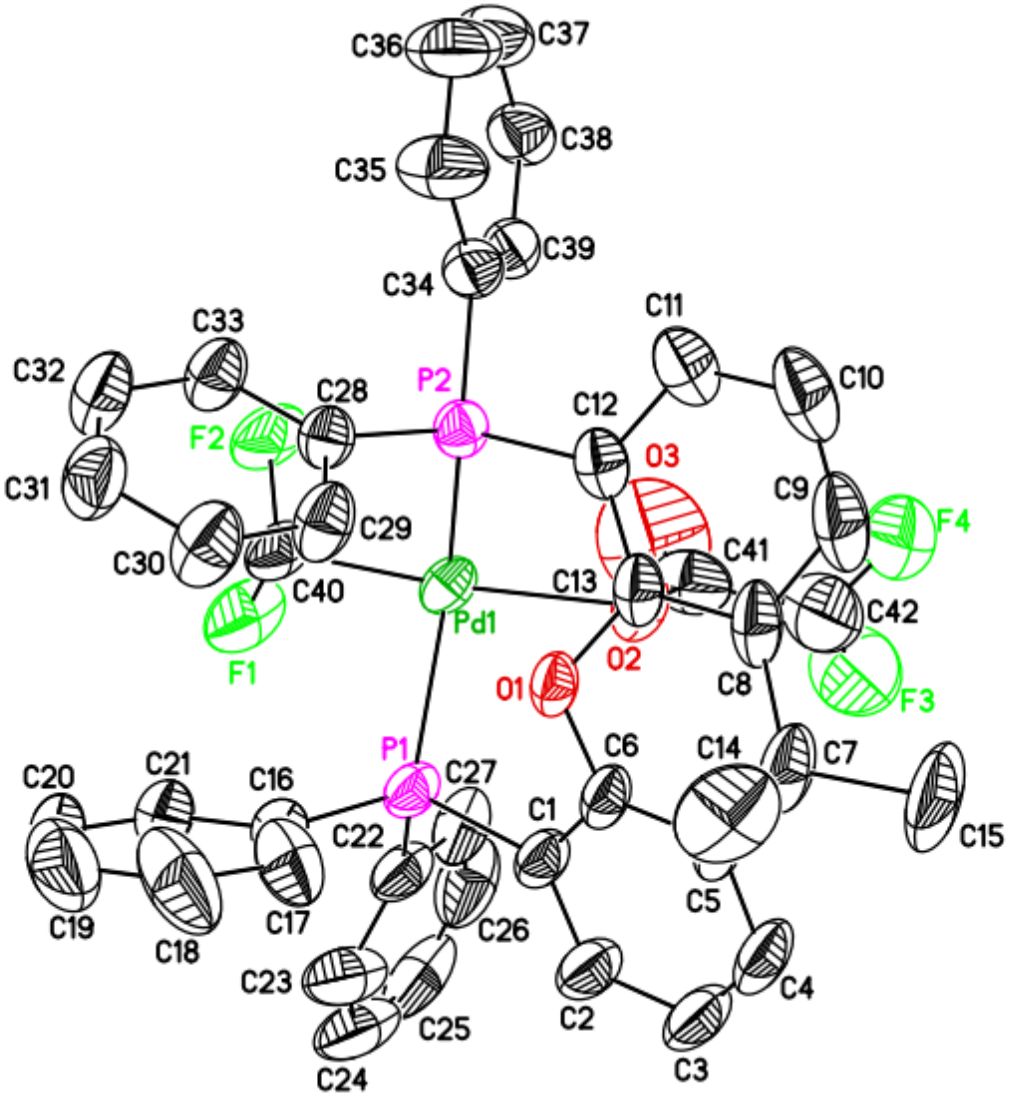

Structure Determination of Xant-II-CHF$_2$. Orange prisms of **Xant-II-CHF$_2$** were grown from a dichloromethane/di-isopropyl ether/pentane solution of the compound at 25 deg. C. A crystal of dimensions 0.14 x 0.14 x 0.14 mm was mounted on a Rigaku AFC10K Saturn 944+ CCD-based X-ray diffractometer equipped with a low temperature device and Micromax-007HF Cu-target micro-focus rotating anode (l = 1.54187 A) operated at 1.2 kW power (40 kV, 30 mA). The X-ray intensities were measured at 225(1) K with the detector placed at a distance 42.00 mm from the crystal. A destructive phase change precluded collection at lower temperature. A total of 2028 images were collected with an oscillation width of 1.0° in w. The exposure times were 1 sec. for

the low angle images, 5 sec. for high angle. Rigaku d*trek images were exported to CrysAlisPro for processing and corrected for absorption. The integration of the data yielded a total of 56484 reflections to a maximum 2q value of 139.24° of which 6959 were independent and 6640 were greater than 2s(I). The final cell constants (Table 1) were based on the xyz centroids of 29316 reflections above 10s(I). Analysis of the data showed negligible decay during data collection. The structure was solved and refined with the Bruker SHELXTL (version 2018/3) software package, using the space group P2(1)/n with Z = 4 for the formula $C_{42}H_{34}O_3F_4P_2Pd$. All non-hydrogen atoms were refined anisotropically with the hydrogen atoms placed in idealized positions. The difluoroacetato ligand is disordered over two rotationally related orientations. Full matrix least-squares refinement based on F^2 converged at R1 = 0.0388 and wR2 = 0.1063 [based on I > 2sigma(I)], R1 = 0.0401 and wR2 = 0.1082 for all data. Additional details are presented in Table 1 and are given as Supporting Information in a CIF file. Acknowledgement is made for funding from NSF grant CHE-0840456 for X-ray instrumentation.

G.M. Sheldrick (2015) "Crystal structure refinement with SHELXL", Acta Cryst., C71, 3-8 (Open Access).

CrystalClear Expert 2.0 r16, Rigaku Americas and Rigaku Corporation (2014), Rigaku Americas, 9009, TX, USA 77381-5209, Rigaku Tokyo, 196-8666, Japan.

CrysAlisPro 1.171.40.53 (Rigaku Oxford Diffraction, 2019).

Empirical formula	$C_{42}H_{34}F_4O_3P_2Pd$
Formula weight	831.03
Temperature	225(2) K
Wavelength	1.54184 A
Crystal system	Monoclinic
space group	P2(1)/n

Unit cell dimensions	a = 9.82100(17) Å α = 90 ° b = 18.93400(10) Å ß = 97.7498(14)° c = 19.6452(3) Å γ = 90 °
Volume	3753.87(10) $Å^3$
Z	4
Calculated density	1.470 Mg/m^3
Absorption coefficient	5.292 mm^{-1}
F(000)	1688
Crystal size	0.140 x 0.140 x 0.140 mm
Theta range for data collection	3.197 to 69.619°
Limiting indices	-11<=h<=11, -23<=k<=23, -23<=l<=23
Reflections collected / unique	56484 / 6959 [R(int) = 0.0525]
Completeness to theta	67.684 99.5 %
Absorption correction	Semi-empirical from equivalents
Max. and min. transmission	1.00000 and 0.70315
Refinement method	Full-matrix least-squares on F^2
Data / restraints / parameters	6959 / 79 / 526
Goodness-of-fit on F^2	1.027
Final R indices [I>2σ(I)]	R1 = 0.0388, wR2 = 0.1063
R indices (all data)	R1 = 0.0401, wR2 = 0.1082
Largest diff. peak and hole	0.414 and -1.023 e.A^-3

Table 3.7. Addition details regarding crystals of **Xant-II-CHF_2**.

	x	y	z	U(eq)
Pd(1)	4699(1)	6398(1)	1856(1)	51(1)
P(1)	5778(1)	7446(1)	2063(1)	54(1)

P(2)	5505(1)	5288(1)	1929(1)	49(1)
O(1)	6910(2)	6290(1)	2959(1)	50(1)
F(1)	4325(3)	7032(1)	595(1)	99(1)
F(2)	4112(3)	5934(1)	527(1)	91(1)
C(1)	6373(3)	7469(2)	2984(1)	56(1)
C(2)	6311(4)	8071(2)	3359(2)	74(1)
C(3)	6652(4)	8069(2)	4064(2)	86(1)
C(4)	7054(3)	7474(2)	4402(2)	80(1)
C(5)	7150(3)	6864(2)	4053(1)	64(1)
C(6)	6803(3)	6879(2)	3339(1)	53(1)
C(7)	7661(4)	6205(2)	4392(2)	78(1)
C(8)	6982(3)	5609(2)	3978(1)	68(1)
C(9)	6716(4)	4983(3)	4259(2)	90(1)
C(10)	6160(5)	4455(2)	3858(2)	95(1)
C(11)	5855(4)	4530(2)	3155(2)	77(1)
C(12)	6088(3)	5149(2)	2842(1)	56(1)
C(13)	6656(3)	5678(2)	3269(1)	54(1)
C(14)	9246(4)	6160(3)	4363(3)	114(2)
C(15)	7403(7)	6190(3)	5140(2)	132(2)
C(16)	7330(4)	7511(2)	1657(2)	67(1)
C(17)	8595(4)	7343(2)	2010(2)	92(1)
C(18)	9756(6)	7316(3)	1681(4)	130(2)
C(19)	9674(9)	7456(3)	1011(4)	144(3)
C(20)	8445(9)	7626(3)	643(3)	136(3)
C(21)	7257(6)	7658(2)	965(2)	99(1)
C(22)	4824(4)	8233(2)	1907(2)	71(1)
C(23)	5420(6)	8851(2)	1789(2)	101(1)
C(24)	4548(8)	9439(2)	1747(2)	121(2)
C(25)	3167(8)	9363(3)	1813(2)	120(2)
C(26)	2631(7)	8771(3)	1906(2)	113(2)
C(27)	3427(4)	8198(2)	1955(2)	83(1)
C(28)	7034(3)	5234(1)	1504(1)	51(1)
C(29)	8312(3)	5429(2)	1838(2)	65(1)
C(30)	9429(3)	5480(2)	1483(2)	80(1)
C(31)	9282(4)	5329(2)	796(2)	81(1)
C(32)	8034(4)	5127(2)	458(2)	79(1)
C(33)	6908(3)	5080(2)	807(2)	67(1)
C(34)	4469(3)	4552(2)	1636(2)	58(1)
C(35)	5035(4)	3934(2)	1482(3)	94(1)
C(36)	4165(6)	3396(2)	1253(3)	114(2)
C(37)	2762(5)	3477(2)	1184(2)	94(1)
C(38)	2211(4)	4078(2)	1337(2)	75(1)
C(39)	3058(3)	4623(2)	1558(1)	60(1)
C(40)	4904(4)	6436(2)	868(2)	67(1)

O(2)	4165(9)	6315(5)	2886(4)	64(2)
C(41)	2952(11)	6346(9)	2960(6)	84(3)
O(3)	2000(10)	6353(7)	2533(7)	200(6)
C(42)	2720(20)	6358(5)	3719(7)	133(4)
F(3)	2063(8)	6797(3)	3895(4)	166(3)
F(4)	2425(9)	5833(3)	4018(3)	135(2)
O(2A)	4081(13)	6531(7)	2845(7)	57(3)
C(41A)	3053(13)	6244(11)	3003(5)	48(3)
O(3A)	2150(9)	5958(5)	2634(4)	83(3)
C(42A)	2950(20)	6323(7)	3786(5)	88(3)
F(3A)	3614(11)	6765(5)	4089(4)	154(4)
F(4A)	3487(15)	5839(6)	4118(5)	163(4)

Table 3.8. Atomic coordinates (x 10^4) and equivalent isotropic displacement parameters (A^2 x 10^3) for **Xant-II-CHF$_2$**. U(eq) is defined as one third of the trace of the orthogonalized Uij tensor.

Pd(1)-C(40)	1.979(3)
Pd(1)-O(2A)	2.129(11)
Pd(1)-O(2)	2.164(7)
Pd(1)-P(2)	2.3177(7)
Pd(1)-P(1)	2.3245(7)
P(1)-C(22)	1.813(4)
P(1)-C(16)	1.818(3)
P(1)-C(1)	1.825(3)
P(2)-C(34)	1.815(3)
P(2)-C(28)	1.816(3)
P(2)-C(12)	1.829(3)
O(1)-C(13)	1.385(3)
O(1)-C(6)	1.388(3)
F(1)-C(40)	1.377(4)
F(2)-C(40)	1.374(4)
C(1)-C(6)	1.388(4)
C(1)-C(2)	1.398(4)
C(2)-C(3)	1.381(5)
C(2)-H(2)	0.9400
C(3)-C(4)	1.376(6)
C(3)-H(3)	0.9400
C(4)-C(5)	1.389(5)
C(4)-H(4)	0.9400

C(5)-C(6)	1.399(3)
C(5)-C(7)	1.511(6)
C(7)-C(8)	1.525(5)
C(7)-C(15)	1.526(5)
C(7)-C(14)	1.568(6)
C(8)-C(9)	1.386(5)
C(8)-C(13)	1.394(4)
C(9)-C(10)	1.370(6)
C(9)-H(9)	0.9400
C(10)-C(11)	1.382(5)
C(10)-H(10)	0.9400
C(11)-C(12)	1.393(4)
C(11)-H(11)	0.9400
C(12)-C(13)	1.403(4)
C(14)-H(14A)	0.9700
C(14)-H(14B)	0.9700
C(14)-H(14C)	0.9700
C(15)-H(15A)	0.9700
C(15)-H(15B)	0.9700
C(15)-H(15C)	0.9700
C(16)-C(17)	1.378(6)
C(16)-C(21)	1.382(5)
C(17)-C(18)	1.386(6)
C(17)-H(17)	0.9400
C(18)-C(19)	1.336(10)
C(18)-H(18)	0.9400
C(19)-C(20)	1.362(10)
C(19)-H(19)	0.9400
C(20)-C(21)	1.401(8)
C(20)-H(20)	0.9400
C(21)-H(21)	0.9400
C(22)-C(23)	1.380(6)
C(22)-C(27)	1.389(5)
C(23)-C(24)	1.433(8)
C(23)-H(23)	0.9400
C(24)-C(25)	1.387(8)
C(24)-H(24)	0.9400
C(25)-C(26)	1.299(8)
C(25)-H(25)	0.9400
C(26)-C(27)	1.366(6)
C(26)-H(26)	0.9400
C(27)-H(27)	0.9400
C(28)-C(29)	1.389(4)
C(28)-C(33)	1.391(4)

C(29)-C(30)	1.380(4)
C(29)-H(29)	0.9400
C(30)-C(31)	1.371(5)
C(30)-H(30)	0.9400
C(31)-C(32)	1.371(5)
C(31)-H(31)	0.9400
C(32)-C(33)	1.381(5)
C(32)-H(32)	0.9400
C(33)-H(33)	0.9400
C(34)-C(39)	1.381(4)
C(34)-C(35)	1.385(5)
C(35)-C(36)	1.394(6)
C(35)-H(35)	0.9400
C(36)-C(37)	1.375(7)
C(36)-H(36)	0.9400
C(37)-C(38)	1.349(6)
C(37)-H(37)	0.9400
C(38)-C(39)	1.389(4)
C(38)-H(38)	0.9400
C(39)-H(39)	0.9400
C(40)-H(40)	0.9900
O(2)-C(41)	1.221(11)
C(41)-O(3)	1.170(11)
C(41)-C(42)	1.540(11)
C(42)-F(3)	1.154(11)
C(42)-F(4)	1.239(11)
C(42)-H(42)	0.9900
O(2A)-C(41A)	1.232(12)
C(41A)-O(3A)	1.204(11)
C(41A)-C(42A)	1.563(10)
C(42A)-F(3A)	1.194(15)
C(42A)-F(4A)	1.229(14)
C(42A)-H(42A)	0.9900
F(3A)-F(4A)	1.824(13)

C(40)-Pd(1)-O(2A)	165.8(4)
C(40)-Pd(1)-O(2)	171.6(3)
C(40)-Pd(1)-P(2)	90.99(9)
O(2A)-Pd(1)-P(2)	101.3(4)
O(2)-Pd(1)-P(2)	89.7(3)
C(40)-Pd(1)-P(1)	91.93(9)
O(2A)-Pd(1)-P(1)	84.9(3)
O(2)-Pd(1)-P(1)	93.7(2)
P(2)-Pd(1)-P(1)	132.67(3)

C(22)-P(1)-C(16)	108.09(16)
C(22)-P(1)-C(1)	103.61(13)
C(16)-P(1)-C(1)	104.95(14)
C(22)-P(1)-Pd(1)	120.80(12)
C(16)-P(1)-Pd(1)	112.05(10)
C(1)-P(1)-Pd(1)	105.85(10)
C(34)-P(2)-C(28)	105.69(13)
C(34)-P(2)-C(12)	106.29(14)
C(28)-P(2)-C(12)	105.86(12)
C(34)-P(2)-Pd(1)	123.84(10)
C(28)-P(2)-Pd(1)	108.85(9)
C(12)-P(2)-Pd(1)	105.06(10)
C(13)-O(1)-C(6)	117.2(2)
C(6)-C(1)-C(2)	118.2(3)
C(6)-C(1)-P(1)	120.8(2)
C(2)-C(1)-P(1)	120.9(3)
C(3)-C(2)-C(1)	120.3(4)
C(3)-C(2)-H(2)	119.8
C(1)-C(2)-H(2)	119.8
C(4)-C(3)-C(2)	120.1(3)
C(4)-C(3)-H(3)	119.9
C(2)-C(3)-H(3)	119.9
C(3)-C(4)-C(5)	121.8(3)
C(3)-C(4)-H(4)	119.1
C(5)-C(4)-H(4)	119.1
C(4)-C(5)-C(6)	117.0(3)
C(4)-C(5)-C(7)	124.1(3)
C(6)-C(5)-C(7)	118.8(3)
C(1)-C(6)-O(1)	117.8(2)
C(1)-C(6)-C(5)	122.6(3)
O(1)-C(6)-C(5)	119.6(3)
C(5)-C(7)-C(8)	109.1(3)
C(5)-C(7)-C(15)	110.7(4)
C(8)-C(7)-C(15)	112.3(4)
C(5)-C(7)-C(14)	107.8(3)
C(8)-C(7)-C(14)	107.6(3)
C(15)-C(7)-C(14)	109.2(4)
C(9)-C(8)-C(13)	116.9(3)
C(9)-C(8)-C(7)	124.1(3)
C(13)-C(8)-C(7)	118.9(3)
C(10)-C(9)-C(8)	121.7(3)
C(10)-C(9)-H(9)	119.2
C(8)-C(9)-H(9)	119.2
C(9)-C(10)-C(11)	120.6(4)

C(9)-C(10)-H(10)	119.7
C(11)-C(10)-H(10)	119.7
C(10)-C(11)-C(12)	120.5(4)
C(10)-C(11)-H(11)	119.7
C(12)-C(11)-H(11)	119.7
C(11)-C(12)-C(13)	117.2(3)
C(11)-C(12)-P(2)	120.9(3)
C(13)-C(12)-P(2)	121.5(2)
O(1)-C(13)-C(8)	119.5(3)
O(1)-C(13)-C(12)	117.4(2)
C(8)-C(13)-C(12)	123.1(3)
C(7)-C(14)-H(14A)	109.5
C(7)-C(14)-H(14B)	109.5
H(14A)-C(14)-H(14B)	109.5
C(7)-C(14)-H(14C)	109.5
H(14A)-C(14)-H(14C)	109.5
H(14B)-C(14)-H(14C)	109.5
C(7)-C(15)-H(15A)	109.5
C(7)-C(15)-H(15B)	109.5
H(15A)-C(15)-H(15B)	109.5
C(7)-C(15)-H(15C)	109.5
H(15A)-C(15)-H(15C)	109.5
H(15B)-C(15)-H(15C)	109.5
C(17)-C(16)-C(21)	118.0(4)
C(17)-C(16)-P(1)	120.9(3)
C(21)-C(16)-P(1)	120.7(3)
C(16)-C(17)-C(18)	121.1(5)
C(16)-C(17)-H(17)	119.5
C(18)-C(17)-H(17)	119.5
C(19)-C(18)-C(17)	120.6(6)
C(19)-C(18)-H(18)	119.7
C(17)-C(18)-H(18)	119.7
C(18)-C(19)-C(20)	120.2(5)
C(18)-C(19)-H(19)	119.9
C(20)-C(19)-H(19)	119.9
C(19)-C(20)-C(21)	120.3(5)
C(19)-C(20)-H(20)	119.9
C(21)-C(20)-H(20)	119.9
C(16)-C(21)-C(20)	119.9(6)
C(16)-C(21)-H(21)	120.1
C(20)-C(21)-H(21)	120.1
C(23)-C(22)-C(27)	120.0(4)
C(23)-C(22)-P(1)	123.8(3)
C(27)-C(22)-P(1)	116.0(3)

C(22)-C(23)-C(24)	117.0(5)
C(22)-C(23)-H(23)	121.5
C(24)-C(23)-H(23)	121.5
C(25)-C(24)-C(23)	119.5(5)
C(25)-C(24)-H(24)	120.3
C(23)-C(24)-H(24)	120.3
C(26)-C(25)-C(24)	121.9(5)
C(26)-C(25)-H(25)	119.0
C(24)-C(25)-H(25)	119.0
C(25)-C(26)-C(27)	120.5(6)
C(25)-C(26)-H(26)	119.8
C(27)-C(26)-H(26)	119.8
C(26)-C(27)-C(22)	121.0(5)
C(26)-C(27)-H(27)	119.5
C(22)-C(27)-H(27)	119.5
C(29)-C(28)-C(33)	118.6(3)
C(29)-C(28)-P(2)	121.1(2)
C(33)-C(28)-P(2)	119.7(2)
C(30)-C(29)-C(28)	120.7(3)
C(30)-C(29)-H(29)	119.7
C(28)-C(29)-H(29)	119.7
C(31)-C(30)-C(29)	119.8(3)
C(31)-C(30)-H(30)	120.1
C(29)-C(30)-H(30)	120.1
C(32)-C(31)-C(30)	120.4(3)
C(32)-C(31)-H(31)	119.8
C(30)-C(31)-H(31)	119.8
C(31)-C(32)-C(33)	120.2(3)
C(31)-C(32)-H(32)	119.9
C(33)-C(32)-H(32)	119.9
C(32)-C(33)-C(28)	120.2(3)
C(32)-C(33)-H(33)	119.9
C(28)-C(33)-H(33)	119.9
C(39)-C(34)-C(35)	119.4(3)
C(39)-C(34)-P(2)	117.8(2)
C(35)-C(34)-P(2)	122.8(3)
C(34)-C(35)-C(36)	119.1(4)
C(34)-C(35)-H(35)	120.4
C(36)-C(35)-H(35)	120.4
C(37)-C(36)-C(35)	120.5(4)
C(37)-C(36)-H(36)	119.7
C(35)-C(36)-H(36)	119.7
C(38)-C(37)-C(36)	120.3(4)
C(38)-C(37)-H(37)	119.8

C(36)-C(37)-H(37)	119.8
C(37)-C(38)-C(39)	120.2(4)
C(37)-C(38)-H(38)	119.9
C(39)-C(38)-H(38)	119.9
C(34)-C(39)-C(38)	120.4(3)
C(34)-C(39)-H(39)	119.8
C(38)-C(39)-H(39)	119.8
F(2)-C(40)-F(1)	104.0(3)
F(2)-C(40)-Pd(1)	109.0(2)
F(1)-C(40)-Pd(1)	108.8(2)
F(2)-C(40)-H(40)	111.5
F(1)-C(40)-H(40)	111.5
Pd(1)-C(40)-H(40)	111.5
C(41)-O(2)-Pd(1)	118.1(8)
O(3)-C(41)-O(2)	127.9(11)
O(3)-C(41)-C(42)	118.9(12)
O(2)-C(41)-C(42)	113.2(11)
F(3)-C(42)-F(4)	107.9(11)
F(3)-C(42)-C(41)	117.7(12)
F(4)-C(42)-C(41)	121.3(10)
F(3)-C(42)-H(42)	102.2
F(4)-C(42)-H(42)	102.2
C(41)-C(42)-H(42)	102.2
C(41A)-O(2A)-Pd(1)	121.2(10)
O(3A)-C(41A)-O(2A)	128.6(11)
O(3A)-C(41A)-C(42A)	120.0(11)
O(2A)-C(41A)-C(42A)	111.3(11)
F(3A)-C(42A)-F(4A)	97.7(13)
F(3A)-C(42A)-C(41A)	117.5(13)
F(4A)-C(42A)-C(41A)	111.5(13)
F(3A)-C(42A)-H(42A)	109.8
F(4A)-C(42A)-H(42A)	109.8
C(41A)-C(42A)-H(42A)	109.8
C(42A)-F(3A)-F(4A)	41.9(7)
C(42A)-F(4A)-F(3A)	40.4(8)

Table 3.9. Bond lengths [A] and angles [deg] for **Xant-II-CHF$_2$.**

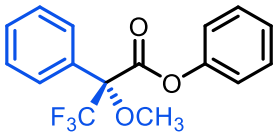

Procedure for the synthesis of phenyl (R)-3,3,3-trifluoro-2-methoxy-2-phenylpropanoate (1) from (R)-3,3,3-trifluoro-2-methoxy-2-phenylpropanoic acid. (R)-3,3,3-trifluoro-2-methoxy-2-phenylpropanoic acid (468 mg, 2 mmol, 1.0 equiv), also known as (R)-(+)-Mosher's Acid, was dissolved in dichloromethane (10 mL) and the solution was cooled to 0 °C in an ice-water bath while stirring. Then, a catalytic amount of DMF (0.05 mL) was added. Following this, oxalyl chloride (0.17 mL, 2 mmol, 1.0 equiv) was added dropwise. The reaction was allowed to slowly warm to room temperature over 3 h. After 3 h, another flask was prepared with phenol (223 mg, 2.4 mmol, 1.2 equiv) and dichloromethane (10 mL) and was cooled to 0 °C in an ice-water bath while stirring. To this solution was added triethylamine (415 mg, 3 mmol, 1.5 equiv). Then, the acid chloride reaction mixture was added dropwise to the flask containing phenol and triethylamine. This reaction mixture was allowed to slowly warm up to room temperature over 18 h. After 18 h, the mixture was diluted with dichloromethane (20 mL) and the reaction was washed twice with deionized H_2O, 1x with NaCl (sat., aq.) brine, then was dried over anhydrous Na_2SO_4. The crude reaction solution was filtered and concentrated en vacuo to yield a yellow oil. The yellow oil was then purified via silica gel chromatography (25g column, gradient elution of 0-5% EtOAc in hexanes). The product was observed to elute at 5% EtOAc in hexanes. Fractions containing the product were collected and concentrated, yielding ester **1** as a colorless oil (426 mg, 1.374 mmol, 69% yield). **^{1}H NMR** (400 MHz, $CDCl_3$) δ 7.72–7.64 (m, 2H), 7.51–7.38 (multiple peaks, 5H), 7.29 (t, *J* = 7.5 Hz, 1H), 7.13 (d, *J* = 8.4 Hz, 2H), 3.70 (s, 3H). **^{19}F NMR** (376 MHz, $CDCl_3$) δ –71.65 (s, 3F). **^{13}C NMR** (126 MHz, $CDCl_3$) δ 165.33, 150.11, 132.13, 130.01, 129.82, 128.78, 127.43, 126.78, 124.54, 122.25, 55.85.

Procedure for the stoichiometric reactions of (R)-3,3,3-trifluoro-2-methoxy-2-phenylpropanoate (1) with Ni(COD)$_2$ and tri-*n*-butylphosphine. In a 4-mL vial fitted with a stirbar, a 0.05 M solution of $Ni(COD)_2$ (0.1 mmol, 27.5 mg, 10.0 equiv) was prepared in THF (2.0 mL). To this mixture was added P(*n*Bu)$_3$ (0.2 mmol, 20.2 mg, 10.0 equiv). The mixture was stirred until homogenous (~ 5 minutes). In a separate 4-mL vial, a 0.05 M THF-solution of 4-fluorotoluene internal standard was prepared. In a tall 10-mL vial, ester 1 (3.1 mg, 0.01 mmol, 1.0 equiv) was weighed and to it was added 0.2 mL of the nickel solution and 0.2 mL of the 4-fluorotoluene

solution. The reaction was sealed with a Teflon-lined screw cap, removed from the glovebox, and heated at temperature (80 °C for 2.5 h or 120 °C for 18 h). After the reaction time, the vial was allowed to cool, brought into the glovebox, and transferred into a screw-cap NMR tube. Subsequent 19F NMR analysis was conducted to identify desired intermediates and undesired by-products. The associated spectra are shown in Schemes 3.21 and 3.22.

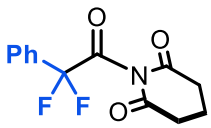

Procedure for the synthesis of 1-(2,2-difluoro-2-phenylacetyl)piperidine-2,6-dione (glut-COCF$_2$Ph) from 2,2-difluorophenylacetic acid. 2,2-difluorophenylacetic acid (516 mg, 3 mmol, 1.0 equiv) was dissolved in dichloromethane (8 mL) and the solution was cooled to 0 °C in an ice-water bath while stirring. Then, a catalytic amount of DMF (0.05 mL) was added. Following this, oxalyl chloride (1.5 mL, 2.0 M in dichloromethane, 3 mmol, 1.0 equiv) was added dropwise. The reaction was allowed to slowly warm to room temperature over 3 h. After 3 h, another flask was prepared with glutarimide (339 mg, 3 mmol, 1.0 equiv) and dichloromethane (10 mL) and was cooled to 0 °C in an ice-water bath while stirring. To this solution was added triethylamine (0.62 mL, 4.5 mmol, 1.5 equiv). Then, the acid chloride reaction mixture was added dropwise to the flask containing glutarimide and triethylamine. This reaction mixture was allowed to slowly warm up to room temperature over 18 h. After 18 h, the mixture was diluted with cold Et_2O (50 mL) to precipitate the triethylamine hydrochloride salt and was subsequently filtered and concentrated en vacuo to yield a yellow oil. The yellow oil was then purified via silica gel chromatography (25g column, gradient elution of 5-50% EtOAc in hexanes). Fractions containing the product were collected and concentrated, yielding **glut-COCF$_2$Ph** as a slightly yellow oil, contrary to the literature protocol.[14] Recrystallization using diethyl ether and heptanes at 0 °C over 18 h yielded **glut-COCF$_2$Ph** as a colorless crystalline solid (575 mg, 2.15 mmol, 72% yield). **^{1}H NMR** (400 MHz, $CDCl_3$) δ 7.63 (dd, *J* = 8.5, 1.5 Hz, 2H), 7.48 (ddd, *J* = 14.4, 8.0, 6.2, 3H), 2.70 (t, *J* = 6.5 Hz, 2H), 2.06 (p, *J* = 6.6 Hz, 2H). **^{19}F NMR** (377 MHz, $CDCl_3$) δ –101.56 (s, 2F). **^{13}C NMR** (176 MHz, $CDCl_3$) δ 173.33, 171.31, 170.99 (td, *J* = 40.6, 3.3 Hz), 131.50 (t, *J* = 25.0 Hz), 131.43, 128.64, 126.36 (t, *J* = 6.2 Hz), 32.19, 17.34.

General procedure for the catalytic optimization of difluorophenylation using glut-COCF$_2$Ph as the limiting reagent. Pd[P(*o*-Tol)$_3$]$_2$ (3,6 mg, 0.005 mmol, 0.1 equiv) was dissolved with a phosphine ligand (0.01 mmol, 0.2 equiv) in 0.3 mL of toluene or THF and pre-stirred for five minutes in a tall 10 mL vial. Electrophile **glut-COCF$_2$Ph** was added as a solid (13 mg, 0.05 mmol, 1 equiv) and the solution was stirred. To the solution was added arene substrate (0.10 mmol, 2 equiv). The vial was sealed with a Teflon-lined screw cap with a septum, removed from the glovebox, and heated to a given temperature for 18 h. After the reaction time, the reaction mixture was allowed to cool to room temperature. To it was added 4-fluorotoluene (25 µL, 2.0 M in DCM, 1.0 equiv) as an internal standard, followed by dichloromethane (1.0 mL). An aliquot of the solution was transferred to an NMR tube and analyzed by ^{19}F NMR spectroscopy. The results of a selection of these optimization reactions are shown in Table 3.2.

General procedure for the catalytic difluorophenylation with excess imide A. Pd[P(*o*-Tol)$_3$]$_2$ (3.6, mg, 0.005 mmol, 0.1 equiv) was dissolved with a phosphine ligand (0.01 mmol, 0.2 equiv) in 0.3 mL of toluene or THF and pre-stirred for five minutes in a tall 10 mL vial. Imide **A** was added as a solid (27 mg, 0.10 mmol, 2 equiv) and the solution was stirred. To the solution was added arene substrate (0.05 mmol, 1 equiv). The vial was sealed with a Teflon-lined screw cap with a septum, removed from the glovebox, and heated to a given temperature for 18 h. After the reaction time, the reaction mixture was allowed to cool to room temperature. To it was added 4-fluorotoluene (25 µL, 2.0 M in DCM, 1.0 equiv) as an internal standard, followed by dichloromethane (1.0 mL). An aliquot of the solution was transferred to an NMR tube and analyzed by ^{19}F NMR spectroscopy. The results of a selection of these optimization reactions are shown in Scheme 3.28.

3.10. References

1. (a) Lalloo, N.; Malapit, C. A.; Taimoory, S. M.; Brigham, C. E.; Sanford, M. S. Decarbonylative fluoroalkylation at palladium(II): from organometallic studies to catalysis. *J. Am. Chem. Soc.* **2021**, *143*, 18617–18625. (b) Malapit, C. A.; Bour, J. R.; Laursen, S. R.; Sanford, M. S. Mechanism and scope of nickel-catalyzed decarbonylative borylation of carboxylic acid fluorides. *J. Am. Chem. Soc.* **2019**, *141*, 17322−17330. (c) Malapit, C. A.; Bour, J. R.; Brigham, C. E.; Sanford, M. S. Base-free nickel-catalysed decarbonylative Suzuki-Miyaura coupling of acid fluorides. *Nature* **2018**, *563*, 100−104.
2. (a) Sakurai, S.; Yoshida, T.; Tobisu, M. Iridium-catalyzed decarbonylative coupling of acyl fluorides with arenes and heteroarenes via C–H activation. *Chem. Lett.* **2019**, *48*, 94–97. (b) Blaser, H. U.; Spencer, A. The palladium-catalysed arylation of activated alkenes with aroyl chlorides. *J. Organometal. Chem.* **1982**, *233*, 267–274. (c) for a comprehensive review: Dermenci, A.; Dong, G. Decarbonylative C–C bond forming reactions mediated by transition metals. *Sci. China Chem.* **2013**, *56*, 685–701.
3. (a) Eicher, T.; Hauptmann, S. The Chemistry of Heterocycles; Wiley-VCH: Weinheim, 2003. (b) Carey, J. S.; Laffan, D.; Thomson, C.; Williams, M. T. Analysis of the reactions used for the preparation of drug candidate molecules. *Org. Biomol. Chem*. **2006**, *4*, 2337−2347. (c) Shibahara, F.; Yamaguchi, E.; Murai, T. Direct multiple C–H bond arylation of heteroarenes catalyzed by cationic palladium complex bearing 1,10-phenanthroline. *Chem. Commun.* **2010**, *46*, 2471–2473. (d) Ranjit, S.; Liu, X. Direct arylation of benzothiazoles and benzoxazoles with aryl boronic acids. *Chem. Eur. J.* **2011**, *17*, 1105–1108. (e) Williams, T. J.; Fairlamb, I. J. S. A key role for iodobenzene in the direct C–H bond functionalization of benzoxazoles using $PhI(OAc)_2$ mediated by a $Pd(OAc)_2$/1,10-phenanthroline catalyst system: in situ formation of well-defined Pd nanoparticles. *Tet. Lett.* **2013**, *54*, 2906–2908. (f) Shelkar, R. S.; Balsane, K. E.; Nagarkar, J. M. Magnetically separable nano CeO_2: a highly efficient catalyst for ligand free direct C–H arylation of heterocycles. *Tet. Lett.* **2015**, *56*, 693–699. (g) Ackermann, L.; Barfusser, S.; Pospech, J. Palladium-catalyzed direct arylations, alkenylations, and benzylations through C–H bond cleavages with sulfamates or phosphates as electrophiles.

Org. Let.. **2010**, *12*, 724–726. (h) Zhu, F.; Tao, J. L.; Wang, Z. X. Palladium-catalyzed C–H arylation of (benzo)oxazoles or (benzo)thiazoles with aryltrimethylammonium triflates. *Org. Lett.* **2015**, *17*, 4926–4929. (i) Zhang, M.; Zhang, S.; Liu, M.; Cheng, J. Palladium-catalyzed desulfinative C-arylation of a benzo[*d*]oxazole C–H bond with arene sulfonyl chlorides. *Chem. Commun.* **2011**, *47*, 11522–11524. (j) Xie, K.; Yang, Z.; Zhou, X.; Li, X.; Wang, S.; Tan, Z.; An, X.; Guo, C. C. Pd-catalyzed decarboxylative arylation of thioazole, benzoxazole, an polyfluorobenzene with substituted benzoic acids. *Org. Lett.* **2010**, *12*, 1564–1567. (k) Balsane, K. E.; Gund, S. H.; Nagarkar, J. M. Atom economical palladium catalyzed novel approach for arylation of benzothiazole and benzoxazole with triarylbismuth reagents via C–H activation. *Catal. Comm.* **2017**, *89*, 29–33. (l) Demmer, C.S.; Bunch, L. Benzoxazoles and oxazolopyridines in medicinal chemistry studies. *Eur. J. Med. Chem.* **2015**, 778–785.

1. (a) Kamer, P. C. J., Reek, J. N. H.; Dierkes, P.; van Leeuwen, P. W. N. M. Ligand bite angle effects in metal-catalyzed C–C bond formation. *Chem. Rev.* **2000**, *100*, 2741–2769. (b) Birkholz, M.N.; Freixa, Z.; van Leeuwen, P. W. N. M. Bite angle effects of disphosphines in C–C and C–X bond forming cross coupling reactions. *Chem. Soc. Rev.* **2008**, 1099–1118. (c) Kamer, P. C. J.; van Leeuwen, P. W. N. M.; Reek, J. N. H. Wide bite angle diphosphines: Xantphos ligands in transition metal complexes and catalysis. *Acc. Chem. Res.* **2001**, *34*, 895–904. (d) Marshall, W. J.; Grushin, V. V. Face Ar–CF_3 bond formation at Pd. Strikingly different outcomes of reductive elimination from [$(Ph_3P)_2Pd(CF_3)Ph$] and [(XantPhos)$Pd(CF_3)Ph$]. *J. Am. Chem. Soc.* **2006**, *128*, 12644–12645. (e) Ji, Y.; Plata, R. E.; Regens, C. S.; Hay, M.; Schmidt, M.; Razler ,T.; Qui, Y.; Geng, P.; Hsiao, Y.; Rosner, T.; Eastgate, M. D.; Blackmond, D. G. Mono-oxidation of bidentate bis-phosphines in catalyst activation: kinetic and mechanistic studies of a Pd/Xantphos-catalyzed C–H functionalization. *J. Am. Chem. Soc.* **2015**, *137*, 13272–13281. (f) Zuideveld, M. A.; Swennenhuis, B. H. G.; Boele, M. D. K.; Guari, Y.; van Strijdonck, G. P. F.; Reek, J. N. H.; Kamer, P. C. J.; Goubitz, K.; Fraanje, J.; Lutz, M.; Spek, A. L.; van Leeuwen, P. W. N. M. The coordination behavior of large natural bite angle disphosphine ligands towards methyl and 4-cyanophenylpalladium(II) complexes.

J. Chem. Soc., Dalton Trans. **2002**, 2308–2317. (g) Yin, J.; Buchwald, S. L. Pd-catalyzed intermolecular amidation of aryl halides: the discovery that Xantphos can be trans-chelating in a palladium complex. *J. Am. Chem. Soc.* **2002**, *124*, 6043–6048.

2. Amaike, K.; Muto, K.; Yamaguchi, J.; Itami, J. Decarbonylative C–H coupling of azoles and aryl esters: unprecedented nickel catalysis and application to the synthesis of muscoride A. *J. Am. Chem. Soc.* **2012**, *134*, 13573–13576.
3. Maleckis, A.; Sanford, M. S. Catalytic cycle for palladium-catalyzed decarbonylative trifluoromethylation using trifluoroacetic esters as the CF_3 source. *Organometallics* **2014**, *33*, 2653–2660.
4. Tasker, S. Z.; Standley, E. A.; Jamison, T. F. Recent advances in homogenous nickel catalysis. *Nature* **2014**, *509*, 299–309.
5. Hoye, T.; Jeffrey, C. S.; Shao, F. Mosher ester analysis for the determination of absolute configuration of stereogenic (chiral) carbinol carbons. *Nature Protocols* **2007**, *2*, 2451–2458.
6. Bekker, R. A.; Asratyan, G. V.; Dyatkin, B. L.; Knunyants, I. L. Polyhalogenated α-oxides. VI. Synthesis of α-substituted difluoroacrylic acids and alkyldifluorovinyl ethers from polyfluorinated α-oxides. *Zhurnal Organicheskoi Khimii* **1975**, *11*, 961–965.
7. Drugbank, http://www.drugbank.ca/ (accessed February 7th, 2022).
8. Geri, J. B.; Wolfe, M. W. W.; Szymczak, N. K. The difluoromethyl group as a masked nucleophile: A Lewis acid/base approach. *J. Am. Chem. Soc.* **2018**, *140*, 9404–9408.
9. Burgey, C. S.; Robinson, K. A.; Lyle, T. A.; Sanderson, P. E. J.; Lewis, S. D.; Lucas, B. J.; Krueger, J. A.; Singh, R.; Miller-Stein, C.; White, R. B.; Wong, B.; Lyle, E. A.; Williams, P. D.; Coburn, C. A.; Dorsey, B. D.; Barrow, J. C.; Stranieri, M. T.; Holahan, M. A.; Sitko, G. R.; Cook, J. J.; McMasters, D. R.; McDonough, C. M.; Sanders, W. M.; Wallace, A. A.; Clayton, F. C.; Bohn, D.; Leonard, Y. M.; Detwiler, T. J., Jr.; Lynch, J. J., Jr.; Yan, Y.; Chen, Z.; Kuo, L.; Gardell, S. J.; Shafer, J. A.; Vacca, J. P. Metabolism-directed optimization of 3-aminopyrazinone acetamide thrombin inhibitors. Development of an orally bioavailable series containing P1 and P3 pyridines. *J. Med. Chem.* **2003**, *46*, 461–473.

10. (a) Ojima, I. Fluorine in Medicinal Chemistry and Chemical Biology; Wiley: Chichester, **2009**. (b) O'Hagan, D. Understanding organofluorine chemistry. An introduction to the C−F bond. *Chem. Soc. Rev.* **2008**, *37*, 308−319. (c) Purser, S.; Moore, P. R.; Swallow, S.; Gouverneur, V. Fluorine in medicinal chemistry. *Chem. Soc. Rev.* **2008**, *37*, 320−330. (d) Hagmann, W. K. The many roles for fluorine in medicinal chemistry. *J. Med. Chem*. **2008**, *51*, 4359−4369. (e) Müller, K.; Faeh, C.; Diederich, F. Fluorine in pharmaceuticals: looking beyond intuition. *Science* **2007**, *317*, 1881−1886. (f) Meanwell, N. A. Synopsis of some recent tactical application of bioisosteres in drug design. *J. Med. Chem*. **2011**, 54, 2529−2591. (g) Zhou, Y.; Wang, J.; Gu, Z.; Wang, S.; Zhu, W.; Aceña, J. L.; Soloshonok, V. A.; Izawa, K.; Liu, H. Next generation of fluorine-containing pharmaceuticals, compounds currently in phase II-III clinical trials of major pharmaceutical companies: new structural trends and therapeutic areas. *Chem. Rev.* **2016**, *116*, 422−518.
11. Reina, A.; Krachko, T.; Onida, K.; Bouyssi, D.; Jeanneau, E.; Monteiro, N.; Amgoune, A. Development and mechanistic investigations of a base-free Suzuki-Miyaura cross-coupling of α,α-difluoroacetamides via C–N cleavage. *ACS Catal.* **2020**, *10*, 2189–2197.
12. (a) G. Meng, M. Szostak.; Sterically controlled Pd-catalyzed chemoselective ketone synthesis via N–C cleavage in twisted amides. *Org. Lett*. **2015**, *17*, 4364; (b) G. Meng, M. Szostak, Palladium-catalyzed Suzuki–Miyaura coupling of amides by carbon–nitrogen cleavage: general strategy for amide N–C bond activation. *Org. Biomol. Chem.* **2016**, *14*, 5690; (c) R. Szostak, M. Szostak, *N*-Acyl-glutarimides: Resonance and proton affinities of rotationally-inverted twisted amides relevant to N–C(O) cross-coupling. *Org. Lett.* **2018**, 20, 1342. (d) G. Meng, M. Szostak, General olefin synthesis by the palladium-catalyzed heck reaction of amides: sterically controlled chemoselective N–C activation. *Angew. Chem. Int. Ed.* **2015**, *54*, 14518.

Chapter 4 – Developments in Decarbonylative Difluoromethylation of Arenes at Nickel

4.1 Introduction

In Chapter 2, we reported the decarbonylative cross-coupling of DFAF with aryl boronate esters catalyzed by a (SPhos)Pd complex.[1] Notably, this reaction was only effective with electron-poor aryl boronate esters (Scheme 4.1). In Chapter 3, we developed a Pd-catalyzed C–H difluoromethylation system that is effective for substituted (benz)azoles (Scheme 4.1).

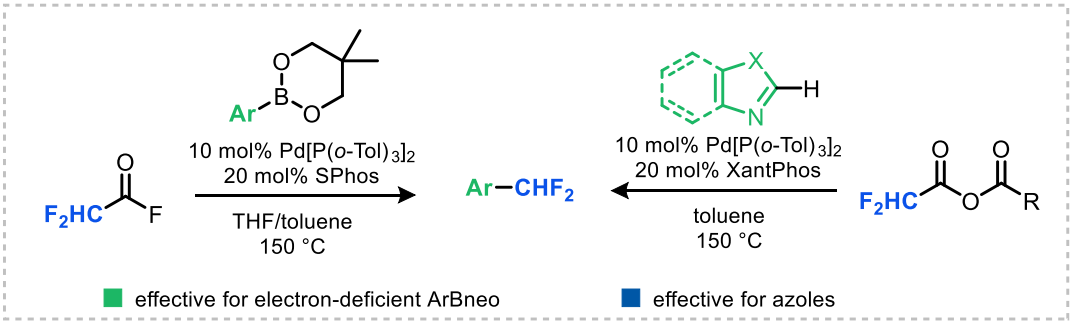

Scheme 4.1. Decarbonylative difluoromethylation reactions developed herein.[1a]

During the optimization of these two Pd-catalyzed transformations, we were unable to effectively difluoromethylate substrates outside of these two limited classes. We reasoned that moving from palladium- to nickel-based catalysts might be and effective approach for expanidng the scope of these transformations. Nickel, the first-row, more electropositive congener of palladium, can catalyze decarbonylative cross-coupling reactions and can exhibit complementary reactivity and selectivity to Pd (Figure 4.1).[2]

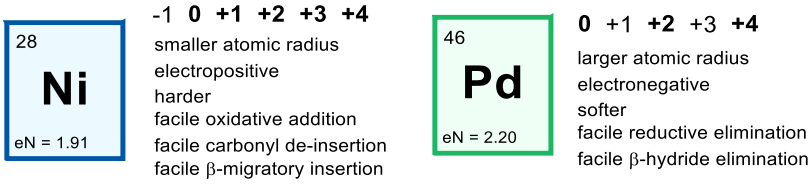

Figure 4.1. Comparison between the reactivity of Ni and Pd. Adapted from ref. 2.

Our lab has demonstrated that Ni-catalyzed decarbonylative coupling reactions are highly effective for C–S[3a,e], C–C[3b], C–B[3c], and C–N[3d] bond formations. In an initial report from our lab on thioetherification,[3a] we observed some complementarity between the substrate scope afforded by Ni-catalysis compared to Pd-catalysis. For instance, as summarized in Figure 4.2, electron-rich thioesters performed worse under the Pd-catalyzed conditions compared to the Ni-catalyzed conditions, presumably due to the more challenging oxidative addition of electron-rich thioesters at Pd^0. However, the Pd catalyst system was effective for the more challenging $C(sp^2)$–$C(sp^3)$ reductive elimination in thioether **3** (Scheme 4.2).

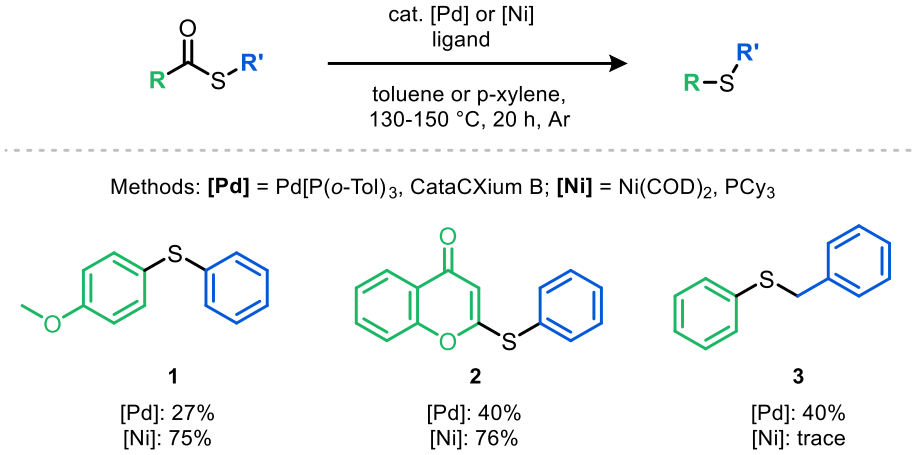

Scheme 4.2. Set of substrates from previous report[3a] that demonstrate complementarity of Ni and Pd in our systems.

Additionally, there has been precedent for aryl difluoromethylation catalyzed by nickel. For instance, Vicic and co-workers reported the room temperature difluoromethylation of aryl iodides using a $L_2Zn^{II}(CHF_2)_2$ nucleophile catalyzed by $Ni(COD)_2$ and a bidentate ligand in DPPF (Scheme 4.3).[4] Similarly, Mikami and co-workers[5] demonstrated the (tmeda)Ni-catalyzed cross-coupling of $ICHF_2$ with aryl Grignard reagents (Scheme 4.4). Both of these transformations

demonstrate the feasibility of room temperature C(sp^2)–CHF_2 bond-forming reductive elimination from Ni centers in cross-coupling reactions. This is a critical observation, considering that reductive elimination is often the slowest/most challenging step in Ni-catalyzed cross-coupling reactions.[4]

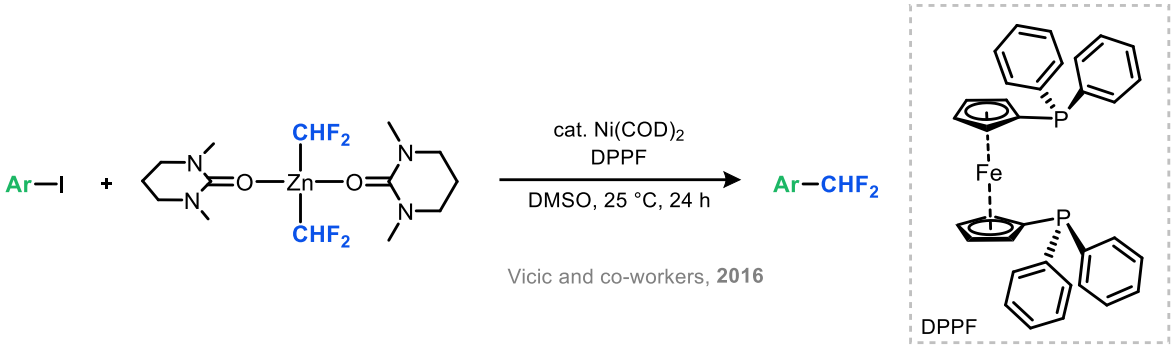

Scheme 4.3. Ni-catalyzed difluoromethylation of aryl iodides reported by Vicic and co-workers.[4]

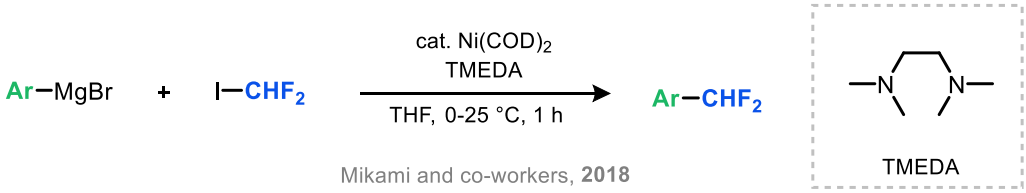

Scheme 4.4. Ni-catalyzed difluoromethylation of aryl Grignard reagents reported by Mikami and co-workers.[5]

4.2 Identifying Compatible Coupling Partners

With these difluoromethylation precedents, we sought to develop a Ni-catalyzed decarbonylative difluoromethylation reaction that utilizes a difluoroacyl electrophile, such as DFAF or DFAAn, with an organometallic nucleophile. Our work in Chapter 2 established the compatibility of DFAF and DFAAn with aryl boronate esters as well as the incompatibility of these electrophiles with more nucleophilic transmetalation diaryl zinc nucleophiles and aryl boronic acids (Scheme 4.5).

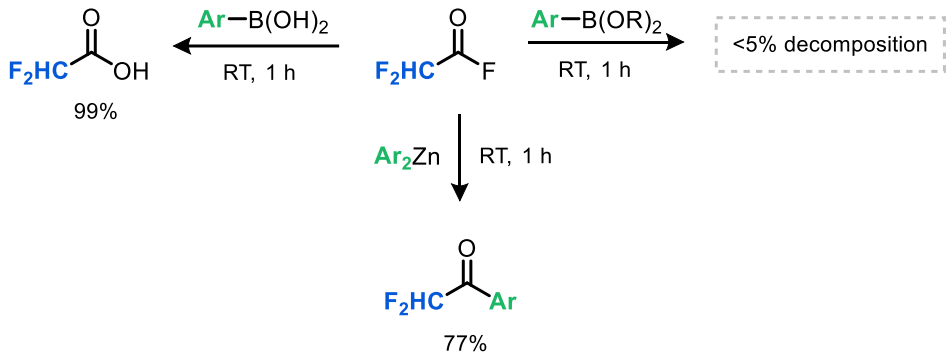

Scheme 4.5. (In)compatibility of DFAF with select organometallics.[1a]

As depicted in Scheme 4.5 and in Figures 2.1 through 2.6 in Chapter 2, difluoroacyl electrophiles (DFAAn, DFAF) are incompatible with highly reactive organometallics, such as aryl boronic acids and diaryl zinc nucleophiles.[1] Therefore, we first tested the reaction of aryl boronate esters with DFAF using a Ni precatalyst and diphosphine ligand at 50 °C. We initially selected a DPPF/Ni catalyst system due to the precedent for this catalyst promoting Ar–CHF_2 reductive elimination under mild conditions.[4] However, as shown in Table 4.1, these conditions were not effective for the formation of the desired product with aryl boronic acids showing complete decomposition of DFAF. In the reactions of boronate esters (entry 2 and 3), significant quantities of DFAF were observed in the crude ^{19}F NMR.

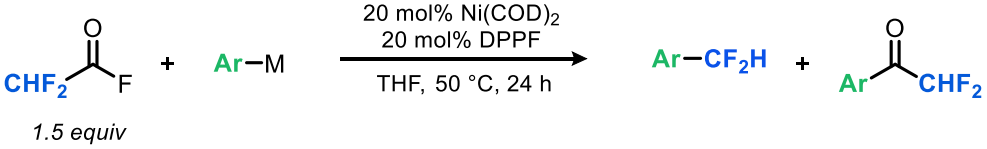

Entry	ArM	**$ArCHF_2$** (% yield)	**$ArCOCHF_2$** (% yield)
1	$PhB(OH)_2$	0	0
2	PhBneo	0	0
3	PhBpin	0	0

Yields determined via ^{19}F NMR

Table 4.1. Initial catalytic reaction with organoboron nucleophiles using Ni/DPPF.

We next posited that aryl tributyltin organometallics could be effective in the reaction, as these undergo faster transmetalation than the analogous boron-based nucleophiles.[6] Before attempting any catalytic reactions, we tested the compatibility of DFAF with tributyl(phenyl)tin and electron-rich tributyl(4-methoxyphenyl)stannane in THF at room temperature and 130 °C for 24 h. Under these conditions, we saw minimal decomposition of DFAF into DFA and no presence of ketone by-product based on the diagnostic resonances in the ^{19}F NMR spectrum. Therefore, we moved to test the reactivity of tin nucleophiles in a Ni-catalyzed decarbonylative difluoromethylation system.

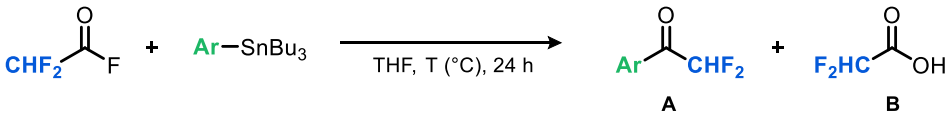

Entry	$ArSnBu_3$	T (°C)	**A** (% yield)	**B** (% yield)
1	$PhSnBu_3$	25	0	0
2	$PhSnBu_3$	130	0	3
3	4-MeOPhSnBu_3	130	0	4

Yields determined via ^{19}F NMR

Table 4.2. Compatibility of DFAF with tributyl(aryl)stannanes in THF.

4.3 Optimizing Ni-catalyzed Decarbonylative Difluoromethylation

First, we attempted the reaction of tributyl(phenyl)stannane with DFAF with our preliminary Ni/DPPF system at 50 °C. Under these conditions, we observed trace amounts of difluoromethylbenzene **1** in the ^{19}F NMR (Table 4.3, entry 1). The remaining mass balance was unreacted DFAF. Under analogous conditions, electron-rich tributyl(4-methoxyphenyl)stannane reacted to afford a significantly higher 12% yield of the difluoromethylarene product **2** (entry 2). Again, the mass balance was unreacted DFAF. Raising the temperature of this reaction from 50 °C to 100 °C and then 130 °C, resulted in higher yields of 30% (entry 3) to 40% (entry 5) of **2**, respectively. Under these conditions, no DFAF remained after the reaction. Less electron-rich tributyl(4-fluorophenyl)stannane showed minimal reactivity even at 100 °C (entry 4).

Interestingly, this electronic trend is opposite to what was observed in our previous difluoromethylation report.[1]

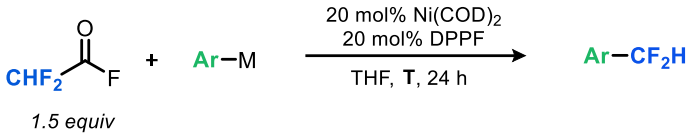

Entry	ArM	T (°C)	DFAF (% yield)	$ArCHF_2$ (% yield)	$ArCOCHF_2$ (% yield)
1	$PhSnBu_3$	50	107	1	0
2	4-$OCH_3PhSnBu_3$	50	92	12	0
3	4-$OCH_3PhSnBu_3$	100	0	30	0
4	4-$FPhSnBu_3$	100	60	0	0
5	4-$OCH_3PhSnBu_3$	130	0	40	0

Yields determined via ^{19}F NMR with internal standard

Table 4.3. Initial catalytic reactions of DFAF with $ArSnBu_3$ reagents using Ni/DPPF.

We next examined the impact of the DPPF to $Ni(COD)_2$ ratio on the yield of the reaction between DFAF and (4-(benzyloxy)phenyl)tributylstannane to form 1-(benzyloxy)-4-(difluoromethyl)benzene, **3** (Table 4.4). We observe a significant increase in the yield when increasing the ratio from 1:1 to 1.5:1 to 2:1 (entries 1-3). However, the yield begins to fall when increasing further to 2.5:1 (entry 4). Overall, at 130 ºC, a 2:1 ratio of DPPF:$Ni(COD)_2$ produced the highest yield of **3** (42% yield, entry 3).

Entry	X mol% DPPF	DPPF:Ni	Yield **3** (%)
1	20	1:1	24
2	30	1.5:1	30
3	40	2:1	42
4	50	2.5:1	35

^{19}F NMR yields w/ fluorobenzene (0.05 mmol)

Table 4.4. Ligand loading screen for (DPPF)Ni-catalyzed decarbonylative difluoromethylation of tributyl(4-benzyloxyphenyl)stannane.

Further optimization of the reaction conditions using 20 mol% of $Ni(COD)_2$ and 40 mol% of other diphosphine ligands revealed the unique efficacy of an unsymmetrical phosphinoferrocene ligand, tBuPPF, in this reaction. As shown in Table 4.5, in the coupling of DFAF with (4-(benzyloxy)phenyl)tributylstannane tBuPPF performed significantly better (entry 6, 42% yield) compared to other phosphinoferrocenes (including analogues DPPF (entry 1, 30 %) and DtBuPF, DiPPF, and DCyPF (all yielding 0% $ArCHF_2$ product with significant DFAF remaining and DFA observed). Notably, tBuPPF was the only mixed phosphinoferrocene that was evaluated in this reaction because it is the only one that is commercially available. Upon increasing the equivalents of DFAF in the reaction from 1.5 to 3.0, we observed a doubling of the yield of the desired product from 42% (entry 8) to 90% (entry 9).

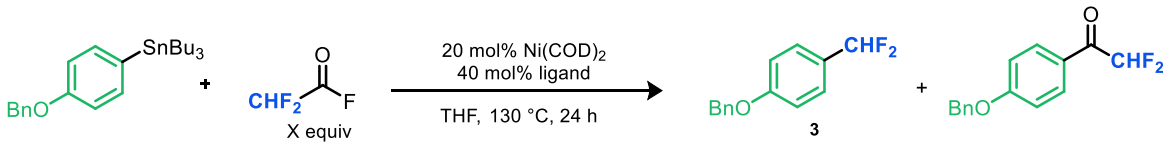

Entry	X equiv	Ligand	yield 3 (%)	yield ketone (%)
1	1.5	DPPF	31	0
2	1.5	DtBPF	0	0
3	1.5	DiPPF	0	0
4	1.5	DCyPF	0	0
5	1.5	DCyPE	0	0
6	1.5	DPPE	0	0
7	1.5	DPPB	0	0
8	1.5	tBuPPF	42	0
9	3	tBuPPF	90	0

Yields determined via ^{19}F NMR

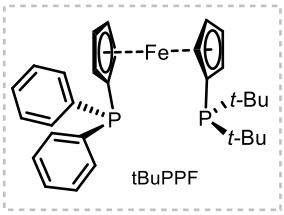

Table 4.5. Ligand screen for Ni-catalyzed decarboynaltive difluoromethylation of tributyl(4-benzyloxyphenyl)stannane.

These optimized conditions (3 equiv of DFAF, 130 ºC, THF) were next applied to a wider range of aryl stannane substrates. The reactions were conducted using 20 mol% of $Ni(COD)_2$ and 40 mol% tBuPPF. A sample of the products obtained are shown in Scheme 4.6. Overall, electron-

rich tributyl(aryl)tin reagents perform exceptionally well under these conditions, yielding greater than 80% yield of the $ArCHF_2$ product in all cases. However, tributyl(4-fluorophenyl)stannane still performed poorly, forming less than 10% yield of the desired difluoromethylation product.

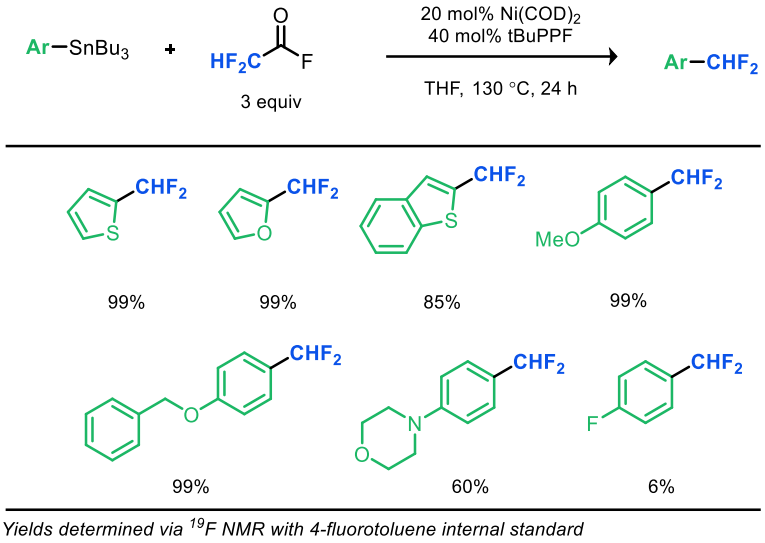

Yields determined via ^{19}F NMR with 4-fluorotoluene internal standard

Scheme 4.6. Preliminary substrate scope for Ni-catalyzed decarbonylative difluoromethylation of $ArSnBu_3$ reagents.

We next evaluated the higher yielding reactions from Scheme 4.6 at lower the loading of catalyst (10 mol% $Ni(COD)_2$ and 20 mol% tBuPPF). As shown in Scheme 4.7, reasonable yields of the difluoromethylation product were maintained for most of the substrates.

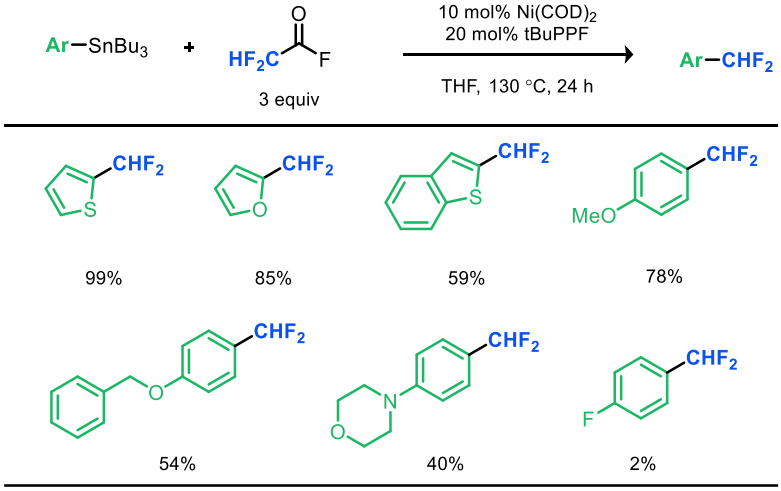

Yields determined via ^{19}F NMR with 4-fluorotoluene internal standard

Scheme 4.7. Substrate scope for Ni-catalyzed decarbonylative difluoromethylation under optimized conditions.

Under these conditions, we also tested a variety of other tributyltin nucleophiles. The results of this screen are shown in Scheme 4.8. In general, both electron rich (e.g. pyrrole) and electron deficient (e.g. pyridine) nitrogen-based nucleophiles were ineffective in the reaction. For example, in the reaction of 1-methyl-4-(tributylstannyl)-1H-pyrazole, significant decomposition of DFAF was observed and undesired ketone by-product was observed (30%) in addition to the desired $ArCHF_2$ product (12%). Based on this result, we conducted the control reaction of DFAF and 1-methyl-4-(tributylstannyl)-1H-pyrazole in THF and observed >95% conversion of the nucleophile to the undesired ketone by-product (Scheme 4.9). Additionally, electron-neutral tributyl(phenyl)stannane and the biphenyl analogue generated the corresponding difluoromethyl products in modest 15 and 25%, respectively, with significant quantities of DFAF remaining.

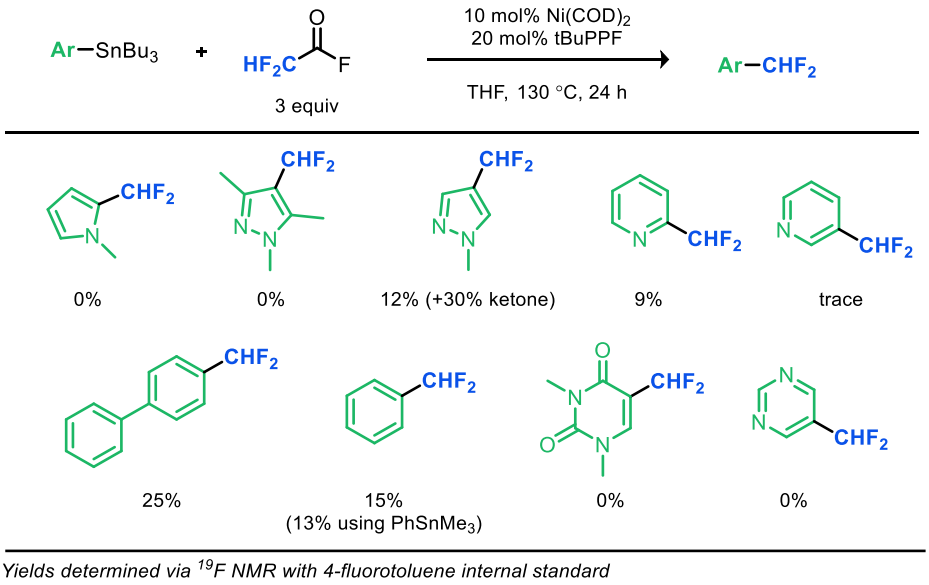

Yields determined via ^{19}F NMR with 4-fluorotoluene internal standard

Scheme 4.8. Limitations in the substrate scope for optimized Ni-catalyzed decarbonylative difluoromethylation system.

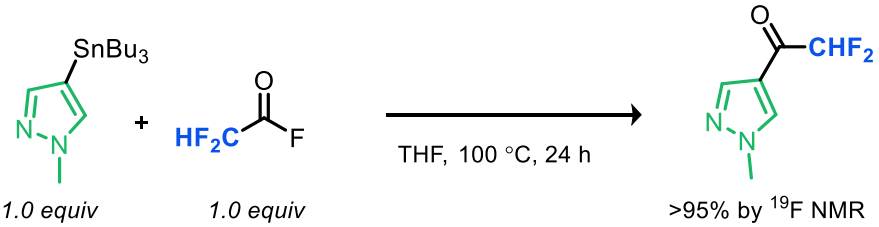

Scheme 4.9. Control reaction of 1-methyl-4-(tributylstannyl)-1H-pyrazole with DFAF at 100 °C for 24 h in THF.

In summary, we successfully identified conditions for the Ni-catalyzed decarbonylative difluoromethylation of electron-rich tributyl(aryl)tin nucleophiles [10 mol% $Ni(COD)_2$, 20 mol% tBuPPF, 3.0 equiv DFAF, 1.0 equiv $ArSnBu_3$, THF (0.17 M), 130 °C, 24 h). However, this transformation works best with electron-rich tin nucleophiles. This is in marked contrast to our previous report of Pd-catalyzed decarbonylative difluoromethylation (Chapter 2) that was only effective for electron-deficient aryl boronate esters.[1] To gain a better understanding of these complementarities, we next pursued a cross-analysis between the substrate scopes of thees two transformations. Therefore, we selected a subset of aryl derivatives that vary electronically[7] and are available both as the tributyltin reagent and the neopentyl boronate esters.[1] We selected the 4-fluorophenyl (σ_p = 0.06), 4-benzyloxyphenyl, and 4-methoxyphenyl (σ_p = -0.24) boron and tin reagents as a series of arenes ranging from electron-deficient to -rich.[6] Scheme 4.9 shows the results of this cross analysis (Scheme 4.10).

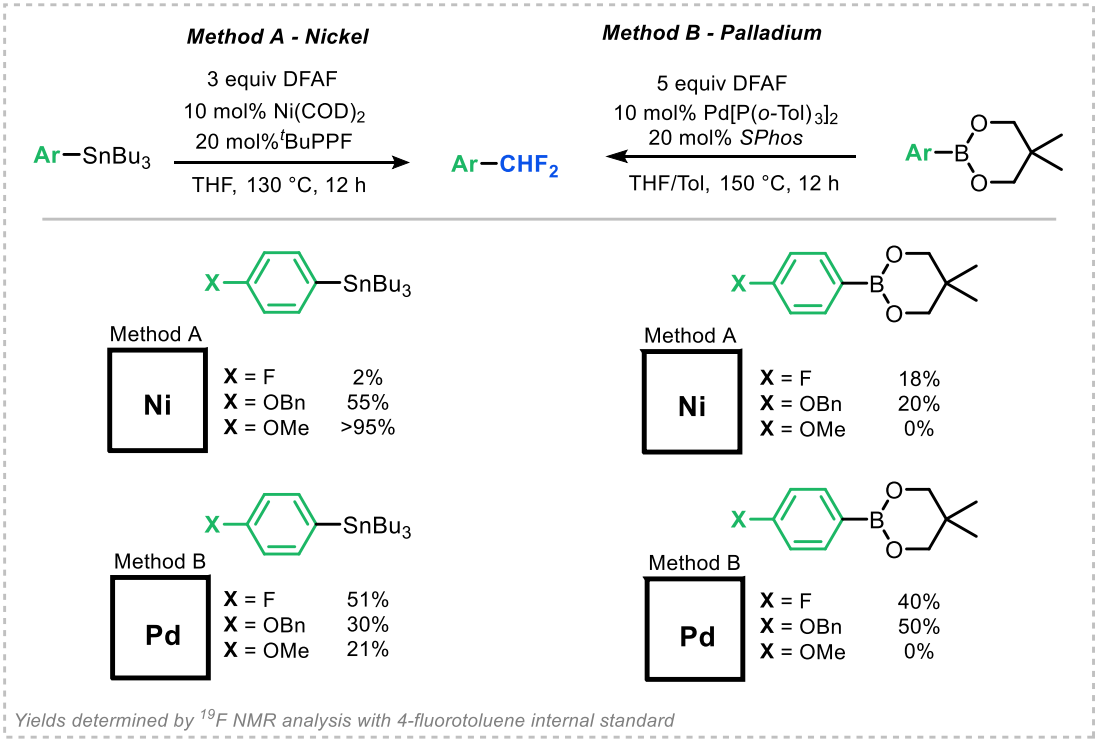

Scheme 4.10. Cross-analysis of newly developed Ni system with previously developed Pd-catalyzed system.[1a]

The results in Scheme 4.10 demonstrate that electron-rich aryl tin reagents are the best substrates for Ni/tBuPPF catalysis and that electron-poor and electron-rich aryl boronate esters perform poorly with this Ni system. They also show that electron-deficient tin and boron organometallic reagents perform well under the Pd/SPhos-catalyzed conditions.[1] To get some idea of the mass balance for the Ni/tBuPPF reaction, we conducted an experiment using tributyl(4-fluorophenyl)stannane and the analogous neopentyl boronate ester. As shown in Scheme 4.10, the results show that the mass balance for the organometallic is mainly the starting material with some protodestannylation observed.

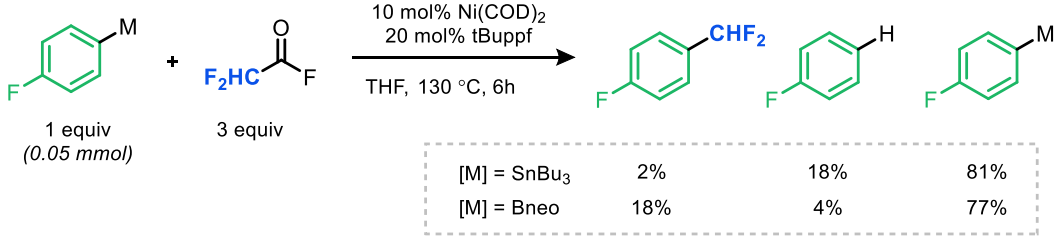

Scheme 4.11. Mass balance experiment with tributyl(4-fluorophenyl)stannane and boronate ester analogue.

We hypothesized that these unique electronic trends may arise from different mechanisms or selectivity in the transmetalation of these organometallics at Ni versus Pd. Therefore, we aimed to study transmetalation of these organometallics at a catalytically-relevant or model metal complex.

4.4 Preliminary Results in Stoichiometric Difluoromethylation

In the decarbonylative difluoromethylation reactions reported in Sections 2.6 and 4.3, we observed complementary substrate scopes. In the Pd-catalyzed system, the scope was limited to electron-deficient aryl boronate esters. In the Ni-catalyzed system, electron-rich tin organometallics are uniquely effective. We hypothesized that the differences in these reactions were likely related to differences in the transmetalation step of the catalytic cycle. As such, we sought to synthesize catalytically relevant and/or model metal-fluoride complexes (intermediate **II** in Scheme 4.12) to evaluate this step in detail.

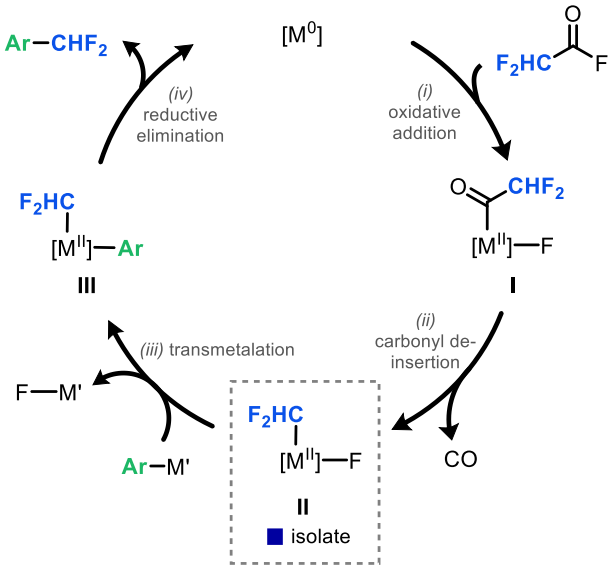

Scheme 4.12. Proposed catalytic cycle for metal-catalyzed decarbonylative difluoromethylation with DFAF.

After obtaining complex **II**, we aimed to test the reactivity of a variety of boron and tin organometallics towards transmetalation. However, we were unable to isolate the reactive (SPhos)$Pd^{II}(CF_2H)(F)$ intermediate that we observed spectroscopically in Chapter 2.[1] Therefore, we posited that the stoichiometric transmetalation study may be more successful using a nickel complex. Further, reductive elimination of the $ArCHF_2$ products in both our systems is proposed to occur at room temperature.[1,4] To study just the transmetalation process and limit Ar–CHF_2 reductive elimination at room temperature, we selected the electron-rich bidentate phosphine ligand DCyPE. Thus, we targeted the synthesis of (DCyPE)$Ni^{II}(CF_2H)(F)$, **II-DCyPE** for studies of transmetalation.

We initially attempted the direct synthesis of **II-DCyPE** via the reaction of a mixture of $Ni(COD)_2$ and DCyPE with DFAF. We proposed that oxidative addition and carbonyl de-insertion (steps *i* and *ii* in Scheme 4.12) would yield the target complex. However, we were unable to determine or isolate the product(s) of this process, and the ^{31}P NMR spectrum of the crude reaction mixture showed complex splitting patterns (Figure 4.2) that were not consistent with the formation of the target complex.

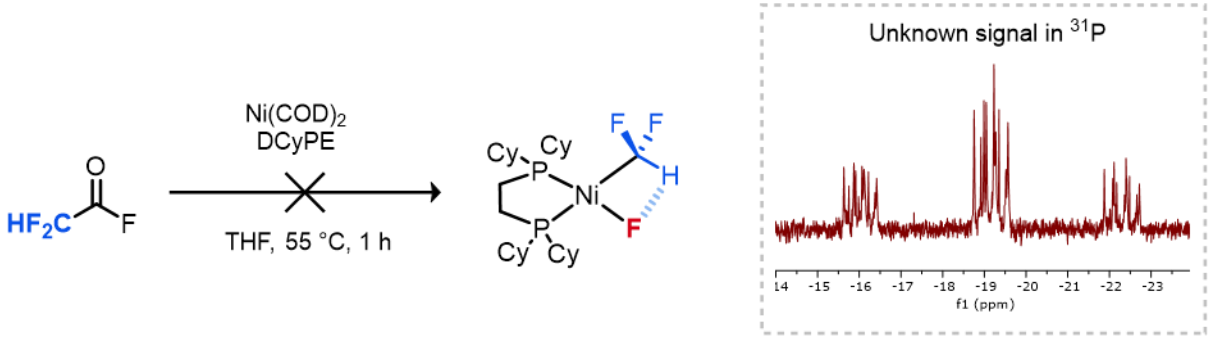

Figure 4.2. Stoichiometric reaction of DFAF with $Ni(COD)_2$ and DCyPE in THF at 55 °C for 1 h showing unidentified product with high order splitting patterns.

Therefore, we designed a multi-step process to synthesis complex **II-DCyPE** based on related work from our lab.[1,8] We first synthesized complex **A** from the two-step reaction of $Ni(COD)_2$ with excess triphenylphosphine followed by oxidative addition and carbonyl de-

insertion with DFAAn (Scheme 4.13). The reaction to form **A** was completed in 3 h, whereas the analogous reaction at our (SPhos)Pd complex in our previous report[1] required 10 h for completion of the reaction.

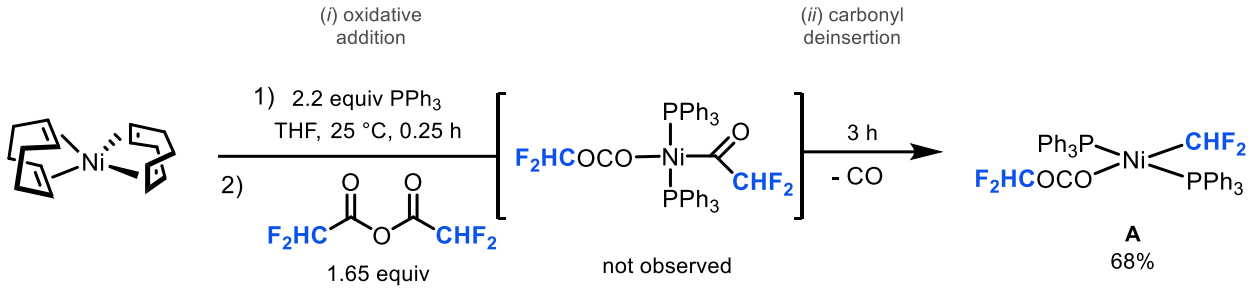

Scheme 4.13. Synthesis of complex **A** from $Ni(COD)_2$ and **DFAAn**.

Complex **A** was isolated in 68% yield, and single crystals were obtained by vapor diffusion. The complex features a diagnostic broad ^{31}P resonance at -32.4 ppm, suggesting a trans orientation of the phosphine ligands. The associated 19F NMR showed two broad resonances at –84.39 and –125.51 ppm, which is consistent with the structure of complex **A**. An ORTEP diagram for **A** is shown in Figure 4.3. Selected bond lengths and angles are shown in the figure caption of Figure 4.3. The X-ray structure confirms the *trans*-orientation of the triphenylphosphine ligands. Rather than being perfectly square-planar, the complex is slightly puckered with a P1–Ni1–P2 angle of 165.2° and a C3–Ni1–O1 angle of 169.0°. Further, complex **A** features a nickel–difluoromethyl bond length of 1.89 Å, which is nearly identical to that in the $(TMEDA)Ni(CHF_2)_2$ complex reported by Vicic and co-workers (1.88 and 1.89 Å).[4]

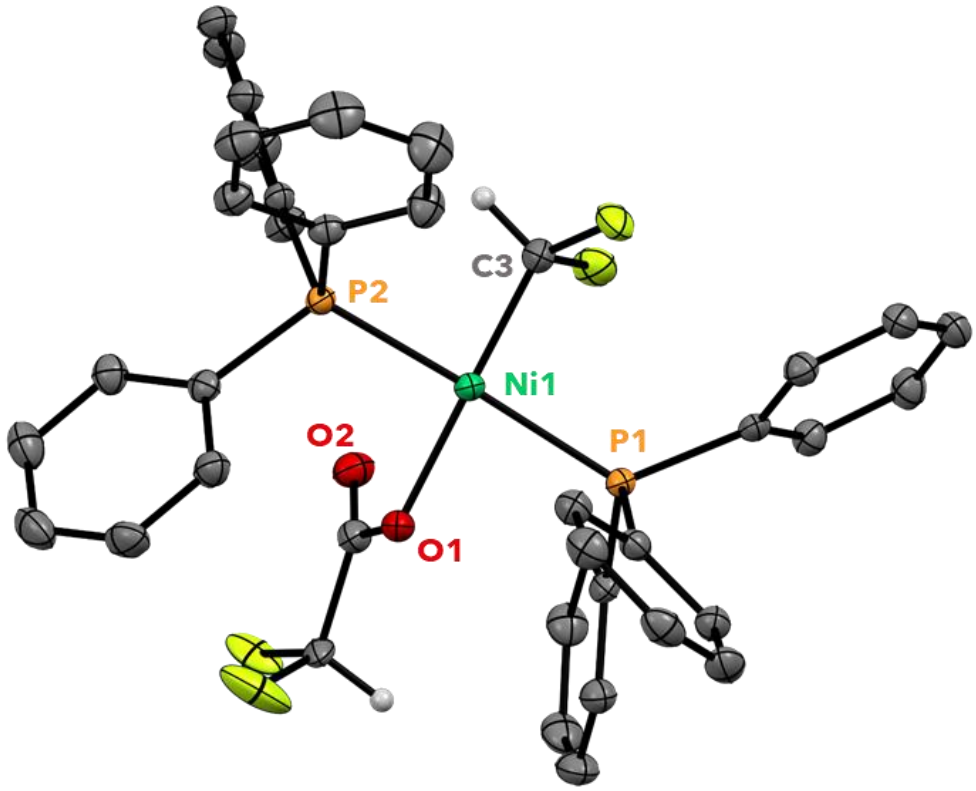

Figure 4.3. ORTEP diagram of complex **A**. Select protons are omitted for clarity. Selected bond lengths (Å) and angles (deg): Ni1–P1 2.24, Ni1–P2 2.23, Ni1–O1 1.96, Ni1–C3 1.89, Ni1---O2 2.71, P1–Ni1–P2 165.2, O1–Ni1–C3 169.0.

We next conducted treated complex **A** with DyCPE at room temperature to promote substitution of the PPh_3 ligands. The target cis-chelated product $(DCyPE)Ni^{II}(CF_2H)(O_2CCF_2H)$ **B** was isolated in 81% yield (Scheme 4.13). The NMR spectra of the crude reaction mixture suggests the formation of the desired complex **B**. Specifically, we observed two resonances in the ^{19}F NMR that supported the presence of the desired complex **B** (ddd, -100.9 ppm, 2F; d, -123.5 ppm, 2F). Additionally, we saw associated phosphorus peaks in the ^{31}P NMR as a dt at 74.7 ppm and a td of 57.9 ppm.

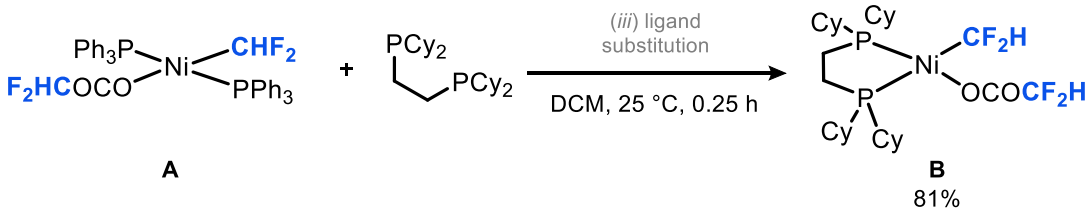

Scheme 4.13. Ligand exchange of complex **A** to form complex **B**.

An x-ray quality crystal of **B** was obtained by single-crystal growth via vapor diffusion (see Experimental details). The ORTEP diagram is shown in Figure 4.4, and selected bond lengths and angles are included in the figure caption. Complex **B** features DCyPE coordinated in a bidentate fashion with a bite angle of 88.8 °, which is within the known range for this ligand.[9] The Ni1–C1 bond length is 1.94 Å, which is slightly longer than that of **A** (1.89 Å). Further, the acidic H1 of complex **B** is only 2.50 Å from the basic O2 of the carboxylate ligand and features a C1–H1---O2 angle of 127.0°. We hypothesize that the electrostatic potential surface of this complex will likely show the presence of an H(δ+)–O(δ–) electrostatic interaction between H1 and O2, similar to that observed in our previous study with an analogous (SPhos)$Pd^{II}(CF_2H)(O_2CCF_2H)$ complex (Figures 2.12 and 2.13).[1]

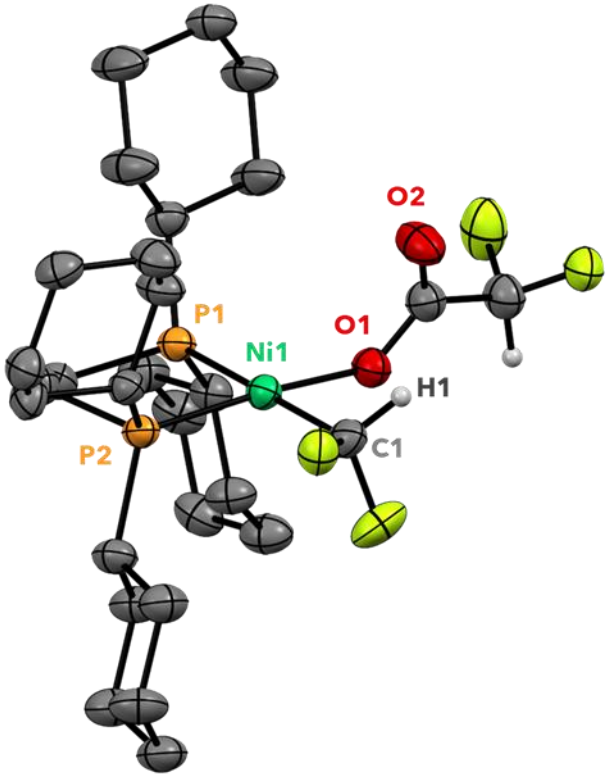

Figure 4.4. ORTEP diagram of complex **B**. Select protons are omitted for clarity. Selected bond lengths (Å) and angles (deg): Ni1–P1 2.24, Ni1–P2 2.15, Ni1–O1 1.91, Ni1–C1 1.94, H1---O1 2.50, H1---O2 2.60, P1–Ni1–P2 88.8, O1–Ni1–C1 86.4, P1–Ni1–C1 175.0, C1–H1---O2 127.0.

With complex **B** in hand, we moved to synthesize our target complex, **II-DCyPE**. This complex would be comparable to intermediate **II** in our proposed catalytic cycle (Scheme 4.11) and would allow us to study the transmetalation with boron and tin organometallics. We synthesized our target complex **II-DCyPE** via the salt metathesis reaction of complex **B** with tetramethylammonium fluoride, as shown in Scheme 4.15.

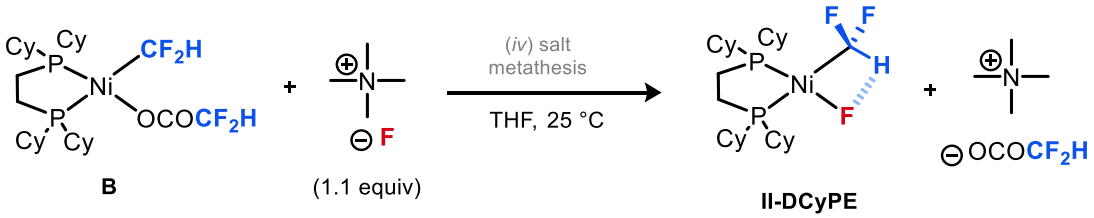

Scheme 4.14. Salt metathesis of **B** with Me_4NF to form Ni–F complex **II-DCyPE**.

The crude ^{19}F NMR of this reaction showed the formation of a new resonance indicative (bs, -317.1 ppm) of a metal–fluoride bond.[10] Isolation of this complex via recrystallization yielded **II-DCyPE** in 30% yield. The ^{19}F NMR spectrum (Figure 4.5) of this purified complex shows the expected splitting for complex **II-DCyPE (**dddd at -97.32 with J = 65.0, 40.2, 23.7, 14.0 Hz; and ddt at -317.91 with J = 93.4, 48.1, 23.4 Hz).

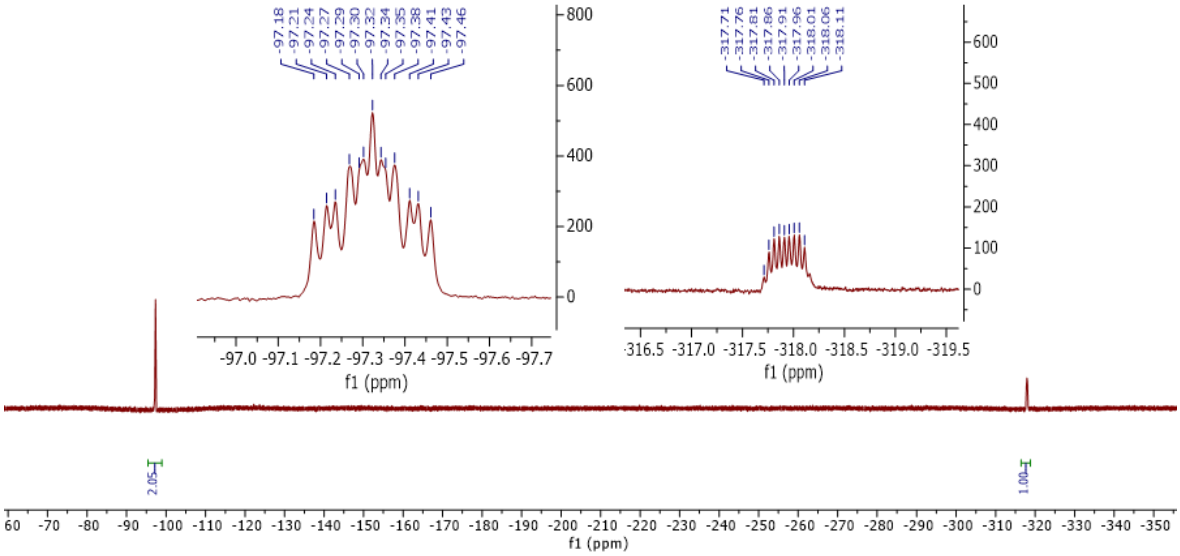

Figure 4.5. ^{19}F NMR spectrum of complex **II-DCyPE** showing diagnostic resonances and high splitting patterns.

An x-ray quality crystal of **A** was obtained via vapor diffusion. Two orientations of the ORTEP diagram of this complex are shown below in Figure 4.6. The DCyPE ligand is bidentate with a bite angle of 88.4° (compared to 88.8° in complex **B**, Figure 4.4). Additionally, this complex shows a notably short contact between the acidic H27 of the Ni–C**H**F_2 and F1 of the Ni–F intermediate (2.36 Å) with a C27–H1---F1 angle of 94.0°. This distance is nearly identical to that in the observed electrostatic interaction (2.38 Å) reported for complex **II-CHF$_2$** in Figure 2.11 and 2.12.[1]

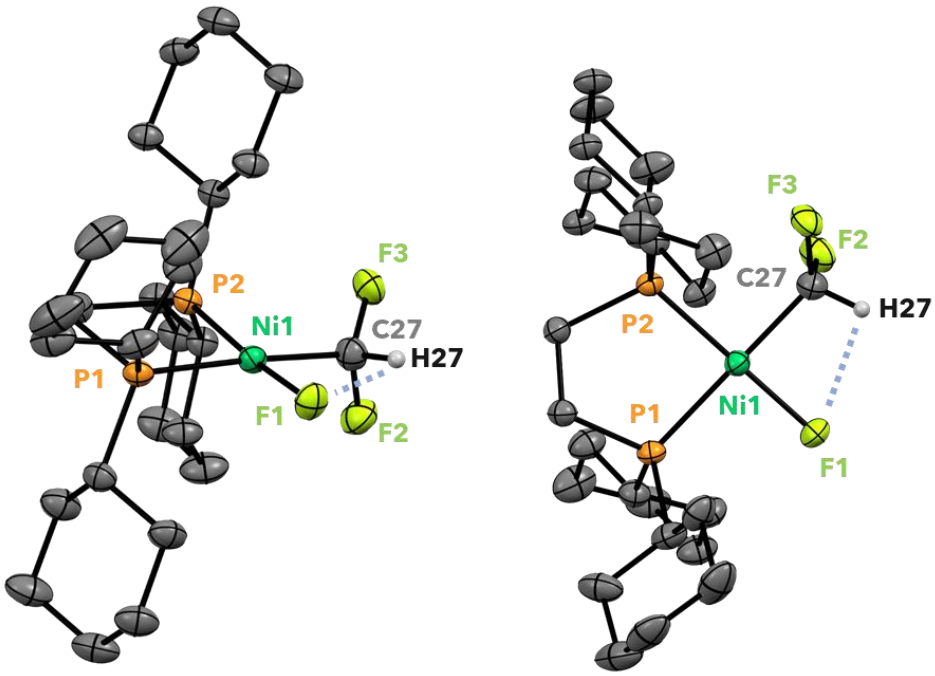

Figure 4.6. ORTEP diagram of complex **II-DCyPE**. Selected protons are omitted for clarity. Selected bond lengths (Å) and angles (deg): Ni1–P1 2.21, Ni1–P2 2.12, Ni1–F1 1.86, Ni1–C27 1.93, H27---F1 2.36, P1–Ni1–P2 88.4, C27–Ni1–F1 88.0, P1–Ni1–C27 177.0.

4.5 Conclusions and Future Work

This chapter describes the development of a Ni-catalyzed decarbonylative difluoromethylation reaction that utilizes DFAF as the difluoroacyl electrophile. This reaction is effective for a range of electron-rich Sn-based organometallics. Future work in the catalytic reaction would be to enable selectivity with N-based nucleophiles, which showed incompatibility with our DFAF electrophile.

Having developed an effective Ni-catalyzed decarbonylative difluoromethylation reaction with complementary scope to that in our previous report[1a], we hypothesized that the difference could be related to electronic trends in transmetalation. As such, we synthesized complexes **A**, **B**, and the unique Ni–F complex **II-DCyPE**. Crystal structures were obtained for all three complexes and elucidate the structural features of these complexes. Overall, we were able to synthesize complex **II-DCyPE** in approximately 16.5% yield over three steps starting from DFAAn.

Complex **II-DCyPE** (like complex **II-CHF$_2$** in Chapter 2) features a short distance between the acidic –C**H**F$_2$ and basic X-type ligand on the complex. We believe this interaction could help stabilize this complex electrostatically.

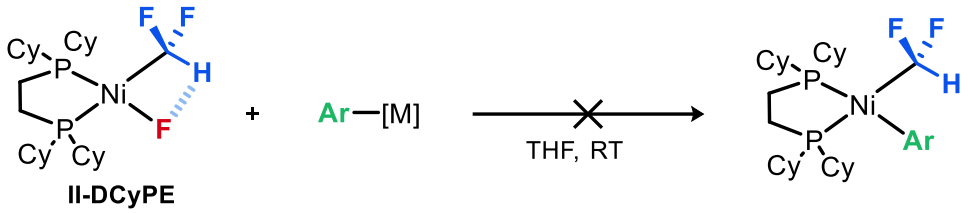

Scheme 4.15. Transmetalation studies of **II-DCyPE** with aryl organometallics.

Addition of 4-methoxyphenylboronic acid to a solution containing **II-DCyPE** led to a complex mixture of signals in the ^{19}F NMR that were not indicative of the desired transmetalation product, which should only have one difluoromethyl signal in ^{19}F NMR. Instead, we observed multiple signals in the metal–difluoromethyl region of the ^{19}F NMR and a new Ni–F signal at -389 ppm. We were unable to isolate a clean complex from this mixture and future work in this area is needed.

Future work will be to conduct a systematic stoichiometric evaluation of the transmetalation activity of **II-DCyPE** with a variety of Sn- and B-based organometallics (Scheme 4.14). From this study, we expect to learn about electronic trends and kinetics observed in transmetalation of our Ni–F complex. Additionally, we will target the isolation of the product of transmetalation and characterize it by X-ray crystallography. A parallel investigation into the differences in these organometallic reagents in a decarbodifluorobenzylation reaction is being conducted catalytically by Alexander W. Bunnell and will be featured in this thesis.

4.6 Experimental Section

General information. All manipulations were performed inside an N_2-filled glovebox unless otherwise noted, and all glassware was oven-dried for a minimum of 24 h in an oven at 150 ºC before use. NMR spectra were obtained on a Varian VNMR 700 (699.76 MHz for 1 H; 175.95 MHz for ^{13}C), Varian VNMR 500 (500.09 MHz for ^{1}H; 470.56 MHz for ^{19}F; 125.75 MHz for ^{13}C), or Varian VNMR 400 (401 MHz for ^{1}H; 376 MHz for ^{19}F; 123 MHz for ^{13}C) spectrometer. ^{1}H and ^{13}C NMR chemical shifts are reported in parts per million (ppm) relative to TMS, with the residual solvent peak used as an internal reference. ^{19}F NMR chemical shifts are reported in ppm and are referenced to 4-fluorotoluene (–119.85 ppm) or trifluoromethoxybenzene (–58.00 ppm). ^{13}C NMR spectra are referenced to the residual $CHCl_3$ peak (77.16 ppm). Abbreviations used in the NMR data are as follows: s, singlet; d, doublet; t, triplet; q, quartet; m, multiplet; br, broad signal. Yields of reactions that generated fluorinated products were determined by ^{19}F NMR spectroscopic analysis.

Abbreviations: tetrahydrofuran (THF), dichloromethane (DCM), diethyl ether (Et_2O), difluoroacetyl fluoride (DFAF), difluoroacetic anhydride (DFAAn), trifluoroacetic anhydride (TFAAn), difluoroacetic acid (DFA), trifluoroacetic acid (TFA), room temperature (RT), 1,2-bis(dicyclohexylphosphino)ethane (DCyPE), 1,1′-bis(diisopropylphosphino)ferrocene (DiPrPF), 1,1′-bis(dicyclohexylphosphino)ferrocene (DCyPF), 1,1′-bis(diphenylphosphino)ferrocene (DPPF), 1,1′-bis(diisopropylphosphino)ferrocene (DiPrPF), 1,1′-Bis(di-*tert*-butylphosphino)ferrocene (DtBPF).

General procedure for the optimization of catalytic decarbonylative difluoromethylation. In a tall 10-mL vial equipped with a stirbar, $Ni(COD)_2$ (2.8 mg, 0.01 mmol, 0.01 equiv or 1.4 mg, 0.005 mmol, 0.05 equiv) and phosphine ligand were stirred in 0.2 mL THF. The yellow suspension was stirred until homogenous, then a select tributyl(aryl)stannane (0.05 mmol, 1.0 equiv) was added. To the resulting mixture was added a cold (–36 °C) solution of DFAF in anhydrous THF. The reaction mixture was then diluted with THF to a total volume of 0.4 mL. The vial was sealed

with a Teflon-lined screw cap with a septum, removed from the glovebox, and heated to a given temperature for 18-24 h. After the reaction time, the reaction mixture was allowed to cool to room temperature. To it was added 4-fluorotoluene (25 µL, 2.0 M in DCM, 1.0 equiv) as an internal standard, followed by dichloromethane (1.0 mL). An aliquot of the solution was transferred to an NMR tube and analyzed by ^{19}F NMR spectroscopy.

General procedure for catalytic decarbonylative difluoromethylation. In a tall 10-mL vial equipped with a stirbar, $Ni(COD)_2$ (1.4 mg, 0.005 mmol, 0.05 equiv) and tBuPPF (5.1 mg, 0.01 mmol, 0.01 equiv) were stirred in 0.2 mL THF. The yellow suspension was stirred until homogenous, then a select tributyl(aryl)stannane (0.05 mmol, 1.0 equiv) was added. To the resulting mixture was added a cold (–36 °C) solution of DFAF (0.05 mL, 0.15 mmol, 2.96 M) in anhydrous THF. The reaction mixture was then diluted with THF to a total volume of 0.4 mL. The vial was sealed with a Teflon-lined screw cap with a septum, removed from the glovebox, and heated to a given temperature for 18-24 h. After the reaction time, the reaction mixture was allowed to cool to room temperature. To it was added 4-fluorotoluene (25 µL, 2.0 M in DCM, 1.0 equiv) as an internal standard, followed by dichloromethane (1.0 mL). An aliquot of the solution was transferred to an NMR tube and analyzed by ^{19}F NMR spectroscopy.

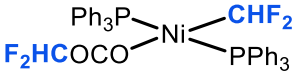

Synthesis of complex A. A 20 mL vial equipped with a stir bar was charged with $Ni(COD)_2$ (275 mg, 1.0 mmol, 1.0 equiv), triphenylphosphine (577 mg, 2.2 mmol, 2.2 equiv), and THF (8 mL). The mixture was stirred at room temperature for fifteen minutes. After this initial time, DFAAn (288 mg, 1.65 mmol, 1.65 equiv) was added the dark red suspension was stirred for 3 h at room temperature. After 3 h, the reaction mixture was concentrated to ca. 1 mL and the product was crashed out by the addition of Et_2O (3.0 mL). The slurry was filtered through a plug of celite (2cm x 2 cm x 2cm) set with Et_2O and the solid crude product was washed with Et_2O (12 mL). The crude orange solid was then eluted through the plug with THF (20 mL) and the filtrate was concentrated yielding crude complex A as

an orange solid (496 mg, 0.68 mmol, 68% yield). To the solid was added benzene (1.0 mL) and the reaction was concentrated (this process was repeated thrice) to remove ethereal solvents. **^{19}F NMR** (376 MHz, Methylene Chloride-d_2) δ –84.39 (bs, 2F), –125.51 (d, *J* = 55.1 Hz). **^{31}P NMR** (162 MHz, Methylene Chloride-d_2) δ 21.00 (bs, 2P). **^{1}H NMR** (400 MHz, Methylene Chloride-d_2) δ 7.94 – 7.06 (*multiple peaks*, 30H), 4.96 (t, *J* = 50.3 Hz, 1H), 4.09 (broad t, *J* = 52.0, 1H). **^{13}C NMR** (176 MHz, Methylene Chloride-d_2) δ 134.94, 130.86, 128.95, 107.56 (t, *J* = 249.1 Hz).

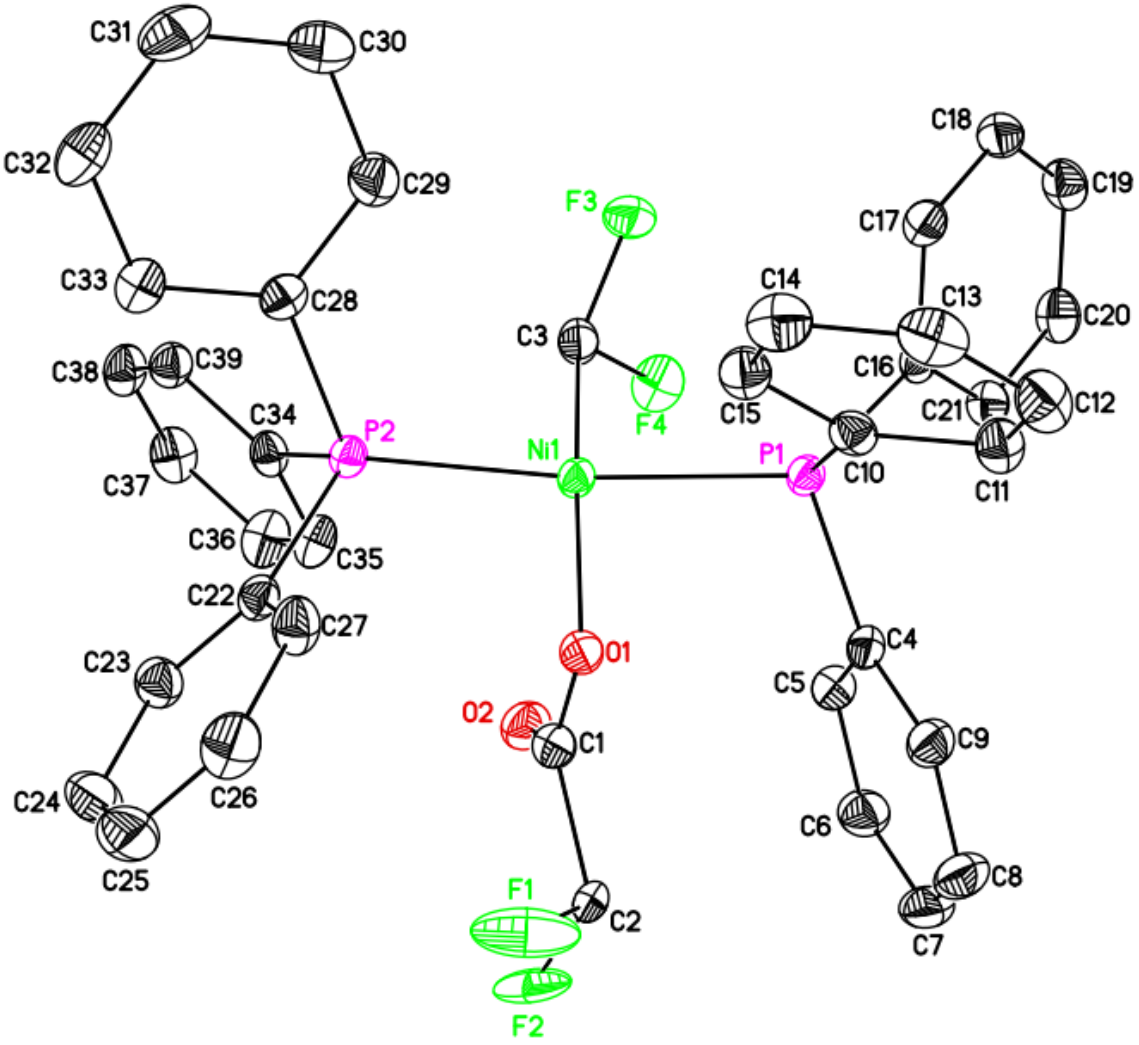

Structure determination of complex A. Orange blocks of **A** were grown from a tetrahydrofuran/diethyl ether solution of the compound at -36 deg. C. A crystal of dimensions

0.12 x 0.12 x 0.08 mm was mounted on a Rigaku AFC10K Saturn 944+ CCD-based X-ray diffractometer equipped with a low temperature device and Micromax-007HF Cu-target micro-focus rotating anode (l = 1.54187 A) operated at 1.2 kW power (40 kV, 30 mA). The X-ray intensities were measured at 85(1) K with the detector placed at a distance 42.00 mm from the crystal. A total of 2028 images were collected with an oscillation width of 1.0° in w. The exposure times were 1 sec. for the low angle images, 4 sec. for high angle. Rigaku d*trek images were exported to CrysAlisPro for processing and corrected for absorption. The integration of the data yielded a total of 24913 reflections to a maximum 2q value of 138.86° of which 6094 were independent and 5979 were greater than 2s(I). The final cell constants (Table 1) were based on the xyz centroids of 20087 reflections above 10s(I). Analysis of the data showed negligible decay during data collection. The structure was solved and refined with the Bruker SHELXTL (version 2018/3) software package, using the space group P1bar with Z = 2 for the formula $C_{39}H_{32}O_2F_4P_2Ni$. All non-hydrogen atoms were refined anisotropically with the hydrogen atoms placed in idealized positions. The difluoroacetato ligand is rotationally disordered in two orientations. Full matrix least-squares refinement based on F^2 converged at R1 = 0.03351 and wR2 = 0.0911 [based on I > 2sigma(I)], R1 = 0.0355 and wR2 = 0.0914 for all data. Additional details are presented in Table 1 and are given as Supporting Information in a CIF file. Acknowledgement is made for funding from NSF grant CHE-0840456 for X-ray instrumentation.
G.M. Sheldrick (2015) "Crystal structure refinement with SHELXL", Acta Cryst., C71, 3-8 (Open Access).
CrystalClear Expert 2.0 r16, Rigaku Americas and Rigaku Corporation (2014), Rigaku Americas, 9009, TX, USA 77381-5209, Rigaku Tokyo, 196-8666, Japan.
CrysAlisPro 1.171.40.53 (Rigaku Oxford Diffraction, 2019).

Empirical formula	$C_{39}H_{32}F_4NiO_2P_2$
Formula weight	729.29
Temperature	85(2) K
Wavelength	1.54184 Å
Crystal system	Triclinic

space group	P-1
Unit cell dimensions	a = 9.74268(18) Å α = 99.4697(16)° b = 9.92318(19) Å ß = 100.4776(16)° c = 18.2324(3) Å γ = 97.7906(16)°
Volume	1684.60(6) $Å^3$
Z	2
Calculated density	1.438 Mg/m^3
Absorption coefficient	2.214 mm^{-1}
F(000)	752
Crystal size	0.12 x 0.12 x 0.08 mm
Theta range for data collection	4.585 to 69.433°
Limiting indices	-11<=h<=11, -12<=k<=12, -20<=l<=21
Reflections collected / unique	24913 / 6094 [R(int) = 0. 0371]
Completeness to theta	67.684 97.8 %
Absorption correction	Semi-empirical from equivalents
Max. and min. transmission	1.00000 and 0.82690
Refinement method	Full-matrix least-squares on F^2
Data / restraints / parameters	6094 / 4 / 461
Goodness-of-fit on F^2	1.098
Final R indices [I>2σ(I)]	R1 = 0.0351, wR2 = 0.0911
R indices (all data)	R1 = 0.0355, wR2 = 0.0914
Largest diff. peak and hole	0.395 and -0.455 e.Å^-3

Table 4.6. Additional crystallography data and structure refinement for complex **A**.

	x	y	z	U(eq)
Ni(1)	4685(1)	6986(1)	7241(1)	16(1)
P(1)	4283(1)	8004(1)	6234(1)	15(1)
P(2)	4737(1)	6343(1)	8359(1)	15(1)

O(1)	6139(1)	8624(1)	7681(1)	19(1)
O(2)	7516(1)	7014(1)	7518(1)	26(1)
F(3)	2142(1)	5279(1)	6451(1)	29(1)
F(4)	4080(1)	4792(1)	6097(1)	29(1)
C(1)	7328(2)	8210(2)	7703(1)	23(1)
C(2)	8663(6)	9367(6)	7820(3)	23(1)
F(1)	8601(4)	10341(5)	8468(3)	54(1)
F(2)	9820(5)	8943(6)	8018(3)	34(2)
C(2A)	8574(6)	9308(6)	8146(5)	46(2)
F(1A)	8472(4)	10568(4)	8082(3)	56(1)
F(2A)	9777(7)	8922(9)	8107(5)	86(3)
C(3)	3558(2)	5267(2)	6734(1)	22(1)
C(4)	5998(2)	8603(2)	6030(1)	19(1)
C(5)	6801(2)	7577(2)	5847(1)	22(1)
C(6)	8167(2)	7936(2)	5741(1)	28(1)
C(7)	8751(2)	9316(2)	5816(1)	31(1)
C(8)	7967(2)	10340(2)	6005(1)	30(1)
C(9)	6598(2)	9994(2)	6117(1)	23(1)
C(10)	3456(2)	9501(2)	6497(1)	18(1)
C(11)	3276(2)	10479(2)	6030(1)	22(1)
C(12)	2571(2)	11566(2)	6231(1)	27(1)
C(13)	2011(2)	11669(2)	6878(1)	27(1)
C(14)	2160(2)	10688(2)	7335(1)	27(1)
C(15)	2887(2)	9614(2)	7146(1)	22(1)
C(16)	3149(2)	7174(2)	5312(1)	17(1)
C(17)	1686(2)	6981(2)	5254(1)	21(1)
C(18)	773(2)	6300(2)	4582(1)	23(1)
C(19)	1310(2)	5791(2)	3957(1)	25(1)
C(20)	2761(2)	5990(2)	4006(1)	25(1)
C(21)	3680(2)	6682(2)	4678(1)	21(1)
C(22)	5999(2)	7492(2)	9148(1)	18(1)
C(23)	7102(2)	7052(2)	9598(1)	24(1)
C(24)	8056(2)	7997(2)	10173(1)	31(1)
C(25)	7919(2)	9383(2)	10301(1)	34(1)
C(26)	6818(2)	9823(2)	9866(1)	31(1)
C(27)	5859(2)	8888(2)	9293(1)	24(1)
C(28)	3080(2)	6307(2)	8693(1)	19(1)
C(29)	1809(2)	6253(2)	8184(1)	27(1)
C(30)	541(2)	6159(2)	8436(1)	36(1)
C(31)	544(2)	6127(2)	9192(1)	36(1)
C(32)	1800(2)	6211(2)	9704(1)	29(1)
C(33)	3066(2)	6296(2)	9454(1)	23(1)
C(34)	5175(2)	4619(2)	8379(1)	18(1)
C(35)	6266(2)	4259(2)	8026(1)	24(1)

C(36)	6624(2)	2947(2)	8005(1)	29(1)
C(37)	5898(2)	1986(2)	8331(1)	27(1)
C(38)	4827(2)	2343(2)	8686(1)	25(1)
C(39)	4449(2)	3651(2)	8707(1)	21(1)

Table 4.7. Atomic coordinates (x 10^4) and equivalent isotropic displacement parameters ($Å^2$ x 10^3) for complex **A**. U(eq) is defined as one third of the trace of the orthogonalized Uij tensor.

Ni(1)-C(3)	1.8897(17)
Ni(1)-O(1)	1.9568(11)
Ni(1)-P(2)	2.2283(5)
Ni(1)-P(1)	2.2360(5)
P(1)-C(4)	1.8204(16)
P(1)-C(10)	1.8215(16)
P(1)-C(16)	1.8299(16)
P(2)-C(22)	1.8211(17)
P(2)-C(34)	1.8225(16)
P(2)-C(28)	1.8232(16)
O(1)-C(1)	1.277(2)
O(2)-C(1)	1.227(2)
F(3)-C(3)	1.3841(19)
F(4)-C(3)	1.390(2)
C(1)-C(2A)	1.519(6)
C(1)-C(2)	1.570(6)
C(2)-F(2)	1.269(7)
C(2)-F(1)	1.414(6)
C(2)-H(2)	1.0000
C(2A)-F(1A)	1.290(7)
C(2A)-F(2A)	1.291(8)
C(2A)-H(2A)	1.0000
C(3)-H(3)	1.0000
C(4)-C(9)	1.396(2)
C(4)-C(5)	1.400(2)
C(5)-C(6)	1.387(2)
C(5)-H(5)	0.9500
C(6)-C(7)	1.384(3)
C(6)-H(6)	0.9500
C(7)-C(8)	1.388(3)
C(7)-H(7)	0.9500
C(8)-C(9)	1.391(3)

C(8)-H(8)	0.9500
C(9)-H(9)	0.9500
C(10)-C(15)	1.390(2)
C(10)-C(11)	1.399(2)
C(11)-C(12)	1.389(2)
C(11)-H(11)	0.9500
C(12)-C(13)	1.382(3)
C(12)-H(12)	0.9500
C(13)-C(14)	1.386(3)
C(13)-H(13)	0.9500
C(14)-C(15)	1.389(2)
C(14)-H(14)	0.9500
C(15)-H(15)	0.9500
C(16)-C(21)	1.394(2)
C(16)-C(17)	1.394(2)
C(17)-C(18)	1.385(2)
C(17)-H(17)	0.9500
C(18)-C(19)	1.388(3)
C(18)-H(18)	0.9500
C(19)-C(20)	1.385(3)
C(19)-H(19)	0.9500
C(20)-C(21)	1.389(2)
C(20)-H(20)	0.9500
C(21)-H(21)	0.9500
C(22)-C(23)	1.394(2)
C(22)-C(27)	1.397(2)
C(23)-C(24)	1.389(3)
C(23)-H(23)	0.9500
C(24)-C(25)	1.386(3)
C(24)-H(24)	0.9500
C(25)-C(26)	1.378(3)
C(25)-H(25)	0.9500
C(26)-C(27)	1.384(3)
C(26)-H(26)	0.9500
C(27)-H(27)	0.9500
C(28)-C(33)	1.391(3)
C(28)-C(29)	1.394(2)
C(29)-C(30)	1.390(3)
C(29)-H(29)	0.9500
C(30)-C(31)	1.385(3)
C(30)-H(30)	0.9500
C(31)-C(32)	1.381(3)
C(31)-H(31)	0.9500
C(32)-C(33)	1.387(3)

C(32)-H(32)	0.9500
C(33)-H(33)	0.9500
C(34)-C(39)	1.393(2)
C(34)-C(35)	1.396(2)
C(35)-C(36)	1.389(2)
C(35)-H(35)	0.9500
C(36)-C(37)	1.386(3)
C(36)-H(36)	0.9500
C(37)-C(38)	1.380(3)
C(37)-H(37)	0.9500
C(38)-C(39)	1.393(2)
C(38)-H(38)	0.9500
C(39)-H(39)	0.9500

C(3)-Ni(1)-O(1)	169.00(6)
C(3)-Ni(1)-P(2)	90.61(5)
O(1)-Ni(1)-P(2)	92.78(4)
C(3)-Ni(1)-P(1)	94.48(5)
O(1)-Ni(1)-P(1)	84.82(3)
P(2)-Ni(1)-P(1)	165.207(19)
C(4)-P(1)-C(10)	108.78(7)
C(4)-P(1)-C(16)	105.41(7)
C(10)-P(1)-C(16)	101.74(7)
C(4)-P(1)-Ni(1)	107.23(5)
C(10)-P(1)-Ni(1)	108.05(6)
C(16)-P(1)-Ni(1)	124.85(5)
C(22)-P(2)-C(34)	105.31(7)
C(22)-P(2)-C(28)	102.43(7)
C(34)-P(2)-C(28)	104.72(7)
C(22)-P(2)-Ni(1)	114.20(5)
C(34)-P(2)-Ni(1)	114.02(5)
C(28)-P(2)-Ni(1)	114.90(6)
C(1)-O(1)-Ni(1)	106.10(10)
O(2)-C(1)-O(1)	126.74(15)
O(2)-C(1)-C(2A)	119.2(3)
O(1)-C(1)-C(2A)	112.9(3)
O(2)-C(1)-C(2)	115.8(3)
O(1)-C(1)-C(2)	116.3(3)
F(2)-C(2)-F(1)	103.3(4)
F(2)-C(2)-C(1)	113.0(5)
F(1)-C(2)-C(1)	105.4(4)
F(2)-C(2)-H(2)	111.6
F(1)-C(2)-H(2)	111.6
C(1)-C(2)-H(2)	111.6

F(1A)-C(2A)-F(2A)	117.2(7)
F(1A)-C(2A)-C(1)	115.7(5)
F(2A)-C(2A)-C(1)	112.4(6)
F(1A)-C(2A)-H(2A)	103.0
F(2A)-C(2A)-H(2A)	103.0
C(1)-C(2A)-H(2A)	103.0
F(3)-C(3)-F(4)	104.38(12)
F(3)-C(3)-Ni(1)	116.72(11)
F(4)-C(3)-Ni(1)	108.26(10)
F(3)-C(3)-H(3)	109.1
F(4)-C(3)-H(3)	109.1
Ni(1)-C(3)-H(3)	109.1
C(9)-C(4)-C(5)	119.16(15)
C(9)-C(4)-P(1)	124.53(13)
C(5)-C(4)-P(1)	116.00(12)
C(6)-C(5)-C(4)	120.42(16)
C(6)-C(5)-H(5)	119.8
C(4)-C(5)-H(5)	119.8
C(7)-C(6)-C(5)	120.25(17)
C(7)-C(6)-H(6)	119.9
C(5)-C(6)-H(6)	119.9
C(6)-C(7)-C(8)	119.65(16)
C(6)-C(7)-H(7)	120.2
C(8)-C(7)-H(7)	120.2
C(7)-C(8)-C(9)	120.69(17)
C(7)-C(8)-H(8)	119.7
C(9)-C(8)-H(8)	119.7
C(8)-C(9)-C(4)	119.81(16)
C(8)-C(9)-H(9)	120.1
C(4)-C(9)-H(9)	120.1
C(15)-C(10)-C(11)	119.10(15)
C(15)-C(10)-P(1)	118.96(12)
C(11)-C(10)-P(1)	121.73(13)
C(12)-C(11)-C(10)	119.92(17)
C(12)-C(11)-H(11)	120.0
C(10)-C(11)-H(11)	120.0
C(13)-C(12)-C(11)	120.49(17)
C(13)-C(12)-H(12)	119.8
C(11)-C(12)-H(12)	119.8
C(12)-C(13)-C(14)	119.93(16)
C(12)-C(13)-H(13)	120.0
C(14)-C(13)-H(13)	120.0
C(13)-C(14)-C(15)	119.90(17)
C(13)-C(14)-H(14)	120.0

C(15)-C(14)-H(14)	120.0
C(14)-C(15)-C(10)	120.62(16)
C(14)-C(15)-H(15)	119.7
C(10)-C(15)-H(15)	119.7
C(21)-C(16)-C(17)	118.87(15)
C(21)-C(16)-P(1)	123.09(12)
C(17)-C(16)-P(1)	117.99(12)
C(18)-C(17)-C(16)	120.70(16)
C(18)-C(17)-H(17)	119.6
C(16)-C(17)-H(17)	119.6
C(17)-C(18)-C(19)	120.12(16)
C(17)-C(18)-H(18)	119.9
C(19)-C(18)-H(18)	119.9
C(20)-C(19)-C(18)	119.56(16)
C(20)-C(19)-H(19)	120.2
C(18)-C(19)-H(19)	120.2
C(19)-C(20)-C(21)	120.50(16)
C(19)-C(20)-H(20)	119.8
C(21)-C(20)-H(20)	119.8
C(20)-C(21)-C(16)	120.23(15)
C(20)-C(21)-H(21)	119.9
C(16)-C(21)-H(21)	119.9
C(23)-C(22)-C(27)	118.97(15)
C(23)-C(22)-P(2)	123.33(13)
C(27)-C(22)-P(2)	117.69(13)
C(24)-C(23)-C(22)	120.19(16)
C(24)-C(23)-H(23)	119.9
C(22)-C(23)-H(23)	119.9
C(25)-C(24)-C(23)	120.16(18)
C(25)-C(24)-H(24)	119.9
C(23)-C(24)-H(24)	119.9
C(26)-C(25)-C(24)	120.01(17)
C(26)-C(25)-H(25)	120.0
C(24)-C(25)-H(25)	120.0
C(25)-C(26)-C(27)	120.28(17)
C(25)-C(26)-H(26)	119.9
C(27)-C(26)-H(26)	119.9
C(26)-C(27)-C(22)	120.38(17)
C(26)-C(27)-H(27)	119.8
C(22)-C(27)-H(27)	119.8
C(33)-C(28)-C(29)	119.30(15)
C(33)-C(28)-P(2)	120.36(13)
C(29)-C(28)-P(2)	120.32(13)
C(30)-C(29)-C(28)	120.03(18)

C(30)-C(29)-H(29)	120.0
C(28)-C(29)-H(29)	120.0
C(31)-C(30)-C(29)	119.88(18)
C(31)-C(30)-H(30)	120.1
C(29)-C(30)-H(30)	120.1
C(32)-C(31)-C(30)	120.53(17)
C(32)-C(31)-H(31)	119.7
C(30)-C(31)-H(31)	119.7
C(31)-C(32)-C(33)	119.67(18)
C(31)-C(32)-H(32)	120.2
C(33)-C(32)-H(32)	120.2
C(32)-C(33)-C(28)	120.56(17)
C(32)-C(33)-H(33)	119.7
C(28)-C(33)-H(33)	119.7
C(39)-C(34)-C(35)	119.40(15)
C(39)-C(34)-P(2)	123.09(13)
C(35)-C(34)-P(2)	117.48(12)
C(36)-C(35)-C(34)	120.15(16)
C(36)-C(35)-H(35)	119.9
C(34)-C(35)-H(35)	119.9
C(37)-C(36)-C(35)	120.30(17)
C(37)-C(36)-H(36)	119.8
C(35)-C(36)-H(36)	119.8
C(38)-C(37)-C(36)	119.68(16)
C(38)-C(37)-H(37)	120.2
C(36)-C(37)-H(37)	120.2
C(37)-C(38)-C(39)	120.63(16)
C(37)-C(38)-H(38)	119.7
C(39)-C(38)-H(38)	119.7
C(34)-C(39)-C(38)	119.82(16)
C(34)-C(39)-H(39)	120.1
C(38)-C(39)-H(39)	120.1

Table 4.8. Bond lengths [Å] and angles [°] for complex **A**.

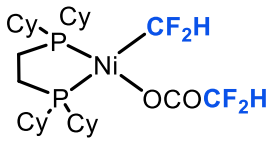

Synthesis of complex B. A 20 mL vial equipped with a stir bar was charged with complex **A** (365 mg, 0.5 mmol, 1.0 equiv), DCyPE (215 mg, 0.51 mmol, 1.02 equiv), and THF (6 mL). Immediately upon dissolving and stirring, the reaction mixture changed color from a red-orange mixture to a yellow-orange

mixture. The mixture was stirred at room temperature for fifteen minutes to form a yellow-orange solution. After fifteen minutes, the reaction mixture was concentrated to ca. 1 mL and filtered through celite (2.0 x 2.0 x 2.0 cm, set with THF) to remove Pd^0 impurities. The orange-yellow filtrate was concentrated to ca. 1 mL and bulk recrystallization at -36 °C was attempted by layering the THF-residue of the product with *i*Pr$_2$O and placing the vial in the freezer for 48 h. After 48 h, orange crystals had formed and were collected and subsequently washed and dried en vacuo. To the solid was added benzene (1.0 mL) and the reaction was concentrated (this process was repeated thrice) to remove ethereal solvents and yield pure complex **B** (254 mg, 0.405 mmol, 81% yield) as a light orange solid. **^{19}F NMR** (376 MHz, Methylene Chloride-d_2) δ -100.90 (dddd, J = 49.5, 35.9, 14.8, 7.8 Hz, 2F), -123.49 (d, J = 55.0 Hz, 2F). **^{31}P NMR** (162 MHz, Methylene Chloride-d_2) δ 74.75 (dtd, J = 17.8, 14.6, 3.1 Hz, 1P), 57.96 (tdd, J = 36.2, 19.7, 3.3 Hz, 1P). **^{1}H NMR** (400 MHz, Methylene Chloride-d_2) δ 7.62 (t, J = 55.5 Hz, 1H), 7.57 (tdd, J = 48.8, 13.0, 4.5 Hz, 1H), 4.48 (t, J = 9.5 Hz, 2H), 4.20 (dd, J = 11.8, 5.5 Hz, 2H), 3.99 (q, J = 11.0 Hz, 2H), 3.74 (*multiple peaks*, 20H), 3.53 – 3.10 (*multiple peaks*, 22H). **^{13}C NMR** (176 MHz, Chloroform-*d*) δ 167.20 (t, J = 24.8 Hz), 137.04 (tdd, J = 295.0, 107.7, 31.6 Hz), 111.73 – 107.27 (m), 36.33 (d, J = 24.5 Hz), 34.11 (d, J = 16.1 Hz), 31.40 (d, J = 2.5 Hz), 29.64 (dd, J = 17.1, 4.2 Hz), 29.16 (d, J = 1.9 Hz), 28.05 (d, J = 13.9 Hz), 27.75 (d, J = 12.3 Hz), 27.61, 22.86 (dd, J = 27.8, 19.0 Hz), 17.63 (dd, J = 23.1, 8.4 Hz).

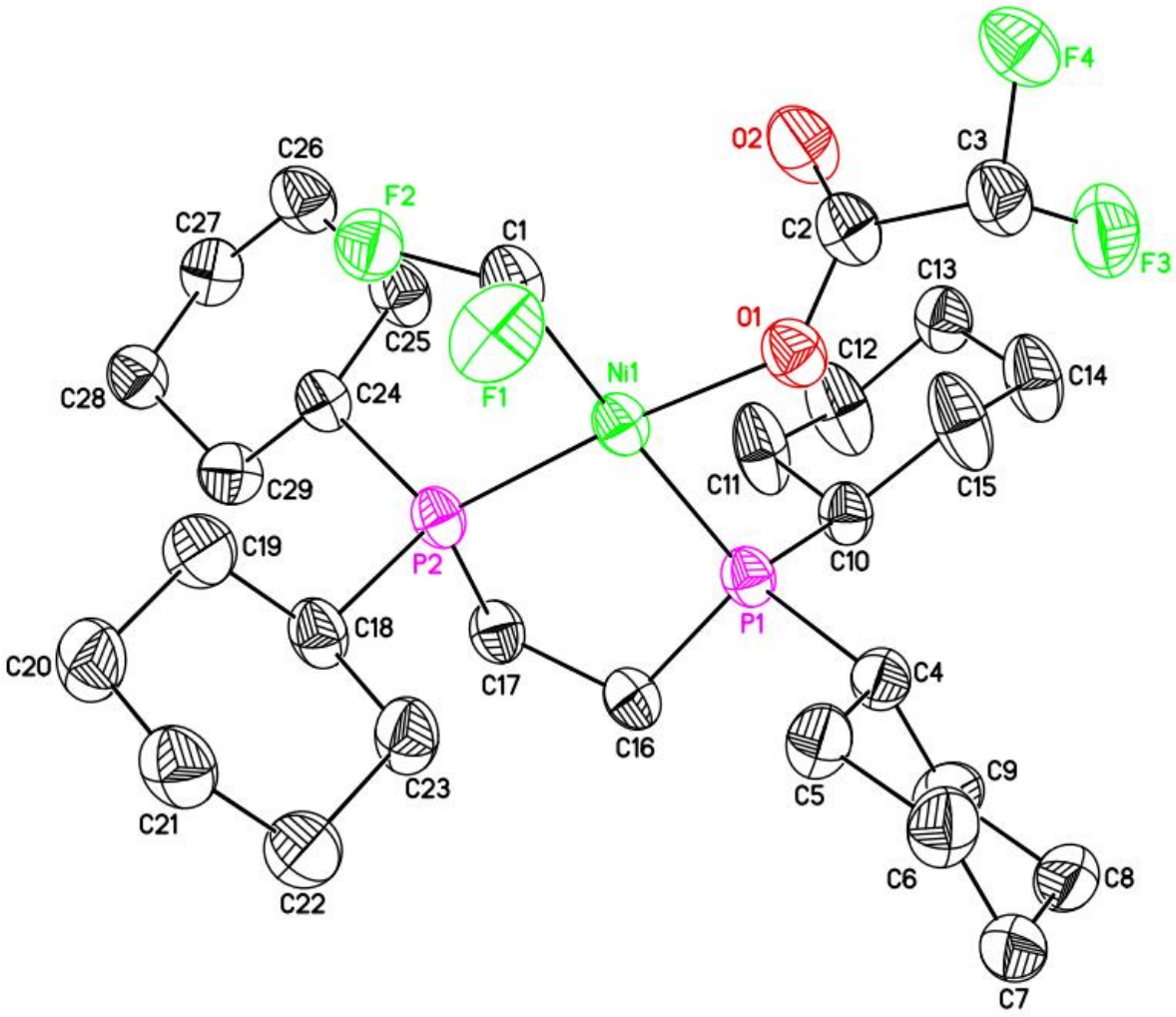

Structure Determination of complex B. Yellow prisms of **B** were grown from a pentanes/tetrahydrofuran/diethyl ether solution of the compound at -36 deg. C. A crystal of dimensions 0.24 x 0.23 x 0.14 mm was mounted on a Rigaku AFC10K Saturn 944+ CCD-based X-ray diffractometer equipped with a low temperature device and Micromax-007HF Cu-target micro-focus rotating anode (l = 1.54187 A) operated at 1.2 kW power (40 kV, 30 mA). The X-ray intensities were measured at 85(1) K with the detector placed at a distance 42.00 mm from the crystal. A total of 2028 images were collected with an oscillation width of 1.0° in w. The exposure times were 1 sec. for the low angle images, 3 sec. for high angle. Rigaku d*trek images were exported to CrysAlisPro for processing and corrected for absorption. The crystal was determined

to be a two-component, non-merohrdral twin. The refined twin fraction was 0.274(1). Reflections from both domains as well as overlaps were used as the basis of a HKLF5 format input file. The integration of the data yielded a total of 82885 reflections to a maximum 2q value of 139.48° of which 111086 were independent and 10388 were greater than 2s(I). The final cell constants (Table 1) were based on the xyz centroids of 22785 reflections above 10s(I). Analysis of the data showed negligible decay during data collection. The structure was solved and refined with the Bruker SHELXTL (version 2018/3) software package, using the space group P2(1)/n with Z = 4 for the formula C29H50O2F4P2Ni. All non-hydrogen atoms were refined anisotropically with the hydrogen atoms placed in idealized positions. Full matrix least-squares refinement based on F2 converged at R1 = 0.0647 and wR2 = 0.1912 [based on I > 2sigma(I)], R1 = 0.0666 and wR2 = 0.1926 for all data. Additional details are presented in Table 1 and are given as Supporting Information in a CIF file. Acknowledgement is made for funding from NSF grant CHE-0840456 for X-ray instrumentation.

G.M. Sheldrick (2015) "Crystal structure refinement with SHELXL", Acta Cryst., C71, 3-8 (Open Access).

CrystalClear Expert 2.0 r16, Rigaku Americas and Rigaku Corporation (2014), Rigaku Americas, 9009, TX, USA 77381-5209, Rigaku Tokyo, 196-8666, Japan.

CrysAlisPro 1.171.40.53 (Rigaku Oxford Diffraction, 2019).

Empirical formula	$C_{29}H_{50}F_4NiO_2P_2$
Formula weight	627.34
Temperature	85(2) K
Wavelength	1.54184 Å
Crystal system	Monoclinic
space group	P2(1)/n

Unit cell dimensions	a = 11.2538(3) Å α = 90° b = 17.0547(3) Å ß = 103.807(2)° c = 16.3136(4) Å γ = 90°
Volume	3040.61(12) $Å^3$
Z	4
Calculated density	1.370Mg/m^3
Absorption coefficient	2.336 mm^{-1}
F(000)	1336
Crystal size	0.240 x 0.230 x 0.140 mm
Theta range for data collection	3.808 to 69.739°
Limiting indices	-13<=h<=13, -20<=k<=20, -19<=l<=19
Reflections collected / unique	82885 / 11086 [R(int) = 0.0859]
Completeness to theta	99.9 %
Absorption correction	Semi-empirical from equivalents
Max. and min. transmission	1.00000 and 0. 61666
Refinement method	Full-matrix least-squares on F^2
Data / restraints / parameters	11086 / 0 / 345
Goodness-of-fit on F^2	1.131
Final R indices [I>2σ(I)]	R1 = 0.0647, wR2 = 0.1912
R indices (all data)	R1 = 0.0666, wR2 = 0.1926
Largest diff. peak and hole	0 0.795 and -0.478 e.$Å^{-3}$

Table 4.9. Additional crystallography data and structure refinement for complex **B**.

	x	y	z	U(eq)
Ni(1)	5174(1)	3157(1)	4154(1)	31(1)
P(1)	3448(1)	2602(1)	4322(1)	31(1)
P(2)	4963(1)	2524(1)	2992(1)	30(1)
O(1)	5231(2)	3787(1)	5132(2)	38(1)
O(2)	6824(3)	3188(2)	6004(2)	52(1)

F(1)	6299(2)	4466(1)	3726(2)	57(1)
F(2)	7366(2)	3450(1)	3530(1)	43(1)
F(3)	5213(3)	3865(2)	7021(2)	64(1)
F(4)	6887(2)	4477(1)	7024(1)	48(1)
C(1)	6624(4)	3724(2)	4041(2)	38(1)
C(2)	6016(4)	3681(2)	5829(2)	40(1)
C(3)	5814(4)	4254(2)	6507(2)	43(1)
C(4)	2315(3)	3317(2)	4524(2)	35(1)
C(5)	2204(4)	4021(2)	3928(2)	42(1)
C(6)	1340(4)	4638(2)	4139(3)	47(1)
C(7)	82(4)	4289(3)	4117(2)	46(1)
C(8)	188(4)	3590(3)	4704(3)	48(1)
C(9)	1049(4)	2965(3)	4503(3)	46(1)
C(10)	3528(3)	1864(2)	5166(2)	35(1)
C(11)	4306(6)	1173(2)	5071(3)	60(1)
C(12)	4318(6)	560(3)	5765(3)	66(2)
C(13)	4782(4)	910(2)	6634(2)	44(1)
C(14)	4004(5)	1601(3)	6739(3)	57(1)
C(15)	3964(6)	2210(2)	6045(3)	61(1)
C(16)	2731(3)	2079(2)	3343(2)	37(1)
C(17)	3724(3)	1797(2)	2912(2)	36(1)
C(18)	4477(4)	3086(2)	1991(2)	38(1)
C(19)	5522(4)	3483(2)	1720(3)	46(1)
C(20)	5059(4)	3934(3)	890(3)	51(1)
C(21)	4084(4)	4536(2)	969(3)	47(1)
C(22)	3028(4)	4128(3)	1225(3)	48(1)
C(23)	3481(4)	3676(2)	2057(2)	44(1)
C(24)	6286(3)	1941(2)	2863(2)	32(1)
C(25)	6956(4)	1535(2)	3686(2)	44(1)
C(26)	8110(4)	1128(2)	3559(3)	48(1)
C(27)	7830(4)	556(2)	2824(3)	43(1)
C(28)	7137(4)	957(2)	2015(2)	40(1)
C(29)	5972(3)	1351(2)	2134(2)	40(1)

Table 4.10. Atomic coordinates (x 10^4) and equivalent isotropic displacement parameters ($Å^2$ x 10^3) for complex **B**. U(eq) is defined as one third of the trace of the orthogonalized Uij tensor.

Ni(1)-O(1)	1.911(2)
Ni(1)-C(1)	1.945(4)
Ni(1)-P(2)	2.1456(10)
Ni(1)-P(1)	2.2349(11)

P(1)-C(16)	1.839(4)
P(1)-C(4)	1.849(4)
P(1)-C(10)	1.852(3)
P(2)-C(24)	1.843(4)
P(2)-C(17)	1.847(4)
P(2)-C(18)	1.860(4)
O(1)-C(2)	1.276(5)
O(2)-C(2)	1.221(5)
F(1)-C(1)	1.381(4)
F(2)-C(1)	1.395(4)
F(3)-C(3)	1.368(5)
F(4)-C(3)	1.352(5)
C(1)-H(1)	1.0000
C(2)-C(3)	1.533(5)
C(3)-H(3)	1.0000
C(4)-C(5)	1.531(5)
C(4)-C(9)	1.539(5)
C(4)-H(4)	1.0000
C(5)-C(6)	1.527(5)
C(5)-H(5A)	0.9900
C(5)-H(5B)	0.9900
C(6)-C(7)	1.528(6)
C(6)-H(6A)	0.9900
C(6)-H(6B)	0.9900
C(7)-C(8)	1.516(6)
C(7)-H(7A)	0.9900
C(7)-H(7B)	0.9900
C(8)-C(9)	1.527(6)
C(8)-H(8A)	0.9900
C(8)-H(8B)	0.9900
C(9)-H(9A)	0.9900
C(9)-H(9B)	0.9900
C(10)-C(11)	1.498(5)
C(10)-C(15)	1.519(5)
C(10)-H(10)	1.0000
C(11)-C(12)	1.539(6)
C(11)-H(11A)	0.9900
C(11)-H(11B)	0.9900
C(12)-C(13)	1.512(6)
C(12)-H(12A)	0.9900
C(12)-H(12B)	0.9900
C(13)-C(14)	1.501(6)
C(13)-H(13A)	0.9900
C(13)-H(13B)	0.9900

C(14)-C(15)	1.529(5)
C(14)-H(14A)	0.9900
C(14)-H(14B)	0.9900
C(15)-H(15A)	0.9900
C(15)-H(15B)	0.9900
C(16)-C(17)	1.534(5)
C(16)-H(16A)	0.9900
C(16)-H(16B)	0.9900
C(17)-H(17A)	0.9900
C(17)-H(17B)	0.9900
C(18)-C(19)	1.512(6)
C(18)-C(23)	1.529(5)
C(18)-H(18)	1.0000
C(19)-C(20)	1.535(5)
C(19)-H(19A)	0.9900
C(19)-H(19B)	0.9900
C(20)-C(21)	1.530(6)
C(20)-H(20A)	0.9900
C(20)-H(20B)	0.9900
C(21)-C(22)	1.518(6)
C(21)-H(21A)	0.9900
C(21)-H(21B)	0.9900
C(22)-C(23)	1.538(5)
C(22)-H(22A)	0.9900
C(22)-H(22B)	0.9900
C(23)-H(23A)	0.9900
C(23)-H(23B)	0.9900
C(24)-C(29)	1.533(5)
C(24)-C(25)	1.538(5)
C(24)-H(24)	1.0000
C(25)-C(26)	1.530(6)
C(25)-H(25A)	0.9900
C(25)-H(25B)	0.9900
C(26)-C(27)	1.519(6)
C(26)-H(26A)	0.9900
C(26)-H(26B)	0.9900
C(27)-C(28)	1.525(5)
C(27)-H(27A)	0.9900
C(27)-H(27B)	0.9900
C(28)-C(29)	1.526(5)
C(28)-H(28A)	0.9900
C(28)-H(28B)	0.9900
C(29)-H(29A)	0.9900
C(29)-H(29B)	0.9900

O(1)-Ni(1)-C(1)	86.46(13)
O(1)-Ni(1)-P(2)	174.27(8)
C(1)-Ni(1)-P(2)	94.84(11)
O(1)-Ni(1)-P(1)	89.58(8)
C(1)-Ni(1)-P(1)	175.02(11)
P(2)-Ni(1)-P(1)	88.81(4)
C(16)-P(1)-C(4)	107.22(17)
C(16)-P(1)-C(10)	104.41(16)
C(4)-P(1)-C(10)	103.26(16)
C(16)-P(1)-Ni(1)	108.22(12)
C(4)-P(1)-Ni(1)	113.51(12)
C(10)-P(1)-Ni(1)	119.31(13)
C(24)-P(2)-C(17)	104.25(16)
C(24)-P(2)-C(18)	104.72(16)
C(17)-P(2)-C(18)	103.05(17)
C(24)-P(2)-Ni(1)	116.75(11)
C(17)-P(2)-Ni(1)	108.84(12)
C(18)-P(2)-Ni(1)	117.63(12)
C(2)-O(1)-Ni(1)	122.8(2)
F(1)-C(1)-F(2)	103.2(3)
F(1)-C(1)-Ni(1)	109.7(3)
F(2)-C(1)-Ni(1)	121.7(2)
F(1)-C(1)-H(1)	107.1
F(2)-C(1)-H(1)	107.1
Ni(1)-C(1)-H(1)	107.1
O(2)-C(2)-O(1)	128.7(3)
O(2)-C(2)-C(3)	120.0(3)
O(1)-C(2)-C(3)	111.2(3)
F(4)-C(3)-F(3)	104.7(3)
F(4)-C(3)-C(2)	111.4(3)
F(3)-C(3)-C(2)	108.3(3)
F(4)-C(3)-H(3)	110.8
F(3)-C(3)-H(3)	110.8
C(2)-C(3)-H(3)	110.8
C(5)-C(4)-C(9)	110.9(3)
C(5)-C(4)-P(1)	111.1(2)
C(9)-C(4)-P(1)	114.4(3)
C(5)-C(4)-H(4)	106.7
C(9)-C(4)-H(4)	106.7
P(1)-C(4)-H(4)	106.7
C(6)-C(5)-C(4)	110.9(3)
C(6)-C(5)-H(5A)	109.5
C(4)-C(5)-H(5A)	109.5

C(6)-C(5)-H(5B)	109.5
C(4)-C(5)-H(5B)	109.5
H(5A)-C(5)-H(5B)	108.0
C(5)-C(6)-C(7)	111.2(3)
C(5)-C(6)-H(6A)	109.4
C(7)-C(6)-H(6A)	109.4
C(5)-C(6)-H(6B)	109.4
C(7)-C(6)-H(6B)	109.4
H(6A)-C(6)-H(6B)	108.0
C(8)-C(7)-C(6)	111.0(3)
C(8)-C(7)-H(7A)	109.4
C(6)-C(7)-H(7A)	109.4
C(8)-C(7)-H(7B)	109.4
C(6)-C(7)-H(7B)	109.4
H(7A)-C(7)-H(7B)	108.0
C(7)-C(8)-C(9)	111.8(3)
C(7)-C(8)-H(8A)	109.3
C(9)-C(8)-H(8A)	109.3
C(7)-C(8)-H(8B)	109.3
C(9)-C(8)-H(8B)	109.3
H(8A)-C(8)-H(8B)	107.9
C(8)-C(9)-C(4)	110.8(3)
C(8)-C(9)-H(9A)	109.5
C(4)-C(9)-H(9A)	109.5
C(8)-C(9)-H(9B)	109.5
C(4)-C(9)-H(9B)	109.5
H(9A)-C(9)-H(9B)	108.1
C(11)-C(10)-C(15)	109.8(3)
C(11)-C(10)-P(1)	112.6(3)
C(15)-C(10)-P(1)	112.6(3)
C(11)-C(10)-H(10)	107.2
C(15)-C(10)-H(10)	107.2
P(1)-C(10)-H(10)	107.2
C(10)-C(11)-C(12)	111.1(4)
C(10)-C(11)-H(11A)	109.4
C(12)-C(11)-H(11A)	109.4
C(10)-C(11)-H(11B)	109.4
C(12)-C(11)-H(11B)	109.4
H(11A)-C(11)-H(11B)	108.0
C(13)-C(12)-C(11)	111.3(4)
C(13)-C(12)-H(12A)	109.4
C(11)-C(12)-H(12A)	109.4
C(13)-C(12)-H(12B)	109.4
C(11)-C(12)-H(12B)	109.4

H(12A)-C(12)-H(12B)	108.0
C(14)-C(13)-C(12)	109.6(4)
C(14)-C(13)-H(13A)	109.7
C(12)-C(13)-H(13A)	109.7
C(14)-C(13)-H(13B)	109.7
C(12)-C(13)-H(13B)	109.7
H(13A)-C(13)-H(13B)	108.2
C(13)-C(14)-C(15)	111.3(4)
C(13)-C(14)-H(14A)	109.4
C(15)-C(14)-H(14A)	109.4
C(13)-C(14)-H(14B)	109.4
C(15)-C(14)-H(14B)	109.4
H(14A)-C(14)-H(14B)	108.0
C(10)-C(15)-C(14)	112.4(4)
C(10)-C(15)-H(15A)	109.1
C(14)-C(15)-H(15A)	109.1
C(10)-C(15)-H(15B)	109.1
C(14)-C(15)-H(15B)	109.1
H(15A)-C(15)-H(15B)	107.9
C(17)-C(16)-P(1)	109.5(2)
C(17)-C(16)-H(16A)	109.8
P(1)-C(16)-H(16A)	109.8
C(17)-C(16)-H(16B)	109.8
P(1)-C(16)-H(16B)	109.8
H(16A)-C(16)-H(16B)	108.2
C(16)-C(17)-P(2)	112.1(2)
C(16)-C(17)-H(17A)	109.2
P(2)-C(17)-H(17A)	109.2
C(16)-C(17)-H(17B)	109.2
P(2)-C(17)-H(17B)	109.2
H(17A)-C(17)-H(17B)	107.9
C(19)-C(18)-C(23)	111.1(3)
C(19)-C(18)-P(2)	113.7(3)
C(23)-C(18)-P(2)	110.1(2)
C(19)-C(18)-H(18)	107.2
C(23)-C(18)-H(18)	107.2
P(2)-C(18)-H(18)	107.2
C(18)-C(19)-C(20)	111.0(3)
C(18)-C(19)-H(19A)	109.4
C(20)-C(19)-H(19A)	109.4
C(18)-C(19)-H(19B)	109.4
C(20)-C(19)-H(19B)	109.4
H(19A)-C(19)-H(19B)	108.0
C(21)-C(20)-C(19)	111.2(3)

C(21)-C(20)-H(20A)	109.4
C(19)-C(20)-H(20A)	109.4
C(21)-C(20)-H(20B)	109.4
C(19)-C(20)-H(20B)	109.4
H(20A)-C(20)-H(20B)	108.0
C(22)-C(21)-C(20)	109.9(3)
C(22)-C(21)-H(21A)	109.7
C(20)-C(21)-H(21A)	109.7
C(22)-C(21)-H(21B)	109.7
C(20)-C(21)-H(21B)	109.7
H(21A)-C(21)-H(21B)	108.2
C(21)-C(22)-C(23)	110.9(3)
C(21)-C(22)-H(22A)	109.5
C(23)-C(22)-H(22A)	109.5
C(21)-C(22)-H(22B)	109.5
C(23)-C(22)-H(22B)	109.5
H(22A)-C(22)-H(22B)	108.0
C(18)-C(23)-C(22)	111.2(3)
C(18)-C(23)-H(23A)	109.4
C(22)-C(23)-H(23A)	109.4
C(18)-C(23)-H(23B)	109.4
C(22)-C(23)-H(23B)	109.4
H(23A)-C(23)-H(23B)	108.0
C(29)-C(24)-C(25)	110.8(3)
C(29)-C(24)-P(2)	113.6(2)
C(25)-C(24)-P(2)	112.6(2)
C(29)-C(24)-H(24)	106.4
C(25)-C(24)-H(24)	106.4
P(2)-C(24)-H(24)	106.4
C(26)-C(25)-C(24)	110.0(3)
C(26)-C(25)-H(25A)	109.7
C(24)-C(25)-H(25A)	109.7
C(26)-C(25)-H(25B)	109.7
C(24)-C(25)-H(25B)	109.7
H(25A)-C(25)-H(25B)	108.2
C(27)-C(26)-C(25)	112.1(3)
C(27)-C(26)-H(26A)	109.2
C(25)-C(26)-H(26A)	109.2
C(27)-C(26)-H(26B)	109.2
C(25)-C(26)-H(26B)	109.2
H(26A)-C(26)-H(26B)	107.9
C(26)-C(27)-C(28)	111.3(3)
C(26)-C(27)-H(27A)	109.4
C(28)-C(27)-H(27A)	109.4

C(26)-C(27)-H(27B)	109.4
C(28)-C(27)-H(27B)	109.4
H(27A)-C(27)-H(27B)	108.0
C(27)-C(28)-C(29)	111.4(3)
C(27)-C(28)-H(28A)	109.4
C(29)-C(28)-H(28A)	109.4
C(27)-C(28)-H(28B)	109.4
C(29)-C(28)-H(28B)	109.4
H(28A)-C(28)-H(28B)	108.0
C(28)-C(29)-C(24)	110.0(3)
C(28)-C(29)-H(29A)	109.7
C(24)-C(29)-H(29A)	109.7
C(28)-C(29)-H(29B)	109.7
C(24)-C(29)-H(29B)	109.7
H(29A)-C(29)-H(29B)	108.2

Table 4.11. Bond lengths [Å] and angles [°] for complex **B.**

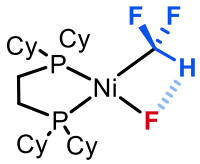

Synthesis of complex II-DCyPE. A 20 mL vial equipped with a stir bar was charged with complex **B** (86 mg, 0.137 mmol, 1.0 equiv) and THF (6 mL). To this solution was added TMAF (mg, 0.24 mmol, 1.5 equiv) and the suspension was stirred at room temperature for 24 h. After 1 h, the reaction mixture was filtered through a plug of celite (2cm x 2cm x 2cm) set with THF. The filtrate was concentrated to ca. 1 mL and layered with a Et_2O:pentanes (1:1) and placed in the freezer at -36 °C for 24 h. After 24 h, a tan solid had precipitated. The solid was filtered over celite set with pentanes and eluted through with THF. The THF-solution was concentrated to yield a tan solid. The complex was only characterized by ^{19}F NMR and X-ray crystallography. **^{19}F NMR** (470 MHz, THF-d_8) δ -97.32 (dddd, J = 65.0, 40.2, 23.7, 14.0 Hz), -317.91 (ddt, J = 93.4, 48.1, 23.4 Hz). **^{31}P NMR** (202 MHz, Methylene Chloride-d_2) δ 74.24 (ddt, J = 95.1 Hz, 19.0 Hz, 13.1 Hz, 1P), 57.98 (m, 1P).

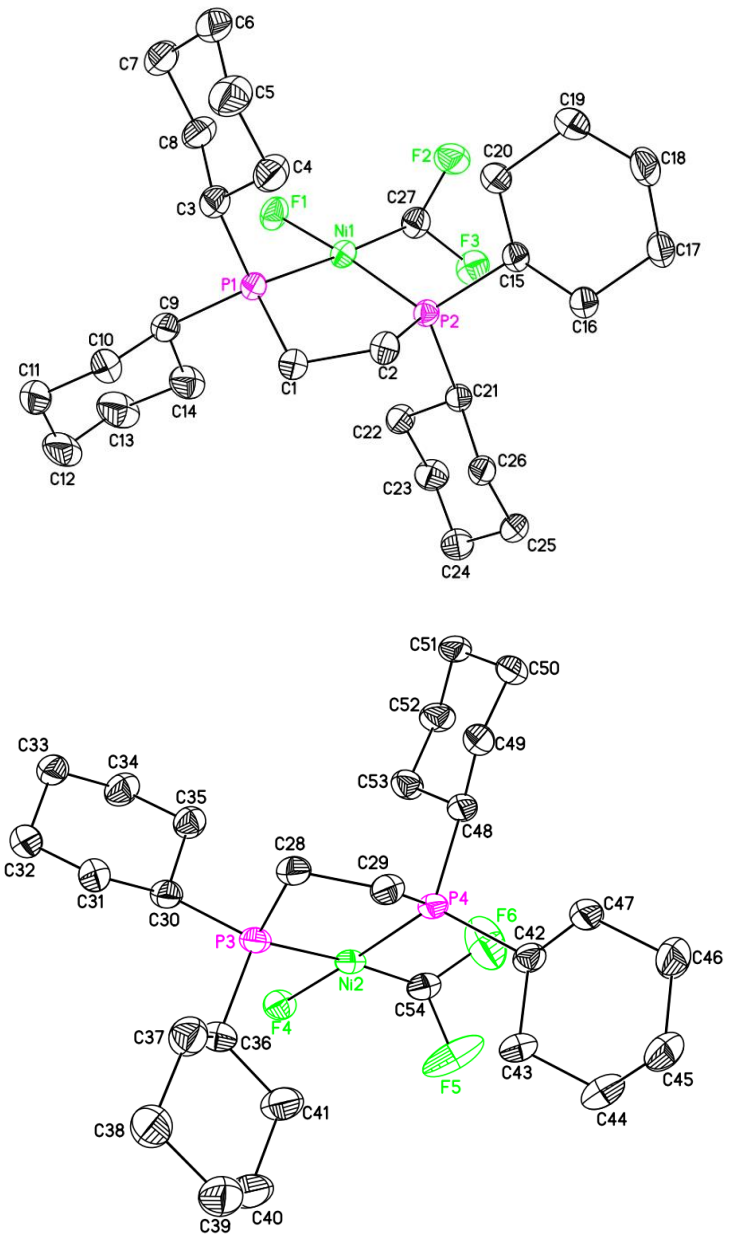

Structure determination of complex II-DCyPE. Yellow plates of **II-DCyPE** were grown from a tetrahydrofuran/diethyl ether/pentanes solution of the compound at 22 deg. C. A crystal of dimensions 0.15 x 0.11 x 0.07 mm was mounted on a Rigaku AFC10K Saturn 944+ CCD-based X-ray diffractometer equipped with a low temperature device and Micromax-007HF Cu-target micro-focus rotating anode (l = 1.54187 A) operated at 1.2 kW power (40 kV, 30 mA). The X-ray intensities were measured at 85(1) K with the detector placed at a distance 42.00 mm from the

crystal. A total of 2028 images were collected with an oscillation width of 1.0° in w. The exposure times were 1 sec. for the low angle images, 4 sec. for high angle. Rigaku d*trek images were exported to CrysAlisPro for processing and corrected for absorption. The integration of the data yielded a total of 42583 reflections to a maximum 2q value of 138.93° of which 10066 were independent and 10013 were greater than 2s(I). The final cell constants (Table 1) were based on the xyz centroids of 33554 reflections above 10s(I). Analysis of the data showed negligible decay during data collection. The structure was solved and refined with the Bruker SHELXTL (version 2018/3) software package, using the space group P2(1) with Z = 4 for the formula $C_{27}H_{49}F_3P_2Ni$. All non-hydrogen atoms were refined anisotropically with the hydrogen atoms placed in idealized positions. One cyclohexyl ligand is disordered in wo orientations. Full matrix least-squares refinement based on F^2 converged at R1 = 0.0337 and wR2 = 0.0878 [based on I > 2sigma(I)], R1 = 0.0338 and wR2 = 0.0880 for all data. Additional details are presented in Table 1 and are given as Supporting Information in a CIF file. Acknowledgement is made for funding from NSF grant CHE-0840456 for X-ray instrumentation.

G.M. Sheldrick (2015) "Crystal structure refinement with SHELXL", Acta Cryst., C71, 3-8 (Open Access).

CrystalClear Expert 2.0 r16, Rigaku Americas and Rigaku Corporation (2014), Rigaku Americas, 9009, TX, USA 77381-5209, Rigaku Tokyo, 196-8666, Japan.

CrysAlisPro 1.171.38.41 (Rigaku Oxford Diffraction, 2015).

Empirical formula	$C_{27}H_{49}F_3NiP_2$
Formula weight	551.31
Temperature	85(2) K
Wavelength	1.54184 Å
Crystal system	Monoclinic
space group	P2(1)

Unit cell dimensions	a = 11.2538(3) Å α = 90° b = 21.2227(2) Å ß = 103.807(2)° c = 11.7770(2) Å γ = 90°
Volume	2780.06(8) $Å^3$
Z	4
Calculated density	1.317 Mg/m^3
Absorption coefficient	2.370 mm^{-1}
F(000)	1184
Crystal size	0.150 x 0.110 x 0.070 mm
Theta range for data collection	3.928 to 69.465°
Limiting indices	-14<=h<=14, -25<=k<=25, -14<=l<=14
Reflections collected / unique	42583 / 10066 [R(int) = 0.0467]
Completeness to theta	99.9 %
Absorption correction	Semi-empirical from equivalents
Max. and min. transmission	1.00000 and 0.80847
Refinement method	Full-matrix least-squares on F^2
Data / restraints / parameters	10066 / 13 / 642
Goodness-of-fit on F^2	1.056
Final R indices [I>2σ(I)]	R1 = 0.0337, wR2 = 0.0878
R indices (all data)	R1 = 0.0338, wR2 = 0.0880
Largest diff. peak and hole	0.432 and -0.333 $e.Å^{-3}$

Table 4.12. Crystal data and structure refinement for complex **II-DCyPE**.

	x	y	z	U(eq)
Ni(1)	2478(1)	4149(1)	3703(1)	23(1)
Ni(2)	1544(1)	6677(1)	7299(1)	25(1)
P(1)	2899(1)	3311(1)	4862(1)	23(1)

P(2)	2487(1)	3561(1)	2249(1)	21(1)
P(3)	543(1)	5812(1)	7455(1)	26(1)
P(4)	3134(1)	6127(1)	7660(1)	24(1)
F(1)	2321(2)	4652(1)	4943(2)	34(1)
F(2)	3276(2)	5137(1)	2596(2)	42(1)
F(3)	1476(2)	4870(1)	1541(2)	38(1)
F(4)	120(2)	7140(1)	7017(2)	33(1)
F(5)	2261(4)	7524(1)	5887(3)	78(1)
F(6)	3531(3)	7547(1)	7641(3)	70(1)
C(1)	2678(3)	2606(2)	3917(3)	27(1)
C(2)	3017(3)	2762(2)	2780(3)	27(1)
C(3)	4449(3)	3294(2)	5862(3)	29(1)
C(4)	5395(3)	3113(2)	5254(3)	37(1)
C(5)	6640(4)	3097(2)	6165(4)	47(1)
C(6)	6966(3)	3729(2)	6775(3)	43(1)
C(7)	6026(3)	3926(2)	7366(3)	40(1)
C(8)	4765(3)	3931(2)	6480(3)	35(1)
C(9)	1983(3)	3182(2)	5880(3)	34(1)
C(10)	2159(4)	2529(2)	6468(4)	45(1)
C(11)	1387(5)	2453(2)	7313(4)	57(1)
C(12)	85(5)	2571(2)	6687(4)	54(1)
C(13)	-87(5)	3221(2)	6123(5)	55(1)
C(14)	654(3)	3300(2)	5251(4)	39(1)
C(15)	3456(3)	3822(2)	1358(3)	25(1)
C(16)	3434(3)	3405(2)	287(3)	28(1)
C(17)	4211(3)	3692(2)	-421(3)	34(1)
C(18)	5496(3)	3803(2)	353(3)	41(1)
C(19)	5527(4)	4202(2)	1440(4)	44(1)
C(20)	4756(3)	3911(2)	2154(3)	33(1)
C(21)	963(3)	3479(2)	1199(3)	24(1)
C(22)	-9(3)	3635(2)	1807(3)	30(1)
C(23)	-1247(3)	3665(2)	886(3)	37(1)
C(24)	-1544(3)	3049(2)	195(3)	37(1)
C(25)	-565(3)	2874(2)	-369(3)	33(1)
C(26)	669(3)	2840(2)	567(3)	27(1)
C(27)	2210(3)	4893(2)	2724(3)	32(1)
C(28)	1633(3)	5175(2)	8030(3)	30(1)
C(29)	2722(3)	5282(2)	7574(3)	28(1)
C(30)	-433(3)	5865(2)	8434(3)	30(1)
C(31)	-1104(3)	5255(2)	8556(3)	35(1)
C(32)	-1911(3)	5368(2)	9346(3)	38(1)
C(33)	-1204(3)	5606(2)	10566(3)	34(1)
C(34)	-533(4)	6209(2)	10470(3)	39(1)
C(35)	273(3)	6115(2)	9658(3)	33(1)

C(36)	-465(3)	5565(2)	5998(3)	32(1)
C(37)	-611(4)	4858(2)	5773(3)	40(1)
C(38)	-1514(4)	4714(2)	4570(4)	46(1)
C(39)	-1133(4)	5027(2)	3578(4)	46(1)
C(40)	-1008(5)	5739(2)	3774(4)	51(1)
C(41)	-105(4)	5884(2)	4995(4)	44(1)
C(42)	4085(3)	6198(2)	6665(3)	29(1)
C(43)	3355(3)	6158(2)	5354(3)	32(1)
C(44)	4174(4)	6248(2)	4556(3)	41(1)
C(45)	5195(4)	5771(2)	4830(3)	44(1)
C(46)	5919(4)	5799(3)	6134(4)	50(1)
C(47)	5103(3)	5717(2)	6930(3)	41(1)
C(48)	4186(3)	6258(2)	9176(3)	33(1)
C(49)	4862(5)	5734(3)	9839(5)	31(1)
C(50)	5792(5)	5955(3)	10986(5)	33(1)
C(51)	5197(5)	6314(3)	11789(5)	34(1)
C(52)	4472(7)	6860(3)	11127(6)	36(1)
C(53)	3565(5)	6650(4)	9961(5)	33(1)
C(48A)	4186(3)	6258(2)	9176(3)	33(1)
C(49A)	5072(11)	6711(6)	9373(9)	43(3)
C(50A)	5891(10)	6715(6)	10653(9)	44(3)
C(51A)	5169(14)	6769(7)	11536(11)	44(3)
C(52A)	4261(16)	6264(8)	11371(10)	68(5)
C(53A)	3410(11)	6254(9)	10081(9)	47(4)
C(54)	2324(3)	7443(2)	7056(3)	32(1)

Table 4.13. Atomic coordinates (x 10^4) and equivalent isotropic displacement parameters ($Å^2$ x 10^3) for **II-DCyPE**. U(eq) is defined as one third of the trace of the orthogonalized Uij tensor.

Ni(1)-F(1)	1.8602(19)
Ni(1)-C(27)	1.925(4)
Ni(1)-P(2)	2.1210(9)
Ni(1)-P(1)	2.2081(9)
Ni(2)-F(4)	1.871(2)
Ni(2)-C(54)	1.925(4)
Ni(2)-P(4)	2.1238(10)
Ni(2)-P(3)	2.2113(10)
P(1)-C(1)	1.837(3)
P(1)-C(3)	1.841(3)

P(1)-C(9)	1.844(3)
P(2)-C(15)	1.839(3)
P(2)-C(21)	1.847(3)
P(2)-C(2)	1.850(3)
P(3)-C(28)	1.841(3)
P(3)-C(30)	1.844(3)
P(3)-C(36)	1.847(4)
P(4)-C(42)	1.839(3)
P(4)-C(29)	1.851(3)
P(4)-C(48A)	1.864(3)
P(4)-C(48)	1.864(3)
F(2)-C(27)	1.394(4)
F(3)-C(27)	1.404(4)
F(5)-C(54)	1.367(4)
F(6)-C(54)	1.387(5)
C(1)-C(2)	1.540(4)
C(1)-H(1A)	0.9900
C(1)-H(1B)	0.9900
C(2)-H(2A)	0.9900
C(2)-H(2B)	0.9900
C(3)-C(4)	1.528(5)
C(3)-C(8)	1.529(5)
C(3)-H(3)	1.0000
C(4)-C(5)	1.529(5)
C(4)-H(4A)	0.9900
C(4)-H(4B)	0.9900
C(5)-C(6)	1.516(7)
C(5)-H(5A)	0.9900
C(5)-H(5B)	0.9900
C(6)-C(7)	1.518(6)
C(6)-H(6A)	0.9900
C(6)-H(6B)	0.9900
C(7)-C(8)	1.531(5)
C(7)-H(7A)	0.9900
C(7)-H(7B)	0.9900
C(8)-H(8A)	0.9900
C(8)-H(8B)	0.9900
C(9)-C(14)	1.526(6)
C(9)-C(10)	1.536(6)
C(9)-H(9)	1.0000
C(10)-C(11)	1.533(6)
C(10)-H(10A)	0.9900
C(10)-H(10B)	0.9900
C(11)-C(12)	1.498(8)

C(11)-H(11A)	0.9900
C(11)-H(11B)	0.9900
C(12)-C(13)	1.518(8)
C(12)-H(12A)	0.9900
C(12)-H(12B)	0.9900
C(13)-C(14)	1.534(5)
C(13)-H(13A)	0.9900
C(13)-H(13B)	0.9900
C(14)-H(14A)	0.9900
C(14)-H(14B)	0.9900
C(15)-C(16)	1.534(4)
C(15)-C(20)	1.539(5)
C(15)-H(15)	1.0000
C(16)-C(17)	1.527(4)
C(16)-H(16A)	0.9900
C(16)-H(16B)	0.9900
C(17)-C(18)	1.523(5)
C(17)-H(17A)	0.9900
C(17)-H(17B)	0.9900
C(18)-C(19)	1.527(6)
C(18)-H(18A)	0.9900
C(18)-H(18B)	0.9900
C(19)-C(20)	1.529(5)
C(19)-H(19A)	0.9900
C(19)-H(19B)	0.9900
C(20)-H(20A)	0.9900
C(20)-H(20B)	0.9900
C(21)-C(26)	1.535(4)
C(21)-C(22)	1.543(4)
C(21)-H(21)	1.0000
C(22)-C(23)	1.529(5)
C(22)-H(22A)	0.9900
C(22)-H(22B)	0.9900
C(23)-C(24)	1.525(6)
C(23)-H(23A)	0.9900
C(23)-H(23B)	0.9900
C(24)-C(25)	1.524(5)
C(24)-H(24A)	0.9900
C(24)-H(24B)	0.9900
C(25)-C(26)	1.533(5)
C(25)-H(25A)	0.9900
C(25)-H(25B)	0.9900
C(26)-H(26A)	0.9900
C(26)-H(26B)	0.9900

C(27)-H(27)	1.0000
C(28)-C(29)	1.532(5)
C(28)-H(28A)	0.9900
C(28)-H(28B)	0.9900
C(29)-H(29A)	0.9900
C(29)-H(29B)	0.9900
C(30)-C(35)	1.528(5)
C(30)-C(31)	1.541(5)
C(30)-H(30)	1.0000
C(31)-C(32)	1.523(5)
C(31)-H(31A)	0.9900
C(31)-H(31B)	0.9900
C(32)-C(33)	1.516(6)
C(32)-H(32A)	0.9900
C(32)-H(32B)	0.9900
C(33)-C(34)	1.521(6)
C(33)-H(33A)	0.9900
C(33)-H(33B)	0.9900
C(34)-C(35)	1.538(5)
C(34)-H(34A)	0.9900
C(34)-H(34B)	0.9900
C(35)-H(35A)	0.9900
C(35)-H(35B)	0.9900
C(36)-C(37)	1.523(5)
C(36)-C(41)	1.524(5)
C(36)-H(36)	1.0000
C(37)-C(38)	1.526(6)
C(37)-H(37A)	0.9900
C(37)-H(37B)	0.9900
C(38)-C(39)	1.520(6)
C(38)-H(38A)	0.9900
C(38)-H(38B)	0.9900
C(39)-C(40)	1.529(7)
C(39)-H(39A)	0.9900
C(39)-H(39B)	0.9900
C(40)-C(41)	1.542(6)
C(40)-H(40A)	0.9900
C(40)-H(40B)	0.9900
C(41)-H(41A)	0.9900
C(41)-H(41B)	0.9900
C(42)-C(47)	1.525(5)
C(42)-C(43)	1.530(5)
C(42)-H(42)	1.0000
C(43)-C(44)	1.534(5)

C(43)-H(43A)	0.9900
C(43)-H(43B)	0.9900
C(44)-C(45)	1.522(6)
C(44)-H(44A)	0.9900
C(44)-H(44B)	0.9900
C(45)-C(46)	1.520(6)
C(45)-H(45A)	0.9900
C(45)-H(45B)	0.9900
C(46)-C(47)	1.529(5)
C(46)-H(46A)	0.9900
C(46)-H(46B)	0.9900
C(47)-H(47A)	0.9900
C(47)-H(47B)	0.9900
C(48)-C(49)	1.450(6)
C(48)-C(53)	1.570(6)
C(48)-H(48)	1.0000
C(49)-C(50)	1.535(7)
C(49)-H(49A)	0.9900
C(49)-H(49B)	0.9900
C(50)-C(51)	1.531(8)
C(50)-H(50A)	0.9900
C(50)-H(50B)	0.9900
C(51)-C(52)	1.510(9)
C(51)-H(51A)	0.9900
C(51)-H(51B)	0.9900
C(52)-C(53)	1.531(9)
C(52)-H(52A)	0.9900
C(52)-H(52B)	0.9900
C(53)-H(53A)	0.9900
C(53)-H(53B)	0.9900
C(48A)-C(49A)	1.379(11)
C(48A)-C(53A)	1.588(11)
C(48A)-H(48A)	1.0000
C(49A)-C(50A)	1.528(14)
C(49A)-H(49C)	0.9900
C(49A)-H(49D)	0.9900
C(50A)-C(51A)	1.522(16)
C(50A)-H(50C)	0.9900
C(50A)-H(50D)	0.9900
C(51A)-C(52A)	1.477(16)
C(51A)-H(51C)	0.9900
C(51A)-H(51D)	0.9900
C(52A)-C(53A)	1.550(15)
C(52A)-H(52C)	0.9900

C(52A)-H(52D)	0.9900
C(53A)-H(53C)	0.9900
C(53A)-H(53D)	0.9900
C(54)-H(54)	1.0000

F(1)-Ni(1)-C(27)	87.97(12)
F(1)-Ni(1)-P(2)	174.79(8)
C(27)-Ni(1)-P(2)	92.12(11)
F(1)-Ni(1)-P(1)	91.82(7)
C(27)-Ni(1)-P(1)	176.62(12)
P(2)-Ni(1)-P(1)	88.39(3)
F(4)-Ni(2)-C(54)	87.84(13)
F(4)-Ni(2)-P(4)	177.75(7)
C(54)-Ni(2)-P(4)	94.16(11)
F(4)-Ni(2)-P(3)	89.44(7)
C(54)-Ni(2)-P(3)	175.82(11)
P(4)-Ni(2)-P(3)	88.62(4)
C(1)-P(1)-C(3)	107.92(16)
C(1)-P(1)-C(9)	105.55(15)
C(3)-P(1)-C(9)	103.09(16)
C(1)-P(1)-Ni(1)	108.43(11)
C(3)-P(1)-Ni(1)	114.11(12)
C(9)-P(1)-Ni(1)	117.09(13)
C(15)-P(2)-C(21)	106.00(14)
C(15)-P(2)-C(2)	105.60(15)
C(21)-P(2)-C(2)	107.35(15)
C(15)-P(2)-Ni(1)	115.69(11)
C(21)-P(2)-Ni(1)	111.40(10)
C(2)-P(2)-Ni(1)	110.31(11)
C(28)-P(3)-C(30)	107.42(15)
C(28)-P(3)-C(36)	108.29(17)
C(30)-P(3)-C(36)	104.97(16)
C(28)-P(3)-Ni(2)	108.55(12)
C(30)-P(3)-Ni(2)	115.93(12)
C(36)-P(3)-Ni(2)	111.38(12)
C(42)-P(4)-C(29)	103.90(15)
C(42)-P(4)-C(48A)	104.44(15)
C(29)-P(4)-C(48A)	106.44(17)
C(42)-P(4)-C(48)	104.44(15)
C(29)-P(4)-C(48)	106.44(17)
C(42)-P(4)-Ni(2)	118.66(12)
C(29)-P(4)-Ni(2)	108.96(11)
C(48A)-P(4)-Ni(2)	113.43(12)
C(48)-P(4)-Ni(2)	113.43(12)

C(2)-C(1)-P(1)	109.0(2)
C(2)-C(1)-H(1A)	109.9
P(1)-C(1)-H(1A)	109.9
C(2)-C(1)-H(1B)	109.9
P(1)-C(1)-H(1B)	109.9
H(1A)-C(1)-H(1B)	108.3
C(1)-C(2)-P(2)	110.2(2)
C(1)-C(2)-H(2A)	109.6
P(2)-C(2)-H(2A)	109.6
C(1)-C(2)-H(2B)	109.6
P(2)-C(2)-H(2B)	109.6
H(2A)-C(2)-H(2B)	108.1
C(4)-C(3)-C(8)	109.8(3)
C(4)-C(3)-P(1)	114.3(2)
C(8)-C(3)-P(1)	109.9(2)
C(4)-C(3)-H(3)	107.5
C(8)-C(3)-H(3)	107.5
P(1)-C(3)-H(3)	107.5
C(3)-C(4)-C(5)	110.0(3)
C(3)-C(4)-H(4A)	109.7
C(5)-C(4)-H(4A)	109.7
C(3)-C(4)-H(4B)	109.7
C(5)-C(4)-H(4B)	109.7
H(4A)-C(4)-H(4B)	108.2
C(6)-C(5)-C(4)	111.5(4)
C(6)-C(5)-H(5A)	109.3
C(4)-C(5)-H(5A)	109.3
C(6)-C(5)-H(5B)	109.3
C(4)-C(5)-H(5B)	109.3
H(5A)-C(5)-H(5B)	108.0
C(5)-C(6)-C(7)	110.3(3)
C(5)-C(6)-H(6A)	109.6
C(7)-C(6)-H(6A)	109.6
C(5)-C(6)-H(6B)	109.6
C(7)-C(6)-H(6B)	109.6
H(6A)-C(6)-H(6B)	108.1
C(6)-C(7)-C(8)	111.4(3)
C(6)-C(7)-H(7A)	109.3
C(8)-C(7)-H(7A)	109.3
C(6)-C(7)-H(7B)	109.3
C(8)-C(7)-H(7B)	109.3
H(7A)-C(7)-H(7B)	108.0
C(3)-C(8)-C(7)	111.5(3)
C(3)-C(8)-H(8A)	109.3

C(7)-C(8)-H(8A)	109.3
C(3)-C(8)-H(8B)	109.3
C(7)-C(8)-H(8B)	109.3
H(8A)-C(8)-H(8B)	108.0
C(14)-C(9)-C(10)	110.3(3)
C(14)-C(9)-P(1)	111.0(2)
C(10)-C(9)-P(1)	113.7(3)
C(14)-C(9)-H(9)	107.2
C(10)-C(9)-H(9)	107.2
P(1)-C(9)-H(9)	107.2
C(11)-C(10)-C(9)	111.2(4)
C(11)-C(10)-H(10A)	109.4
C(9)-C(10)-H(10A)	109.4
C(11)-C(10)-H(10B)	109.4
C(9)-C(10)-H(10B)	109.4
H(10A)-C(10)-H(10B)	108.0
C(12)-C(11)-C(10)	111.4(4)
C(12)-C(11)-H(11A)	109.4
C(10)-C(11)-H(11A)	109.4
C(12)-C(11)-H(11B)	109.4
C(10)-C(11)-H(11B)	109.4
H(11A)-C(11)-H(11B)	108.0
C(11)-C(12)-C(13)	110.6(4)
C(11)-C(12)-H(12A)	109.5
C(13)-C(12)-H(12A)	109.5
C(11)-C(12)-H(12B)	109.5
C(13)-C(12)-H(12B)	109.5
H(12A)-C(12)-H(12B)	108.1
C(12)-C(13)-C(14)	111.3(4)
C(12)-C(13)-H(13A)	109.4
C(14)-C(13)-H(13A)	109.4
C(12)-C(13)-H(13B)	109.4
C(14)-C(13)-H(13B)	109.4
H(13A)-C(13)-H(13B)	108.0
C(9)-C(14)-C(13)	110.3(4)
C(9)-C(14)-H(14A)	109.6
C(13)-C(14)-H(14A)	109.6
C(9)-C(14)-H(14B)	109.6
C(13)-C(14)-H(14B)	109.6
H(14A)-C(14)-H(14B)	108.1
C(16)-C(15)-C(20)	110.3(3)
C(16)-C(15)-P(2)	115.5(2)
C(20)-C(15)-P(2)	110.3(2)
C(16)-C(15)-H(15)	106.7

C(20)-C(15)-H(15)	106.7
P(2)-C(15)-H(15)	106.7
C(17)-C(16)-C(15)	110.5(3)
C(17)-C(16)-H(16A)	109.6
C(15)-C(16)-H(16A)	109.6
C(17)-C(16)-H(16B)	109.6
C(15)-C(16)-H(16B)	109.6
H(16A)-C(16)-H(16B)	108.1
C(18)-C(17)-C(16)	111.7(3)
C(18)-C(17)-H(17A)	109.3
C(16)-C(17)-H(17A)	109.3
C(18)-C(17)-H(17B)	109.3
C(16)-C(17)-H(17B)	109.3
H(17A)-C(17)-H(17B)	107.9
C(17)-C(18)-C(19)	111.4(3)
C(17)-C(18)-H(18A)	109.3
C(19)-C(18)-H(18A)	109.3
C(17)-C(18)-H(18B)	109.3
C(19)-C(18)-H(18B)	109.3
H(18A)-C(18)-H(18B)	108.0
C(18)-C(19)-C(20)	111.3(3)
C(18)-C(19)-H(19A)	109.4
C(20)-C(19)-H(19A)	109.4
C(18)-C(19)-H(19B)	109.4
C(20)-C(19)-H(19B)	109.4
H(19A)-C(19)-H(19B)	108.0
C(19)-C(20)-C(15)	110.2(3)
C(19)-C(20)-H(20A)	109.6
C(15)-C(20)-H(20A)	109.6
C(19)-C(20)-H(20B)	109.6
C(15)-C(20)-H(20B)	109.6
H(20A)-C(20)-H(20B)	108.1
C(26)-C(21)-C(22)	108.9(3)
C(26)-C(21)-P(2)	116.2(2)
C(22)-C(21)-P(2)	111.0(2)
C(26)-C(21)-H(21)	106.7
C(22)-C(21)-H(21)	106.7
P(2)-C(21)-H(21)	106.7
C(23)-C(22)-C(21)	110.3(3)
C(23)-C(22)-H(22A)	109.6
C(21)-C(22)-H(22A)	109.6
C(23)-C(22)-H(22B)	109.6
C(21)-C(22)-H(22B)	109.6
H(22A)-C(22)-H(22B)	108.1

C(24)-C(23)-C(22)	111.2(3)
C(24)-C(23)-H(23A)	109.4
C(22)-C(23)-H(23A)	109.4
C(24)-C(23)-H(23B)	109.4
C(22)-C(23)-H(23B)	109.4
H(23A)-C(23)-H(23B)	108.0
C(25)-C(24)-C(23)	111.1(3)
C(25)-C(24)-H(24A)	109.4
C(23)-C(24)-H(24A)	109.4
C(25)-C(24)-H(24B)	109.4
C(23)-C(24)-H(24B)	109.4
H(24A)-C(24)-H(24B)	108.0
C(24)-C(25)-C(26)	111.2(3)
C(24)-C(25)-H(25A)	109.4
C(26)-C(25)-H(25A)	109.4
C(24)-C(25)-H(25B)	109.4
C(26)-C(25)-H(25B)	109.4
H(25A)-C(25)-H(25B)	108.0
C(25)-C(26)-C(21)	109.6(3)
C(25)-C(26)-H(26A)	109.8
C(21)-C(26)-H(26A)	109.8
C(25)-C(26)-H(26B)	109.8
C(21)-C(26)-H(26B)	109.8
H(26A)-C(26)-H(26B)	108.2
F(2)-C(27)-F(3)	101.9(3)
F(2)-C(27)-Ni(1)	112.2(2)
F(3)-C(27)-Ni(1)	120.7(2)
F(2)-C(27)-H(27)	107.1
F(3)-C(27)-H(27)	107.1
Ni(1)-C(27)-H(27)	107.1
C(29)-C(28)-P(3)	108.2(2)
C(29)-C(28)-H(28A)	110.1
P(3)-C(28)-H(28A)	110.1
C(29)-C(28)-H(28B)	110.1
P(3)-C(28)-H(28B)	110.1
H(28A)-C(28)-H(28B)	108.4
C(28)-C(29)-P(4)	110.7(2)
C(28)-C(29)-H(29A)	109.5
P(4)-C(29)-H(29A)	109.5
C(28)-C(29)-H(29B)	109.5
P(4)-C(29)-H(29B)	109.5
H(29A)-C(29)-H(29B)	108.1
C(35)-C(30)-C(31)	110.4(3)
C(35)-C(30)-P(3)	110.6(2)

C(31)-C(30)-P(3)	115.4(3)
C(35)-C(30)-H(30)	106.6
C(31)-C(30)-H(30)	106.6
P(3)-C(30)-H(30)	106.6
C(32)-C(31)-C(30)	110.3(3)
C(32)-C(31)-H(31A)	109.6
C(30)-C(31)-H(31A)	109.6
C(32)-C(31)-H(31B)	109.6
C(30)-C(31)-H(31B)	109.6
H(31A)-C(31)-H(31B)	108.1
C(33)-C(32)-C(31)	111.8(3)
C(33)-C(32)-H(32A)	109.3
C(31)-C(32)-H(32A)	109.3
C(33)-C(32)-H(32B)	109.3
C(31)-C(32)-H(32B)	109.3
H(32A)-C(32)-H(32B)	107.9
C(32)-C(33)-C(34)	110.9(3)
C(32)-C(33)-H(33A)	109.5
C(34)-C(33)-H(33A)	109.5
C(32)-C(33)-H(33B)	109.5
C(34)-C(33)-H(33B)	109.5
H(33A)-C(33)-H(33B)	108.0
C(33)-C(34)-C(35)	110.9(3)
C(33)-C(34)-H(34A)	109.5
C(35)-C(34)-H(34A)	109.5
C(33)-C(34)-H(34B)	109.5
C(35)-C(34)-H(34B)	109.5
H(34A)-C(34)-H(34B)	108.0
C(30)-C(35)-C(34)	112.0(3)
C(30)-C(35)-H(35A)	109.2
C(34)-C(35)-H(35A)	109.2
C(30)-C(35)-H(35B)	109.2
C(34)-C(35)-H(35B)	109.2
H(35A)-C(35)-H(35B)	107.9
C(37)-C(36)-C(41)	110.2(3)
C(37)-C(36)-P(3)	116.7(3)
C(41)-C(36)-P(3)	110.4(3)
C(37)-C(36)-H(36)	106.3
C(41)-C(36)-H(36)	106.3
P(3)-C(36)-H(36)	106.3
C(36)-C(37)-C(38)	111.7(3)
C(36)-C(37)-H(37A)	109.3
C(38)-C(37)-H(37A)	109.3
C(36)-C(37)-H(37B)	109.3

C(38)-C(37)-H(37B)	109.3
H(37A)-C(37)-H(37B)	107.9
C(39)-C(38)-C(37)	110.4(3)
C(39)-C(38)-H(38A)	109.6
C(37)-C(38)-H(38A)	109.6
C(39)-C(38)-H(38B)	109.6
C(37)-C(38)-H(38B)	109.6
H(38A)-C(38)-H(38B)	108.1
C(38)-C(39)-C(40)	110.6(4)
C(38)-C(39)-H(39A)	109.5
C(40)-C(39)-H(39A)	109.5
C(38)-C(39)-H(39B)	109.5
C(40)-C(39)-H(39B)	109.5
H(39A)-C(39)-H(39B)	108.1
C(39)-C(40)-C(41)	110.3(4)
C(39)-C(40)-H(40A)	109.6
C(41)-C(40)-H(40A)	109.6
C(39)-C(40)-H(40B)	109.6
C(41)-C(40)-H(40B)	109.6
H(40A)-C(40)-H(40B)	108.1
C(36)-C(41)-C(40)	111.5(4)
C(36)-C(41)-H(41A)	109.3
C(40)-C(41)-H(41A)	109.3
C(36)-C(41)-H(41B)	109.3
C(40)-C(41)-H(41B)	109.3
H(41A)-C(41)-H(41B)	108.0
C(47)-C(42)-C(43)	109.7(3)
C(47)-C(42)-P(4)	113.0(2)
C(43)-C(42)-P(4)	112.3(2)
C(47)-C(42)-H(42)	107.2
C(43)-C(42)-H(42)	107.2
P(4)-C(42)-H(42)	107.2
C(42)-C(43)-C(44)	110.6(3)
C(42)-C(43)-H(43A)	109.5
C(44)-C(43)-H(43A)	109.5
C(42)-C(43)-H(43B)	109.5
C(44)-C(43)-H(43B)	109.5
H(43A)-C(43)-H(43B)	108.1
C(45)-C(44)-C(43)	112.0(3)
C(45)-C(44)-H(44A)	109.2
C(43)-C(44)-H(44A)	109.2
C(45)-C(44)-H(44B)	109.2
C(43)-C(44)-H(44B)	109.2
H(44A)-C(44)-H(44B)	107.9

C(46)-C(45)-C(44)	110.7(3)
C(46)-C(45)-H(45A)	109.5
C(44)-C(45)-H(45A)	109.5
C(46)-C(45)-H(45B)	109.5
C(44)-C(45)-H(45B)	109.5
H(45A)-C(45)-H(45B)	108.1
C(45)-C(46)-C(47)	110.9(3)
C(45)-C(46)-H(46A)	109.5
C(47)-C(46)-H(46A)	109.5
C(45)-C(46)-H(46B)	109.5
C(47)-C(46)-H(46B)	109.5
H(46A)-C(46)-H(46B)	108.1
C(42)-C(47)-C(46)	112.5(3)
C(42)-C(47)-H(47A)	109.1
C(46)-C(47)-H(47A)	109.1
C(42)-C(47)-H(47B)	109.1
C(46)-C(47)-H(47B)	109.1
H(47A)-C(47)-H(47B)	107.8
C(49)-C(48)-C(53)	111.1(4)
C(49)-C(48)-P(4)	120.0(3)
C(53)-C(48)-P(4)	110.9(3)
C(49)-C(48)-H(48)	104.4
C(53)-C(48)-H(48)	104.4
P(4)-C(48)-H(48)	104.4
C(48)-C(49)-C(50)	111.8(4)
C(48)-C(49)-H(49A)	109.3
C(50)-C(49)-H(49A)	109.3
C(48)-C(49)-H(49B)	109.3
C(50)-C(49)-H(49B)	109.3
H(49A)-C(49)-H(49B)	107.9
C(51)-C(50)-C(49)	111.4(4)
C(51)-C(50)-H(50A)	109.3
C(49)-C(50)-H(50A)	109.3
C(51)-C(50)-H(50B)	109.3
C(49)-C(50)-H(50B)	109.3
H(50A)-C(50)-H(50B)	108.0
C(52)-C(51)-C(50)	110.4(4)
C(52)-C(51)-H(51A)	109.6
C(50)-C(51)-H(51A)	109.6
C(52)-C(51)-H(51B)	109.6
C(50)-C(51)-H(51B)	109.6
H(51A)-C(51)-H(51B)	108.1
C(51)-C(52)-C(53)	111.8(5)
C(51)-C(52)-H(52A)	109.2

C(53)-C(52)-H(52A)	109.2
C(51)-C(52)-H(52B)	109.2
C(53)-C(52)-H(52B)	109.2
H(52A)-C(52)-H(52B)	107.9
C(52)-C(53)-C(48)	111.5(4)
C(52)-C(53)-H(53A)	109.3
C(48)-C(53)-H(53A)	109.3
C(52)-C(53)-H(53B)	109.3
C(48)-C(53)-H(53B)	109.3
H(53A)-C(53)-H(53B)	108.0
C(49A)-C(48A)-C(53A)	115.8(7)
C(49A)-C(48A)-P(4)	120.9(5)
C(53A)-C(48A)-P(4)	107.4(4)
C(49A)-C(48A)-H(48A)	103.5
C(53A)-C(48A)-H(48A)	103.5
P(4)-C(48A)-H(48A)	103.5
C(48A)-C(49A)-C(50A)	112.9(8)
C(48A)-C(49A)-H(49C)	109.0
C(50A)-C(49A)-H(49C)	109.0
C(48A)-C(49A)-H(49D)	109.0
C(50A)-C(49A)-H(49D)	109.0
H(49C)-C(49A)-H(49D)	107.8
C(51A)-C(50A)-C(49A)	111.4(10)
C(51A)-C(50A)-H(50C)	109.4
C(49A)-C(50A)-H(50C)	109.4
C(51A)-C(50A)-H(50D)	109.4
C(49A)-C(50A)-H(50D)	109.4
H(50C)-C(50A)-H(50D)	108.0
C(52A)-C(51A)-C(50A)	111.9(10)
C(52A)-C(51A)-H(51C)	109.2
C(50A)-C(51A)-H(51C)	109.2
C(52A)-C(51A)-H(51D)	109.2
C(50A)-C(51A)-H(51D)	109.2
H(51C)-C(51A)-H(51D)	107.9
C(51A)-C(52A)-C(53A)	111.5(12)
C(51A)-C(52A)-H(52C)	109.3
C(53A)-C(52A)-H(52C)	109.3
C(51A)-C(52A)-H(52D)	109.3
C(53A)-C(52A)-H(52D)	109.3
H(52C)-C(52A)-H(52D)	108.0
C(52A)-C(53A)-C(48A)	109.4(9)
C(52A)-C(53A)-H(53C)	109.8
C(48A)-C(53A)-H(53C)	109.8
C(52A)-C(53A)-H(53D)	109.8

C(48A)-C(53A)-H(53D)	109.8
H(53C)-C(53A)-H(53D)	108.2
F(5)-C(54)-F(6)	103.1(4)
F(5)-C(54)-Ni(2)	111.5(3)
F(6)-C(54)-Ni(2)	120.9(2)
F(5)-C(54)-H(54)	106.8
F(6)-C(54)-H(54)	106.8
Ni(2)-C(54)-H(54)	106.8

Table 4.14. Bond lengths [Å] and angles [°] for complex **II-DCyPE**.

4.7 References

1. Lalloo, N.; Malapit, C. A.; Taimoory, S. M.; Brigham, C. E.; Sanford, M. S. Decarbonylative fluoroalkylation at palladium(II): from organometallic studies to catalysis. *J. Am. Chem. Soc.* **2021**, *143*, 18617–18625.
2. Tasker, S. Z.; Standley, E. A.; Jamison, T. F. Recent advances in homogenous nickel catalysis. *Nature* **2014**, *509*, 299–309.
3. (a) Ichiishi, N.; Malapit, C. A.; Wozniak, L.; Sanford, M. S. Palladium- and nickel-catalyzed decarbonylative C–S coupling to convert thioesters to thioethers. *Org. Lett.* **2017**, *20*, 44–47. (b) Malapit, C. A.; Bour, J. R.; Brigham, C. E.; Sanford, M. S. Base-free nickel-catalysed decarbonylative Suzuki-Miyaura coupling of acid fluorides. *Nature* **2018**, *563*, 100–104. (c) Malapit, C. A.; Bour, J. R.; Laursen, S. R.; Sanford, M. S. Mechanism and scope of nickel-catalyzed decarbonylative borylation of carboxylic acid fluorides. *J. Am. Chem. Soc.* **2019**, *141*, 17322–17330. (d) Malapit, C. A.; Borrell, M.; Milbauer, M. W.; Brigham, C. E.; Sanford, M. S. Nickel-catalyzed decarbonylative amination of carboxylic acid esters. *J. Am. Chem. Soc.* **2020**, *142*, 5918–5923. (e) Brigham, C.; Malapit, C.; Lalloo, N.; Sanford, M. S. Nickel-catalyzed decarbonylative synthesis of fluoroalkylthioethers. *ACS Catal*. **2020**, *10*, 8315–8320.
4. Xu, L.; Vicic, D. A.; Direct difluoromethylation of aryl halides via base metal catalysis at room temperature. *J. Am. Chem. Soc.* **2016**, *138*, 2536–2539.
5. Motohashi, H.; Mikami, K. Nickel-catalyzed aromatic cross-coupling difluoromethylation of Grignard reagents with difluoroiodomethane. *Org. Lett*. **2018**, *20*, 5430–5434.
6. Regens, C. S.; Denmark, S. E. Palladium-catalyzed cross coupling reactions of organosilanols and their salts: practical alternatives to boron- and tin-based methods. *Acc. Chem. Res.* **2008**, *41*, 1486–1499.
7. Hansch, C.; Leo, A.; Taft, R. W. A survey of Hammet substituents constants and resonance and field parameters. *Chem. Rev.* **1991**, *91*, 165–195.

8. Maleckis, A.; Sanford, M. S. Catalytic cycle for palladium-catalyzed decarbonylative trifluoromethylation using trifluoroacetic esters as the CF3 source. *Organometallics* **2014**, *33*, 2653−2660.
9. Dierkes, P.; van Leeuwen, P. W. N. M. The bite angle makes the difference: a practical ligand parameters for disphosphine ligands. *J. Chem Soc., Dalton. Trans.* **1999**, 1519–1530.
10. Beweries, T.; Brammer, L.; Jasim, N. A.; McGrady, J. E.; Perutz, R. N.; Whitwood, A. C. Energetics of halogen bonding of group 10 metal fluoride complexes. *J. Am. Chem. Soc*. **2011**, *133*, 14338−14348.

Chapter 5 – Developing New Lab Modules for Organic Chemistry II Lab Experiments

5.1 Introduction

The following was the result of undertaking a Future Faculty Graduate Student Instructor position, which are available for Chemistry graduate student instructors at the University of Michigan. This program allows the graduate student instructor to create or contribute to an instructional development and/or educational research project as 50% of their normal teaching load. Encouraged by Professor Brian Coppola and working with Professor Ginger Shultz, I focused on developing a two-week lab module for a high-enrollment course that draws from recent organic chemistry literature. While reading papers related to my thesis research in the Sanford Lab, I discovered a recent report of amide bond formation that proceeds through acid fluoride intermediates.[1] This chapter describes the motivation behind this work, the translation of the literature protocol to a lab module, and future directions therein. The two-week lab module developed herein will be conducted in the large-enrollment organic chemistry 2 lab (CHEM 216) at the University of Michigan during Winter 2022. It will also be the subject of additional Future Faculty Graduate Student Instructor positions and is being prepared for submission as an article for the *Journal of Chemical Education*.

Figure 5.1. Chemistry building at the University of Michigan

5.2 Motivation for New Lab Experiments in CH216 at UM

One of the goals in modern undergraduate science education is to make science learning better resemble the true practice of science.[2] Established methods to accomplish this goal include formal research experiences, such as Research Experience for Undergraduate (REU) programs, and research-type problems into the undergraduate curricula.[3a] However, limitations with respect to financial resources, laboratory space, and large enrollment numbers challenge the ability of many academic institutions to incorporate such experiences into the curriculum.[3a]

An effective method for introducing students to "real" scientific practice is to develop lab experiments that engage students in critical thinking and problem-based learning (PBL).[4a-d] Practicing chemists regularly encounter day-to-day problems regarding project design, synthesis, and methodology that require critical thinking and problem-solving.[3] An authentic experience in this problem-solving and critical thinking is thought to improve student understanding of the nature of scientific research, encourage continued education in chemistry, and increase interest in careers in chemistry.[3a]

To best align our organic chemistry lab curriculum with scientific practice, we were motivated to develop new experiments for the first-year organic chemistry 2 lab course at the University of Michigan (UM) that draw from recent literature. However, the revision of a lab curriculum to be

more aligned with true practice is associated with challenges regarding the practicality of the experiment in an undergraduate setting.[3b]

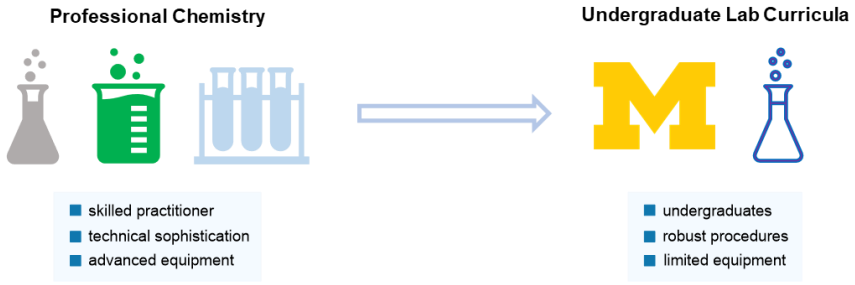

Figure 5.2. Translation of professional chemistry into undergraduate lab procedures.

Protocols developed in academic and industrial settings are most often developed by skilled practitioners.[3b] These practitioners have access to equipment and materials that are not usually available in an undergraduate lab. In an undergraduate lab setting, certain restrictions are in place to mitigate potential safety risks, minimize cost and waste generation, and limit complexity (both in instrumentation and technical ability required). Thus, commonly employed experiments in undergraduate organic chemistry labs, such as the synthesis of Aspirin and extraction of limonene or thymol, while highly robust, are often not particularly effective for teaching critical thinking.[5] As such, a central goal of this work was to translate a literature protocol into a robust lab module for a large-enrollment undergraduate organic chemistry 2 lab course.

5.3 Amide Bond Formation via Deoxyfluorination

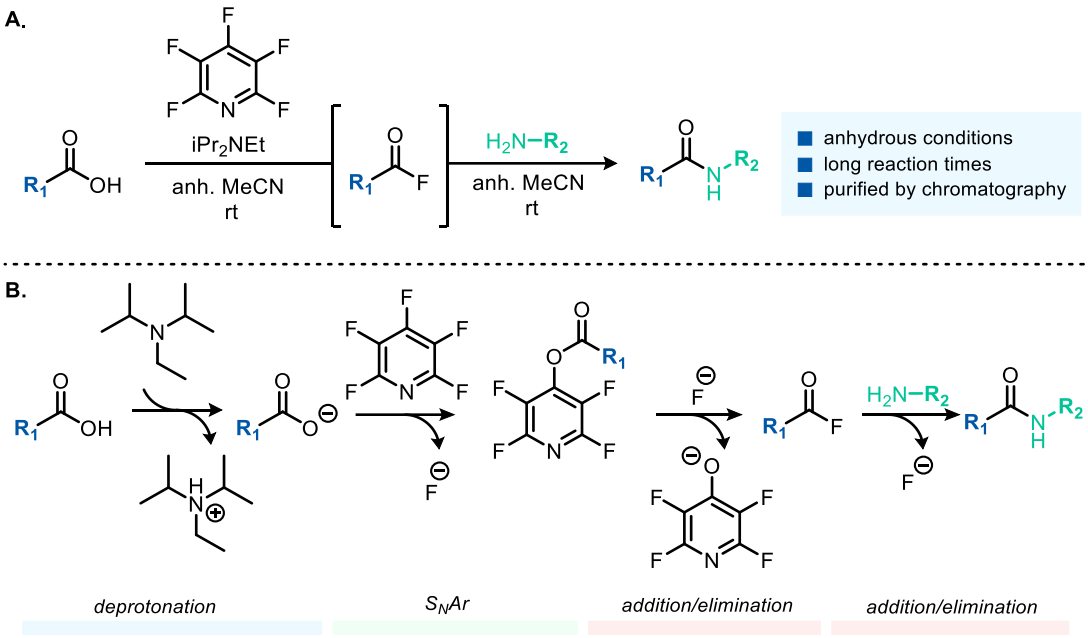

Scheme 5.1. Reaction reported in the original protocol and proposed mechanism.[1]

We noted a recent report in the literature that synthesizes amide bonds from carboxylic acids through deoxyfluorination with pentafluoropyridine (Scheme 5.1).[1] Amides via a one pot, two-step reaction that proceeds through an acid fluoride intermediate. As shown in Scheme 5.1B, the first step of the mechanism involves an S_NAr reaction of a carboxylate (formed in situ using diisopropylethylamine) with perfluoropyridine in anhydrous MeCN to form an activated ester. This ester then undergoes an addition/elimination reaction with the fluoride anion generated as a by-product of the initial S_NAr. The acid fluoride intermediate then participates in a second addition/elimination sequence with an amine to ultimately yield the amide product and an equivalent of 2,3,5,6-tetrafluoropyridin-4-ol. The amide product is then directly purified and isolated via silica gel chromatography.[1]

We were attracted to this protocol because amides are an important functional group taught in introductory chemistry, biochemistry, and biology courses.[6] In an introductory biology or biochemistry course, amide bonds are often highlighted as a critical feature in proteins, peptides, and other biomolecules. They are also ubiquitous in synthetic materials, small molecule drug candidates, and commercial pharmaceuticals. A study from 2008 of lab notebooks from three major pharmaceutical companies showed that amide formation representing 16% of all reactions

conducted.[7a] A 2014 study reported on the most frequently used reactions in medicinal chemistry papers and concluded that amide bond formation was observed at least once in greater than 50% of all manuscripts studied (Figure 5.3).[7b] Further, the top eight most profitable small molecule pharmaceuticals by retail sales in 2020 each contained at least one amide bond.[8]

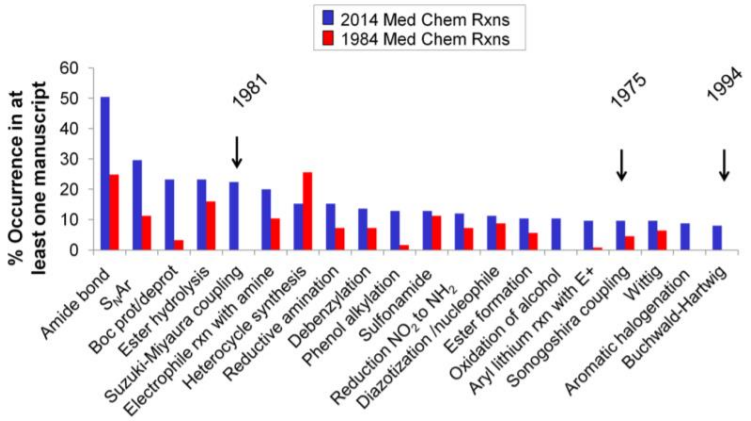

Figure 1. Occurrence of a particular reaction, plotted as the percentage of which it shows up in at least one manuscript (n = 125; representative data set taken from 2014, *J. Med. Chem.*, blue; 1985, *J. Med. Chem.*, red). The arrows (and years) indicated the first citation of this technology in the primary literature.

Figure 5.3. Prevalence of amide bond reactions over time. Taken directly from ref. 7b.

While deoxyfluorination is not specifically taught in an undergraduate organic chemistry lecture, the process of activating an –OH group to become a "leaving group" and conducting a net substitution reaction is a repeated theme in the course. Deoxyfluorination is a cutting-edge method for the synthesis of important fluorinated molecules, such as acid fluorides.[9d] Research groups around the world (including the Sanford Lab) are currently working on developing new deoxyfluorination reagents and exploring their reactivity for the synthesis of bioactive molecules (Figure 5.4).[9a-c] We were particularly excited about the prospect of developing a lab module that is related to chemistry that is conducted in the UM chemistry department. We anticipate that a new lab module developed around this report will (1) introduce students to novel chemistry in an active research field, (2) link classroom learning with practical applications in research, and (3) engender interest in scientific research and the chemistry conducted at UM.

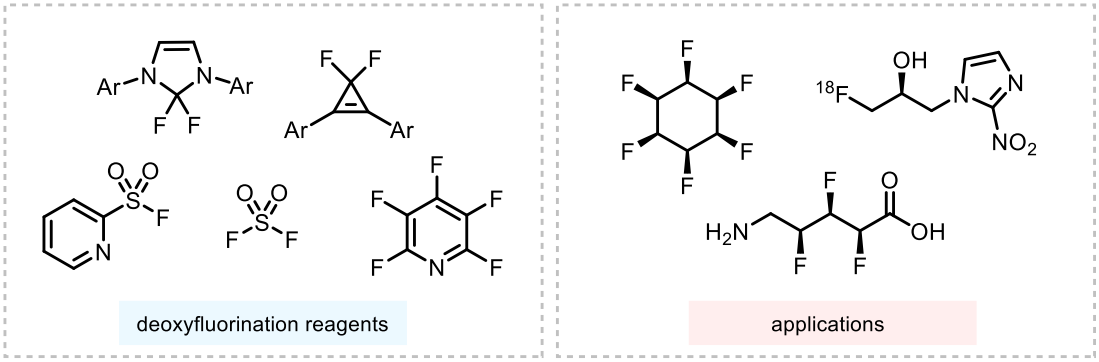

Figure 5.4. Sample of deoxyfluorination reagents and examples of incorporation of fluorine into bioactive molecules. Adapted from ref. 9d.

In most introductory organic chemistry courses, two distinct pathways are taught for the synthesis of amides.[6] The first method (A in Scheme 5.2) involves the conversion of the carboxylic acid to an electrophilic acid derivative, most commonly an acid chloride or anhydride, and subsequent reaction with an amine. The second method (B in Scheme 5.2) accesses amides via the use of a coupling reagent, such as a carbodiimide or uronium reagent.

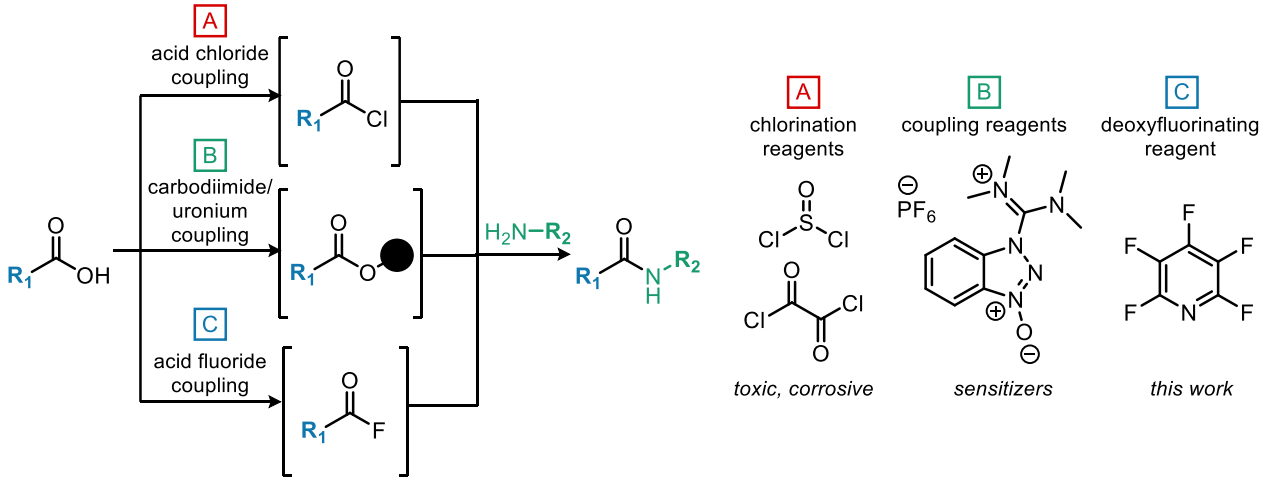

Scheme 5.2 Various methods for synthesis of amides using (A) chlorination reagents, (B) coupling reagents, and (C) deoxyfluorination reagents.

While effective, both methods have drawbacks, particularly in the context of a high-enrollment undergraduate chemistry lab course. First, the reagents used to form acid chlorides,

such as thionyl chloride and oxalyl chloride, are highly corrosive and toxic. Second, the acid chloride intermediates often have poor functional group tolerance and are sensitive to handle. As a consequence, in other reported amide syntheses that were conducted in undergraduate lab settings, these reactions are often lower yielding for the students. Third, these reactions are conducted under inert atmosphere with oven- or flame-dried glassware. Fourth, the formation of gaseous by-products when using oxalyl chloride or thionyl chloride can lead to violent exotherms, particularly when conducted without sufficient venting and cooling.

While coupling reagents, such as HATU, are easier to handle and form more stable intermediates, uronium reagents have been reported as sensitizers that should be handled with extreme care.[10] Accordingly, recent research has explored new methods for the synthesis of amide bonds.[11] In this context, the deoxyfluorination of an acid to make the acid fluoride derivative presents an attractive route for the formation of amide bonds. In terms of stability, acid fluorides show higher stability towards water and are less prone to racemization compared to their acid chloride analogues.[12]

While the report was attractive to us for these reasons, the protocol for the reaction had several key procedural challenges that needed to be addressed prior to implementation in an undergraduate lab. First, the reaction utilized anhydrous acetonitrile as solvent. Second, it had specific reaction times that were not readily compatible with two 4 h lab periods separated by 1 week. Third, the procedure required concentrating the reaction mixture in vacuo and isolating the product via silica gel chromatography, both of which are not feasible in our high enrollemnt introductory labs. Thus, the key goals of my work were to develop a lab module that: (1) does not require anhydrous solvent or reagents, (2) templates well onto the prescribed time periods of the organic chemistry 2 undergraduate lab course (two four-hour sessions a week apart), and (3) enables a simple purification and isolation procedure for a small scope (3-4) reaction products. (2). After developing a lab module that meets these conditions, we intend to incorporate PBL to enhance the learning outcomes from this lab module beyond technical skill development.

5.4 Translation of the Experiment for an Undergraduate Lab

To begin the experimental development, we selected a subset of amide products that were reported by Cobb and Brittain. In their report, the authors posit that electron-rich amine derivatives performed best in the reaction.[1] Informed by this and by the bulk commercial availability of potential reagents, we selected benzoic acid as the single carboxylic acid substrate and initially selected a series of amine derivatives: aniline, benzylamine, and *p*-anisidine (Scheme 5.3).

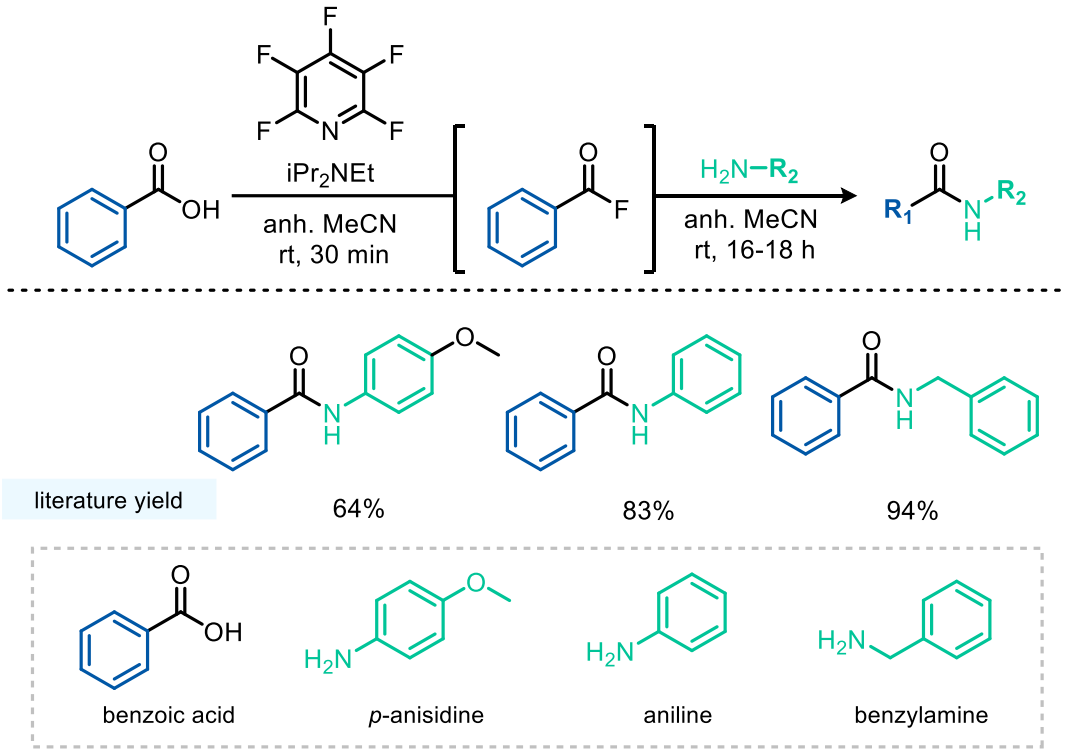

Scheme 5.3. Selected substrates for preliminary testing and reported yields from the literature protocol.[1]

Initial experiments tested the reaction under very similar conditions to those reported in the original protocol. First benzoic acid was reacted with pentafluoropyridine and *i*PrNEt$_2$ in anhydrous acetonitrile (0.27 M in benzoic acid). After a period of 0.5 h, p-anisidine was added to the reaction mixture, and the reaction was allowed to stir for 18 h. After 18 h, the reaction solution was diluted with Et$_2$O and washed with dilute HCl followed by dilute NaOH. Diethyl ether was selected as the extraction solvent for amide **1** as it is highly volatile, easier to evaporate than EtOAc, and less toxic than dichloromethane. We hypothesized that washing the organic layer with aqueous NaOH (1 M), aqueous HCl (1 M), and saturated aqueous brine would be effective for

removing organic impurities (benzoic acid, amine, diisopropylethylamine, perfluoropyridine, and 2,3,5,6-tetrafluoropyridin-4-ol, and acetonitrile).

Drying the ethereal solution over solid Na_2SO_4 afforded a lightly colored solution. Solvent was evaporated via nitrogen flow to obtain a tan solid in 63% theoretical yield of product **1**. However, ^{1}H NMR spectroscopic analysis of this material in $CDCl_3$ revealed the presence of minor impurities (~5%) in the aryl region. Subsequent ^{19}F NMR spectroscopic analysis revealed a significant amount of pyridinol by-product[1] as well as a small amount of unreacted benzoyl fluoride (Figure 5.5).

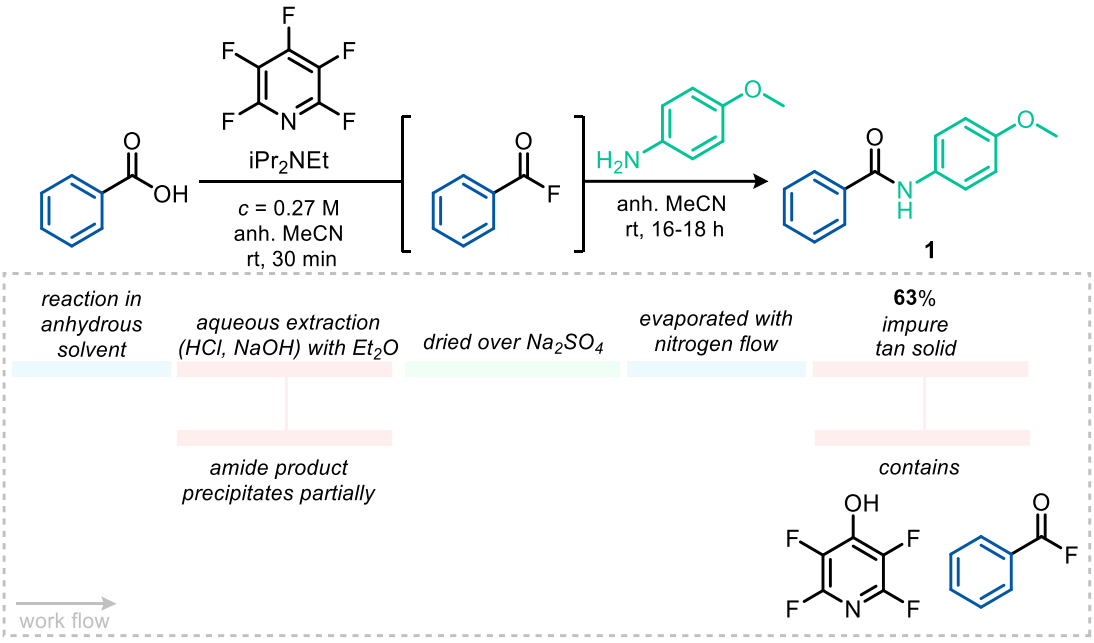

Figure 5.5. Work-flow for reaction with *p*-anisidine and purification using liquid-liquid extraction.

The results in Figure 5.5 show that the liquid-liquid extraction was not completely effective in removing the organic impurities from the reaction mixture. Further, ether extraction of product **1** proved challenging, as some product precipitated out of the organic layer during the extraction and washes. When conducting the same protocol with benzylamine, impure amide product containing significant amounts of pyridinol by-product was obtained.

When the reaction between benzoic acid and *p*-anisidine was conducted at a higher concentration (0.54 M vs 0.27 M), a white solid precipitate during the reaction. To leverage this

low solubility, the crude reaction mixture was filtered, and the resulting solid was washed with cold Et_2O and allowed to dry under ambient conditions. Subsequent ^1H and ^{19}F NMR spectroscopic analysis in d_6-DMSO showed that solid was highly pure, completely devoid of benzoyl fluoride and pyridinol by-product (Figure 5.6). The product **1** was obtained in 52% isolated yield under these conditions.

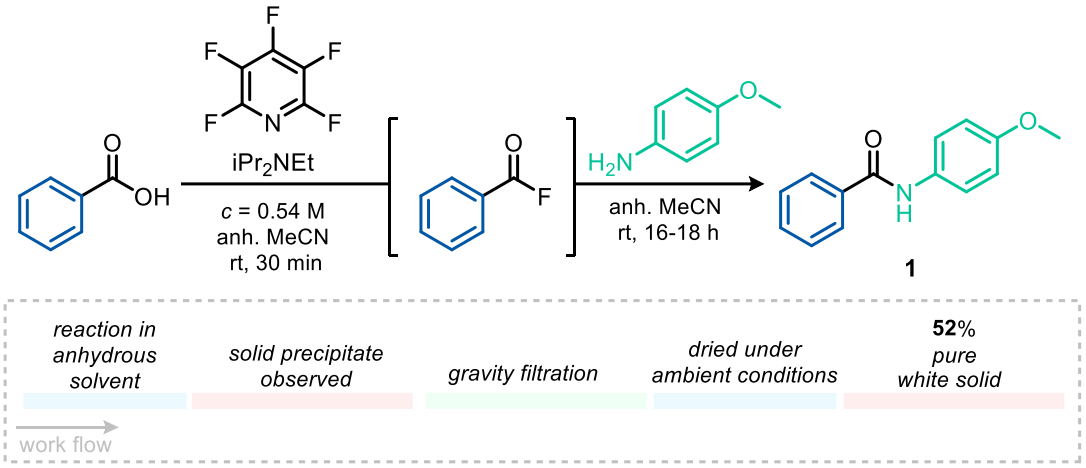

Figure 5.6. Work-flow for reaction with *p*-anisidine featuring precipitation during the reaction.

With a preliminary set of conditions in hand, we next sought to evaluate whether anhydrous solvent was critical for the reaction. Under similar conditions, except using commercial acetonitrile directly out of the bottle, we observed only a 7% reduction in the isolated yield (45% **1** rather than 52%). This simple experiment demonstrates that the reaction does not require, but benefits from, anhydrous solvent.

Analogous reactions of benzoic acid were next conducted with the two other amine substrates: aniline and benzylamine. In the reaction of aniline with in situ generated benzoyl fluoride at 0.54 M concentration only small amounts of precipitate formed during the reaction. As such, upon gravity filtration of the crude reaction mixture, only 25% yield of a white solid was obtained. However, the obtained solid was highly pure, as determined by ^{19}F and ^1H NMR spectroscopic analysis in $CDCl_3$. Attempts to precipitate or recrystallize the remaining product from the filtrate via a two-solvent mixture (Et_2O/heptane or Et_2O/hexanes) over 18 h at 0 °C did provide some additional amide product. However, this isolation and purification method was

deemed infeasible for the large enrollment lab course, as the undergraduate organic chemistry labs do not have facilities for storing samples at 0 ºC over extended times.

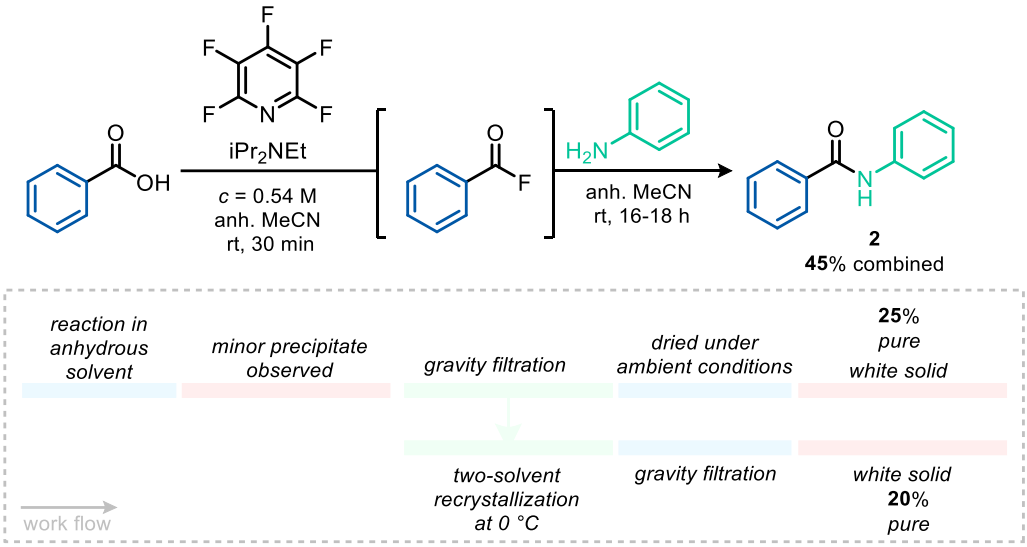

Figure 5.7. Work-flow for reaction with aniline featuring precipitation and recrystallization attempts.

Further, while this method was mild effective for obtaining **1** and **2,** it was largely ineffective for the isolation of the *N*-benzylbenzamide. We posit that this is due to the lower crystallinity of this amide (compared to the biaryl amide **2**) due to the methylene group of benzylamine that disrupts the planarity of the amide.

Moving forward, we removed benzylamine as a substrate and added two other aniline derivatives, *p*-toluidine and 3,4-dimethylaniline. The updated substrate table is shown below in Scheme 5.4. Our second iteration of amine substrates was informed by the potential for isolation of the amide products via precipitation. Thus, we selected only small aromatic amines derivatives bearing different substituents on the ring.

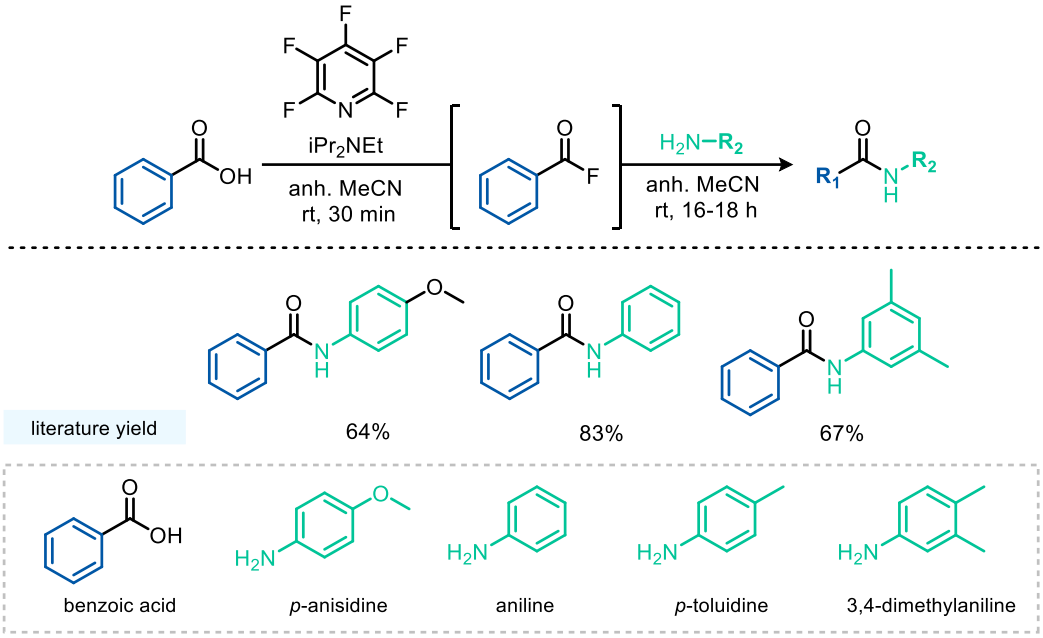

Scheme 5.4. Updated substrate table for isolation of amide products via precipitation.

We next aimed to utilize the water-solubility of benzoic acid and other small organics in the reaction mixture to purify and isolate the amide products. We hypothesized that the addition of water to the reaction mixture would precipitate the biaryl amide product and leave the organics in solution. While precipitation was observed, the solid obtained after vacuum filtration contained the amide product **1** in only ~90% purity, along with significant quantities of the aniline starting material and pyridinol by-product (Figure 5.8).[1]

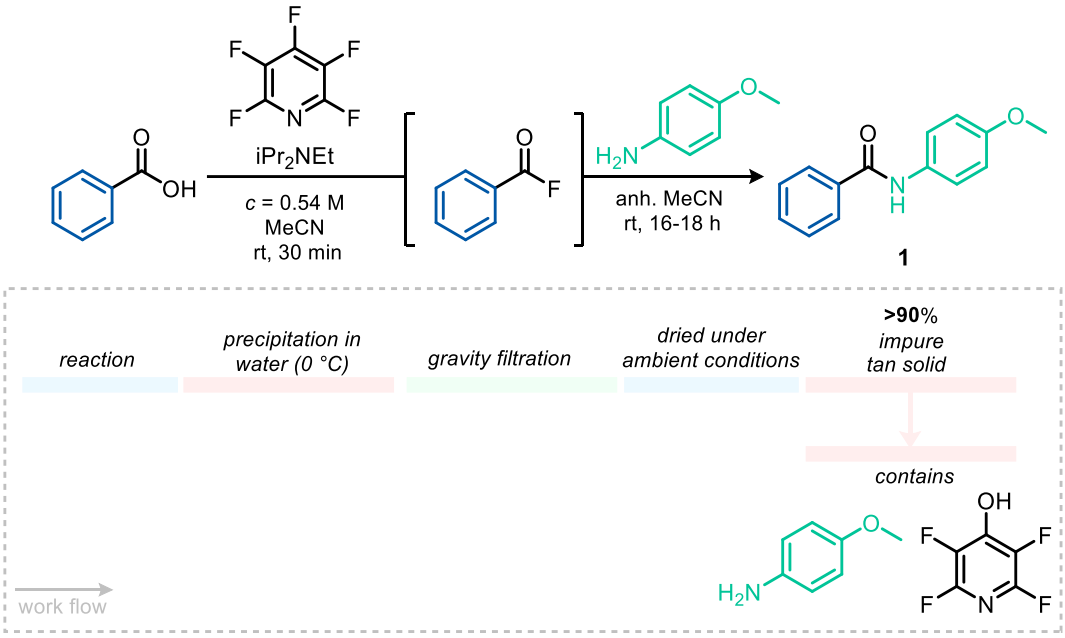

Figure 5.8. Work-flow for reaction with *p*-anisidine with purification via precipitation in ice-water.

We next reasoned that we could optimize this isolation process via the addition of dilute aqueous hydrochloric acid. This should protonate any remaining aniline to solubilize it in the aqueous phase. The *p*-anisidine reaction was thus carried out under the optimized conditions and then poured into 75 mL of dilute HCl solution (0.1 M) in an Erlenmeyer flask. This suspension was stirred while cooling to 0 °C in an ice-water bath, resulting in the precipitation of a solid. The solid was collected via vacuum filtration, washed with water, and then dried under vacuum. However, the ^{19}F NMR spectrum of this solid revealed the presence of small amounts of 2,3,5,6-tetrafluoropyridin-4-ol.[1] Ultimately, we found that washing this solid with a mixture of diethyl ether and hexanes (1:2) and subsequent drying under vacuum yielded pure amide product in 70-89% yield. Notably, these yields are comparable to, and in some cases higher than, those obtained via chromatography.[1] A pictorial supporting information highlighting the optimized process is shown in the Experimental section.

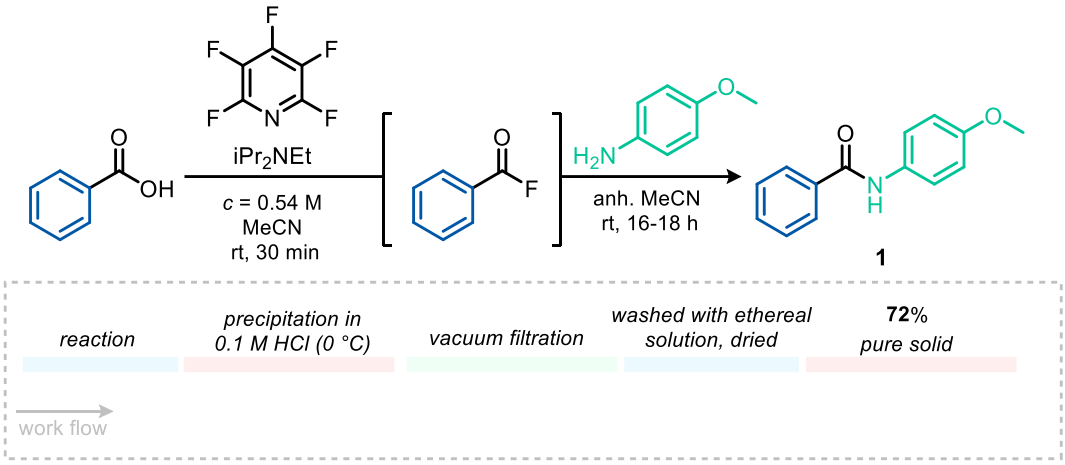

Figure 5.9. Work-flow for reaction with *p*-anisidine with purification via precipitation in acidic ice-water.

Having developed a working experimental protocol, we sought to template it onto the prescribed time periods and restrictions of a two-week module in the organic chemistry 2 labs. We first doubled the scale of the reaction to 1.64 mmol (rather than 0.82 mmol) and adjusted the concentration of the reaction to ca. 0.8 M to increase the amount of product the students would be working with. We conducted the reaction to form benzoyl fluoride from benzoic acid under these conditions but allowed the reaction to stir for one hour before the addition of the aniline derivative. After addition of *p*-anisidine, the reaction was stirred for the remainder of the lab period (ca. 2.5 h). After this period, the reaction was removed from the stirplate and allowed to sit, undisturbed for one week. After the one-week period, the product had crystallized out of the reaction mixture. This suspension was poured into 0.1 M HCl with cooling in an ice-water bath, and the solids were collected via vacuum filtration and washed with diethyl ether: hexanes (1: 2). This afforded pure product in 76% yield.

Finally, we conducted this same protocol with the aniline derivatives in Scheme 5.5 and observed 68-89% yield of the corresponding amide products. In the case of products **1** and **2**, higher yields were obtained using our protocol as compared to the reported protocol.[1] All yields reported below are an average of three entries that vary in yield by less than 5% demonstrating the reproducibility of this method.

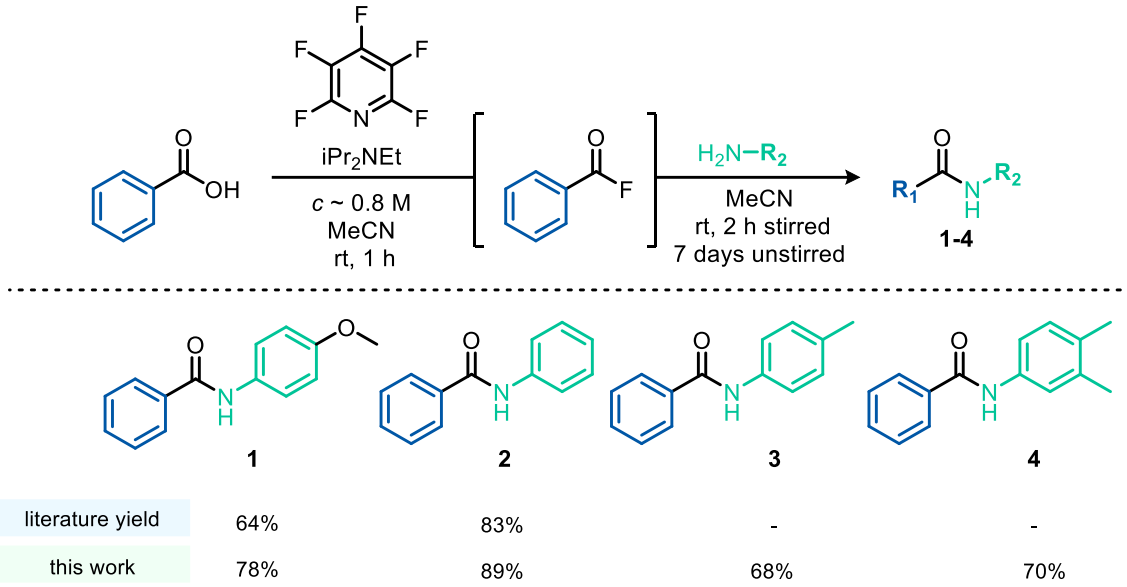

Scheme 5.5. Finalized substrate table with isolated yields compared to yields in original protocol.[1]

In conclusion, we were able to translate an experimental protocol conducted by skilled workers in an academic lab setting into a two-week lab module for a large-enrollment organic chemistry 2 lab course. This lab is being deployed as the last lab module in the Winter 2022 semester of CHEM 216 at UM.

5.5 Conclusions and Future Directions

This chapter describes the development of a new lab module for the organic chemistry 2 lab course at the University of Michigan. This work was conducted as a semester-long FFGSI project in which efforts were focused on developing a practical protocol for the reaction that can be conducted in a large-enrollment lab course. Having met that initial goal, we are focused on how to use the experiment to engage students in critical thinking and problem-based learning. As such, another student in the department at UM is undertaking an FFGSI project to develop a argument-based post-lab assignment to help students gain mechanistic insight from the experiment. One of the foci is to understand how students think about electrophile and nucleophiles.

5.6 Experimental Section

Optimized method in synthetic lab, isolation, and characterization data

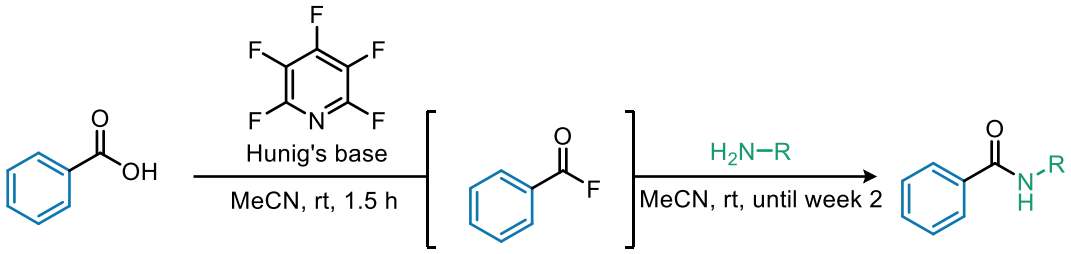

General procedure for synthesis of amides 1-4: In a 5-mL reaction vial equipped with a stirbar, dissolve benzoic acid (200 mg, 1.64 mmol, 1.0 equiv) in MeCN (ca. 2 mL). Add pentafluoropyridine (305 mg, 1.8 mmol, 1.1 equiv), then diisopropylethylamine (424 mg, 3.28 mmol, 2.0 equiv), and stir for 30 minutes to two hours at room temperature. After this initial period, amine was added (1.64 mmol, 1.0 equiv) and the reaction was stirred overnight, approximately 16 to 18 h. After 18 h, the reaction mixture was transferred to an Erlenmeyer flask, washing thrice with minimal acetonitrile. To the diluted crude reaction mixture was added 75 mL 0.1 M HCl and the mixture was stirred for thirty minutes to 1 h in a prepared ice-water bath. After the stirring period, vacuum filtration was conducted and the obtained solid was washed water (3x 5 mL), then a 1:2 solution of Et_2O:hexanes (5 mL), then only hexanes (10 mL). Drying the solid under vacuum resulted in pure solid that was directly analyzed via NMR spectroscopy in $CDCl_3$.

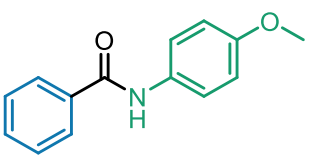

Preparation of *N*-(4-methoxyphenyl)benzamide (1). The general procedure was followed using *p*-anisidine and product **1** was isolated as an light purple solid (286 mg, 77%). **^{1}H NMR** (401 MHz, Chloroform-*d*) δ 7.91 – 7.68 (multiple peaks, 3H), 7.62 – 7.41 (multiple peaks, 5H), 6.92 (d, *J* = 2.1 Hz, 2H), 3.81 (s, 3H). **^{13}C NMR** (176 MHz, Chloroform-*d*) δ 165.75, 156.74, 135.15, 131.84, 131.10, 128.88, 127.10, 122.22, 114.36, 55.65. **^{19}F NMR** in $CDCl_3$ was silent.

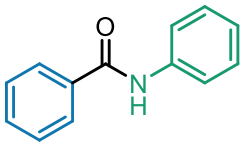

Preparation of *N*-phenylbenzamide (2). The general procedure was followed using aniline and product **2** was isolated as an off-white solid (300 mg, 93%). **^{1}H NMR** (401 MHz, Chloroform-*d*) δ 7.96 – 7.78 (multiple peaks, 3H), 7.64 (d, *J* = 7.7 Hz, 2H), 7.59 – 7.50 (m, 1H), 7.47 (m, 2H), 7.40 – 7.33 (m, 2H), 7.15 (t, *J* = 7.4 Hz, 1H). **^{13}C NMR** (176 MHz, Chloroform-*d*) δ 165.97, 138.01, 135.08, 131.97, 129.21, 128.90, 127.15, 124.71, 120.37. **^{19}F NMR** in $CDCl_3$ was silent.

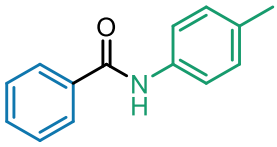

Preparation of *N*-(p-tolyl)benzamide (**3**). The general procedure was followed using *p*-toluidine and product **3** was isolated as an white solid (236 mg, 68%). **^{1}H NMR** (401 MHz, Chloroform-*d*) δ 7.97 – 7.73 (multiple peaks, 3H), 7.59 – 7.45 (multiple peaks, 5H), 7.18 (d, *J* = 8.2 Hz, 2H), 2.35 (s, 3H). **^{13}C NMR** (176 MHz, Chloroform-*d*) δ 165.80, 135.47, 135.18, 134.34, 131.84, 129.69, 128.86, 127.12, 120.42, 21.05. **^{19}F NMR** in $CDCl_3$ was silent.

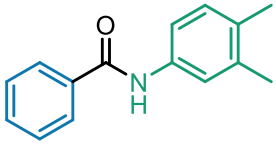

Preparation of *N*-(3,4-dimethylphenyl)benzamide (**4**). The general procedure was followed using 3,4-dimethylaniline and product **4** was isolated as a white solid (259 mg, 70%).. **^{1}H NMR** (401 MHz, Chloroform-*d*) δ 7.96 – 7.69 (multiple peaks, 3H), 7.57 – 7.41 (multiple peaks, 4H), 7.35 (dd, *J* = 8.2, 2.3 Hz, 1H), 7.11 (d, *J* = 8.1 Hz, 1H), 2.30 – 2.21 (multiple peaks, 6H). **^{13}C NMR** (176 MHz, Chloroform-*d*) δ 165.71, 137.48, 135.73, 135.26, 133.09, 131.82, 130.17, 128.87, 127.10, 121.70, 117.83, 20.08, 19.39. **^{19}F NMR** in $CDCl_3$ was silent.

Lab Experiment Protocol (as described in the W22 CH216 Lab Manual)

Week 1: In a 5-mL reaction vial equipped with a stirbar, dissolve benzoic acid (200 mg, 1.64 mmol, 1.0 equiv) in MeCN (ca. 2 mL). Add pentafluoropyridine (305 mg, 1.8 mmol, 1.1 equiv), then diisopropylethylamine (424 mg, 3.28 mmol, 2.0 equiv), and stir for 1 h at room temperature. After 1 h, add selected aniline derivative from Table 1 (1.64 mmol, 1.0 equiv) and stir the reaction until the end of the lab period. Each group member should do the reaction with a

different aniline derivative (Table 1). Your reaction will be stored until the next week. Pictures of the reaction have been provided on the final page of this document for your reference.

Week 2: The reaction may be either a solution or the amide product may have precipitated or crystallized out of the reaction mixture. If your reaction mixture is a solution or free flowing suspension containing fine solids, use a glass pipette to transfer the reaction mixture to a 125-mL Erlenmeyer flask equipped with a medium to large stirbar, leaving the small stirbar behind. If your reaction mixture has formed a large crystalline solid that cannot be pipetted, carefully decant your reaction mixture along with the solid into a 125-mL Erlenmeyer flask equipped with a medium to large stirbar, leaving the small stirbar behind. Add MeCN (1 mL) to the reaction vial and transfer the mixture to the Erlenmeyer flask (repeat twice). Prepare an ice bath (ice and water) and place the Erlenmeyer flask in the ice bath while stirring (ensure you clamp the flask so that it does not spill into the ice bath). Add 40-mL of HCl solution (0.2 M) and allow the mixture to stir for 0.5 h in the ice bath. During this time, prepare for vacuum filtration with a Buchner funnel, filter paper, and a 125-mL filter flask attached to a vacuum. While pulling vacuum, wet the filter paper with water (repeat twice and make sure it is wet before filtering the reaction through). Slowly pour the reaction mixture through the Buchner funnel in portions. No solids should go through or under the filter paper. If solid goes through into the filtrate, recombine it with the rest of the reaction, reset your Buchner funnel, and try again. After the initial filtration, dump the filtrate into the waste then re-clamp the filter flask and attach the Buchner funnel containing your crude product. Wash the crude solid with three portions of 5 mL H_2O. Dump the waste again and reconnect the flask. Dry the solid under vacuum 5 minutes. Prepare a 1:2 Et_2O:hexanes solution (ca. 15 mL). Pipette the ethereal solution over the crude solid (some material will go into the filtrate - this is desired this time). Wash the solid with 10 mL hexanes, dump the waste, then dry under vacuum for 10 minutes. Use a weigh paper and spatula to carefully transfer the solid to a tared vial. Record the mass of your product and characterize by NMR and IR spectroscopy.

Pictorial experimental protocol to make benzamide 1.

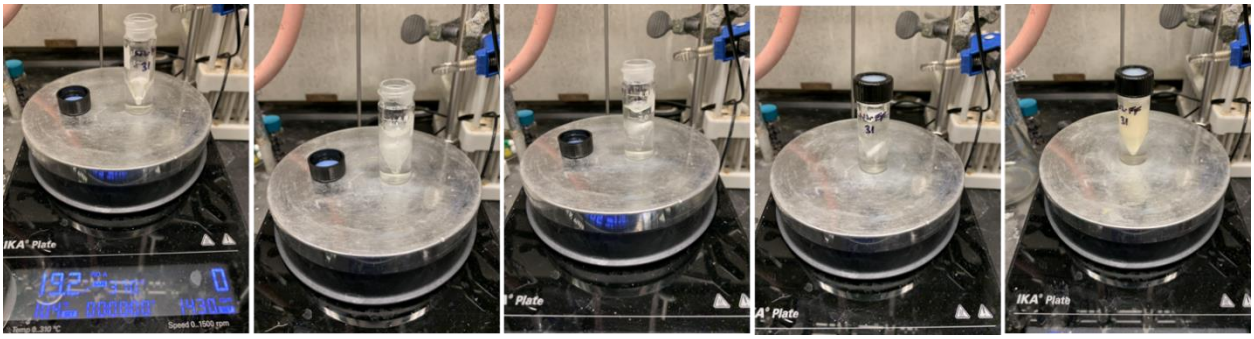
IKA Plate


MeCN
IKA Plate


125 ml
PYREX

5.6 References

1. Brittain, W. D. G.; Cobb, S. L. Carboxylic acid deoxyfluorination and one-pot amide bond formation using pentafluoropyridine (PFP). *Org. Lett.* **2021**, *23*, 5793–5798.
2. Schwingruber, H.; Keller, T.; Quinn, H. *A Framework for K-12 Science Education: Practices, Crosscutting Concepts, and Core Ideas*; National Academies Press: Washington, D.C., 2012.
3. (a) Raker, J. R.; Towns, M. H. Problem types in synthetic organic chemistry research: Implications for the development of curricular problems for second-year level organic chemistry instruction. *Chem. Educ. Res. Pract.* **2012**, *13*, 179–185. (b) Raker, J. R.; Towns, M. H. Designing undergraduate-level organic chemistry instructional problems: Seven ideas from a problem-solving study of practicing synthetic organic chemists. *Chem. Educ. Res. Pract.* **2012**, *13*, 277–285.
4. (a) Savery, J. R., Overview of problem-based learning: Definitions and distinctions. *Interdiscip. J. Probl.-based Learn.* **2006**, *1*, 9–20. (b) Overton, T.; Potter, N.; Leng, C. A study of approaches to solving open-ended problems in chemistry. *Chem. Educ. Res. Pract*. **2013**, *14*, 468. (c) Hmelo-Silver, C. E. *Problem-based learning: What and how do students learn?* Edu. Psychol. Rev. **2004**, *16*, 235−266. (d) Dochy, F.; Segers, M.; Van den Bossche, P.; Gijbels, D. *Effects of problem-based learning: A meta-analysis.* Learn Instr. **2003**, *13*, 533−568.
5. (a) Hofstein, A.; Lunetta, V. N. The Laboratory in Science Education: Foundations for the Twenty-First Century. *Sci. Educ.* **2004**, *88*, 28−54. (b) Hart, C.; Mulhall, P.; Berry, A.; Loughran, J.; Gunstone, R. What is the purpose of this experiment? Or can students learn something from doing experiments? *J. Res. Sci. Teach.* **2000**, *37*, 655−675.
6. (a) Solomons, T. W. G.; Fryhle, C.; Snyder, S. *Organic Chemistry*, 11th ed.; Wiley Global Education: Hoboken, NJ, 2012; pp 796−798. (b) Karty, J. *Organic Chemistry: Principles and Mechanisms*; W. W. Norton & Company Incorporated: New York, 2014; pp 971−974, 1049−1052. (c) Sorrell, T. N. *Organic Chemistry*; University Science Books: Sausalito, CA, 2006; pp 710−715, 938. (d) McMurry, J. E. *Organic Chemistry, 9th ed*.; Cengage Learning: Boston, MA, 2015; pp 692−707.

7. (a) Roughley, S. D.; Jordan, A. M. The medicinal chemist's toolbox: an analysis of reactions used in the pursuit of drug candidates. *J. Med. Chem.* **2011**, 54, 3451−3479. (b) Brown, D. G.; Bostrom, J. Analysis of past and present synthetic methodologies on medicinal chemistry: where have all the new reactions gone? *J. Med. Chem.* **2016**, *59*, 4443–4458.
8. Njardarson poster: <https://njardarson.lab.arizona.edu/sites/njardarson.lab.arizona.edu/files/Top%20200%20Pharmaceuticals%20Small%20Molecule%202020V3.pdf>
9. (a) Schimler, S. D.; Cismesia, M. A.; Hanley, P. S.; Froese, R. D. J.; Jansma, M. J.; Bland, D. C.; Sanford, M. S. S. Nucleophilic deoxyfluorination of phenols via aryl fluorosulfonate intermediates. *J. Am. Chem. Soc.* **2017**, *139*, 1452–1455. (b) Melvin, P. R.; Ferguson, D. M.; Schimler, S. D.; Bland, D. C.; Sanford, M. S. Room temperature deoxyfluorination of benzaldlehydes and ß-ketoesters with sulfuryl fluoride and tetramethylammonium fluoride. *Org. Lett.* **2019**, *21*, 1350–1353. (c) Nielsen, M. K.; Ugaz, C. R.; Li, W.; Doyle, A. G. PyFluor: A low-cost, stable, and selective deoxyfluorination reagent. *J. Am. Chem. Soc.* **2015**, *137*, 9571–9574. (d) Hu, W. L.; Hu, X. G.; Hunter, L. Recent developments in the deoxyfluorination of alcohols and phenols: new reagents, mechanistic insights, and applications. *Synthesis* **2017**, *49*, 4917–4930.
10. McKnelly, K. J.; Sokol, W.; Nowick, J. S. Anaphylaxis Induced by Peptide Coupling Agents: Lessons Learned from Repeated Exposure to HATU, HBTU, and HCTU. *J. Org. Chem.* **2019**, *85*, 1764–1768.
11. Pattabiraman, V. R.; Bode, J. W. Rethinking Amide Bond Synthesis. *Nature* **2011**, *480*, 471−479.
12. Blanchard, N.; Bizet, V. Acid fluoride in transition-metal catalysis: a good balance between stability and reactivity. *Angew. Chem. Int. Ed.* **2019**, *58*, 6814–6817.

Chapter 6 - Conclusions

Chapters 2 through 4 of this thesis describe the development of a four distinct decarbonylative fluoroalkylation reactions[1] that are catalyzed by Ni and Pd catalysts bearing phosphine ligands. In general, these systems were developed by evaluating the compatibility of potential reactants in tandem with studying their elementary reactivity with either a Pd or Ni complex. We then optimized the catalytic reactions informed by these initial data to achieve selectivity for the desired Ar–R_F (R_F = fluoroalkyl group) bond forming reaction.

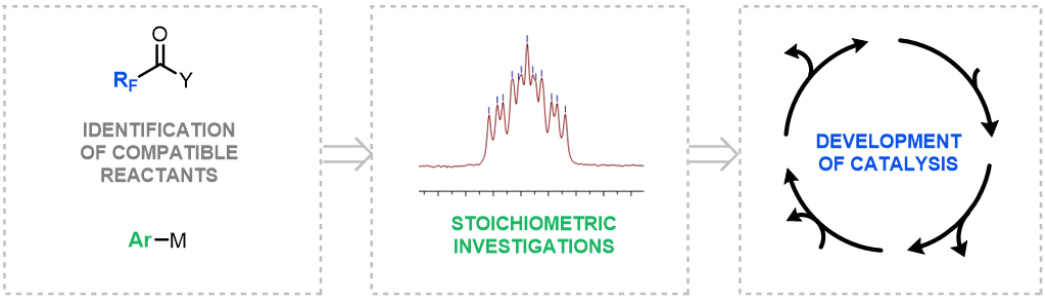

Figure 6.1. Work-flow for the development of decarbonylative catalysis.

In Chapter 2, we used the process outlined in Figure 6.1, to identify, synthesize and utilize difluoromethylacylfluoride (DFAF) as a compatible electrophile for a (SPhos)Pd-catalyzed decarbonylative difluoromethylation reaction of organoboronate esters.[1] Notable findings in Chapter 2 were the identification of a stabilizing weak H(δ+)−O(δ−) electrostatic contact (3.59 Å) between the acidic –C**H**F_2 proton and the basic difluoroacetate ligand of complex **II-CHF$_2$** (Figure 6.2). We propose that this interaction is critical to the low barrier for carbonyl de-insertion of the difluoromethyl group at this (SPhos)Pd complex.

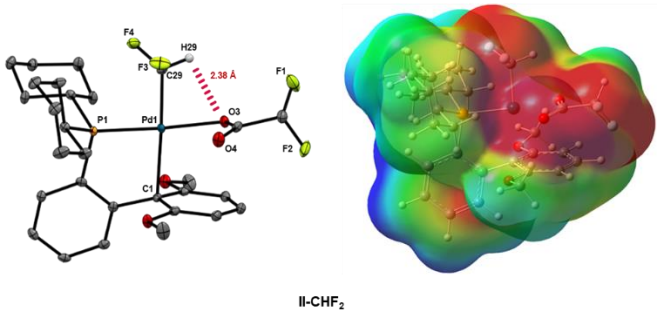

Figure 6.2. ORTEP diagram and electrostatic potential surface for **II-CHF$_2$**.[1]

Then, we utilized a transmetalation-active Pd–F intermediate for transmetalation with aryl boronate esters and developed the catalytic reaction reported in ref 1. We expect that this work on decarbonylative difluoromethylation will engender interest in the unique properties of the difluoromethyl group and the reactivity of metal–fluoride intermediates for transmetalation. Specifically, we propose the study of other M(CHF$_2$)(X) complexes to gain insight about the generality of the contribution of electrostatic interactions in stabilizing metal–difluoromethyl complexes.

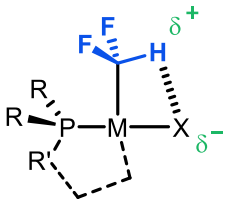

Figure 6.3. Proposed stabilization of metal–difluoromethyl complexes by electrostatic interaction.

In chapter 3, we developed our difluoromethylation catalysis to enable C–H difluoromethylation using a (XantPhos)Pd catalyst system and difluoromethyl anhydride-type electrophiles. We were also able to synthesize and obtain a crystal structure for the tentative Pd complex responsible for C–H activation, **Xant-II-CHF$_2$**, which shows a unique bite angle of 132 ° which is in between known ranges of cis- and trans-chelated (XantPhos)Pd complexes (Figure 3.6 and 6.4). [2] We aim to utilize this complex to study the C–H activation as a function on arene

and ligand to understand the selectivity and reactivity limits of this complex. We expect this study to enable the C–H activation of a wider array of arenes.

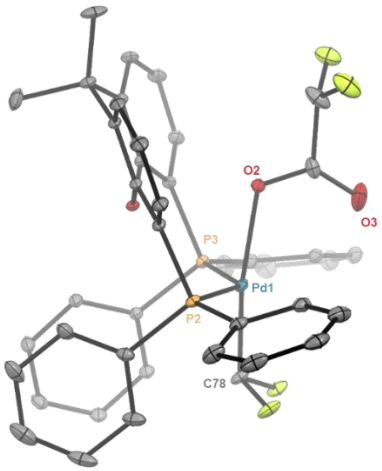

Figure 6.4. ORTEP diagram of complex **Xant-II-CHF$_2$**.

We also initiated studies of chiral acid coupling using the phenyl ester derivative of Mosher's acid. However, during stoichiometric oxidative addition and carbonyl de-insertion studies of this ester, we observed rapid ß-fluoride elimination at Ni complex and decomposition of the chiral group to form an undesired alkene by-product. Based on these results, we designed a systematic set of (fluoroalkyl)carboxylic acid derivatives increasing in complexity, as depicted in Figure 3.7. This set of derivatives would ideally inform us about the impact of the structure of the RCOY electrophile on the various elementary steps of the catalytic reaction. Based on this set of substrates, we developed the Pd-catalyzed decarbonylative difluorobenzylation of aryl boronate esters. This work was inspired by a recent report from the Amgoune group that forms difluorobenzyl ketones via a non-decarbonylative process.[3] We then translated this reaction to a decarbonylative difluorobenzylation reaction via optimization of the ligand and organometallic nucleophile to attain selectivity for the desired decarbonylative process. We expect that this work will engender interest in the development of other catalytic decarbonylative processes via rational

design of the reaction components. Future work will focus on the development of a metal-catalyze decarbonylative monofluorobenzylation reaction, as this is the next substrate featured in Figure 3.7. We propose that this substrate could exhibit stabilizing electrostatic interactions (similar to complex **II-CHF$_2$** in Figure 6.2), as depicted in Figure 6.5.

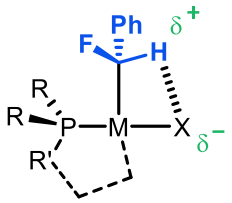

Figure 6.5. Proposed stabilization of (X)M–CHFPh complex due to electrostatic interactions with X-type ligand.

In Chapter 4, we developed a Ni-catalyzed difluoromethylation reaction with a complementary substrate scope to our Pd-catalyzed method.[1] Accordingly, we were interested in the origins of the substrate selectivity and conducted organometallic syntheses of model complexes to study transmetalation. As such, we synthesized catalytically-relevant Ni–F complex **II-DCyPE** via a three-step process starting from commercially available difluoroacetic anhydride (DFAAn). Future work in this area will systematically evaluate the transmetalation activity of a set of organoboron and organotin nucleophiles. We expect this work will inform on the transmetalation-activity of B- and Sn-organometallics in Pd- and Ni-catalyzed cross-coupling reactions.

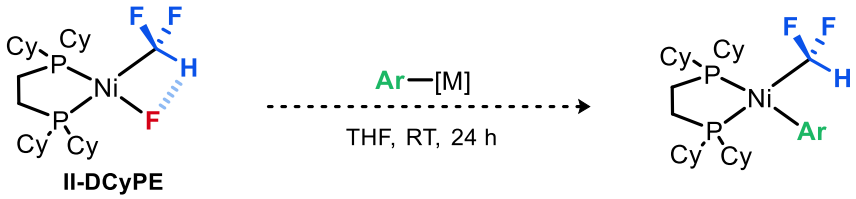

Scheme 6.1. Proposed transmetalation of (X)M–CHFPh complex.

In summary, we have developed a variety of decarbonylative fluoroalkylation reactions via reactant compatibility studies, stoichiometric studies at metal complexes, and finally through optimization of the catalytic processes. To our knowledge, no new decarbonylative fluoroalkylation studies have been reported based on this work. However, we expect this work to

be highly informative on the unique properties of the difluoromethyl group and on the development of fluoroalkylation catalysis at Pd and Ni complexes.

Moving forward, we are interested in using the information gained in these studies to develop new catalytic processes. We are focused on conducting a second iteration of our chiral acid coupling reaction that is informed from our previous work. Given that we were able to develop the intramolecular thioester coupling reaction of fluoroalkyl groups[4], we have proposed a system for the intramolecular decarbonylative coupling of thioester derivative of Mosher's acid as a model system for the development of decarbonylative chiral acid coupling (Scheme 6.2).

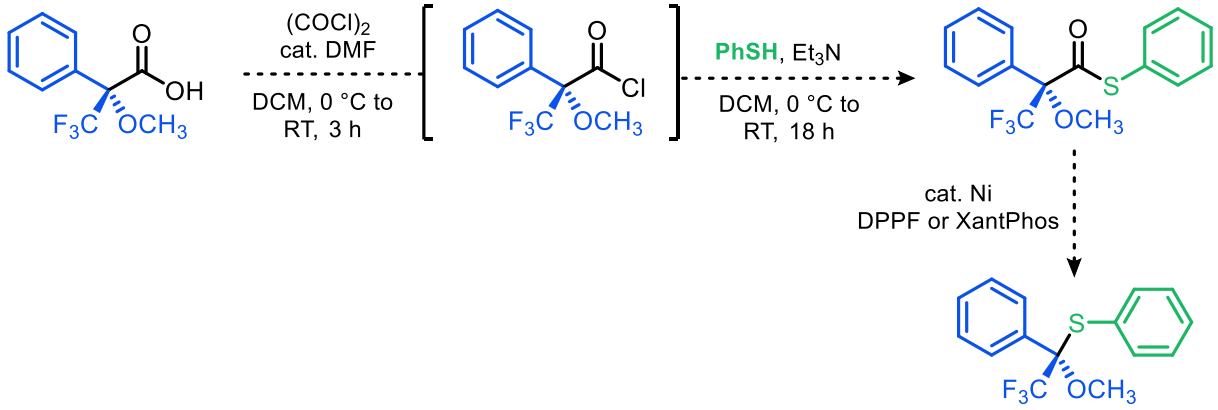

Scheme 6.2. Proposed intramolecular decarbonylative coupling of chiral thioester informed by previous studies.[4]

A central aim within this work is to minimize or prevent the potential decomposition pathways (such as ß-fluoride elimination) through a fast, intramolecular coupling process. We expect this work to serve as an excellent model system for the development of other decarbonylative chiral acid coupling reactions in our lab and others.

6.1. References

1. Lalloo, N.; Malapit, C. A.; Taimoory, S. M.; Brigham, C. E.; Sanford, M. S. Decarbonylative fluoroalkylation at palladium(II): from organometallic studies to catalysis. *J. Am. Chem. Soc.* **2021**, *143*, 18617–18625.
2. Kamer, P. C. J., Reek, J. N. H.; Dierkes, P.; van Leeuwen, P. W. N. M. Ligand bite angle effects in metal-catalyzed C–C bond formation. *Chem. Rev.* **2000***, 100*, 2741–2769. (b) Birkholz, M.N.; Freixa, Z.; van Leeuwen, P. W. N. M. Bite angle effects of disphosphines in C–C and C–X bond forming cross coupling reactions. *Chem. Soc. Rev.* **2008**, 1099–1118. (c) Kamer, P. C. J.; van Leeuwen, P. W. N. M.; Reek, J. N. H. Wide bite angle diphosphines: Xantphos ligands in transition metal complexes and catalysis. *Acc. Chem. Res.* **2001**, *34*, 895–904. (d) Marshall, W. J.; Grushin, V. V. Face Ar–CF_3 bond formation at Pd. Strikingly different outcomes of reductive elimination from [$(Ph_3P)_2Pd(CF_3)Ph$] and [(XantPhos)$Pd(CF_3)Ph$]. *J. Am. Chem. Soc.* **2006**, *128,* 12644–12645. (e) Ji, Y.; Plata, R. E.; Regens, C. S.; Hay, M.; Schmidt, M.; Razler ,T.; Qui, Y.; Geng, P.; Hsiao, Y.; Rosner, T.; Eastgate, M. D.; Blackmond, D. G. Mono-oxidation of bidentate bis-phosphines in catalyst activation: kinetic and mechanistic studies of a Pd/Xantphos-catalyzed C–H functionalization. *J. Am. Chem. Soc.* **2015**, *137*, 13272–13281. (f) Zuideveld, M. A.; Swennenhuis, B. H. G.; Boele, M. D. K.; Guari, Y.; van Strijdonck, G. P. F.; Reek, J. N. H.; Kamer, P. C. J.; Goubitz, K.; Fraanje, J.; Lutz, M.; Spek, A. L.; van Leeuwen, P. W. N. M. The coordination behavior of large natural bite angle disphosphine ligands towards methyl and 4-cyanophenylpalladium(II) complexes. *J. Chem. Soc., Dalton Trans*. **2002**, 2308–2317. (g) Yin, J.; Buchwald, S. L. Pd-catalyzed intermolecular amidation of aryl halides: the discovery that Xantphos can be trans-chelating in a palladium complex. *J. Am. Chem. Soc.* **2002**, *124*, 6043–6048.

3. Reina, A.; Krachko, T.; Onida, K.; Bouyssi, D.; Jeanneau, E.; Monteiro, N.; Amgoune, A. Development and mechanistic investigations of a base-free Suzuki-Miyaura cross-coupling of α,α-difluoroacetamides via C–N cleavage. *ACS Catal.* **2020**, *10*, 2189–2197.
4. Brigham, C. E.; Malapit, C. A.; Lalloo, N.; Sanford, M. S. Nickel-catalyzed decarbonylative synthesis of fluoroalkyl thioethers. *ACS Catal.* **2020**, *10*, 8315−8320.